DEPARTAMENTO DE QUÍMICA ORGÁNICA

DESIGN, SYNTHESIS AND *IN VITRO* EVALUATION OF NOVEL (SUB)PHTHALOCYANINE-BASED PHOTOSENSITIZERS FOR PHOTODYNAMIC THERAPY

Doctoral Thesis presented by

EVELINE VAN DE WINCKEL

to opt for the grade of

DOCTOR IN ORGANIC CHEMISTRY

Madrid, February 24, 2017

The present work has been developed at the Organic Chemistry Department of Universidad Autónoma de Madrid, under the supervision of Dr. Rudolf Schneider, Dr. Andrés de la Escosura Navazo and Prof. Tomás Torres Cebada.

The research in this work has been funded by the People Programme (Marie Curie Actions) of the European Union's Seventh Framework Programme FP7-PEOPLE-2012-ITN under REA grant agreement n° GA 316975.

During the development of the present work, predoctoral internships have been conducted in the following research centres:

1. Laboratory for Organic and Biomimetic Chemistry, Department of Organic and Macromolecular Chemistry , Ghent University, Ghent, Belgium

   Supervision: Prof. Annemieke Madder
   Date: January 4th to 15th, 2016

2. Grupo de Ingeniería Molecular, IQS, Universidad Ramon Llull, Barcelona, Spain

   Supervision: Prof. Santi Nonell Marrugat
   Date: September 19th to 23rd, 2016

To date, the results reported in this thesis have led to the following patent application and publications in scientific journals:

(i) "Multifunctional Logic in a Photosensitizer with Triple-Mode Fluorescent and Photodynamic Activity" , E. van de Winckel, R. Schneider, A. de la Escosura and T. Torres, *Chem. Eur. J*, **2015**, *21*, 18551 –18556.

(ii) "Polymeric Micelle Phthalocyanine Nano-systems for Photodynamic Therapy and/or Fluorescence Based Imaging", European Patent, Application No. 16177001.1 / Patent No. 1453, Filing date 29th of June **2016**

(iii) "Synthesis and Photosensitizing Properties of an Activatable Phthalocyanine-Subphthalocyanine Triad", E. van de Winckel, A. de la Escosura and T. Torres, *Org. Chem. Res.* **2016**, *Accepted.*

(iv) "Photoactive Cellulose Nanocrystals by Supramolecular Surface Immobilization of Phthalocyanine Phtotosensitizers", E. Anaya-Plaza, E. van de Winckel, J. Mikkilä, J.-M. Malho, O. Ikkala, O. Gulías, R. Bresolí-Obach, M. Agut, S. Nonell, T. Torres, M. A. Kostiainen and A. de la Escosura, *Chem. Eur. J.* **2016**, *Accepted.*

Other manuscripts that are related to this thesis are in preparation, including:

(v) "Phthalocyanine based biohybrid materials for biomedical applications", E. van de Winckel, E. Anaya-Plaza, A. de la Escosura, T. Torres, *Chem. Soc. Rev.* **2017**, *Review in preparation*

(vi) "Cell Penetrating Peptides enhancing Cell Uptake of Subphthalocyanine and Phthalocyanine Photosensitizers", E. van de Winckel, E. M. Llamas, A. Van Driessche, B. de Geest, A. de la Escosura, A. Madder and T. Torres, *Manuscript in preparation*

(vii) "Silicon Phthalocyanines and Subphthalocyanines as Photosensitizers for Triggering Apoptosis and Necrosis in Cancer Cells", A. Zamarrón, E. van de Winckel, A. de la Escosura, T. Torres and A. Juarranz de la Fuente, *Manuscript in preparation*

(viii) "Broad-spectrum Photodynamic Inactivation with Octacationic Silicon Phthalocyanines", E. van de Winckel, J. A. González-Delgado, M. Moreno-Simoni, Â. Cunha, A. de la Escosura and T. Torres, *Manuscript in preparation*

Foreword

Photodynamic therapy (PDT) is a photochemical approach that uses light to activate specific chemicals that, in the activated state, impart cytotoxicity. Historically, the concept of combining light with chemical agents dates back over 5000 years, when ancient civilizations in Egypt and India applied this combination to treat several disorders.

Over the years, PDT has received regulatory approval worldwide for several indications, and there have been major milestones in the basic understanding of the underlying processes and expanded vision of its applications. However, it has by no means achieved the recognition and the breadth of applications that it deserves. Therefore, within the field of PDT, there is a general consensus that the best is yet to come.

With this work I hope to make a contribution, however small it may be, to the development of this fast growing field and I hope that in the future PDT will find its well-deserved place in modern-day medicine, by the means of new and better clinical treatments than the ones offered today.

Eveline van de Winckel
Madrid, February 2017

Agradecimientos

Escribir una Tesis Doctoral no es una tarea fácil, ni lo ha sido el camino para llegar a este momento. Por suerte, en este camino me ha acompañado gente increíble. A todos ellos, me gustaría dar mis más sinceros agradecimientos.

En primer lugar, me gustaría agradecer a mis directores de tesis. A **Tomás**, por darme la oportunidad de trabajar en su grupo de investigación, y por el trato amable y cercano desde que llegué a Madrid hace un poco más que tres años y me recogió en el aeropuerto hasta ahora. A **Andrés**, que ha sido un excelente supervisor que desde el primer momento ha confiado en mí, y por su ayuda y el esfuerzo que ha depositado en este trabajo.

Siendo extranjera y llegando a Madrid sin conocer a nadie, los compañeros en el laboratorio tienen una importancia fundamental. Por ello quiero expresar mi más sincera gratitud a toda la gente del labo que me ha hecho sentir como en casa, me acogió como una familia y me ha ayudado a aprender español y a entender la cultura española. En especial la gente del L301, con quien he compartido más tiempo: **Ana**, **Edu**, **Lara**, **Giulia**, **Germán**, **Sara** y **Ismael**. También hay personas fuera del L301 que merecen una mención especial, como **Ettore**, **David** y **Joana**, los cofundadores del grupo 'Dos Cervezas Por Favor', **Lara**, la mejor vecina del mundo, y **Miguel-Angel**, mi 'rijstvriendje'. Finalmente quiero agradecer a todos los que han pasado por nuestro grupo, todos han aportado al buen ambiente que existe en la tercera planta: **María**, **Carol**, **Nico**, **Luis**, **Julia**, **Javi**, **Virtu**, **Francesca**, **Olga**, **Max**, **Vero**, **Isa**, **Marta**, **Beatrice**, **Diana**, **Miguel**, **Gema**, **Mariví**, **Gianni**, **Puri**, y **Salome.** No quiero olvidarme de los que han venido de estancia pero que han llegado a ser buenos amigos en muy poco tiempo, como **Nunzio**, **Vanesa**, **Mafalda** y sobre todo **Elisa**.

Como siempre, algunas personas consiguen reservarse un hueco especial en tu corazón. En mi caso, entre ellos está **Germán**, por ser mi peor enemigo en el squash, pero mi mejor amigo en otros momentos. Creo que es la persona con quien más tiempo he compartido y me llevo incontables recuerdos que me hacen sonreír cuando pienso en ellos (los memes, los viajes en tren y el aparato que hace tsjk-tsjk-tsjk, la noche en el karaoke o la

de Elche, nuestro amigo Jimmy, …). Qué bien nos lo pasamos! **Sara**, por introducirme en el maravilloso mundo de los vermuts (cuándo repetimos?!) y simplemente por ser la persona tan bonita que es y siempre poder confiar en ella. Dijo que quería secuestrarme para tenerme siempre consigo. Ahora que nuestro tiempo juntas llega a su fin, más que nunca querría que fuera verdad. **Edu**, tanto por las muchas conversaciones científicas como por todas nuestras tonterías, que han hecho el día a día en el laboratorio bastante más divertido! Nunca me olvidaré de las "patatas fritas" de Sigma Aldrich ni de la cara de Nicolas Cage! La princesa **Ana**, por su manera de enseñarme español un tanto particular (sigo dudando si al final es sapo o príncipe) pero sobre todo por su apoyo incondicional, tanto en lo científico como en lo personal. Por último, **Astrid** y **Iñigo**, completando así el famoso "Tea Time". Como he disfrutado todas nuestras cenas, escapadas, brunch, el viaje a Canarias, etc. A por muchos Tea Times más, sean donde sea!

Without a shadow of doubt I want to thank my family, in particular my parents, **Lieve** and **Franckie**, and my brother **Thomas**. Without their continuous support all of this would have been impossible. I always looked forward to our weekly skype-sessions, your visits to Madrid and surroundings, and my visits to Belgium.

Of course, my visits to Belgium would not have been the same without the bunch of friends that were always waiting there for me. I am extremely grateful that, after three and a half years of living abroad, our friendships have not vanished, if not, they have only become stronger. Thanks to **Sophie**, **Mere**l, **Olivier**, **Jonas**, **Sam**, **Ward**, **Kevin**, **Joke**, **Willem** and **Nils**, my friends from university. We were always joking of who would become a doctor and who would not. Well here I am, almost a doctor! Also thanks to **Xantippe**, **Kari**, **Eva**, **Laura**, **Jolien**, **Michael** and all the others from Kinepolis. Although I love working in the laboratory a lot more than in the movie theatre, we had a great time and I always look forward to our reunions. And last, but definitely not least, a big thanks to **Joni**, **An-Katrien**, **Lieselot**, **Katrijn**, **Katrien**, **Jessica**, **Stéphanie**, **Elien**, **Charlotte**, **Hannelore**, **Lien**, and everyone from "**De bende van de Bosklapper**". In my life, I have never laughed so hard as we do almost every time we meet. You lot are the best.

Gracias!
Thank you!
Dankjewel!

Table of contents

Abbreviations & Acronyms

Throughout the present thesis 'Standard Organic Chemistry Abbreviations and Acronyms' following the recommendation of the "guidelines for authors" published by *J. Org. Chem.* **2016**, have been used, which can be found on the journal webpage (http://pubs.acs.org/paragonplus/submission/joceah/joceah_authguide.pdf).

Furthermore, the next abbreviations and acronyms have also been used:

$^1O_2$	Singlet oxygen
$^3O_2$	Molecular (triplet) oxygen
ALA	5-aminolevulinic acid
aPDT	Antibacterial PDT
Arg	Arginine
CFU	Colony forming unit
CNC	Cellulose nanocrystal
CPP	Cell penetrating peptide
Cys	Cysteine
DIPEA	*N,N*-Diisopropylethylamine
DLS	Dynamic light scattering
DMEM	Dulbecco's Modified Eagle's Medium
DPBF	1,3-Diphenylisobenzofuran
DTT	Dithiothreitol
EDC	1-Ethyl-3-(3-dimethylaminopropyl)carbodiimide
EET	Electronic energy transfer
FRET	Fluorescence resonance energy transfer
FBS	Fetal Bovine Serum
HMME	Hp monomethyl ether
Hp	Hematoporphyrin

HpD	Hematoporphyrin derivative
IC_{50}	Half maximal inhibitory concentration
LED	Light emitting diode
Lys	Lysine
MAL	Methylated ALA
MAP	Model amphipathic peptide
MRSA	Methycillin resistant *Staphylococcus Aureus*
m-THPC	*meta*-Tetrahydroxyphenylchlorin
MTT	3-(4,5- Dimethylthiazol-2-yl)-2,5-diphenyltetrazolium bromide
NADH	Nicotinamide adenine dinucleotide hydride
NIR	Near-infrared
NLS	Nuclear localization sequence
PACT	Photodynamic antimicrobial chemotherapy
PBS	Phosphate buffered saline
Pc	Phthalocyanine
PCI	Photochemical internalization
PEG	Polyethylene glycol
PhC	Phase contrast
PCI	Photochemical internalization
pO_2	Oxygen partial pressure
Por	Porphyrin
PS	Photosensitizer
PDI	Photodynamic inactivation
PDT	Photodynamic therapy
PET	Photoinduced electron transfer
ROS	Reactive oxygen species

RPMI	Roswell Park Memorial Institute medium
S	Substrate
SEC	Size exclusion chromatography
SiPc	Silicon phthalocyanine
$SiPcCl_2$	Silicon phthalocyanine dichloride
$SiPc(OH)_2$	Silicon phthalocyanine dihydroxide
SubPc	Subphthalocyanine
Tat	Transcription trans-activating protein
TBO	Toluidine blue O
TEM	Transition electron microscopy
TLC	Thin layer chromatography
TP	Transportan
TSA	Tryptic soy agar
TSB	Tryptic soy broth
YGCA	Yeast extract glucose chloramphenicol agar
ZnPc	Zinc phthalocyanine

Introduction

Photodynamic therapy (PDT) is a clinically approved[1] form of phototherapy using nontoxic light-sensitive compounds, called photosensitizers or photosensitizing agents (PS), which, when exposed selectively to light of a certain wavelength, become toxic to targeted malignant and other diseased cells or organisms.

PDT is becoming widely recognized as a valuable treatment option for localized cancers, being both minimally invasive and minimally toxic.[2] Furthermore, PDT has proven ability to kill microbial cells, including bacteria, yeast, fungi and viruses.[3] In the latter case, people also refer to the treatment as photodynamic inactivation (PDI), antimicrobial PDT (aPDT) or photodynamic antimicrobial chemotherapy (PACT).

History of Photodynamic Therapy

The use of light as a therapy in medicine and surgery can be dated back to ancient times, and found its origin in Ancient Egypt, Greece and India (Figure 1a), where it was used to treat various diseases such as psoriasis, rickets, vitiligo, and skin cancer.[4]

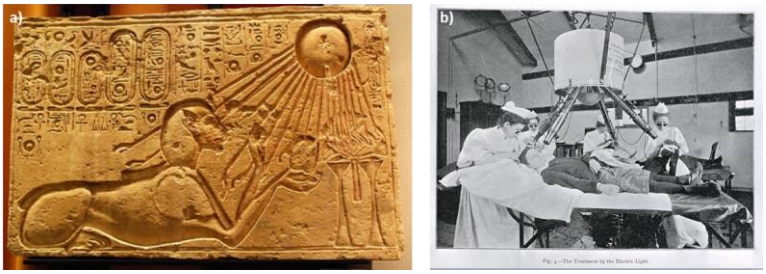

Figure 1. a) Ancient Egyptians worshipped the sun, which eventually led them to discover the connection between sunlight and health.[5] b) Set of apparatus devised by N.R. Finsen for treating lupus with light.[6]

Although later on the interest in phototherapy disappeared for many centuries, it was rediscovered by western civilization at the beginning of end of the 20th century when Niels

---

1 CenterWatch, "Photodynamic Therapy New FDA Drug Approval | CenterWatch," can be found under http://www.centerwatch.com/drug-information/fda-approved-drugs/drug/37/photodynamic-therapy, **1996**.

2 S. B. Brown, E. A. Brown, I. Walker, *Lancet Oncol.* **2004**, *5*, 497–508.

3 a] M. R. Hamblin, G. Jori, *Photodynamic Inactivation of Microbial Pathogens: Medical and Environmental Applications*, RSC Publishing, London, **2011**; b) M. Wainwright, T. Maisch, S. Nonell, K. Plaetzer, A. Almeida, G. P. Tegos, M. R. Hamblin, *Lancet Infect. Dis.* **2016**, *0*, DOI 10.1016/S1473-3099(16)30268-7.

4 a] R. V. Bensasson, G. Jori, E. J. Land, T. G. Truscott, Eds. , *Primary Photo-Processes in Biology and Medicine*, Springer US, Boston, MA, **1985**; b) M. D. Daniell, J. S. Hill, *Aust. N. Z. J. Surg.* **1991**, *61*, 340–348.

5 "Akhenaten," can be found under https://upload.wikimedia.org/wikipedia/commons, **2008**.

6 "N. R. Finsen," can be found under http://wellcomeimages.org/, **2002**.

R. Finsen found that sun exposure of his patients showed beneficial effects in their treatment of lupus vulgaris (skin tuberculosis) and smallpox.[7] He went on to successfully demonstrate this form of phototherapy by employing heat-filtered light from a carbon-arc lamp in the treatment of cutaneous tuberculosis (Figure 1b),[8] for which he won the Nobel Prize in Physiology and Medicine in 1903.

The idea of using a dye as a PS came from an observation by Oscar Raab, a student of Professor H. Tappenheimer at the Pharmacological Institute of the Ludwig-Maximilian University of Munich, in the winter of 1897-1898. He noticed that the toxic effect of the acridine dye (Figure 2a) on paramecia (microscopic single-cell organisms that live in ponds, rivers, lakes, streams and puddles) was minimal on a day where there was a thunderstorm in comparison to its efficacy on a normal day. From this observation he concluded that light, in some way, activated the acridine dye and that the combined cytotoxic effect was greater than that of the individual components.[9] A few years later, in 1904, Professor H. Tappenheimer was the first to introduce the term "Photodynamische Wirkung" (Photodynamic Action), when he successfully treated a skin tumor using a combination of white light and topical application of Eosin Y as PS (Figure 2 b and c).[10]

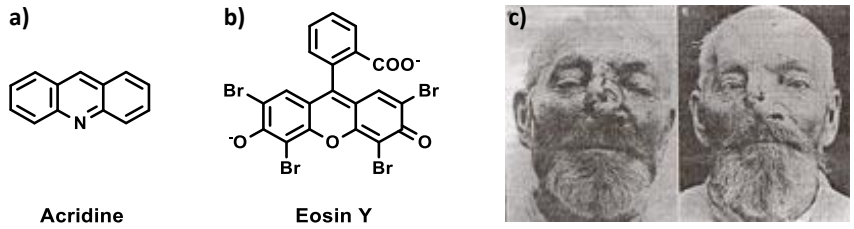

Figure 2. Chemical structure of a) Acridine and b) Eosin Y, the first dyes used as a PS by Oscar Raab and H. Tappenheimer, respectively. c) Topical PDT treatment of facial basal cell carcinoma with Eosin Y as PS, before and after long-term exposure either to sunlight or arc-lamp light.[11]

The more recent era of PDT was initiated by Lipson in the 1960s, when he discovered Hematoporphyrin derivative (HpD), a complex mixture of porphyrins (Por) derived from Hematoporphyrin (Hp, Figure 3a), which had tumor-localizing properties.[7a,8,12] The final breakthrough of the therapeutical application of PDT came in 1975, when Dougherty and co-workers first reported that the administration of HpD and red light could completely

---

7 a] T. Patrice, J. Moan, Q. Peng, *An Outline of the History of PDT*, The Royal Society Of Chemistry, **2003**; b) N. R. Finsen, *Br. Med. J.* **1903**, *1*, 1297–1298.

8 R. Bonnet, *Chem. Soc. Rev.* **1995**, *24*, 19–33.

9 O. Raab, *Ztg. Biol.* **1900**, *39*, 524–526.

10 A. Jesionek, H. von Tappenheimer, *Arch Klin. Med.* **1905**, *82*, 223–227.

11 M. H. Abdel-Kader, *Photodynamic Therapy - From Theory to Application*, Springer, **2014**.

12 a] R. L. Lipson, E. J. Baldes, *Arch. Dermatol.* **1960**, *82*, 508–516; b) R. L. Lipson, E. J. Baldes, A. M. Olsen, *J. Natl. Cancer Inst.* **1961**, *26*, 1–11; c] R. L. Lipson, E. J. Baldes, A. M. Olsen, *J. Thorac. Cardiovasc. Surg.* **1961**, *42*, 623–629.

eradicate mammary tumor growth in mice,[13] while Kelly and co-workers reported that light activation of HpD could also eliminate bladder carcinoma in mice.[14] A few years later, Photofrin® (Figure 3b), a fraction of HpD purified by removal of the Hp monomers, became the first PS to be approved by regulatory authorities. In 1993, it was first approved in Canada, for the treatment of bladder cancer. In 1995, it was approved by de Food and Drug Administration in the United States, for the palliation of obstructive esophageal cancer.[15]

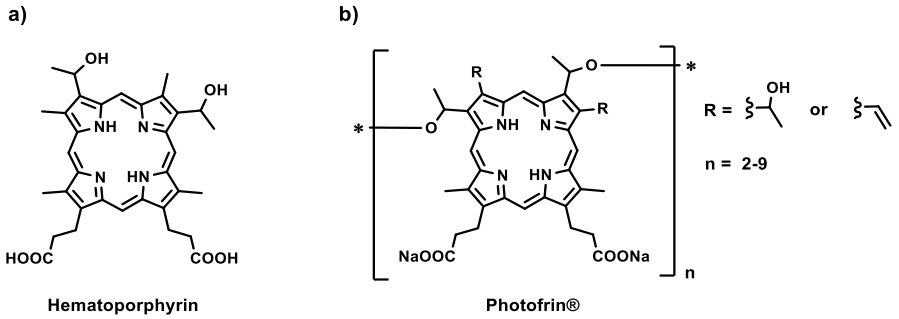

Figure 3. a) Hp structure. b) Photofrin® structure; a purified HpD derivative consisting of a complex mixture of dimers and oligomers ranging from two to nine Por units connected by ether bonds (does not contain any monomers unlike HpD).

The success of treatments and subsequent approvals of using Photofrin® generated worldwide interest in PDT as a treatment modality.

---

[13] T. J. Dougherty, G. B. Grindey, R. Fiel, K. R. Weishaupt, D. G. Boyle, *J. Natl. Cancer Inst.* **1975**, *55*, 115–121.

[14] a] J. K. Kelly, M. E. Snell, *Br. J. Cancer* **1975**, *31*, 237–244; b) *J. Urol.* **1976**, *115*, 150–151.

[15] Z. Huang, *Technol. Cancer Res. Treat.* **2005**, *4*, 283–293.

Key components of Photodynamic Therapy

PDT is a form of phototherapy that, apart from a light source, involves two other main components: a PS and the presence of molecular oxygen ($^3O_2$). Only when these three components are combined together, they become toxic to targeted cells.

Photosensitizers

As a general definition, PS are compounds that are capable of absorbing light of a specific wavelength and transforming it into other forms of energy. In medicine, a PS is considered a drug when, upon excitation by light, it can utilize and convert this energy to induce photochemical reactions that may ultimately cause lethal toxic effects in the direct neighbourhood of the PS.[16] In this respect, the ideal PS should preferentially accumulate only in the targeted diseased tissue.

First, second and third generation photosensitizers

Historically, PS are classified into three generations.[17] First generation PS solely include HpD and porfimer sodium (Photofrin®). They were the first effective PS, but showed various problematic side effects such as low selectivity and prolonged skin photosensitization. Second generation PS are synthetic derivatives of the first generation PS, designed with the intention to overcome these shortcomings. They are chemically pure compounds, at least as efficient as the first generation PS, that absorb at longer wavelengths and cause significantly less post-treatment photosensitization. Finally, third generation PS are second generation PS covalently conjugated to site-specific delivery agents for selective accumulation within targeted tissue (Figure 4).[17] If such delivery agents are of biological nature (eg. monoclonal antibodies, specific peptides, protein cages, low-density lipoproteins, liposomes, nucleic acids, folic acid, carbohydrates, etc.), the PS-conjugates are called biohybrids.[18] Other non-biological delivery platforms could be for example semisolid hydrogel formulations, polymeric micelles, nanoparticles, etc.[19]

---

16 a] J. F. Lovell, T. W. B. Liu, J. Chen, G. Zheng, *Chem. Rev.* **2010**, *110*, 2839–2857; b) F. Dumoulin, *Photosensitizers in Medicine, Environment and Security*, Springer New York, **2012**.

17 a] J. G. Moser, *Photodynamic Tumor Therapy : 2nd and 3rd Generation Photosensitizers*, Harwood Academic Publishers, Amsterdam, **1998**; b) D. Wöhrle, A. Hirth, T. Bogdahn-Rai, G. Schnurpfeil, M. Shopova, *Russ. Chem. Bull.* **1998**, *47*, 807–816.

18 E. van de Winckel, E. Anaya, A. de la Escosura, T. Torres, *Chem. Soc. Rev.*, *manuscript in preparation.*

19 a] M. E. Wieder, D. C. Hone, M. J. Cook, M. M. Handsley, J. Gavrilovic, D. A. Russell, *Photochem. Photobiol. Sci.* **2006**, *5*, 727–734; b) M. Camerin, M. Magaraggia, M. Soncin, G. Jori, M. Moreno, I. Chambrier, M. J. Cook, D. A. Russell, *Eur. J. Cancer* **2010**, *46*, 1910–1918; c] B. Kogan, A. Pankratov, A. Butenin, R. Feyzulova, T. Andreeva, O. Yuzhakova, R. Yakubovskaya, V. Negrimovsky, E. Lukyanets, G. Vorozhtsov, *Photodiagnosis Photodyn. Ther.* **2011**, *8*, 209; d) X. Jia, L. Jia, *Curr. Drug Metab.* **2012**, *13*, 1119–1122.

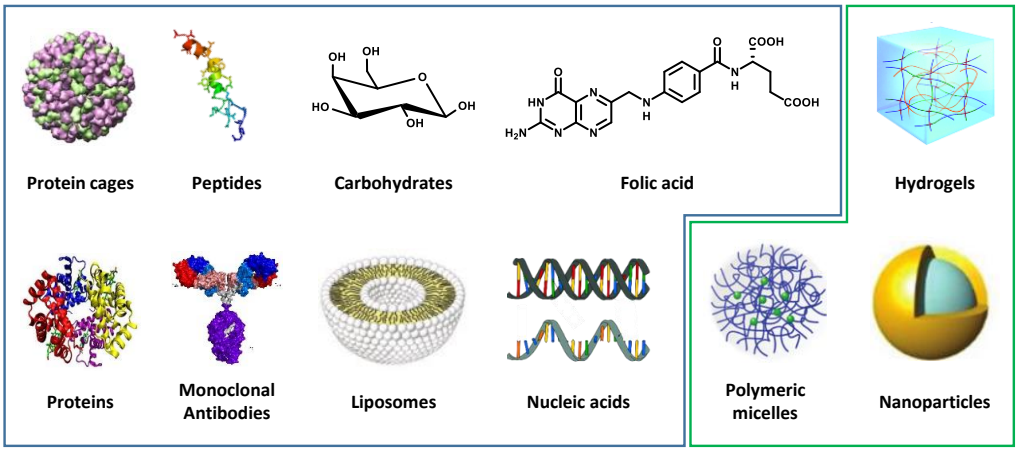

Figure 4. Some examples of biological (blue) and non-biological (green) delivery agents for selective delivery of PS to the targeted malignant tissues or organisms.

Classification of photosensitizers according to chemical structure

Apart from the above-mentioned classification in three generations, which wrongly implies that third-generation PS are better than the first- and second-generation ones, PS have also been categorized according to their chemical structure. In this way, three broad categories are distinguished: (i) Pors, (ii) chlorins and (iii) synthetic dyes.

The first category solely consists of Pors, such as Hp and its derivatives (Figure 3), while the second category consists of chlorophyll-like substances that were discovered through photosynthesis processes (chlorins) and in bacteria and algae (bacteriochlorins) (Figure 5). They are in fact reduced forms of Pors and were found to possess equally great photosensitizing properties.

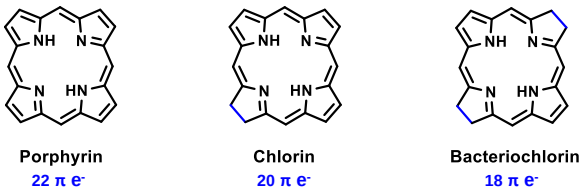

Figure 5. Chemical structures of Por, and the reduced Por derivatives chlorin and bacteriochlorin.

The third and biggest family is that of the synthetic dyes, which can be subdivided into two categories: porphyrinoid and non-porphyrinoid dyes. The chemical structures of some of the most common synthetic dyes that are able to photogenerate singlet oxygen ($^1O_2$) are summarized in Figure 6.

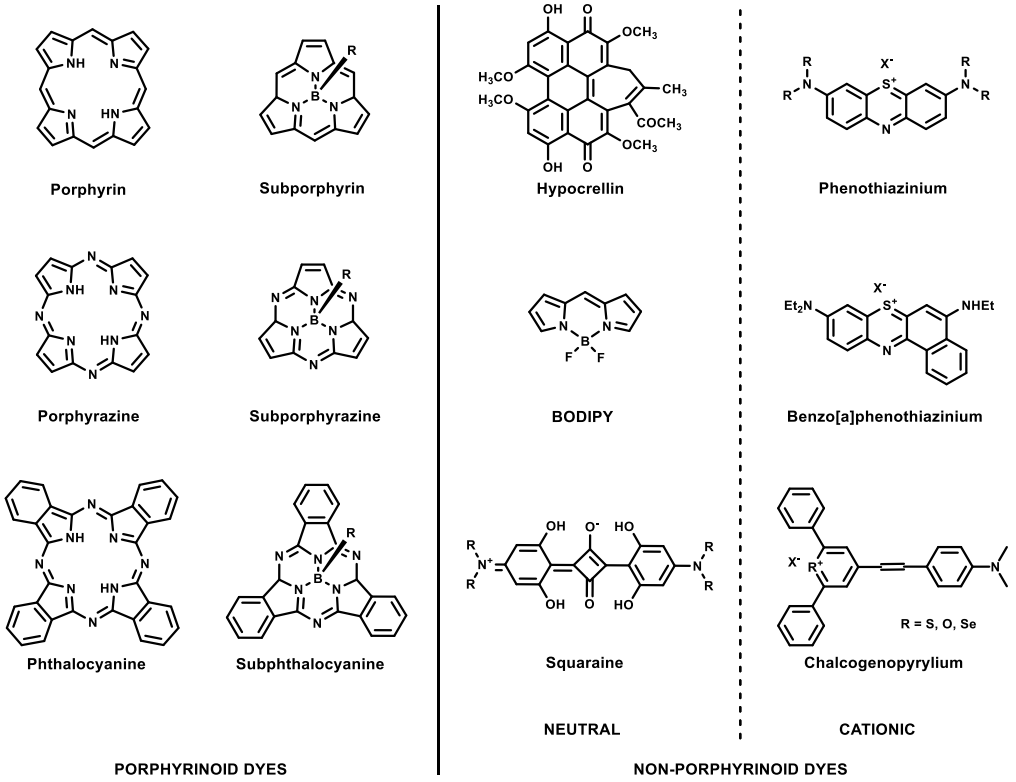

Figure 6. Chemical structures of some of the most common synthetic dyes able to photogenerate $^1O_2$. On the left some common porphyrinoid dyes can be seen, while the right column depicts neutrally charged (middle) and cationic (right) non-porphyrinoid dyes.

Until now, the porphyrinoid dyes are the most investigated and most important ones among the synthetic dyes.[20] Indeed, the only clinically approved PS up to date are all porphyrinoid derivatives. In this thesis, in particular, we will focus on two of these porphyrinoid families, which are also heavily studied compounds in our research group, namely phthalocyanines (Pcs) and subphthalocyanines (SubPcs). Their general characteristics and synthesis will be discussed in detail later on in this introduction.

Characteristics of ideal photosensitizers

In order to develop PS with high potency and selectivity, the characteristics of efficient PS must first be known. A good PS is preferably a single and well characterized compound with a known and constant composition, low manufacturing costs and good stability when

[20] a] M. R. Detty, S. L. Gibson, S. J. Wagner, *J. Med. Chem.* **2004**, *47*, 3897–3915; b) A. E. O'Connor, W. M. Gallagher, A. T. Byrne, *Photochem. Photobiol.* **2009**, *85*, 1053–1074; c] S. Yano, S. Hirohara, M. Obata, Y. Hagiya, S. Ogura, A. Ikeda, H. Kataoka, M. Tanaka, T. Joh, *J. Photochem. Photobiol. C* **2011**, *12*, 46–67; d) A. B. Ormond, H. S. Freeman, *Materials* **2013**, *6*, 817–840; e] A. Kamkaew, S. H. Lim, H. B. Lee, L. V. Kiew, L. Y. Chung, K. Burgess, *Chem. Soc. Rev.* **2013**, *42*, 77–88.

stored. Furthermore, it should ideally fulfil most of the following criteria, mentioned in Table 1.

Table 1. Recommended characteristics for ideal PS.[21]

Parameter	Description of the ideal PS characteristics
Toxicity	The PS should not show any intrinsic dark toxicity, and no toxic byproducts should be generated when it is metabolized. Furthermore, the PS should not be mutagenic or carcinogenic, as it should not cause a new disease when curing another.
Administration	The PS should preferably be administrated close to the site of action (e.g. topically for skin cancer, inhalation for lung cancer, etc.) In the case of intravenous administration, the PS should show a good selectivity for the target tissue.
Selectivity	The PS should preferably accumulate in the targeted malignant tissue. Special attention should be given to determining the correct site of action, which can either be intracellular (e.g. mitochondrial membranes) or extracellular (e.g. cell membrane).
Activation	The PS should exclusively be activated by light of a certain wavelength to prevent accidental treatment, while at the same time the light of this wavelength should provide the PS with sufficient energy to excite $^3O_2$ to its singlet excited state. To this end, the PS should show maximal absorption in the range of 600-800 nm.
Functioning	The PS should show a high triplet quantum yield (ϕ_t) and triplet state energy (ΔE_t), higher than that of $^1O_2$ (ΔE_t = 94 kJ mol^{-1}), so that energy transfer can occur to generate $^1O_2$. In this regard, the PS should not aggregate in physiological environment, since aggregation decreases ϕ_t and therefore the $^1O_2$ quantum yield (ϕ_Δ).
Integrative ability	The PS should easily be integrated in a multi-treatment therapy, and perform well in conjugated use with chemotherapy, surgery and/or radiation.
Imaging	The PS should ideally be (or contain) a fluorescent moiety, which allows for *in situ* imaging of its localization, functioning and elimination.
Elimination	The PS should be effectively eliminated from the body to avoid generalized skin photosensitization, while it should on the other hand have an acceptable half-life to enable repeated treatments without having to re-administer the drug.

[21] a] A. J. MacRobert, S. G. Bown, Philips, D., *Photosensitizing Compounds: Their Chemistry, Biology and Clinical Use, No. 146*, Wiley, Chichester, **1989**; b) G. Jori, *J. Photochem. Photobiol. Chem.* **1992**, *62*, 371–376; c] S. B. Brown, T. G. Truscott, *Chem. Br.* **1993**, *29*, 955–959; d) E. D. Sternberg, D. Dolphin, C. Brückner, *Tetrahedron* **1998**, *54*, 4151–4202; e] E. Waszkowska, Z. Zarębska, J. Poznański, I. Zhukov, *J. Photochem. Photobiol. B* **2000**, *55*, 145–154; f) R. R. Allison, G. H. Downie, R. Cuenca, X.-H. Hu, C. J. Childs, C. H. Sibata, *Photodiagnosis Photodyn. Ther.* **2004**, *1*, 27–42.

Tissue oxygen and its conversion into $^1O_2$

Absolutely essential for PDT to work is the presence of $^3O_2$ in the near proximity of the site of action. Luckily the human body requires and regulates a very precise and specific balance of $^3O_2$ in the blood and tissues.[22] Using the respiratory system, red blood cells, specifically hemoglobin, gather oxygen in the lungs and distribute it to the rest of the body. The quantity of oxygen in blood and tissues can be expressed by their oxygen partial pressure (pO_2). Typical pO_2 values for various tissues can be seen in Table 2.

Table 2. Typical pO_2 values in different tissues.

	pO_2 (mmHg)	**pO_2 (%)**
Air	160	21.1
Arterial blood	100	13.2
Brain	33.8 ± 2.6	1.3-2.5
Lungs	42.8	5.6
Intestine	8 ± 3.2	1.1 ± 0.4
Liver	40.6 ± 5.4	5.4 ± 0.7
Kidney	72 ± 20	9.5 ± 2.6
Bone marrow	48.9 ± 4.5	6.5 ± 0.6

In its ground state, $^3O_2$ has an unusual electronic structure: the ground state is a triplet, paramagnetic because of two parallel electronic spins (Figure 7a). When an excited PS (also in its triplet state) collides with $^3O_2$, a process of triplet-triplet energy transfer takes place, converting the $^3O_2$ into the is extremely short-lived and reactive $^1O_2$ (Figure 7b).[23] This process involves "flipping the spin" of the outermost electron and shifting it into the orbital containing the other electron, which in turn leaves one orbital entirely unoccupied (a violation of Hund's rule).

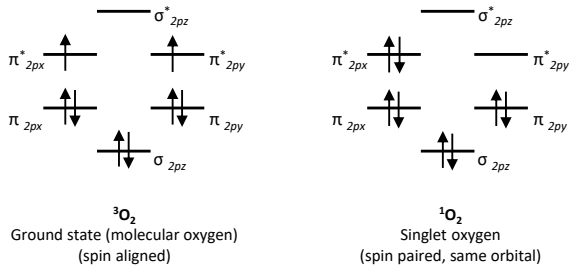

Figure 7. Molecular orbital diagrams of molecular triplet oxygen and highly reactive $^1O_2$.

---

22 a] P. Vaupel, F. Kallinowski, P. Okunieff, *Cancer Res.* **1989**, *49*, 6449–6465; b) A. Carreau, B. E. Hafny-Rahbi, A. Matejuk, C. Grillon, C. Kieda, *J. Cell. Mol. Med.* **2011**, *15*, 1239–1253; c] K. Mayer, S. Trzeciak, N. K. Puri, *Curr. Opin. Crit. Care* **2016**, *22*, 437–443.

23 a] M. C. De Rosa, R. J. Crutchley, *Coord. Chem. Rev.* **2002**, *233–234*, 351–371; b) C. Schweitzer, R. Schmidt, *Chem. Rev.* **2003**, *103*, 1685–1757; c] R. Schmidt, *Photochem. Photobiol.* **2006**, *82*, 1161–1177; d) P. R. Ogilby, *Chem. Soc. Rev.* **2010**, *39*, 3181–3209.

$^1O_2$ is the main reactive species in PDT and, as a result of its electron configuration instability and therefore short lifetime, it reacts only with substrates in close proximity to its site of generation. Furthermore, its lifetime depends on the solvent in which it is generated. In organic solvents it is estimated to be 10-100 µs, while in water it is about 3-4 µs, and under physiological conditions it is only around 100-250 ns. As a consequence, the diffusion range of $^1O_2$ is predicted to be around 45 nm,[24] making it possible to use PDT as a highly selective form of local treatment.

Light source

The first light sources used in PDT were conventional non-coherent lamps where the output was defined by the use of filters.[25] However, these lamps generated significant heat, and calculating the exact light dose was difficult.

Nowadays, a wide range of coherent and non-coherent light sources can be used. Coherent light sources such as lasers are the most common light sources used in PDT, as they produce monochromatic light of a known wavelength and the light dosimetry is easy to calculate.[26] Furthermore, the light can be passed down an optical fiber for localized treatments. Laser sources include dye lasers pumped by argon, or metal vapour lasers and frequency-doubled neodymium-doped-yttrium aluminium garnet lasers (Nd: YAG). The non-laser sources include tungsten filament, xenon arc, metal halide, and fluorescent lamps. New exciting developments such as light emitting diodes (LEDs) and femtosecond lasers are also being used.[27]

No single light source is ideal for all PDT applications, even if the same PS is used. The choice of light source should not only be based on PS absorption, but should also take into consideration the specific characteristics of the disease being treated such as the location, the size of the treated area, the accessibility, and local tissue characteristics. Endoscopic guided and interstitial PDT, for example, require the use of lasers, preferably of the exact wavelength of the absorption maximum of the PS (Figure 8a). For topical PDT in dermatology on the other hand, the most important factor is that the total light dose should be administered in a homogeneous fashion over the total treatment area. This favours the use of LED-arrays for larger areas, or lasers with a flat profile fiber applicator for smaller areas (Figure 8b).[11]

---

[24] E. Skovsen, J. W. Snyder, J. D. C. Lambert, P. R. Ogilby, *J. Phys. Chem. B* **2005**, *109*, 8570–8573.
[25] C. Whitehurst, J. D. Humphries, J. V. Moore, *Lasers Med. Sci.* **1995**, *10*, 121–126.
[26] R. Ackroyd, C. Kelty, N. Brown, M. Reed, *Photochem. Photobiol.* **2001**, *74*, 656–669.
[27] L. Brancaleon, H. Moseley, *Lasers Med. Sci.* **2014**, *17*, 173–186.

Figure 8. a) Interstitial PDT with the use of an optical fiber laser light source.[28] b) Topical PDT with the use of a LED light source.[29]

As mentioned in the previous paragraph, the choice of the light source should take into consideration the tissue characteristics of the zone that needs to be treated. The biological media is inhomogeneous and causes light scattering and reflection, which both limit effective tissue penetration.[30] Depending on the treatment area, endogenous absorption by tissue components such as nucleic acids, hemoglobin and melanin can also cause a drastic decrease of intensity and penetration depth of the light beam. Since both the absorption and the scattering of light by tissue increase as the wavelength decreases, light penetration is very low at 500 nm. However, as can be seen in Figure 9, it almost doubles from 550 nm to 600 nm and doubles again in going to 750 nm.[30b]

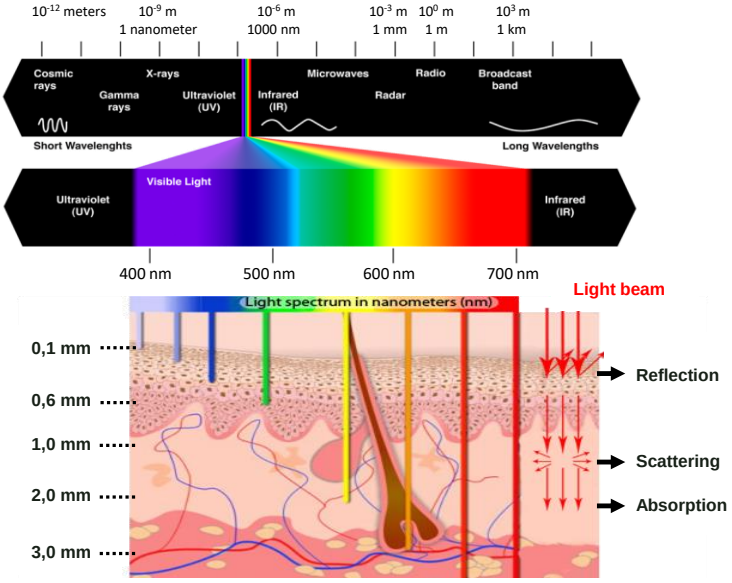

Figure 9. Light penetration and propagation through biological tissues.

---

28 J. Crawford, "Photodynamic Therapy: The use of fiber-optic probes," can be found under https://visualsonline.cancer.gov/details.cfm?imageid=2267, **1987**.

29 "Topical PDT is administered using an Aktilite 128 LED source (Photocure ASA/Galderma)," can be found under http://www.bioopticsworld.com/articles/print/volume-3/issue6/features/dermatology-photodynamic-therapy-the-benefits-of-topical-photodynamic-therapy-in-dermatology.html, **2010**.

30 a] A. Juarranz, P. Jaén, F. Sanz-Rodríguez, J. Cuevas, S. González, *Clin. Transl. Oncol.* **2008**, *10*, 148–154; b) M. Ethirajan, Y. Chen, P. Joshi, R. K. Pandey, *Chem. Soc. Rev.* **2010**, *40*, 340–362.

Although the penetration depth of light increases with increasing wavelength, wavelengths higher than 850-900 nm are not desirable because at those wavelengths the light no longer has sufficient energy to initiate a photodynamic reaction and convert tissue oxygen into $^1O_2$ and other reactive oxygen species (ROS).[31] This, in combination with the fact that hemoglobin and water in tissue absorb light over a broad spectral regime, results in an optical therapeutic window for PDT in the range of 650 nm to 900 nm (Figure 10).[32]

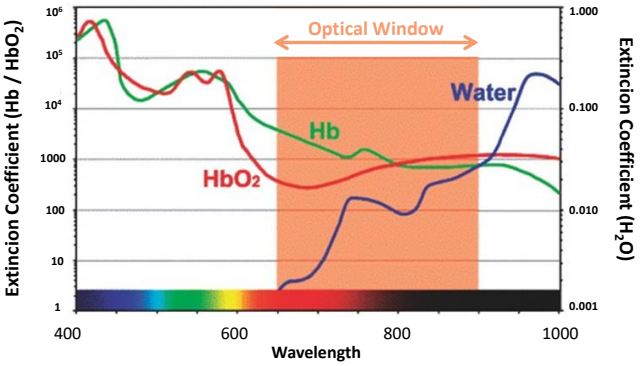

Figure 10. Hemoglobin and water in tissue absorb light over a broad spectral regime, creating an optical window in the near-infrared (NIR) region, between 650 and 900 nm, which represents an optimal trade-off between image resolution and tissue penetration for *in vivo* imaging and PDT.[32b]

---

31 A. Juzeniene, K. P. Nielsen, J. Moan, *J. Environ. Pathol. Toxicol. Oncol.* **2006**, *25*, 7–28.

32 a] B. P. Joshi, T. D. Wang, *Cancers* **2010**, *2*, 1251–1287; b) H. Kobayashi, M. Ogawa, R. Alford, P. L. Choyke, Y. Urano, *Chem. Rev.* **2010**, *110*, 2620–2640.

Molecular mechanisms in photodynamic therapy

Despite considerable investigation and debate, the mechanism of PDT is still not fully understood. Many different biological mechanisms of cell destruction (for PDT) or microbial inactivation (for PDI) play a role and influence one another. In the next subchapters, these biological mechanisms and their underlying photophysical mechanisms will be explained in detail.

Photophysical mechanisms

The general "map" for the processes taking place after electronic excitation of a molecule is the so-called Jablonski-scheme,[33] such as the one shown for a PS in Figure 11.

The molecular structure of most PS is typified by conjugated double bonds containing a delocalized system of π-electrons that are spin paired in low energy orbitals. The total spin of the PS is therefore 0, so its ground electronic state is (as for most molecules) a singlet state (S_0). Upon application of light corresponding to the absorption peak of the PS, the electron in the highest occupied molecular orbital (HOMO) of the PS is promoted to the lowest unoccupied molecular orbital (LUMO), exciting the PS to an unstable and short lived singlet excited state S_1 ($^1PS^*$) (process 1 in Figure 11). In this state, several processes may rapidly occur.[34] $^1PS^*$ can return to the S_0 state by emitting the absorbed energy as fluorescence (2) or by internal conversion (thermal decay, 3). Alternatively, and most importantly to the PDT process, the PS can undergo a reversal of the excited electrons spin to give rise to the first triplet excited state T_1 of the PS ($^3PS^*$), a process which is known as intersystem crossing (4). The resulting triplet excited state T_1 is less energetic than the singlet excited state S_1, but has a much longer lifetime (microseconds as opposed to nanoseconds), since transitions from T_1 to S_0 are "spin forbidden". Importantly, the biologically relevant photochemistry is often mediated by this triplet state.[34,35] The energy of $^3PS^*$ can be dissipated by emitting it as phosphorescence (5) returning to the ground state S_0 by changing the spin orientation of the excited electron in the PS triplet state (a relatively slow process). Alternatively, $^3PS^*$ may interact with molecules abundant in its immediate environment. Because of the selection rules that specify that triplet–triplet interactions are spin-allowed while triplet–singlet interactions are spin-forbidden, the PS triplet can react readily with $^3O_2$, which is one of the few molecules that are a triplet in the ground state.

---

33 J. R. Lakowicz, *Principles of Fluorescence Spectroscopy*, Springer US, **2006**.

34 C. S. Foote, *Photochem. Photobiol.* **1991**, *54*, 659.

35 J. P. Celli, B. Q. Spring, I. Rizvi, C. L. Evans, K. S. Samkoe, S. Verma, B. W. Pogue, T. Hasan, *Chem. Rev.* **2010**, *110*, 2795–2838.

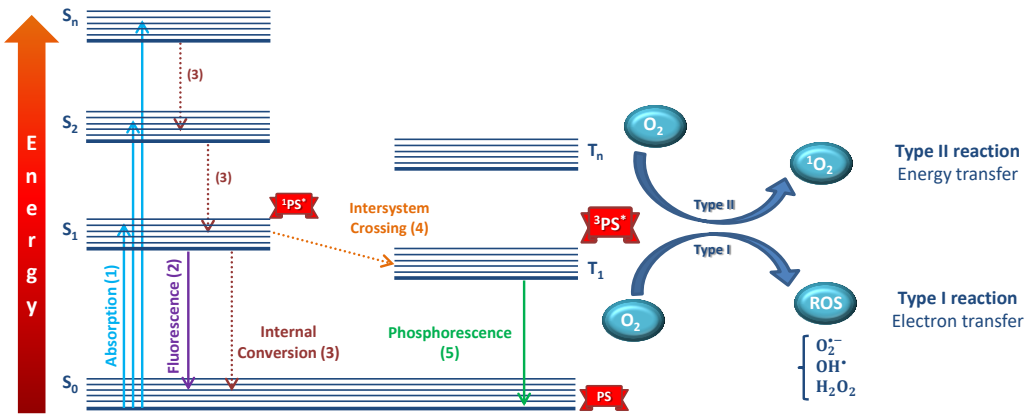

Figure 11. Modified Jablonski diagram outlining the characteristic possible radiative (full line) and non-radiative (dashed line) transitions between electronic states of PS, i.e. photon absorption (1), fluorescence (2), internal conversion (3), intersystem crossing (4) and phosphorescence (5). $^3PS^*$ can participate in Type I and Type II photodynamic reactions, resulting in $^1O_2$ and ROS.

As can already be seen from Figure 11, the excited $^3PS^*$ can react with surrounding molecular $^3O_2$ by participating in two types of photodynamic reactions titled Type I and Type II reactions.[34] Details of both types of photoreactions can be seen in Figure 12. In Type I reactions, the excited PS transfers an electron to a nearby substrate (S), sometimes in concert with proton donation to $^3O_2$, yielding the superoxide anion $O_2^{\bullet-}$. The direction of the electron transfer is controlled by the relative redox potentials of the PS and the substrate. The $O_2^{\bullet-}$ superoxide anion then goes on to form other ROS including the hydroxyl radical ($OH^\bullet$), and hydrogen peroxide (H_2O_2). Alternatively, in type II reactions, $^3PS^*$ undergoes an electronic energy transfer upon collision with $^3O_2$, resulting in the formation of cytotoxic $^1O_2$.

Type I photoreactions

$$^3PS^* + S \rightarrow PS^{\bullet-} + S^{\bullet+}$$
$$^3PS^* + {}^3O_2 \rightarrow PS + O_2^{\bullet-}$$
$$PS^{\bullet-} + {}^3O_2 \rightarrow PS^{\bullet+} + O_2^{\bullet-}$$
$$S^{\bullet+} + {}^3O_2 \rightarrow \text{oxidative damage}$$
$$S^{\bullet} + O_2^{\bullet-} \rightarrow \text{oxidative damage}$$

Type II photoreactions

$$^3PS^* + {}^3O_2 \rightarrow PS + {}^1O_2$$
$$^1O_2 + S \rightarrow \text{oxidative damage}$$

Figure 12. Overview of Type I and Type II photoreactions during PDT, which result in oxidative damage of biological targets.

Both Type I and Type II mechanisms cause oxidative damage within the target tissues which lead to cell death and tumor destruction in case of PDT and microbial inactivation in case of PDI. However, it is generally accepted that the generation of $^1O_2$ from Type II mechanism predominates in both treatment modalities.

Biological mechanisms

The ROS formed through the Type I processes have a range of different reactivities.[36] $^{\bullet}OH$, arguably the most reactive of the three ROS formed, is a strong electrophile that is able to chemically attack a wide range of biomolecules such as nuclear DNA, mitochondrial DNA, proteins and membrane lipids.[37] H_2O_2 is less reactive than $^{\bullet}OH$, and $O_2^{\bullet-}$ is the least reactive of all. Nonetheless, $O_2^{\bullet-}$ may be converted into H_2O_2 and O_2 by superoxide dismutase. H_2O_2 is only considered truly reactive when it reacts with ferrous iron in what is known as the Fenton reaction:

$$H_2O_2 + Fe^{2+} \rightarrow OH^- + {}^{\bullet}OH + Fe^{3+}.$$

This reaction results in homolytic fission of the oxygen-oxygen bond in H_2O_2, to yield a hydroxide ion and $^{\bullet}OH$ *via* the oxidation of ferrous iron to ferric iron.[38] Importantly, their exist various ways of deactivation for these ROS. For example, H_2O_2 can be removed through catalase, forming water and oxygen gas. $^{\bullet}OH$, just like $^1O_2$, cannot be broken down by an enzymatic reaction, but may be quenched by antioxidants, including antioxidant peptides (e.g. glutathione) or by antioxidant vitamins (e.g. ascorbic acid).[39]

Because $^1O_2$ is not a radical, it reacts with biological molecules through quite different mechanisms, making the Type II pathway responsible for different macromolecular reaction pathways. The oxidative attack is of electrophilic nature, hence (as can be seen in Figure 13) it is specifically directed to groups with high electron densities such as:

(i) double bonds in unsaturated lipids (e.g. oleic, linoleic and arachidonic acids)

(ii) double bounds in steroids (e.g. cholesterol)

(iii) sulphur atoms in amino acids (e.g. methionine, cysteine)

(iv) aromatic or heterocyclic groups in amino acids (e.g. tryptophan, tyrosine, histidine)

(v) aromatic or heterocyclic groups in pyrimidine and purine bases of DNA and RNA (e.g. guanosine).

---

36 M. Ochsner, *J. Photochem. Photobiol. B* **1997**, *39*, 1–18.

37 S. K. Borra, J. Mahendra, P. Gurumurthy, Jayamathi, S. S. Iqbal, L. Mahendra, *J. Clin. Diagn. Res.* **2014**, *8*, CC01–CC05.

38 M. Valko, H. Morris, M. T. D. Cronin, *Curr. Med. Chem.* **2005**, *12*, 1161–1208.

39 T. Dai, B. B. Fuchs, J. J. Coleman, R. A. Prates, C. Astrakas, T. G. St. Denis, M. S. Ribeiro, E. Mylonakis, M. R. Hamblin, G. P. Tegos, *Front. Microbiol.* **2012**, *3*, 120.

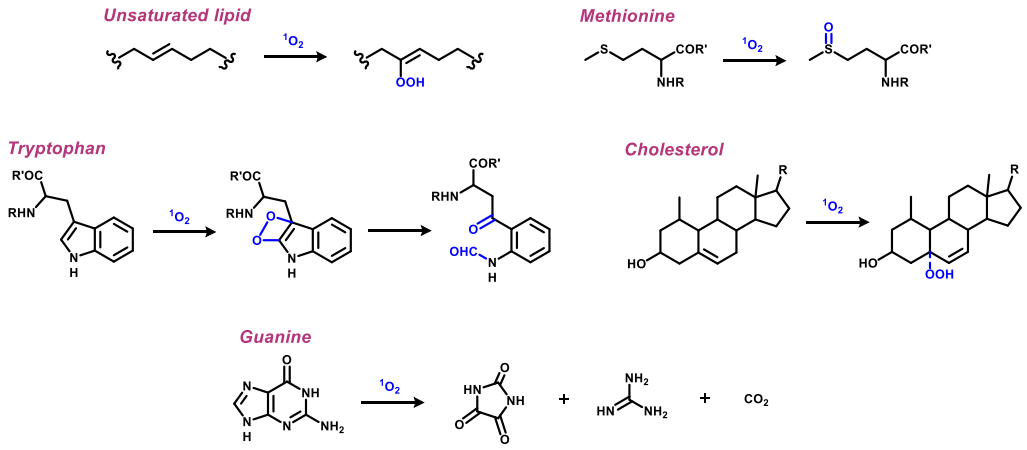

Figure 13. Typical reactions of $^1O_2$ with selected biomolecules.[40]

Specific mechanisms of tumor destruction in PDT

It is now known that there are three main biological mechanisms involved in the tumor shrinkage and disappearance followed by photodynamic treatment,[41] being (i) direct tumor cell destruction, (ii) vascular destruction, and (iii) elicitation of an antitumor immune response. These three mechanisms can influence each other and their combination is required for achieving long-term tumor control. In the following subsections, these three mechanisms are briefly discussed.

(i) Direct damage and cell death

In this case, the ROS generated during PDT can kill tumor cells directly by apoptosis and/or necrosis.[42] Necrosis is a violent and quick form of degeneration that results from extensive cellular damage. It is characterized by the destruction of organelles and disruption of the plasma membrane leading to the release of intracellular contents into the extracellular environment. In contrast, apoptosis is a mechanism of genetically programmed death of old cells in both physiological and pathological conditions of a living organism. It is characterized by a common sequence of morphological and biochemical

---

40 a] A. G. Leach, K. N. Houk, *Chem. Commun.* **2002**, 1243–1255; b) M.-F. Zuluaga, N. Lange, *Curr. Med. Chem.* **2008**, *15*, 1655–1673; c] B. Lipinski, *Oxid. Med. Cell. Longev.* **2011**, 809696; d) J. T. F. Lau, *Towards Dual and Targeted Cancer Therapy with Novel Phthalocyanine-Based Photosensitizers*, Springer International Publishing, Switzerland, **2013**.

41 a] T. J. Dougherty, C. J. Gomer, B. W. Henderson, G. Jori, D. Kessel, M. Korbelik, J. Moan, Q. Peng, *J. Natl. Cancer Inst.* **1998**, *90*, 889–905; b) A. P. Castano, T. N. Demidova, M. R. Hamblin, *Photodiagnosis Photodyn. Ther.* **2005**, *2*, 91–106.

42 a] I. J. Macdonald, T. J. Dougherty, *J. Porphyr. Phthalocyanines* **2001**, *5*, 105–129; b) P. Agostinis, E. Buytaert, H. Breyssens, N. Hendrickx, *Photochem. Photobiol. Sci.* **2004**, *3*, 721–729; c] A. P. Castano, T. N. Demidova, M. R. Hamblin, *Photodiagnosis Photodyn. Ther.* **2005**, *2*, 1–23; d) D. Kessel, *J. Porphyr. Phthalocyanines* **2016**, *20*, 302–306.

changes including condensation of chromatin and formation of apoptotic bodies. The crucial factors in determining the type of cell death are the cell type, the subcellular localization of the PS and the light dose applied to activate it locally. In general, it is believed that lower dose PDT leads to more apoptosis, while higher doses lead to proportionally more necrosis.[43]

(ii) Vascular damage

PDT also damages the tumor-associated vasculature, leading to tissue deprivation of oxygen and nutrients.[44] Since the viability of tumor cells depends on the amount of nutrients supplied by surrounding blood vessels, this vascular damage can lead to consequent tumor infarction and can contribute to long-term tumor control.[45] Over the last two decades, there have been various reports of PDT-induced damage to tumor microvasculature leading to persistent post-PDT tumor hypoxia/anoxia and nutrient deficiency and finally to complete tumor disappearance.[35,42b,46] The mechanisms underlying the vascular occlusion differ greatly with different PS, but include vessel constriction, macromolecular leakage, leukocyte adhesion, blood flow stasis, and thrombus formation.[47] Importantly, to obtain maximal effects, PDT should also be applied to the healthy vasculature surrounding the tumor zone, as studies have shown the lack of tumor curability when only irradiating the malignant tumor zone.[48] A crucial parameter for controlling the effect of vascular damage is the drug-light interval, as this can determine whether the drug is mostly free flowing in the blood, binding to the blood vessel walls or leaking out into the tumor interstitium, resulting in very different outcomes after PDT treatment.[49]

(iii) Inflammatory and immune response

Photodynamically induced changes in the plasma membrane and the membrane of cell organelles can trigger an immune response against tumor cells by activating multiple

---

43 K. Plaetzer, T. Kiesslich, B. Krammer, P. Hammer, *Photochem. Photobiol. Sci.* **2002**, *1*, 172–177.

44 a] W. Wang, L. T. Moriyama, V. S. Bagnato, *Laser Phys. Lett.* **2013**, *10*, 23001; b) A. Kawczyk-Krupka, A. M. Bugaj, M. Potempa, K. Wasilewska, W. Latos, A. Sieroń, *Photodiagnosis Photodyn. Ther.* **2015**, *12*, 161–175.

45 J. Usuda, T. Okunaka, K. Furukawa, T. Tsuchida, Y. Kuroiwa, Y. Ohe, N. Saijo, K. Nishio, C. Konaka, H. Kato, *Int. J. Cancer* **2001**, *93*, 475–480.

46 a] R. Bonneau, R. Pottier, O. Bagno, J. Joussot-Dubien, *Photochem. Photobiol.* **1975**, *21*, 159–163; b) B. W. Henderson, V. H. Fingar, *Cancer Res.* **1987**, *47*, 3110–3114.

47 V. H. Fingar, K. A. Siegel, T. J. Wieman, K. W. Doak, *Photochem. Photobiol.* **1993**, *58*, 393–399.

48 V. H. Fingar, T. J. Wieman, K. W. Doak, *Cancer Res.* **1990**, *50*, 2599–2603.

49 a] A. Ferrario, D. Kessel, C. J. Gomer, *Cancer Res.* **1992**, *52*, 2890–2893; b) K. Kurohane, A. Tominaga, K. Sato, J. R. North, Y. Namba, N. Oku, *Cancer Lett.* **2001**, *167*, 49–56; c] B. Chen, T. Roskams, P. A. M. de Witte, *Photochem. Photobiol.* **2002**, *76*, 509–513; d) B. Chen, B. W. Pogue, I. A. Goodwin, J. A. O'Hara, C. M. Wilmot, J. E. Hutchins, P. J. Hoopes, T. Hasan, *Radiat. Res.* **2003**, *160*, 452–459; e] P. Cramers, M. Ruevekamp, H. Oppelaar, O. Dalesio, P. Baas, F. A. Stewart, *Br. J. Cancer* **2003**, *88*, 283–290.

signal transduction pathways.[50] These include a variety of protein kinase signalling cascades, which elicit an inflammatory or immune response leading to cell death.[51] In fact, studies in the late 1980s and early 1990s have reported the infiltration of lymphocytes, leukocytes, and macrophages into PDT-treated tissue, which indicates an activation of the immune response.[52] One of the key experiments demonstrating this effect was carried out by Korbelik *et al*., who grew the same tumor in immunocompetent and immunodeficient mice of the same background, with PDT leading to tumor ablation in both of them but only obtaining a long-term curing in the immunocompetent mice.[53] Furthermore, the differences in the nature and intensity of the inflammatory response between normal and cancerous tissues may contribute to the selectivity of PDT-induced damage.[41,54]

Specific mechanisms of microbial inactivation in PDI

Microbial cells display a truly large variety of size, sub-cellular architecture, and biochemical composition. Nevertheless, the photosensitized processes in most microorganisms, ranging from fungi, viruses and parasitic protozoa to Gram-positive and Gram-negative bacteria, occur in a similar to almost identical way.[3]

(i) Cytoplasmic membrane

The first and most frequent target of microbial cell inactivation by PDI is the cytoplasmic membrane.[55] Various studies have demonstrated that the photoinduced damage progresses from the outer to the inner leaflet of the cytoplasmic membrane and that it takes place *via* various simultaneous mechanisms.[56] The generation of ROS and $^1O_2$ leads to the inactivation of several co-factors and enzymes that are associated with the cytoplasmic membrane, such as NADH, succinic dehydrogenase and lactic dehydrogenase. Meanwhile several outer membrane and cytoplasmic membrane proteins also undergo extensive crosslinking causing a loss of membrane barrier properties and resulting in the

---

50 M. Wachowska, A. Muchowicz, U. Demkow, *Cent.-Eur. J. Immunol.* **2015**, *40*, 481–485.

51 a] T. J. Dougherty, C. J. Gomer, B. W. Henderson, G. Jori, D. Kessel, M. Korbelik, J. Moan, Q. Peng, *J. Natl. Cancer Inst.* **1998**, *90*, 889–905; b) G. Canti, A. D. Simone, M. Korbelik, *Photochem. Photobiol. Sci.* **2002**, *1*, 79–80.

52 a] B. P. Shumaker, F. W. Hetzel, *Photochem. Photobiol.* **1987**, *46*, 899–901; b) B. W. Henderson, T. J. Dougherty, *Photochem. Photobiol.* **1992**, *55*, 145–157.

53 M. Korbelik, G. Krosl, J. Krosl, G. J. Dougherty, *Cancer Res.* **1996**, *56*, 5647–5652.

54 D. E. J. G. J. Dolmans, A. Kadambi, J. S. Hill, C. A. Waters, B. C. Robinson, J. P. Walker, D. Fukumura, R. K. Jain, *Cancer Res.* **2002**, *62*, 2151–2156.

55 M. Bhatti, S. P. Nair, A. J. Macrobert, B. Henderson, P. Shepherd, J. Cridland, M. Wilson, *Curr. Microbiol.* **2001**, *43*, 96–99.

56 S. A. G. Lambrechts, M. C. G. Aalders, J. Van Marle, *Antimicrob. Agents Chemother.* **2005**, *49*, 2026–2034.

collapse of the K^+ and ionic balance.[57] This consequently leads to a massive reduction of the transport capacity for a variety of solutes, which results in a shortage of essential substrates for anabolic and catabolic pathways.[58] The inhibition of these metabolic processes leads, in turn, to the inhibition of glucose transport and DNA synthesis (and therefore also RNA and protein synthesis).

(ii) Intracellular damage

Although the PS is initially partitioned in the cytoplasmic membrane, some reports have shown that, as irradiation progresses, the PS gradually diffuses to inner cellular districts.[59] It is thus reasonable to expect that a variety of non-membranous sites, including DNA, are involved in the photooxidative reactions at later stages of the overall photoprocess. However, it has been pointed out by several research groups that such additional damage is not directly correlated with cell death, which is already quite extensive when the cytoplasmic membrane has been heavily disrupted.[60]

The overall process is obviously of multi-target nature, making it extremely difficult for microbial cells to develop resistance to the photodynamic treatment. Taking into account the current antibiotic resistance crisis,[61] this represents one of the major advantages of antimicrobial PDT.

---

57 a] M. Paardekooper, P. J. A. Van den Broek, A. W. De Bruijne, J. G. R. Elferink, T. M. A. R. Dubbelman, J. Van Steveninck, *Biochim. Biophys. Acta* **1992**, *1108*, 86–90; b) Z. Malik, T. Babushkin, S. Sher, J. Hanania, H. Ladan, Y. Nitzan, S. Salzberg, *Int. J. Biochem.* **1993**, *25*, 1399–1406.

58 M. Salmon-Divon, Y. Nitzan, Z. Malik, *Photochem. Photobiol. Sci.* **2004**, *3*, 423–429.

59 G. Jori, C. Fabris, M. Soncin, S. Ferro, O. Coppellotti, D. Dei, L. Fantetti, G. Chiti, G. Roncucci, *Lasers Surg. Med.* **2006**, *38*, 468–481.

60 a] Z. Malik, H. Ladan, Y. Nitzan, *J. Photochem. Photobiol. B* **1992**, *14*, 262–266; b) M. Wainwright, *J. Antimicrob. Chemother.* **1998**, *42*, 13–28; c] M. R. Hamblin, T. Hasan, *Photochem. Photobiol. Sci.* **2004**, *3*, 436–450.

61 J. O'Neill, *Tackling Drug-Resistant Infections Globally: A Final Report and Recommendations*, **2016**.

(Sub)Phthalocyanines as photosensitizers in PDT

Out of all the PS employed in different PDT applications, Pcs (Figure 14, top) are, together with Pors, the current golden standard in PDT, among the most studied ones. They present several advantages such as their absorption at higher wavelengths and higher molar extinction coefficients as compared to Pors. Structurally related to Pcs, SubPcs (Figure 14, bottom) also show these favourable characteristics. However, their use as PS remains little investigated. On these bases, in the next subsections we will introduce the chemistry of Pcs and SubPcs, in general, and their utility in the field PDT, in particular.

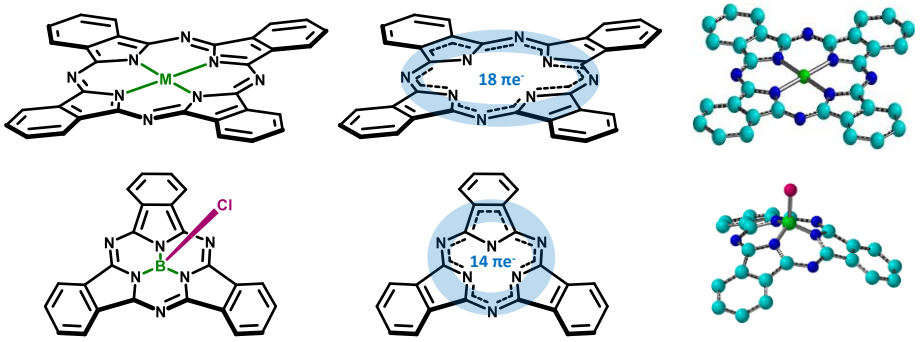

Figure 14. Molecular structure, electron delocalization and 3D-shape of Pcs (top) versus SubPcs (bottom).

Phthalocyanines

Phthalocyanines are planar 18 π-electron aromatic macroheterocycles consisting of four isoindole subunits linked together through aza bridges, with or without a metal atom in the central cavity.[62] The delocalization of these 18 π-electrons generates their typical absorption spectra with two major intense bands: the Q- and B- or Soret band, both due to π-π* transitions. The Q-band (S_0 to S_1 transition), between 620-720 nm, is generally sharp and intense, and gives to the characteristic blue/green color of these molecules. The Soret band (S_0 to S_2 transition), around 350 nm, is usually broad and low in intensity. Metallophthalocyanines (MPcs) generally show one single Q-band, while in the case of free base Pcs (H_2Pc) a splitting of the Q-band can be observed due to their doubly

[62] a] C. C. Leznoff, A. B. P. Lever, *Wiley: Phthalocyanines, Properties and Applications, Volume 4 -*, VHC Publishers (LSK) Ltd., Cambridge, **1996**; b) N. B. McKeown, *Phthalocyanine Materials. Synthesis, Structure and Function*, Cambridge University Press, **1998**; c] C. G. Claessens, U. Hahn, T. Torres, *Chem. Rec.* **2008**, *8*, 75–97; d) G. de la Torre, G. Bottari, U. Hahn, T. Torres, in *Funct. Phthalocyanine Mol. Mater.*, **2010**, pp. 1–44; e] F. Dumoulin, M. Durmuş, V. Ahsen, T. Nyokong, *Coord. Chem. Rev.* **2010**, *254*, 2792–2847; f) J. Mack, N. Kobayashi, *Chem. Rev.* **2011**, *111*, 281–321; g] K. M. Kadish, K. M. Smith, R. Guilard, *Handbook of Porphyrin Science*, World Scientific, Singapore, **2013**.

degenerated LUMO as a consequence of their lower symmetry (D_2h) as compared to that of MPcs (D_4h).

As can be seen in Figure 6, Pcs are structurally very similar to Pors. However, due to their four additional peripheral benzene rings, their absorption maximum or Q-band lies at longer wavelengths, usually in the red visible region, falling inside the optical therapeutic window and allowing a deeper light penetration (Figure 15). Furthermore, the Pc Q-band has a significantly higher molar extinction coefficient, about two orders of magnitude, compared to Pors ($\varepsilon_{Pc} \sim 10^5\ M^{-1}\ cm^{-1}$, $\varepsilon_{HpD} \sim 10^3\ M^{-1}\ cm^{-1}$).

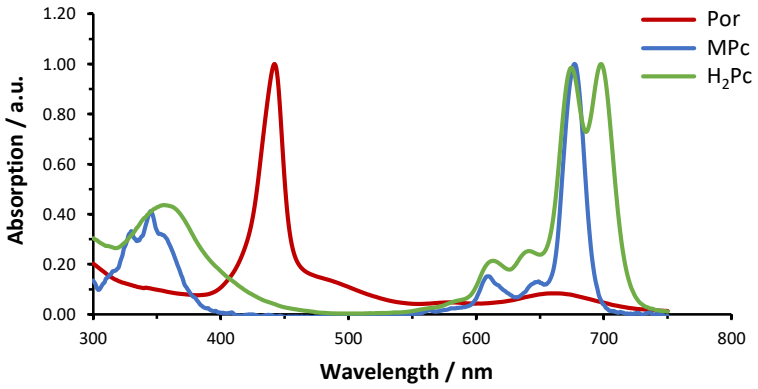

Figure 15. Typical normalized UV-Vis absorption spectra of Por, metal-free Pcs (H_2Pc) and Pcs containing a metal ion in their central cavity (MPc) in DMF.

Because of these molecular characteristics, Pcs possess very desirable photophysical and photochemical properties for their use in PDT. Furthermore, these properties can in many cases easily be tuned through rational modification of the peripheral and/or axial substituents of the Pcs and by varying the central metal atom. More than 70 different atoms can be included in their central cavity, influencing their fluorescence, phosphorescence and excited triplet state generation.[63] Pcs containing a closed d shell and diamagnetic metal center, such as Zn^{2+}, Al^{3+} and Ga^{3+}, generally have higher triplet state quantum yields (ϕ_t >0.4) and longer lifetimes (τ_T > 200 µs), as compared to Pcs containing transition metal ions (τ_T in the nanosecond range).[62,63,64] Apart from this, the heavy atom effects promotes the intersystem crossing from the singlet to the triplet excited state as the central atom mass increases.[65]

---

63 a] A. Morandeira, I. López-Duarte, M. V. Martínez-Díaz, B. O'Regan, C. Shuttle, N. A. Haji-Zainulabidin, T. Torres, E. Palomares, J. R. Durrant, *J. Am. Chem. Soc.* **2007**, *129*, 9250–9251; b) Y. Rio, M. S. Rodríguez-Morgade, T. Torres, *Org. Biomol. Chem.* **2008**, *6*, 1877–1894; c] A. Listorti, I. López-Duarte, M. V. Martínez-Díaz, T. Torres, T. DosSantos, P. R. F. Barnes, J. R. Durrant, *Energy Environ. Sci.* **2010**, *3*, 1573–1579; d) X.-F. Zhang, X. Shao, H. Tian, X. Sun, K. Han, *Dyes Pigments* **2013**, *99*, 480–488.

64 J. R. Darwent, P. Douglas, A. Harriman, G. Porter, M.-C. Richoux, *Coord. Chem. Rev.* **1982**, *44*, 83–126.

65 a] J. W. Perry, D. Alvarez, I. Choong, K. Mansour, S. R. Marder, K. J. Perry, *Opt. Lett.* **1994**, *19*, 625; b) A. V. Vannikov, A. D. Grishina, Y. G. Gorbunova, V. I. Zolotarevskii, T. V. Krivenko, A. S. Laryushkin, L.

Synthesis and versatility of Pcs

Pcs were first synthesized by Braun and Tchernlac in 1907.[66] They are generally synthesized by cyclotetramerization of the appropriate precursors, usually phthalonitriles or 1,3-diiminoisoindolines (Scheme 1).[62g] MPcs are synthesized, either starting from phthalonitriles or a 1,3- diiminoisoindolines, in the presence of a metallic salt that acts as a template, or by later metalation of a H_2Pc. H_2Pc, on the other hand, can be synthesized starting from 1,3-diiminoisoindolines, by heating a phthalonitrile in the presence of DBU or hydroquinone, or by the formation of a lithium Pc followed by subsequent demetallation by treatment with a mineral acid. More recently, various new methods to prepare Pcs have been described, such as the treatment of phthalonitriles with metal salts and hexamethyldisilazane in DMF,[67] the double-addition of oximes to phthalonitriles[68] and microwave-assisted synthesis.[69]

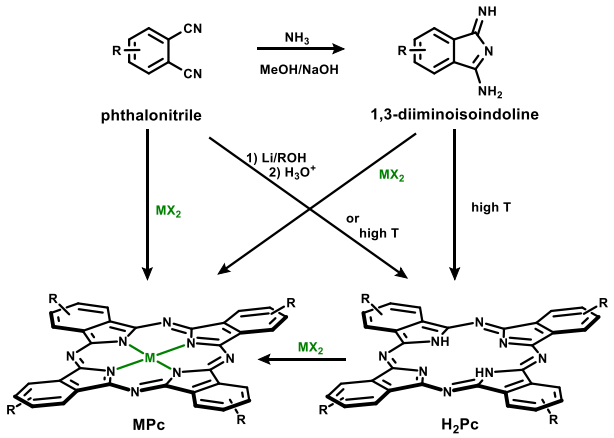

Scheme 1. General schematic representation of the synthesis of H_2Pc and MPcs.

The mechanism at the basis of the formation of Pcs is still not completely understood, nevertheless there exist various mechanistic hypotheses, all bearing some common features that are generally accepted.[70] The macrocyclization in the presence of a

A. Lapkina, V. V. Savel'ev, A. Y. Tsivadze, *High Energy Chem.* **2014**, *49*, 36–43; c] M. E. Alberto, B. C. D. Simone, G. Mazzone, E. Sicilia, N. Russo, *Phys. Chem. Chem. Phys.* **2015**, *17*, 23595–23601.

66 A. Braun, J. Tcherniac, *Ann Ber* **1907**, *40*, 2709–2714.

67 a] H. Uchida, H. Tanaka, H. Yoshiyama, P. Y. Reddy, S. Nakamura, T. Toru, *Synlett* **2002**, 1649–1652; b) H. Uchida, M. Mitsui, P. Y. Reddy, S. Nakamura, T. Toru, *ARKIVOC* **2005**, *11*, 17–23.

68 M. N. Kopylovich, V. Y. Kukushkin, M. Haukka, K. V. Luzyanin, A. J. L. Pombeiro, *J. Am. Chem. Soc.* **2004**, *126*, 15040–15041.

69 a] A. Burczyk, A. Loupy, D. Bogdal, A. Petit, *Tetrahedron* **2005**, *61*, 179–188; b) İ. Acar, H. Kantekin, Z. Bıyıklıoğlu, *J. Organomet. Chem.* **2010**, *695*, 151–155; c] C. Kantar, H. Akal, B. Kaya, F. Islamoğlu, M. Türk, S. Şaşmaz, *J. Organomet. Chem.* **2015**, *783*, 28–39.

70 a] V. W. Day, T. J. Marks, W. A. Wachter, *J. Am. Chem. Soc.* **1975**, *97*, 4519–4527; b) D. H. Bush, N. Stephenson, *Coord. Chem. Rev.* **1990**, *100*, 119–154; c] C. Rager, G. Schmid, M. Hanack, *Chem. Eur. J.* **1999**, *5*, 280–288; d) C. C. Leznoff, A. M. D'Ascanio, S. Z. Yildiz, *J. Porphyr. Phthalocyanines* **2000**, *4*, 103–111.

nucleophile sodium or lithium alkoxide usually starts with the formation of the corresponding salt of 1-imido-3-alkoxyindoline (Scheme 2 – step 1),[71] followed by the nucleophilic attack of this intermediate to the cyano group of another phthalonitrile molecule (step 2). The resulting dimer can either react with a third phthalonitrile molecule in the same way, to form a trimer (step 3a) or undergo self-condensation with another dimer (step 3b), both mediated by the metallic cation as a template.

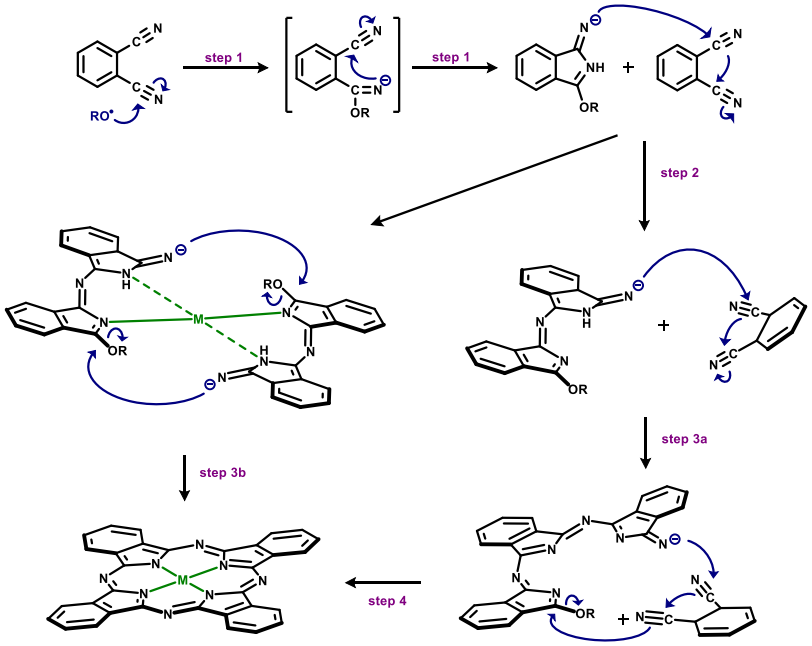

Scheme 2. Hypothetical mechanism for the synthesis of MPcs by cyclotetramerization of phthalonitrile in the presence of a metal salt.

When using more than one different phthalonitrile and/or 1,3-diiminoisondoline (A and B) in this synthesis, the library of possible Pcs is amplified even more, and differently substituted Pcs (Figure 16) are obtained in a statistical manner.[62f,72] The selective synthesis of these unsymmetrically substituted Pcs is also possible,[73] however it will not be detailed over here as it lies outside the scope of the present thesis.

---

71 S. W. Oliver, T. D. Smith, *J. Chem. Soc. Perkin Trans. 2* **1987**, 1579–1582.

72 a] N. Kobayashi, Y. Kobayashi, T. Osa, *J. Am. Chem. Soc.* **1993**, *115*, 10994–10995; b) T. Torres, *J. Porphyr. Phthalocyanines* **2000**, *4*, 325–330; c] G. de la Torre, T. Torres, *J. Porphyr. Phthalocyanines* **2002**, *6*, 274–284.

73 a] C. C. Leznoff, T. W. Hall, *Tetrahedron Lett.* **1982**, *23*, 3023–3026; b) J. G. Young, W. Onyebuagu, *J. Org. Chem.* **1990**, *55*, 2155–2159; c] N. Kobayashi, T. Ashida, T. Osa, *Chem. Lett.* **1992**, 2031–2034; d) A. Sastre, T. Torres, M. Hanack, *Tetrahedron Lett.* **1995**, *36*, 8501–8504; e] A. Weitemeyer, H. Kliesch, D. Woehrle, *J. Org. Chem.* **1995**, *60*, 4900–4904; f) Á. Sastre, B. del Rey, T. Torres, *J. Org. Chem.* **1996**, *61*, 8591–8597; g] A. Hirth, A. K. Sobbi, D. Wöhrle, *J. Porphyr. Phthalocyanines* **1997**, *1*, 275–279; h) W. M. Sharman, J. E. van Lier, *J. Porphyr. Phthalocyanines* **2005**, *9*, 651–658; i] S. S. Erdem, I. V. Nesterova, S. A. Soper, R. P. Hammer, *J. Org. Chem.* **2008**, *73*, 5003–5007; j) *J. Org. Chem.* **2009**, *74*,

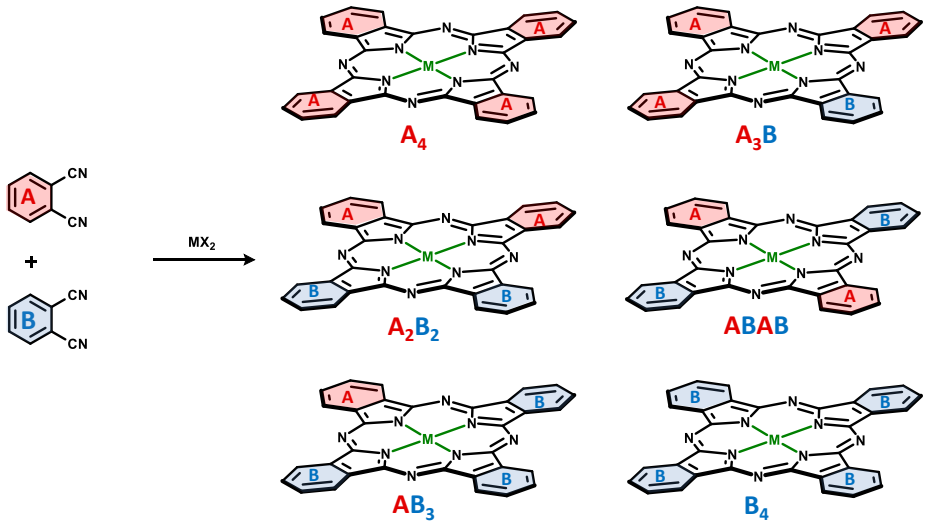

Figure 16. Schematic representation of the set of Pc compounds obtained *via* statistical cyclotetramerization of two differently functionalized phthalonitriles, A and B. The relative percentages of each compound in the mixture will depend on the reactivity of the respective phthalonitriles.

Furthermore, depending on the central atom incorporated in the macrocycle cavity, it is in some cases possible to further amplify the versatility of Pcs by incorporating different functional groups at axial positions of the metal atom. This is the case for ruthenium (RuPc), aluminium (AlPc) and silicon (SiPc) Pcs, among others. For SiPcs and AlPcs (Figure 17a and c) the axial substituents are covalently linked to the central atom, while for RuPcs bearing N-containing ligands (Figure 17b) the bond is supramolecular in nature.

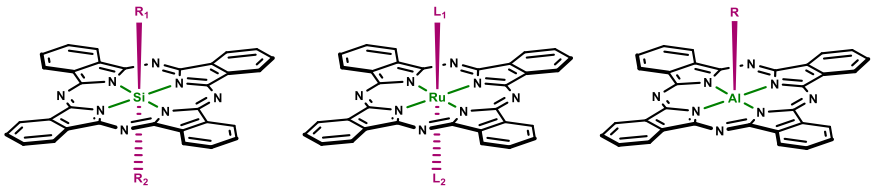

Figure 17. General structure of axially coordinating Pcs: a) SiPc (where R = alkoxy, phenoxy, silyloxy), b) RuPc (where L = N-containing ligands able to coordinate to the central metal or CO), and c) AlPc (where R = alkoxy, phenoxy, silyloxy).

In case the central metal allows the conjugation of two axial ligands, such as for SiPcs and RuPcs, symmetrically and asymmetrically substituted Pcs can be obtained in a statistical manner, as can be seen in Figure 18 for SiPcs.

9280–9286; k] M. Mudyiwa, M. W. Ndinguri, S. A. Soper, R. P. Hammer, *J. Porphyr. Phthalocyanines* **2010**, *14*, 891–903; l) K. N. Porchelvi, S. Meenakshi, K. Pandian, *Adv. Mater. Res.* **2014**, *938*, 40–45; m] L. Zhao, K. Wang, H. Shang, J. Jiang, *Dyes Pigments* **2015**, *120*, 52–56.

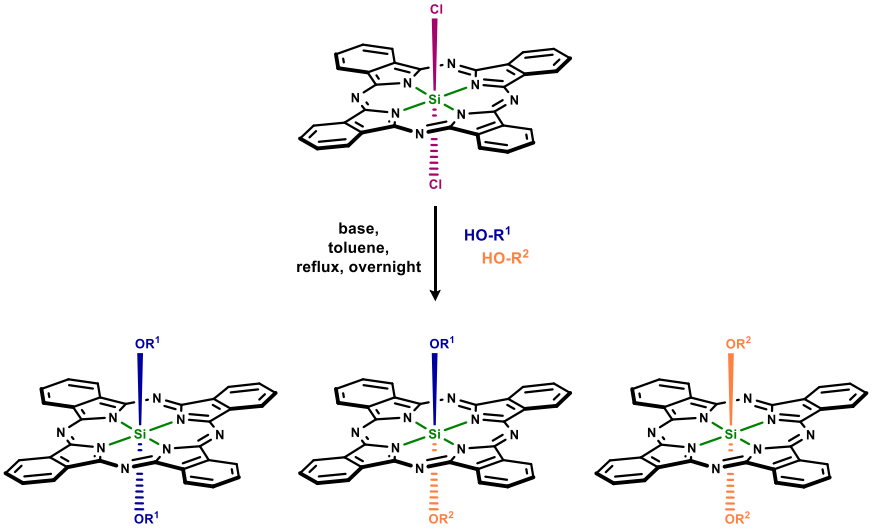

Figure 18. Schematic representation of the set of Pc compounds obtained *via* statistical functionalization of Pcs with a tetravalent central metal atom, such as SiPcs. The relative percentages of each compound will depend on the reactivity of the respective axial substituents.

Silicon: the metalloid of choice

In the present thesis, SiPcs have been chosen as the object of study for various reasons. As most Pcs, they fulfil several of the requirements for ideal PS mentioned in Table 1: i.e. intense absorption inside the range of the therapeutic window, high molar extinction coefficients, high ϕ_t and long lifetimes of their triplet excited state (τ_t). Besides, one of the biggest drawbacks of the use of Pcs in PDT is their tendency to aggregate in aqueous solution, an inherent characteristic caused by the intrinsic planarity of these large aromatic systems. Any kind of aggregation immediately kills the generation of $^1O_2$ and its diffusion to the site of action, making the PS completely useless.[74] Since Si is a tetravalent metalloid, this problem is easily circumvented in SiPcs, since they offer the possibility to incorporate up to two voluminous substituents at the axial positions of the Si atom, preventing any form of aggregation. Furthermore, apart from introducing bulky substituents to avoid aggregation, substituents with desired characteristics could be introduced at the axial positions, further enhancing the interesting properties of these systems. Some examples of substituents that could be introduced are chromophores (e.g. pyrene, …) for imaging applications and theranostics, selective targeting units (e.g. antibodies, peptide sequences, carbohydrates, etc.), or specific ligands enabling activatable $^1O_2$ generation.

---

[74] a] X. Damoiseau, F. Tfibel, M. Hoebeke, M.-P. Fontaine-Aupart, *Photochem. Photobiol.* **2002**, *76*, 480–485; b) X.-F. Zhang, Q. Xi, J. Zhao, *J. Mater. Chem.* **2010**, *20*, 6726–6733; c] M. Nishida, H. Horiuchi, A. Momotake, Y. Nishimura, H. Hiratsuka, T. Arai, *J. Porphyr. Phthalocyanines* **2011**, *15*, 47–53.

Conveniently, SiPcs are easily accessible. They can be synthesized either by tetramerization of the corresponding 1,3-diiminoisoindolines in the presence of $SiCl_4$,[75] or by silylation of the corresponding free-base Pcs with $HSiCl_3$,[76] although this last alternative easily leads to the formation of dimers and oligomers and is therefore seldom used. Notably, silicon phthalocyanine dichloride ($SiPcCl_2$), the most commonly used starting material for derivatization at the axial positions, is commercially available from Sigma Aldrich.[77]

Although a large number of Pcs have been synthesized as PS for PDT applications, only a few have made it to the stage of clinical trials (Figure 19).[78] Pc 4, a SiPc, has been one of the most successful PS out of this series, which greatly stimulated the interest in the design of new SiPcs. The clinical evaluation of Pc 4, which localizes almost exclusively in the mitochondria and causes localized damage upon irradiation, has been assessed in cutaneous and subcutaneous lesions from diverse solid tumor origins.[79,80] A Phase I clinical trial of topically applied Pc 4 for treatment of mycosis fungoides, the most common form of cutaneous T-cell lymphoma has recently been completed, although no final results have been reported yet.[81] However, preliminary findings from this Phase I trial have been promising with no local or systemic toxicities observed.[82]

---

[75] a] K. A. Bello, I. A. Bello, *Dyes Pigments* **1997**, *35*, 261–267; b) N. Sasa, K. Okada, K. Nakamura, S. Okada, *J. Mol. Struct.* **1998**, *446*, 163–178; c] N. Kobayashi, F. Furuya, G.-C. Yug, H. Wakita, M. Yokomizo, N. Ishikawa, *Chem. Eur. J.* **2002**, *8*, 1474–1484.

[76] a] G. Cheng, X. Peng, G. Hao, V. O Kennedy, I. N. Ivanov, K. Knappenberger, T. J. Hill, M. A. J. Rodgers, M. E. Kenney, *J Phys Chem A* **2003**, *107*, 3503–3514; b) N. Kobayashi, M. Yokoyama, A. Muranaka, A. Ceulemans, *Tetrahedron Lett.* **2004**, *45*, 1755–1758; c] J. Ranta, R. Viljanen, H. Lemmetyinen, A. Efimov, *Dyes Pigments* **2009**, *83*, 317–323.

[77] "Silicon phthalocyanine dichloride," can be found under http://www.sigmaaldrich.com/catalog/, **2016**.

[78] a) N. Sekkat, H. van den Bergh, T. Nyokong, N. Lange, *Molecules* **2012**, *17*, 98–144.; b) R. K. Pandey, D. Kessel, T. J. Dougherty, *Handbook of Photodynamic Therapy: Updates on Recent Applications of Porphyrin-Based Compounds*, World Scientific, Singapore, **2016**

[79] N. L. Oleinick, A. R. Antunez, M. E. Clay, B. D. Rihter, M. E. Kenney, *Photochem. Photobiol.* **1993**, *57*, 242–247.

[80] a] E. D. Baron, C. L. Malbasa, D. Santo-Domingo, P. Fu, J. D. Miller, K. K. Hanneman, A. H. Hsia, N. L. Oleinick, V. C. Colussi, K. D. Cooper, *Lasers Surg. Med.* **2010**, *42*, 728–735; b) M. Lam, Y. Lee, M. Deng, A. H. Hsia, K. A. Morrissey, C. Yan, K. Azzizudin, N. L. Oleinick, T. S. McCormick, K. D. Cooper, E. D. Baron, M. Lam, Y. Lee, M. Deng, A. H. Hsia, K. A. Morrissey, C. Yan, K. Azzizudin, N. L. Oleinick, T. S. McCormick, K. D. Cooper, E. D. Baron, *Adv. Hematol.* **2010**, *2010*, 896161; c] T. J. Kinsella, E. D. Baron, V. C. Colussi, K. D. Cooper, C. L. Hoppel, S. T. Ingalls, M. E. Kenney, X. Li, N. L. Oleinick, S. R. Stevens, S. C. Remick, *Front. Oncol.* **2011**, *1*, 14; d) M. Lam, M. L. Dimaano, P. Oyetakin-White, M. A. Retuerto, J. Chandra, P. K. Mukherjee, M. A. Ghannoum, K. D. Cooper, E. D. Baron, *Antimicrob. Agents Chemother.* **2014**, *58*, 3029–3034.

[81] "Photodynamic Therapy Using Silicon Phthalocyanine 4 in Treating Patients With Actinic Keratosis, Bowen's Disease, Skin Cancer, or Stage I or Stage II Mycosis Fungoides," can be found under https://clinicaltrials.gov/ct2/show/NCT00103246, **2016**.

[82] D. C. Soler, J. Ohtola, H. Sugiyama, M. E. Rodriguez, L. Han, N. L. Oleinick, M. Lam, E. D. Baron, K. D. Cooper, T. S. McCormick, *Photochem. Photobiol. Sci.* **2016**, *15*, 822–831.

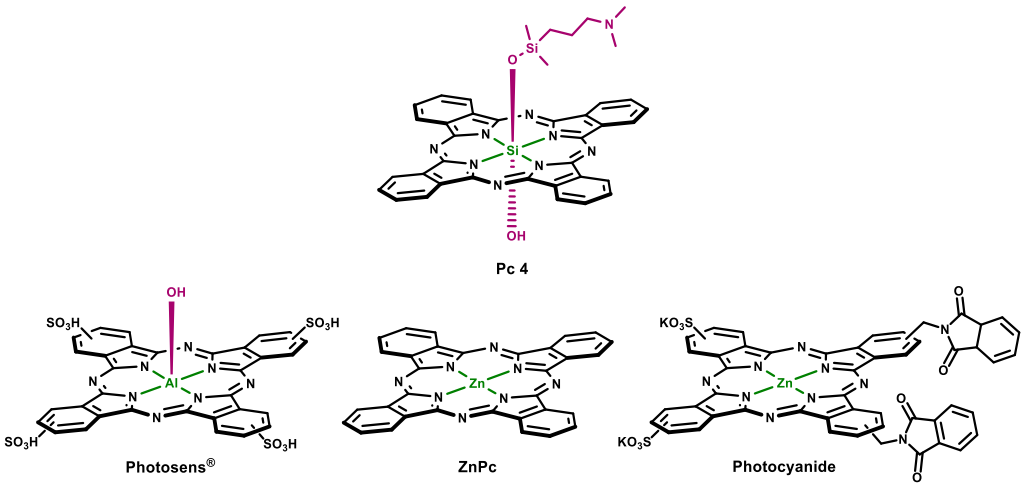

Figure 19. Chemical structures of four Pc-based PS, which are currently in clinical use or trial, with the SiPc Pc 4 being one of the most successful Pc-based PS in PDT so far.[78]

Subphthalocyanines

SubPcs are lower homologues of Pcs, consisting of three isoindole subunits linked together through aza bridges (instead of 4 in the case of Pcs) (Figure 14). In their central cavity they always bear a boron atom, which is tetracoordinated to three nitrogen atoms of the macrocycle and one axial substituent.[83] Their aromatic system consists of 14 π-electrons which are delocalized over the internal aromatic ring, consisting of 6 carbon and 6 nitrogen atoms. Importantly, and in contrast to Pcs, they are not planar, but show a conical structure.[84] Similarly to Pcs, the delocalization of these 14 π-electrons generates an absorption spectrum with the same two characteristic bands, corresponding to the π-π* transitions of S_0 to S_1 and S_0 to S_2, respectively (Figure 20): the Q-band (in this case centered between 460 and 570 nm) and the B- or Soret band (around 350 nm). Depending on the exact wavelength of the absorption maximum of their Q-band, SubPcs display a

[83] a] C. G. Claessens, D. González-Rodríguez, T. Torres, *Chem. Rev.* **2002**, *102*, 835–853; b) T. Torres, *Angew. Chem. Int. Ed.* **2006**, *45*, 2834–2837; c] A. Medina, C. G. Claessens, *J. Porphyr. Phthalocyanines* **2009**, *13*, 446–454; d) C. G. Claessens, D. González-Rodríguez, M. S. Rodríguez-Morgade, A. Medina, T. Torres, *Chem. Rev.* **2014**, *114*, 2192–2277.

[84] a] H. Kietaibl, *Monatshefte Für Chem.* **1974**, *105*, 405–418 b) K. Kasuga, T. Idehara, M. Handa, Y. Ueda, T. Fujiwara, K. Isa, *Bull. Chem. Soc. Jpn.* **1996**, *69*, 2559–2563 c] M. K. Engel, J. Yao, H. Maki, H. Takeuchi, H. Yonehara, C. Pac, *Rep. Kawamura Inst Chem Res* **1997**, *9*, 53–57 d) R. Potz, M. Göldner, H. Hückstädt, U. Cornelissen, A. Tutaß, H. Homborg, *Z. Für Anorg. Allg. Chem.* **2000**, *626*, 588–596 e] M. S. Rodríguez-Morgade, C. G. Claessens, A. Medina, D. González-Rodríguez, E. Gutiérrez-Puebla, A. Monge, I. Alkorta, J. Elguero, T. Torres, *Chem. Eur. J.* **2008**, *14*, 1342–1350 f) F. Camerel, G. Ulrich, P. Retailleau, R. Ziessel, *Angew. Chem. Int. Ed.* **2008**, *47*, 8876–8880 g] A. S. Paton, A. J. Lough, T. P. Bender, *Acta Crystallogr. E* **2010**, *66*, 3246 h) A. S. Paton, G. E. Morse, J. F. Maka, A. J. Lough, T. P. Bender, *Acta Crystallogr. E* **2010**, *66*, 3059 i] J. D. Virdo, Y. H. Kawar, A. J. Lough, T. P. Bender, *Cryst Eng Comm* **2013**, *15*, 3187–3199 j) J. D. Virdo, A. J. Lough, T. P. Bender, *Acta Crystallogr. C* **2016**, *72*, 297–307.

color varying from intense pink to dark purple. On the other hand, the molar extinction coefficient of SubPcs is generally in de order of 10^4 M^{-1} cm^{-1}, situated between that of Pors (ε_{HpD} ~10^3 M^{-1} cm^{-1}) and Pcs (ε_{Pc} ~ 10^5 M^{-1} cm^{-1}).

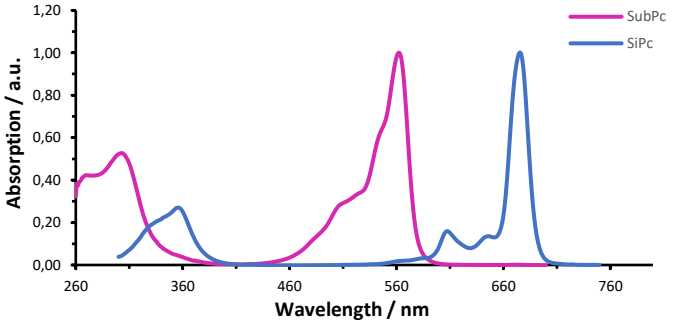

Figure 20. Normalized UV-Vis spectra of a SubPc (pink) and a SiPc (blue) in DMF.

Synthesis and versatility of SubPcs

Although SubPcs were discovered in 1972,[85] it took various years to optimize their synthesis.[86] Today, they can be easily synthesized with reasonable to high yields by the cyclotrimerization of phthalonitrile in the presence of a boron trihalide, generally BBr_3 or BCl_3, in a variety of high-boiling solvents, such as *p*-xylene, naphthalene or *o*-dichlorobenzene (Scheme 3).[83a,83d,87] Recently there also have been advances in their synthesis by microwave heating.[88]

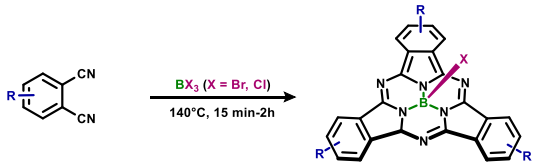

Scheme 3. General synthesis of SubPcs.

Although BBr_3 and BCl_3 are the most commonly used boron trihalides in the synthesis of SubPcs, there exist other possibilities such as BF_3, BPh_3, $PhBF_2$, $PhBCl_2$ or $BuBBr_2$.[16,73d, 84,87a,89] However, both BBr_3 and BCl_3 are commercially available as solutions in *p*-xylene or

---

85 A. Meller, A. Ossko, *Monatshefte Für Chem.* **1972**, *103*, 150–155.

86 a] C. G. Claessens, T. Torres, *Chem. Eur. J.* **2000**, *6*, 2168–2172 b) *Tetrahedron Lett.* **2000**, *41*, 6361–6365 c] C. G. Claessens, D. González-Rodríguez, B. del Rey, T. Torres, G. Mark, H.-P. Schuchmann, C. von Sonntag, J. G. MacDonald, R. S. Nohr, *Eur. J. Org. Chem.* **2003**, *2003*, 2547–2551.

87 a] M. Geyer, F. Plenzig, J. Rauschnabel, M. Hanack, B. del Rey, A. Sastre, T. Torres, *Synthesis* **1996**, *1996*, 1139–1151 b) D. González-Rodríguez, Tesis Doctoral, **2003**.

88 a] L. Giribabu, C. Vijay Kumar, A. Surendar, V. Gopal Reddy, M. Chandrasekharam, P. Yella Reddy, *Synth. Commun.* **2007**, *37*, 4141 b) J. H. Kim, J. Heo, B. M. Kang, D.-H. Son, G.-D. Lee, S.-S. Hong, S. S. Park, *KongopHwahak* **2009**, *20*, 154.

89 a] J. Rauschnabel, M. Hanack, *Tetrahedron Lett.* **1995**, *36*, 1629–1632; b) N. Kobayashi, T. Ishizaki, K. Ishii, H. Konami, *J. Am. Chem. Soc.* **1999**, *121*, 9096–9110; c] N. Kobayashi, *J. Porphyr. Phthalocyanines*

DCM, greatly facilitating their use and making it possible to control the stoichiometry of the reaction. Furthermore, *p*-xylene not only serves as a typical high-boiling solvent (bp = 138.5°C), but has also de capacity to reduce *in situ* the chlorine atoms liberated by BCl_3 during the reaction, effectively preventing the chlorination of the macrocycle periphery.

Various studies have been conducted on the mechanism of formation of SubPcs and with the aid of theoretical calculations, they have resulted in the mechanism postulated in Scheme 4.[83d,90] The process starts with the formation of a phthalonitrile-BX_3 adduct, leading to intermediate A, which subsequently reacts with another phthalonitrile molecule. Addition of a third phthalonitrile molecule leads to the formation of the intermediate macrocycle B, which, after elimination of Cl_2 (catalyzed by BX_3), leads to the final SubPc product.

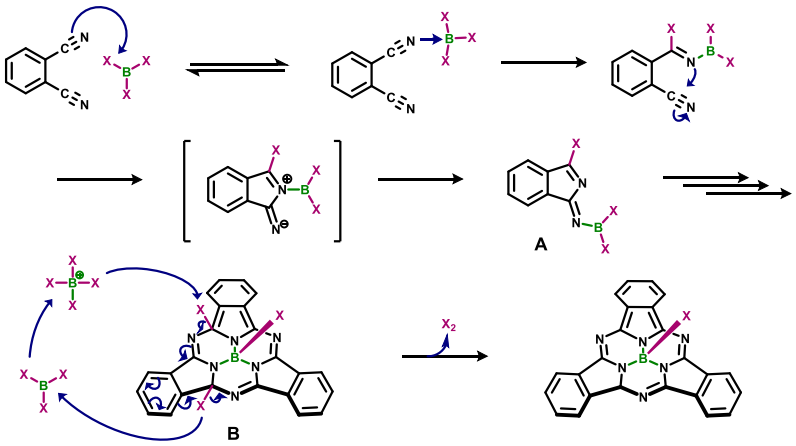

Scheme 4. Postulated mechanism for the formation of SubPcs.

Similarly as for Pcs, more than one different phthalonitrile can be employed in the synthesis of SubPcs, giving rise to differently substituted derivatives in a statistical manner (Figure 21).[86a,91] However, less variety in the type of substituents of the phthalonitriles is possible, as compared to those accessible in the synthesis of Pcs, since the reaction conditions for the formation of SubPcs are very harsh. Halogen atoms such as iodine and bromine are without doubt the most used substituents, as they provide a way for subsequent functionalization of the SubPc through Pd-catalyzed cross coupling

---

1999, *3*, 453–467; d) M. S. Rodríguez-Morgade, S. Esperanza, T. Torres, J. Barberá, *Chem. Eur. J.* **2005**, *11*, 354–360.

90 a] C. G. Claessens, D. González-Rodríguez, C. M. McCallum, R. S. Nohr, H.-P. Schuchmann, T. Torres, *J. Porphyr. Phthalocyanines* **2007**, *11*, 181–188 b) R. S. Nohr, C. M. McCallum, H.-P. Schuchmann, *J. Porphyr. Phthalocyanines* **2010**, *14*, 271–277.

91 a] H. Ali, S. K. Sim, J. E. van Lier, *J. Chem. Res. Synop.* **1999**, 496–497; b) J. R. Stork, R. J. Potucek, W. S. Durfee, B. C. Noll, *Tetrahedron Lett.* **1999**, *40*, 8055–8058; c] C. D. Zyskowski, V. O. Kennedy, *J. Porphyr. Phthalocyanines* **2000**, *4*, 707–712; d) D. González-Rodríguez, C. G. Claessens, T. Torres, *J. Porphyr. Phthalocyanines* **2009**, *13*, 203–214.

reactions.[92] Other possible SubPc substituents include nitro, thioether, alkyl and sulfonyl groups.[83a,d]

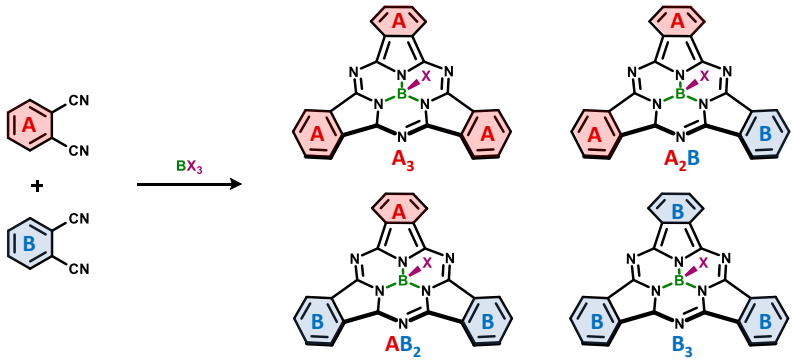

Figure 21. Schematic representation of the set of SubPc derivatives obtained *via* statistical cyclotetramerization of two differently functionalized phthalonitriles, A and B. The relative percentages of each compound will depend on the relative reactivity of the respective phthalonitriles.

[92] a] D. González-Rodríguez, T. Torres, *Eur. J. Org. Chem.* **2009**, *2009*, 1871–1879; b) R. Ziessel, G. Ulrich, K. J. Elliott, A. Harriman, *Chem. Eur. J.* **2009**, *15*, 4980–4984.

Applications of photodynamic therapy

As mentioned before, PDT has numerous applications, which can be divided into two main fields: the photodynamic treatment of malignant cancer cells, known as PDT, on the one hand, and the photodynamic treatment or inactivation of microorganisms, known as PDI, on the other hand. In the next paragraphs some of the most important developments and success stories of both fields will be highlighted .

Oncological applications (PDT)

Although PDT was discovered more than a century ago as an antimicrobial,[9] its most developed application until now has been cancer treatment and it is now being widely used in the clinic.[2] PDT has several advantages over actual cancer therapies such as radiotherapy and chemotherapy: it is comparatively non-invasive, it can be targeted accurately, repeated doses can be given without the total-dose limitations associated with radiotherapy, and the healing process results in little or no scarring. Furthermore, PDT can usually be done in an outpatient or day-case setting, which is convenient for the patient, and has no side-effects. To date, this therapeutic methodology has been used in various branches of oncology, such as dermatology,[2,93] brain malignancies,[94] thoracic oncology,[95] pancreatic cancer,[96] oesophageal cancer,[97] bladder cancer,[98] etc.

Non-oncological applications (PDI)

Although most research around PDT in the last decade has been focussed on oncological applications, recently a renewed interest in antimicrobial PDT has surfaced, accelerated by the advent of antibiotic resistance.[61] PDI has already proven its efficacy against both

---

93 a] S. Collaud, A. Juzeniene, J. Moan, N. Lange, *Curr. Med. Chem.* **2004**, *4*, 301–316; b) D. Ozong, A. M. Rkein, S. G. Fabi, H. Michael, M. Goldman, N. J. Lowe, G. M. Martin, G. S. Munavalli, *Dermatol. Surg.* **2016**, *42*, 804–827.

94 a] H. Kostron, A. Obwegeser, R. Jakober, *J. Photochem. Photobiol. B* **1996**, *36*, 157–168; b) H. Kostron, *Methods Mol. Biol.* **2010**, *635*, 261–280; c] R. Ritz, R. Daniels, S. Noell, G. C. Feigl, V. Schmidt, A. Bornemann, K. Ramina, D. Mayer, K. Dietz, W. S. L. Strauss, M. Tatagiba, *Eur. J. Surg. Oncol.* **2012**, *38*, 352–360; d) J. D. Meyers, Y. Cheng, A.-M. Broome, R. S. Agnes, M. D. Schluchter, S. Margevicius, X. Wang, M. E. Kenney, C. Burda, J. P. Basilion, *Part. Part. Syst. Charact.* **2015**, *32*, 448–457.

95 a] Y. Hayata, H. Kato, C. Konaka, J. Ono, N. Takizawa, *Chest* **1982**, *81*, 269–277; b) C. B. Simone, J. S. Friedberg, E. Glatstein, J. P. Stevenson, D. H. Sterman, S. M. Hahn, K. A. Cengel, *J. Thorac. Dis.* **2012**, *4*, 63–75.

96 S. G. Bown, A. Z. Rogowska, D. E. Whitelaw, W. R. Lees, L. B. Lovat, P. Ripley, L. Jones, P. Wyld, A. Gillams, A. W. R. Hatfield, *Gut* **2002**, *50*, 549–557.

97 a] C. Hopper, *Lancet Oncol.* **2000**, *1*, 212–219; b) C. Compagnin, M. Mognato, L. Celotti, G. Canti, G. Palumbo, E. Reddi, *Cell Prolif.* **2010**, *43*, 262–274.

98 a] M. J. Bader, H. Stepp, W. Beyer, T. Pongratz, R. Sroka, M. Kriegmair, D. Zaak, M. Welschof, D. Tilki, C. G. Stief, R. Waidelich, *Urol. Oncol. Semin. Orig. Investig.* **2013**, *31*, 1178–1183; b) P. M. R. Pereira, S. Silva, M. Bispo, M. Zuzarte, C. Gomes, H. Girão, J. A. S. Cavaleiro, C. A. F. Ribeiro, J. P. C. Tomé, R. Fernandes, *Bioconjug. Chem.* **2016**, *27*, 2762–2769.

drug-resistant and non-resistant pathogens,[99] and it is worthy to note that in general the photosensitizing ability of the bacteria is completely independent of antibiotic-resistance spectrum, since both therapies work through entirely different mechanisms. Furthermore, PDI deserves a notable mention for its ability to kill not only bacteria, but also insects, parasites, viruses, yeast, fungi, etc (Figure 22).[100] Perhaps the most successful application of PDT so far has been in dentistry,[101] with two commercialized products (Periowave®[102] and SaveDents®[103]) so far. Another success story which is worth a special mention is that of Avedro's KXL System®, which has recently been FDA-approved for therapeutic treatment for progressive keratoconus.[104] Furthermore, apart from its use in clinical treatments, PDI has also shown efficacy in various disinfection techniques such as blood disinfection,[105] surface disinfection,[106] food decontamination,[107] and water disinfection.[108]

---

99 a] A. Orenstein, D. Klein, J. Kopolovic, E. Winkler, Z. Malik, N. Keller, Y. Nitzan, *FEMS Immunol. Med. Microbiol.* **1997**, *19*, 307–314; b) Y. Nitzan, A. Balzam-Sudakevitz, H. Ashkenazi, *J. Photochem. Photobiol. B* **1998**, *42*, 211–218; c] K. Lasocki, M. Szpakowska, J. Grzybowski, A. Graczyk, *Pharmacol. Res.* **1999**, *39*, 181–184; d) M. Szpakowska, K. Lasocki, J. Grzybowski, A. Graczyk, *Pharmacol. Res.* **2001**, *44*, 243–246; e] H. M. Tang, M. R. Hamblin, C. M. N. Yow, *J. Infect. Chemother.* **2007**, *13*, 87–91; f) M. Grinholc, B. Szramka, J. Kurlenda, A. Graczyk, K. P. Bielawski, *J. Photochem. Photobiol. B* **2008**, *90*, 57–63.

100 a] G. D. Pimprikar, G. P. Georghiou, *Pestic. Biochem. Physiol.* **1979**, *12*, 10–22; b) T. L. Carpenter, J. R. Heitz, *Environ. Entomol.* **1980**, *9*, 533–537; c] M. H. Abdel-Kader, T. A. El-Tayeb, *Field Application for Malaria Vector Control Using Sunlight Active Formulated Extract.*, **2009**, WO 2009/149720 A1.

101 a] V. V. Tuchin, E. A. Genina, A. N. Bashkatov, G. V. Simonenko, O. D. Odoevskaya, G. B. Altshuler, *Lasers Surg. Med.* **2003**, *33*, 296–310; b) T. K. Boehm, S. G. Ciancio, *J. Int. Acad. Periodontol.* **2011**, *13*, 58–63.

102 "Products | Ondine Biomedical," can be found under http://www.ondinebio.com/products/, **2016**.

103 S. J. Bonsor, R. Nichol, T. M. S. Reid, G. J. Pearson, *Br. Dent. J.* **2006**, *200*, 337–341, discussion 329.

104 Avedro, "Avedro Receives FDA Approval for Photrexa® Viscous, Photrexa® and the KXL® System for Corneal Cross-Linking," can be found under http://avedro.com/en-us/press-releases/avedro-receives-fda-approval/, **2016**.

105 a] U. Schiffner, G. Cachovan, J. Bastian, A. Sculean, S. Eick, *Acta Odontol. Scand.* **2014**, *72*, 673–680; b) V. Bärenfaller, C. Clausen, A. Sculean, S. Eick, *J. Photochem. Photobiol. B* **2016**, *158*, 252–257.

106 a] S. Noimark, C. W. Dunnill, C. W. M. Kay, S. Perni, P. Prokopovich, S. Ismail, M. Wilson, I. P. Parkin, *J. Mater. Chem.* **2012**, *22*, 15388–15396; b) S. Noimark, E. Salvadori, R. Gómez-Bombarelli, A. J. MacRobert, I. P. Parkin, C. W. M. Kay, *Phys. Chem. Chem. Phys.* **2016**, *18*, 28101–28109.

107 P. Delcanale, C. Montali, B. Rodríguez-Amigo, S. Abbruzzetti, S. Bruno, P. Bianchini, A. Diaspro, M. Agut, S. Nonell, C. Viappiani, *J. Agric. Food Chem.* **2016**, *64*, 8633–8639.

108 a] R. Bonnett, M. A. Krysteva, I. G. Lalov, S. V. Artarsky, *Water Res.* **2006**, *40*, 1269–1275; b) A. K. Benabbou, C. Guillard, S. Pigeot-Rémy, C. Cantau, T. Pigot, P. Lejeune, Z. Derriche, S. Lacombe, *J. Photochem. Photobiol. Chem.* **2011**, *219*, 101–108.

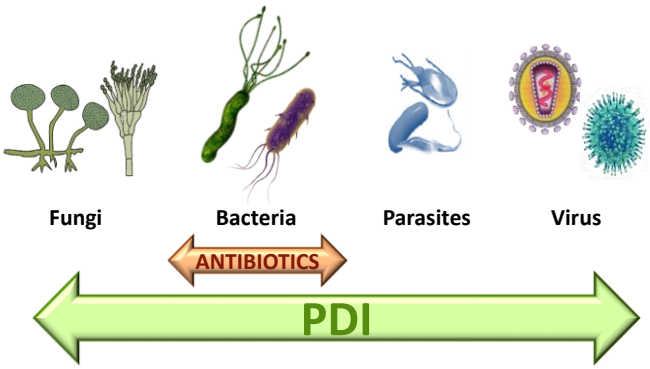

Figure 22. Scope of microorganisms that can be treated by PDI, compared to that of antibiotics.

As a consequence to the positive results already obtained, the interest in PDT is growing steadily and more and more selective and potent PSs are being developed. In the following Tables, an overview of some PS that are already clinically approved, and others that are under investigation in clinical trials, are listed, both for application in PDT (Table 3) and PDI (Table 4).

Table 3. PS for PDT applications currently under investigation in clinical trials (†) and/or already approved for clinical use (‡), in alphabetical order.[11,109]

Trade Name(s)	**Photosensitizer**	**Potential indications**	
Alacare®, Ameluz®	5-aminolevulinic acid (ALA)	Actinic keratosis on face and scalp	(‡)
Alasens®	5-aminolevulinic acid (ALA)	Kidney tumors	(†)
Amphinex	TPCS2a	Head and neck cancers	(†)
Antrin®	Motexafin lutetium	Skin conditions and superficial cancers	(‡)
Antrin®	Motexafin lutetium	Prostate cancer, diseased arteries	(†)
Aptocine®	Talaporfin sodium	Lung cancer	(‡)
BOPP	Boronated protoporphyrin	Brain tumors	(†)
DTBF	Deuteporphyrin	Bladder cancer	(†)
Foscan®, Fosgel®, Foslip®, Fospeg®	*meta*-tetrahydroxyphenyl chlorin	Head, neck, prostate, lung and pancreatic cancers	(‡)
Fotolon®	Chlorin e6	Basal cell carcinoma	(†)
Hemoporfin	Hp monomethyl ether (HMME)	Ovarian cancer	(†)
Levulan Kerastick®	5-aminolevulinic acid (ALA)	Basal cell carcinoma, head, neck, and gynaecological tumors	(‡)
Laserphyrin®	Talaporfin sodium	Lung cancers	(‡)
Laserphyrin®	Talaporfin sodium	Liver, colon and brain tumors	(†)

[109] a] R. R. Allison, G. H. Downie, R. Cuenca, X.-H. Hu, C. J. Childs, C. H. Sibata, *Photodiagnosis Photodyn. Ther.* **2004**, *1*, 27–42; b) A. Serra, M. Pineiro, N. Pereira, A. R. Gonsalves, M. Laranjo, M. Abrantes, F. Botelho, *Oncol. Rev.* **2008**, *2*, 235–249; c] P. Agostinis, K. Berg, K. A. Cengel, T. H. Foster, A. W. Girotti, S. O. Gollnick, S. M. Hahn, M. R. Hamblin, A. Juzeniene, D. Kessel, M. Korbelik, J. Moan, P. Mroz, D. Nowis, J. Piette, B. C. Wilson, J. Golab, *CA. Cancer J. Clin.* **2011**, *61*, 250–281; d) H. Pye, I. Stamati, G. Yahioglu, M. A. Butt, M. Deonarain, *Antibodies* **2013**, *2*, 270–305; e] "PDT - Clinical Trials," can be found under https://clinicaltrials.gov/ct2/results?term=photodynamic+therapy&Search=Search, **2016**.

Lutex®	Lutetium texaphyrin	Breast, cervical, prostate, and brain tumors	(†)
Metvix®	Methylated ALA (MAL)	Basal cell carcinoma	(‡)
Pc4	Silicon Phthalocyanine 4	Cutaneous/subcutaneous lesions from diverse solid tumor origins, EGFR-overexpressing cancers, cervical cancer	(†)
Photochlor®	2-[1-Hexyloxyethyl]-2-devinyl pyropheophorbide-a (HPPH)	Head and neck, esophagus and lung cancer	(‡)
Photofrin®	HpD, porfimer sodium	Cervical, endobronchial, esophageal, bladder, and gastric cancers	(‡)
Photofrin®	HpD, porfimer sodium	Brain tumors, high grade gliomas, lung cancer	(†)
Photogem®	HpD	Various tumors	(†)
Photosan®	HpD	Bile duct cancer, intracranial tumors	(†)
Photosens®	Sulfonated Al Pcs	Bladder, breast, lung and neck cancers	(‡)
Photrex®	Thin ethyl etiopurpurin (SnET2)	Breast cancer	(‡)
Radachlorin	Mixture of 3 chlorophyll a derivatives	Skin cancer	(‡)
TOOKAD	Padoporphyrin	Prostate cancer	(†)
Visudyne®	Verteporfin: Benzoporphyrin derivative monoacid ring A	Basal cell carcinoma	(‡)

Table 4. PS for PDI applications currently under investigation in clinical trials (†) and/or already approved for clinical use (‡), in alphabetical order.[3,109e,110]

Trade Name(s)	**Photosensitizer**	**Formulation**	**Potential indications**	
Fospeg®	*meta*-tetrahydroxyphenyl chlorin	Spray applicator	Wound and burn infections	(†)
KXL System®	riboflavin 5'-phosphate	Eye drops	Corneal injuries; Keratoconus	(‡)
Levulan Kerastick®	5-aminolevulinic acid (ALA)	Oil-in-water cream (20%)	Actinic keratosis of the face or scalp	(‡)
MAL	Methyl 5-aminolevulinate	Cream	Actinic keratosis	(†)
MB Depletion Set®	Methylene blue	MB dry pill	Decontamination of plasma	(‡)
Mycostatin	Nystatin	Topical oral suspension	Denture-related stomatitis	(†)
Periowave®	Methylene blue	Irrigating needle	Periodontitis	(‡)
Photrex®	Thin ethyl etiopurpurin (SnET2)	Intravenous infusion	Age-related macular degeneration	(†)
PPA904	3,7-bis(di-*n*-butylamino)phenothiazine-5-ium bromide	Cream	Infected chronic leg and diabetic foot ulcers	(†)
SaveDent®	Toluidine blue O (TBO)	Irrigating needle	Periodontitis	(‡)
Visudyne®	Verteporfin: Benzoporphyrin derivative monoacid ring A	Infusion	Ocular indications	(‡)
	tetra butyl analogue methylene blue		Sterilization of infected wounds	(†)

[110] a] M. Wainwright, H. Mohr, W. H. Walker, *J. Photochem. Photobiol. B* **2007**, *86*, 45–58; b) V. Engelhardt, B. Krammer, K. Plaetzer, *Photochem. Photobiol. Sci.* **2010**, *9*, 365–369; c] J. A. González-Delgado, P. J. Kennedy, M. Ferreira, J. P. C. Tomé, B. Sarmento, *J. Med. Chem.* **2015**; d) "Adis Insight," can be found under http://adisinsight.springer.com, **2016**.

General Objectives

The aim of this Doctoral Thesis is the preparation, characterization and *in vitro* study of novel PS, based on Pcs and SubPcs, for their use in PDT and PDI.

PDT is a clinically approved form of phototherapy that finds use in both oncological treatments and in the treatment of microbial infections (in that case also referred to as photodynamic inactivation, PDI). Up to now, the most successful PS have all been part of the porphyrinoid PS family. Both Pcs and SubPcs are part of this family, and present various beneficial characteristics for their use as PS, such as their synthetic accessibility, high molar absorption coefficients, and high triplet state, $^1O_2$ and fluorescence quantum yields, encouraging further investigation towards their use as PS.

The **first chapter** is devoted to the synthesis of Pcs and SubPcs as PS for application in oncological PDT treatments. For this purpose, a series of neutrally charged Pcs and SubPcs with different substituents at their axial positions will be prepared (Figure 23) and the influence of the axial substituents on the PS fluorescence and $^1O_2$ generation properties will be thoroughly investigated. Furthermore, it is our aim to make use of axial substituents that can actively quench the singlet excited state of the PS, and therefore its $^1O_2$ generation efficiency and fluorescence, in a reversible way. To this end, activation studies of these quenching processes in function of different external stimuli will be undertaken. Finally, the efficacy as PS of selected Pcs and SubPcs will be studied *in vitro* against various tumor cell lines, such as HEp-2 (from a human larynx carcinoma), SCC-13 (from a human squamous cell carcinoma of the skin) and HeLa (from a human cervical carcinoma). For this, a collaboration with the laboratory of microbiology of prof. Ángeles Juarranz de la Fuente, in the Biology Department of our university, will be established.

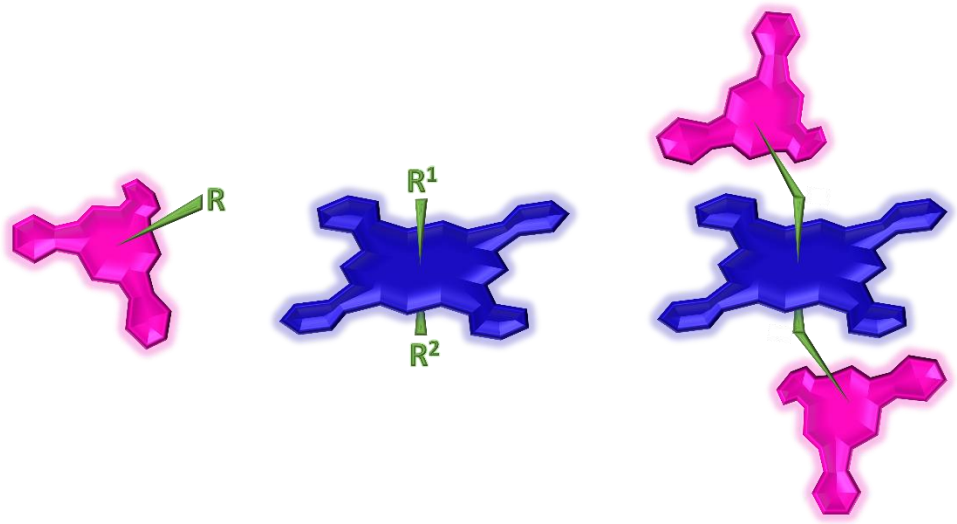

Figure 23. Schematic representation of the target neutrally charged SiPc- and SubPc-based PS that will be studied in Chapter 1.

The **second chapter** is centred in the preparation and characterization of Pcs and SubPcs as PS for application in PDI, a subfield of PDT consisting in the photodynamic inactivation of microorganisms. To this end, a series of cationic Pcs and SubPcs will be synthesized, employing cationic groups at the periphery of the macrocycle, while making use of the same axial substituents as those used in the previous chapter (Figure 24). The influence of the axial substituent on the PS fluorescence and $^1O_2$ generation properties will be thoroughly investigated, and *in vitro* studies of the inactivation efficiency of selected PS will be performed against both Gram-positive and Gram-negative bacteria. To this end, a collaboration with the research group of Prof. Angela Cunha at the Department of Biology of the University of Aveiro (Portugal) has been established.

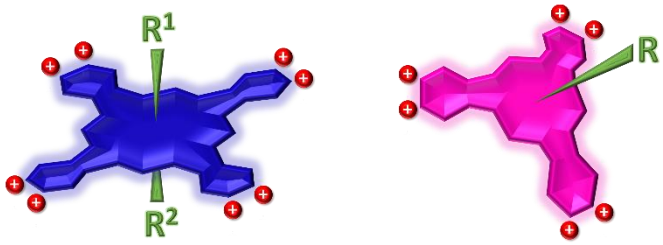

Figure 24. Schematic representation of the target positively charged SiPc (octacationic) and SubPc (hexacationic) PS that will be studied in Chapter 2.

The aim in the **third chapter** is the synthesis of new third-generation PS, based on Pcs and SubPcs. For this, selected Pcs and SubPcs will be covalently or non-covalently linked to site-specific delivery agents or nanostructured delivery platforms, with the goal to improve both the selectivity and cell-uptake of the PS system. In the first place, maleimide-containing Pc and SubPc derivatives will be covalently conjugated with a cysteine C-terminated cell penetrating peptide (CPP), through a ene-thiol "click" reaction. In particular, the Tat CPP is a short peptide sequence that possesses the remarkable property of being able to cross cell membranes and deliver bioactive cargoes inside diseased cells (Figure 25a). Cell-uptake and *in vitro* photodynamic activity studies will be performed in collaboration with the laboratory of Prof. Bruno de Geest at Ghent University (Belgium), to validate the employed strategy. In the second place, cationic zinc Pc (ZnPc) derivatives will be non-covalently deposited onto the negatively charged surface of cellulose nanocrystals (CNC), which are rod-shaped sugar-based nanostructures that can greatly increase the biocompatibility of their cargo (Figure 25b). In this case, detailed photophysical studies and *in vitro* photodynamic activity studies of the resulting biohybrids will be performed in collaboration with the research groups of Profs. Santi Nonell and Montserrat Agut Bonsfills, at the Institut Químic de Sarrià of the Universitat Ramon Llull (Barcelona, Spain). These studies will be conducted against a broad spectrum of microorganisms, including a Gram-positive (*S. aureus*) bacterium, a Gram-negative bacterium (*E. coli*) and a yeast (*C. albicans*).

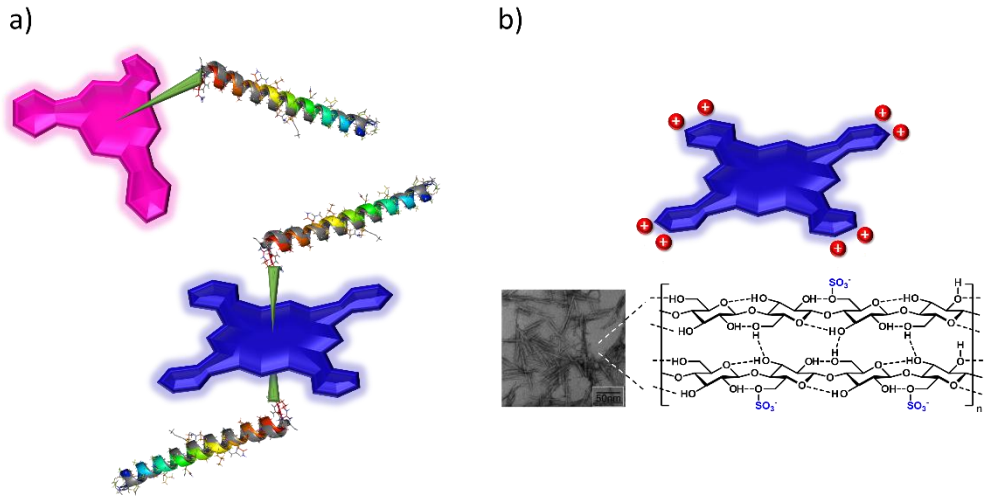

Figure 25. Schematic representation of the target PS-based biohybrids that will be studied in Chapter 3. a) Schematic representation of covalently conjugated SiPc-CPP and SubPc-CPP biohybrids. b) Schematic representation of non-covalently conjugated ZnPc-CNC biohybrids.

The molecular design of each of the target compounds and the corresponding specific research objectives will be detailed in the respective subchapters.

CHAPTER 1

Design, synthesis and *in vitro* evaluation of neutrally charged (sub)phthalocyanines for use in photodynamic therapy

1

Neutral silicon phthalocyanines as photosensitizers for photodynamic therapy

1.1 State of the art

As mentioned in the general introduction of this thesis, Pc 4 is one of the most promising Pcs for PDT applications. Since its discovery, lots of research has been done into the synthesis of Pc 4 analogues and their structure-activity relationships concerning their photodynamic efficacy (Figure 26).[111] From these studies, it could be concluded that an unhindered macrocycle face (bearing one –OH substituent) is not essential for efficient interaction with biological targets, Pc 12 being as effective as Pc 4 , but that the axial substituents should not be too long either, Pc 18 being less effective then Pc 12.[111a,c] Furthermore, terminal amines seem to drastically quench the Pc's excited state, the effect depending on the relative proximity of the amine group to the macrocycle.[111b] Pc 227, on the other hand, is an interesting new analogue, being photosensitive. It bears one alkyl- instead of an alkysiloxy substituent, and yields Pc 4 when irradiated by light.[111d]

---

[111] a] Y.-S. Li, S. I. A. Zaidi, M. A. J. Rodgers, H. Mukhtar, M. E. Kenney, N. L. Oleinick, J. He, H. E. Larkin, B. D. Rihter, *Photochem. Photobiol.* **1997**, *65*, 581–586; b) H. M. Anula, J. C. Berlin, H. Wu, Y.-S. Li, X. Peng, M. E. Kenney, M. A. J. Rodgers, *J. Phys. Chem. A* **2006**, *110*, 5215–5223; c] M. E. Rodriguez, P. Zhang, K. Azizuddin, G. B. Delos Santos, S. Chiu, L. Xue, J. C. Berlin, X. Peng, H. Wu, M. Lam, A.-L. Nieminen, M. E. Kenney, N. L. Oleinick, *Photochem. Photobiol.* **2009**, *85*, 1189–1200; d) J. Li, Y. Yang, P. Zhang, J. R. Sounik, M. E. Kenney, *Photochem. Photobiol. Sci.* **2014**, *13*, 1690–1698.

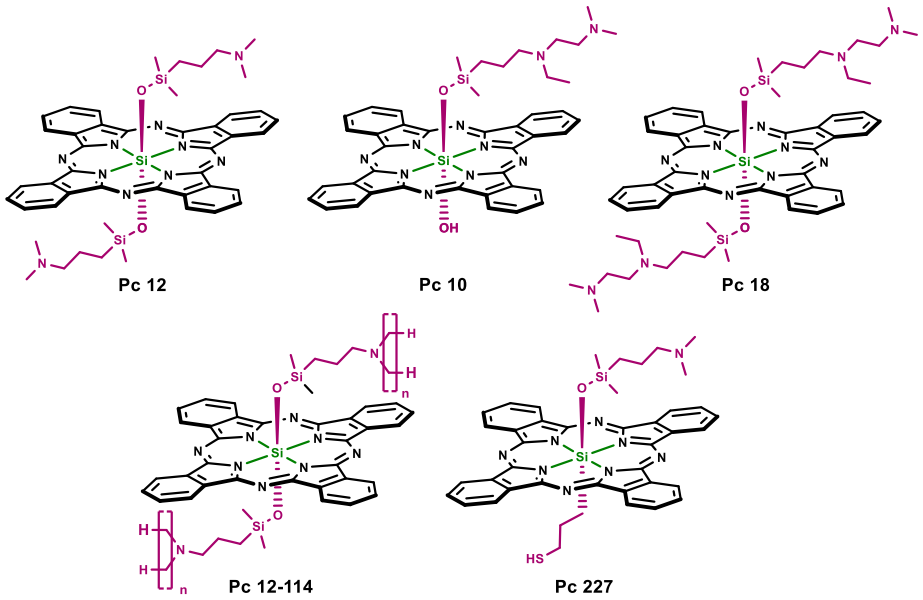

Figure 26. Some examples of already synthesized analogues of Pc 4.[111]

Apart from Pc 4 analogues, a lot of other interesting SiPcs for PDT have been synthesized in the last years, the most important contribution to this field being made by Ng and co-workers. Exploiting the fact that tumor cells are slightly acidic, they have synthesized various SiPcs bearing polyamines as axial substituents. In this way, their fluorescence emission and efficiency of generating ROS are sensitive to the pH environment (Figure 27).[112]

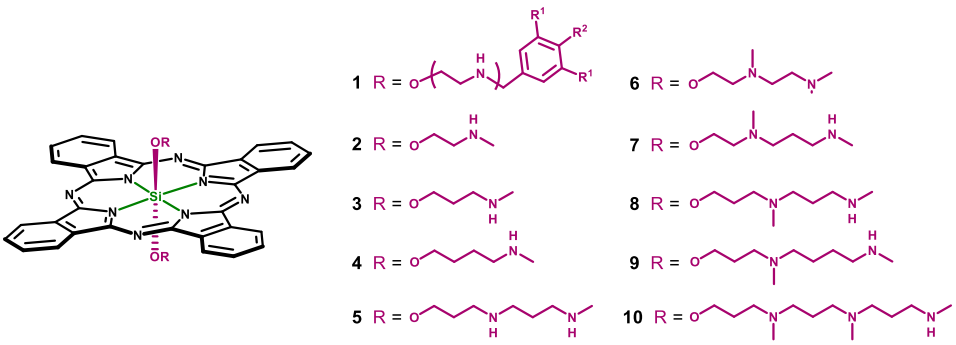

Figure 27. An extensive series of acid-sensitive SiPcs bearing (poly-)amine substituents at the axial positions, synthesized by Ng and co-workers.[112]

More specifically, at neutral pH, both the ROS generation and fluorescence emission are strongly reduced by the photoinduced electron-transfer (PET) deactivation pathway caused by the presence of the amino groups, which quench the singlet excited state of the

[112] a] X.-J. Jiang, P.-C. Lo, Y.-M. Tsang, S.-L. Yeung, W.-P. Fong, D. K. P. Ng, *Chem. Eur. J.* **2010**, *16*, 4777–4783; b) X.-J. Jiang, P.-C. Lo, S.-L. Yeung, W.-P. Fong, D. K. P. Ng, *Chem. Commun.* **2010**, *46*, 3188–3190; c] X.-J. Jiang, S.-L. Yeung, P.-C. Lo, W.-P. Fong, D. K. P. Ng, *J. Med. Chem.* **2001**, *54*, 320–330.

Pc core. At slightly acidic pH (such as that inside tumor cells), however, the amino groups will be protonated and the fluorescence emission and ROS generation activated. This results in a selective functioning of the PS only inside tumor cells, while in healthy cells no ROS should be generated and no cell damage does occur.

Ng and co-workers have later further developed this type of activatable PS by introducing other quenching moieties (i.e. ferrocenyl chalcone) and other activation pathways (i.e. reduction of disulfide bridges or acid sensitive hydrazone linkers), their most interesting system up to date being the dual activatable PS depicted in Figure 28.[113]

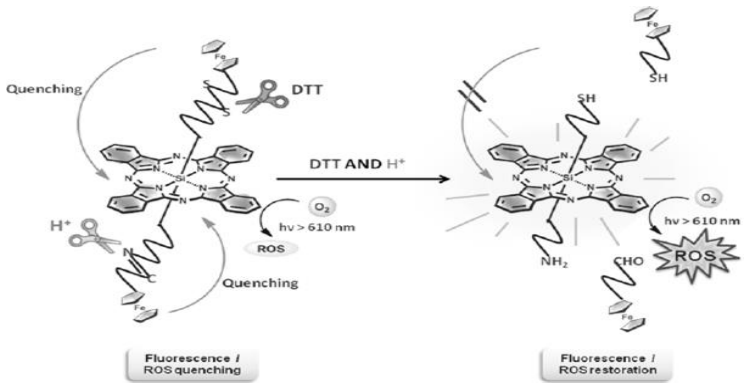

Figure 28. A dual activatable PS and its activation pathways, synthesized by Ng and co-workers.[113b]

Other SiPc-based PS have been designed bearing various interesting moieties at the axial position, such as morpholine[114] (i.e. a well-known antipsychotic drug and radiosensitizer), carboranes[115] (for simultaneous boron neutron capture therapy), β-cyclodextrins[116] (cyclic oligosaccharides that facilitate the anchoring of PS to cellular tissues and surfaces), solketal groups (which can be converted in glycerol in vivo)[117] and parabens[118] (one of the most functional preservative agents used in drugs, cosmetics, foodstuffs as well as in dental materials).

---

113 a] J. T. F. Lau, X.-J. Jiang, D. K. P. Ng, P.-C. Lo, *Chem. Commun.* **2013**, *49*, 4274–4276; b) J. T. F. Lau, P.-C. Lo, X.-J. Jiang, Q. Wang, D. K. P. Ng, *J. Med. Chem.* **2014**, *57*, 4088–4087.

114 Y.-J. Zhu, J.-D. Huang, X.-J. Jiang, J.-C. Sun, *Inorg. Chem. Commun.* **2006**, *9*, 473–477.

115 G. Y. Atmaca, C. Dizman, T. Eren, A. Erdoğmuş, *Spectrochim. Acta A* **2015**, *137*, 244–249.

116 a] J. T. F. Lau, P.-C. Lo, W.-P. Fong, D. K. P. Ng, *Chem. Eur. J.* **2011**, *17*, 7569–7577; b) J. T. F. Lau, P.-C. Lo, Y.-M. Tsang, W.-P. Fong, D. K. P. Ng, *Chem. Commun.* **2011**, *47*, 9657; c] A. Galstyan, U. Kauscher, D. Block, B. J. Ravoo, C. A. Strassert, *ACS Appl Mater Interfaces* **2016**, *8*, 12631–12637.

117 J. W. Hofman, F. van Zeeland, S. Turker, H. Talsma, S. A. G. Lambrechts, D. V. Sakharov, W. E. Hennink, C. F. van Nostrum, *J. Med. Chem.* **2007**, *50*, 1485–1494.

118 G. C. Taşkın, M. Durmuş, F. Yüksel, V. Mantareva, V. Kussovski, I. Angelov, D. Atilla, *J. Photochem. Photobiol. Chem.* **2015**, *306*, 31–40.

1.2 Molecular design, synthesis and characterization of a series of neutral silicon phthalocyanine photosensitizers

The specific objective of this subchapter is the design, synthesis and characterization of a series of axially substituted SiPcs (Figure 29). Furthermore, the efficacy of the resulting PS to generate $^1O_2$ and their applicability in PDT, by leading to tumoral cell death, will be examined *in vitro*.

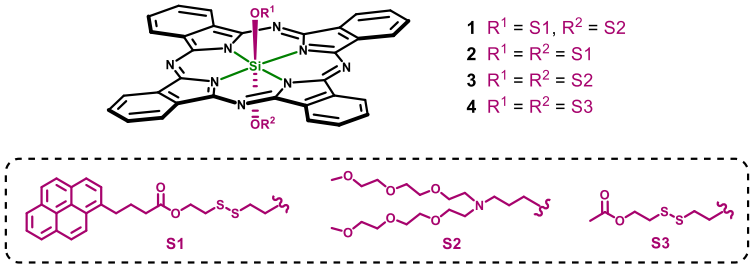

Figure 29. Target compounds of Chapter 1 - Subchapter 1: A series of axially substituted SiPcs bearing different axial substituents.

As explained in the Introduction of this Thesis, Pcs are known to generate $^1O_2$ from their photoinduced singlet excited state (S_1), followed by intersystem crossing to the excited triplet (T_1) and subsequent energy transfer to the triplet ground state of $^3O_2$. Within SiPcs this process can be quenched if photo- or electroactive units are connected to the axial positions of the central silicon atom.[119] As mentioned above, Ng and co-workers have exploited this characteristic to develop a pH- and redox-responsive activatable PS by attaching two ferrocenyl moieties to the axial positions of a SiPc.[113] Amino groups also provoke a pH-dependent quenching of Pc excited states.[112a,b] As a continuation of this work we designed a series of novel SiPcs **1-3** bearing an additional fluorophore (i.e., pyrene), which allows the theranostic use of the resulting PS,[120] and/or an amino group with two methoxy(triethylenoxy) axial chains for increasing hydrophilicity. As shown for other Pc-pyrene covalent dyads, the emission of the pyrene unit (F_{377}) is probably deactivated by electronic energy transfer (EET),[121] yet quenching by photoinduced electron transfer (PET) cannot be excluded. The amino group quenches the SiPc excited state through PET.[112a,b] A SiPc without any of the previously mentioned quenching units, SiPc **4**, was also synthesized for its use as reference compound. Furthermore, from a logical perspective, in all previously published cases,[112a,b,113] $^1O_2$ production and SiPc fluorescence are recovered simultaneously. Thus, these systems present only a single combined output signal and, therefore, a limited capacity for molecular computing. To

[119] X. Li, S. Kolemen, J. Yoon, E. U. Akkaya, *Adv. Funct. Mater.* **2016**, DOI: 10.1002/adfm.201604053.
[120] S. S. Kelkar, T. M. Reineke, *Bioconjug. Chem.* **2011**, *22*, 1879–1903.
[121] J. Bartelmess, B. Ballesteros, G. de la Torre, D. Kiessling, S. Campidelli, M. Prato, T. Torres, D. M. Guldi, *J. Am. Chem. Soc.* **2010**, *132*, 16202–16211.

circumvent these limitations, the asymmetrical SiPc **1** was our target compound. To activate F_{377}, a disulfide linker has been introduced, which can be cleaved selectively under reducing conditions (e.g., with DTT). Since the extent of EET is dependent on and extremely sensitive to the distance of the donor to the acceptor,[122] the EET will no longer be efficient upon cleavage of the disulfide linker, resulting in recuperation of F_{377} and $^1O_2$ generation. Upon protonation of the pendant amino group by slightly lowering the pH of the solution, the SiPc emission (F_{680}) is also recovered. In turn, we found that the propensity of **1** to generate $^1O_2$ is modulated by the presence and/or absence of acid, DTT, and irradiation of the complex in the requisite absorption range (Figure 30). Importantly, two of these inputs are particularly relevant from a medical perspective, considering tumor environments are characterized by being both acidic[123] and highly reducing[124] in nature, more so than healthy cells and extracellular matrix.

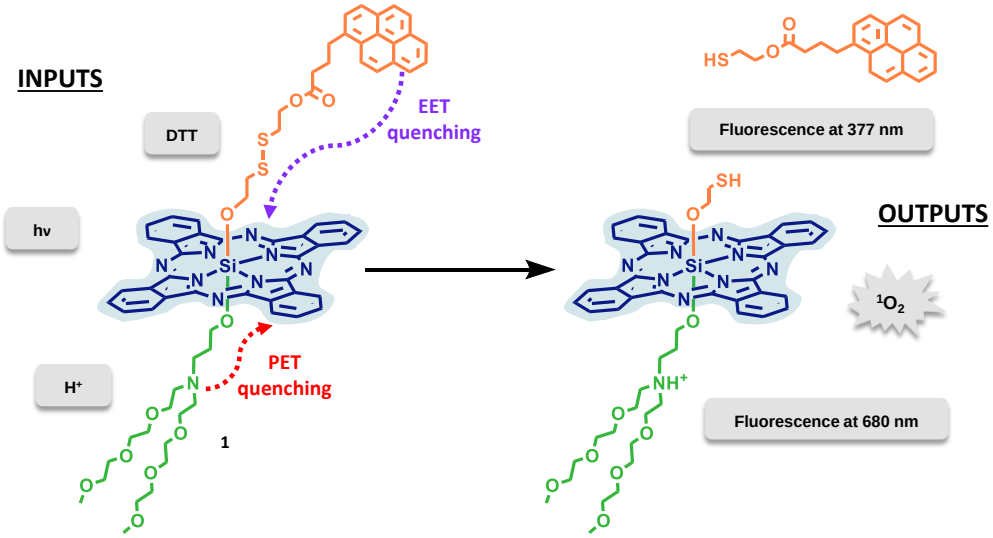

Figure 30. Structure of PS **1** and its activation pathways.

In the next sections, the synthesis and characterization of SiPcs **1-4** will be detailed, whereas the influence of the three different external stimuli (DTT, H^+ and hv) on SiPc **1** will be thoroughly investigated.

---

122 D. C. Harris, in *Quant. Chem. Anal.*, W. H. Freeman And Co, New York, **2010**, pp. 419–444.
123 G. Helmlinger, A. Sckell, M. Dellian, N. S. Forbes, R. K. Jain, *Clin. Cancer Res.* **2002**, *8*, 1284–1291.
124 M. P. Gamcsik, M. S. Kasibhatla, S. D. Teeter, O. M. Colvin, *Biomarkers* **2012**, *17*, 671–691.

1.2.1 Synthesis of building blocks for axial substitution

There exist three commonly used methods to introduce building blocks for axial substitution in SiPcs, starting from SiPc bearing chlorine atoms at the axial positions ($SiPcCl_2$). $SiPcCl_2$ can be treated both with derivatives bearing a free carboxylic acid or a free primary hydroxyl group, yielding the corresponding SiPc silyl ester[125] or SiPc silyl ether[104a] derivatives, respectively, after nucleophilic displacement of the chlorine atoms. In a third method, $SiPcCl_2$ can be subjected to hydrolysis, yielding silicon phthalocyanine dihydroxide ($SiPc(OH)_2$), which can be axially substituted with different trialkylchlorosilane derivatives. In the present thesis, we have made use of both the second and third method, in this subchapter and in subchapter 2.1, respectively. Since in this subchapter we will make use of the first method, primary alcohol derivatives need to be synthesized as building blocks for axial substitution.

To obtain the first building block for axial substitution, 1-pyrenebutyric acid was reacted with 2-hydroxyethyl disulfide (Scheme 5), in the presence of 1-ethyl-3-(3-dimethylaminopropyl) carbodiimide (EDC) and catalytic amounts of DMAP, obtaining 1-pyrenebutanoic acid, 2-[(2-hydroxyethyl)dithio]ethyl ester (**5**). In this variant of the Steglich esterification, EDC was used as carbodiimide for carboxyl activation, instead of DCC.[126] In this case, EDC reacts with the carboxylic acid group of 1-pyrenebutyric acid to form an active O-acylisourea intermediate that is easily displaced by nucleophilic attack by DMAP. This leads to a reactive amide intermediate, which reacts rapidly with one of the alcohol groups of 2-hydroxyethyl disulfide, giving rise to the desired ester. The benefit of using EDC instead of DCC is the fact that its urea, which is formed as a by-product, is water-soluble, for which it can be easily removed by washing the crude reaction mixture with water. The reaction was performed in DCM, overnight, yielding 2-[(2-hydroxyethyl)dithio]ethyl ester in 77% yield after purification by column chromatography using chloroform/methanol (100:1) as the eluent. Importantly, making use of a small excess of 2-hydroxyethyl disulfide (1.2 equivalents), no double esterification of the second alcohol group has been observed.

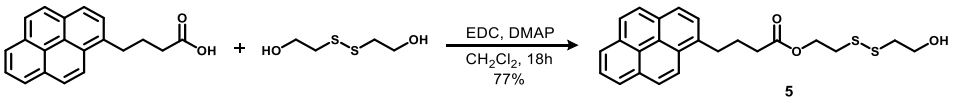

Scheme 5. Synthesis of the first building block for axial substitution: 1-pyrenebutanoic acid, 2-[(2-hydroxyethyl)dithio]ethyl ester (**5**).

The second building block for axial substitution, bearing the methoxy(triethylenoxy) chains in order to increase the biocompatibility of the final PS, has been synthesized in

---

[125] a] C. Farren, S. FitzGerald, M. R. Bryce, A. Beeby, A. S. Batsanov, *J. Chem. Soc. Perkin Trans. 2* **2002**, 59–66; b) F. J. Céspedes-Guirao, L. Martín-Gomis, K. Ohkubo, S. Fukuzumi, F. Fernández-Lázaro, Á. Sastre-Santos, *Chem. Eur. J.* **2011**, *17*, 9153–9163.

[126] S.-Y. Han, Y.-A. Kim, *Tetrahedron* **2004**, *60*, 2447–2467.

two steps (Scheme 6). The commercially available triethylene glycol monomethyl ether was first reacted with *p*-toluenesulfonyl chloride, to convert its alcohol group in a tosyl group, which is a much better leaving group. During this reaction, the alcohol reacts as a nucleophile, attacking the electrophilic centre of *p*-toluenesulfonyl chloride and displacing the chloride atom, yielding **6** with a good yield. The reaction was performed in a mixture of water and THF, and a water-soluble base such as NaOH was added to the reaction mixture in order to neutralize the HCl that is being formed and speed up the reaction. Finally, a double S_N2 nucleophilic substitution reaction between **6** and the amine group of the commercially available 3-amino-1-propanol, which acts as nucleophile, lead to the formation of 3-bis(methoxy(diethylenoxy)ethyl)amino]-1-propanol (**7**). After column chromatography using DCM/methanol (20:1) as the eluent the yield of the purified compound was determined to be 61%. The formation of some mono-substituted product could be detected, although to a small extent. Upon recovery of this product from the column, it could be subjected to another reaction cycle.

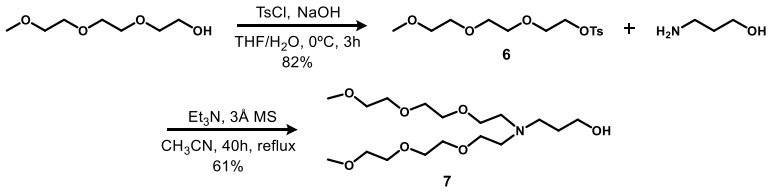

Scheme 6. Synthesis of the second building block for axial substitution: 3-bis(methoxy(diethylenoxy)ethyl)amino]-1-propanol (**7**).

Next, the building block for axial substitution to synthesize the reference SiPc **4** was synthesized by reacting 2-hydroxyethyl disulfide with acetylchloride, through a nucleophilic addition/elimination, resulting in 2-[(2-hydroxyethyl)disulfanyl]ethyl acetate (**8**) (Scheme 7). Similarly as in the tosylation above, the reaction is exothermic and was therefore performed at 0°C. Since in this case the reaction was performed in an organic solvent, HCl was neutralized by the presence of an organic base such as Et_3N. Upon completion of the reaction (30 min), the reaction mixture was quenched with a saturated aqueous solution of $NaHCO_3$. After work-up and purification by column chromatography, **7** was isolated as colorless oil with a yield of 33%. The major cause for this reasonably low yield is the formation of a by-product in which the disulfide bridge has been cleaved, as detected by ^{1}H-NMR spectroscopy, which was isolated with a yield of 59%.

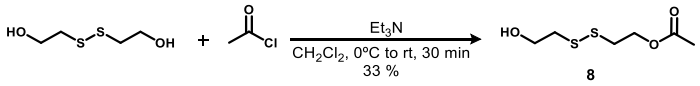

Scheme 7. Synthesis of the building block for axial substitution 2-[(2-hydroxyethyl)disulfanyl]ethyl acetate (**8**).

Finally, 1-pyrenebutanoic acid, N-(3-hydroxypropyl) amide (**11**), was synthesised in order to be used as a reference compound in fluorescence measurements regarding F_{377} (Scheme 8). For this, alcohol group of the commercially available 3-amino-1-propanol was

first protected by a *tert*-butyldimethylsilyl group, enabling the selective reaction of its amine group with the carboxylic acid group of 1-pyrene butyric acid. In this amine formation the carboxylic acid group of 1-pyrene butyric acid was activated by EDC and catalyzed by DMAP, in similar way as in the Steglich esterification detailed above. After the formation of the amide, the *tert*-butyldimethylsilyl ether could be easily deprotected by employing a catalytic amount of acetyl chloride in dry methanol. The final compounds was purified by column chromatography using a gradient of Chloroform to chloroform/methanol (10:1) as the eluent, yielding **11** with a 64% overall yield.

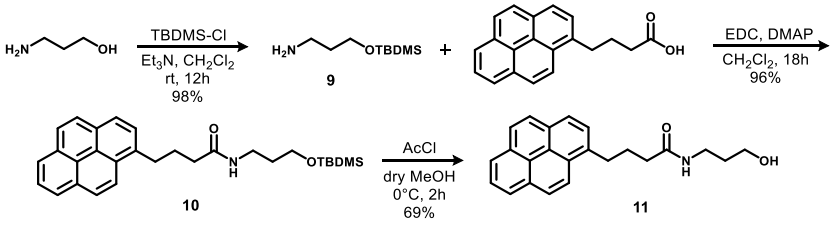

Scheme 8. Synthesis of 1-pyrenebutanoic acid, N-(3-hydroxypropyl) amide (**11**), to be used as a reference compound for fluorescence measurements.

1.2.2 Synthesis of target neutral silicon phthalocyanines

Once all primary alcohol building blocks for axial substitution were synthesized, they were incorporated at the axial positions of $SiPcCl_2$, following a previously published protocol, which has been optimized for these particular axial substituents (Scheme 9).[113a] Unless stated otherwise, pyridine was used as the base for this substitution reaction throughout the present thesis, even though other bases such as NaH or DIPEA could also be used.

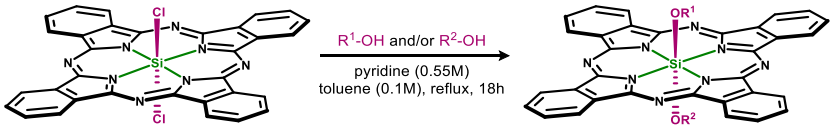

Scheme 9. General synthesis of axially substituted SiPcs using an optimized method.

The symmetrical SiPcs were easily synthesized, using an excess of 5 equivalents of the corresponding building block for axials substitution, with respect to the $SiPcCl_2$ (Scheme 10). After refluxing the reaction mixture overnight, the solvent was evaporated to dryness and the SiPcs were purified by column chromatography using silica gel previously neutralized with Et_3N, since they are unstable in normal silica gel. As a consequence, the compounds elute together with a trimethylammonium cation (Et_3NH^+), which can be removed by consequent washing with water or filtration over a short pad of silica gel using DCM as the solvent. In case of SiPcs **2** and **4**, a final purification step by recrystallization in toluene or methanol, respectively, was performed. In the case of SiPc **3**, which is a sticky

solid due to the presence of the methoxy(triethylenoxy) chains, a final purification step by size exclusion chromatography (SEC), using Bio-Beads as the stationary phase and DCM as the eluent was performed, to remove any traces of remaining free alcohol. In this way, the symmetrical SiPcs **2**-**4** could be obtained with reasonable yields, ranging from 24% to 32%.

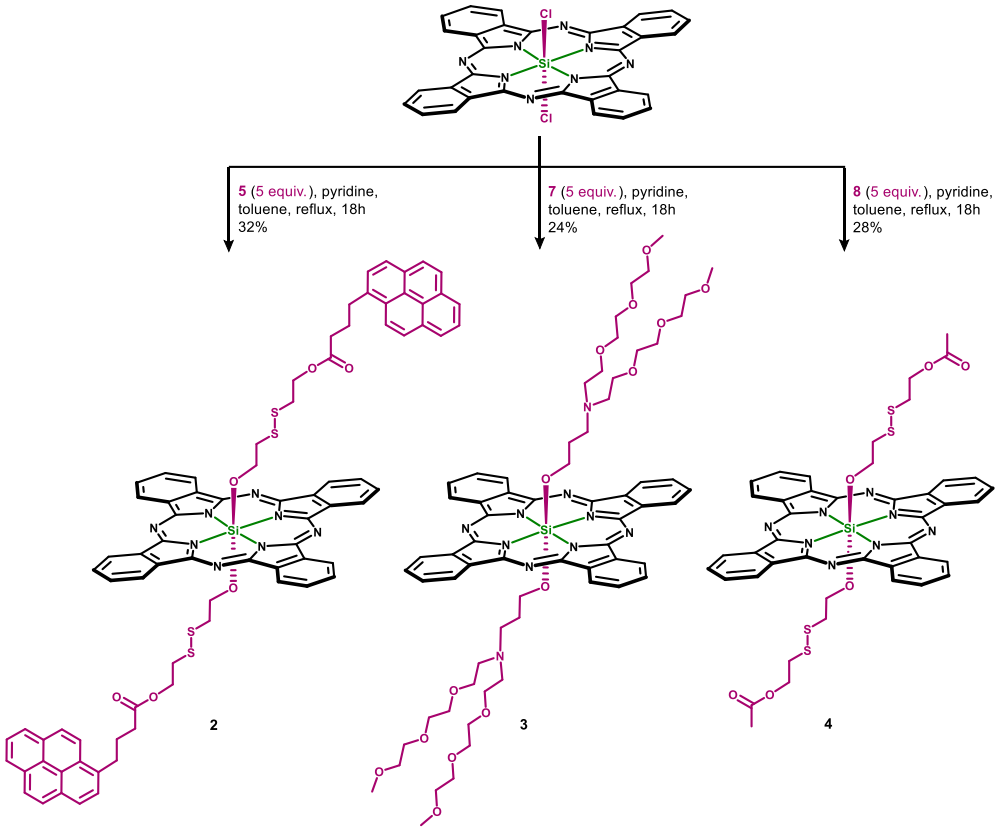

Scheme 10. Synthesis of the symmetrical SiPcs **2**-**4**.

As a representative example of the NMR characterization of these compounds, Figure 31a shows the ^{1}H-NMR spectrum, recorded in $CDCl_3$, of the building block for axial substitution **5** and the corresponding symmetrical SiPc **2**, respectively. The signals for the SiPc aromatic protons, at 9.65 pm and 8.30 ppm, are well resolved, indicating the complete absence of aggregation, as expected. Furthermore, the ring current effect exerted by the π-electron cloud of the SiPc macrocycle over the nearby protons of the axial substituents can be clearly observed. The closer the proton to the SiPc macrocycle, the stronger the shielding effect and the weaker the nuclear magnetic field it experiences.[125] Therefore, the chemical shift of these protons is normally significantly more upfield than in the corresponding building block, and this in order of the proximity of the respective protons to the SiPc macrocycle. Importantly, all CH_2-signals could be unquestionably assigned making use of two-dimensional NMR techniques such as COSY, TOCSY, HSQC and HMBC. Furthermore, using these techniques, it was also possible to unambiguously assign all carbon signals in the ^{13}C-NMR spectrum (Figure 31b).

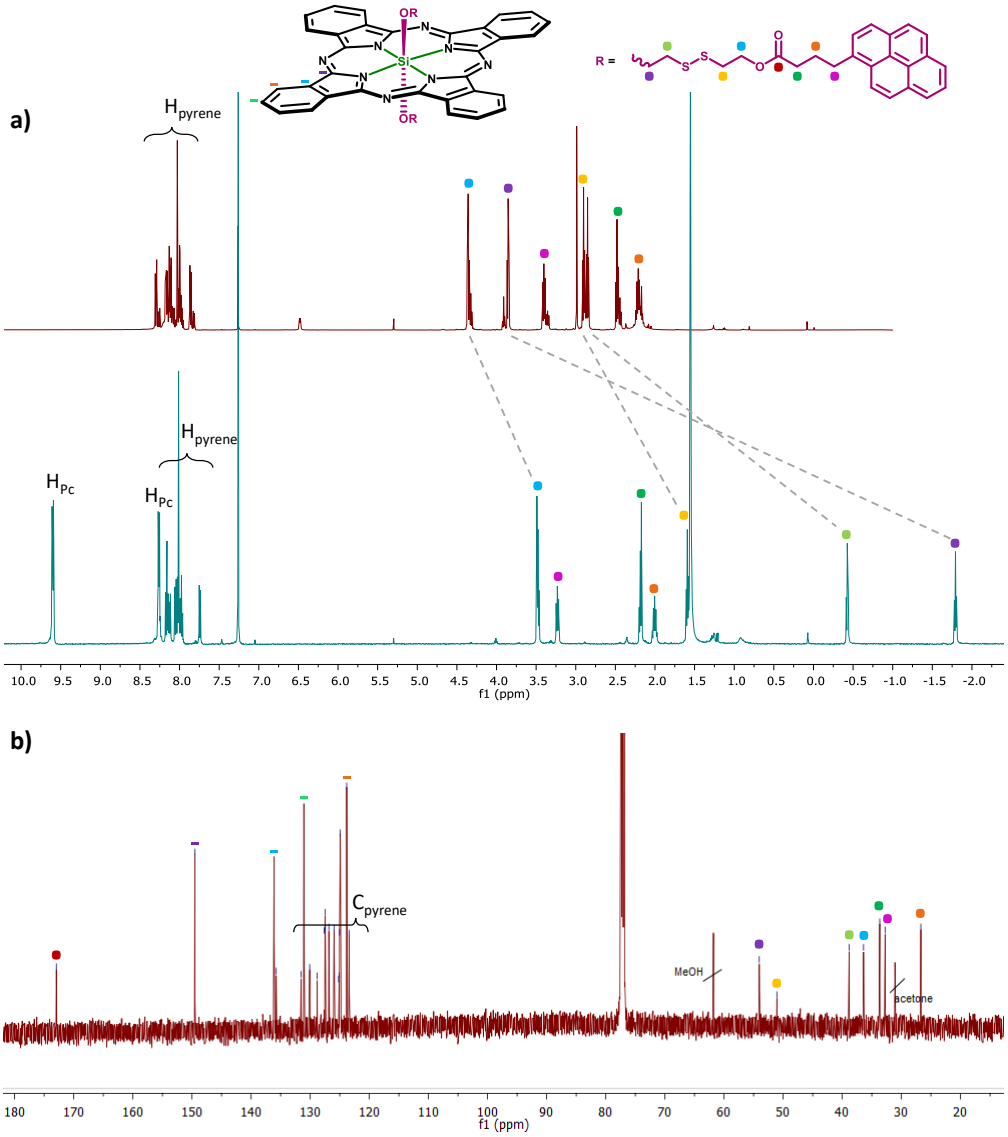

Figure 31. a) ^{1}H-NMR spectrum of building block for axial substitution **5** (top) and symmetrical SiPc **2** bearing **5** as axial substituents (bottom) in $CDCl_3$, showing the effect of the ring current on the protons of the axial substituents: the closer the protons to ring, the greater the upfield displacement of their chemical shift. b) ^{13}C-NMR spectrum of the symmetrical SiPc **2** in $CDCl_3$.

Following the successful synthesis and purification of these symmetrical SiPcs **2-4**, the synthesis of the asymmetric SiPc **1** was tackled. As explained before (Figure 18), asymmetric SiPcs result from a statistical reaction employing two different building blocks for axial substitution. Generally, a first trial with 2,5 equivalents of each building block is taken as a starting point to explore the reactivity of each of the building blocks, in function of which the equivalents employed for each of them are then adapted. In the case of SiPc **1**, the two building blocks **5** and **7** appeared to display a similar reactivity, for which 2,5

equivalents of each resulted to be the optimal building block ratio, giving rise to SiPc **1** with a reasonable 16% yield (Scheme 11). Purification was performed in a similar way as for the symmetrical SiPcs **2**-**4**, that is, purification by column chromatography using silica gel previously neutralized with Et_3N, which is followed by a washing step with water to remove the triethylammonium cation, and a final purification step by SEC with Biobeads as the stationary phase and DCM as the eluent. As side-products from this reaction, the symmetrical SiPcs **2** and **3** are also obtained, with a 14% and 19% yield, respectively.

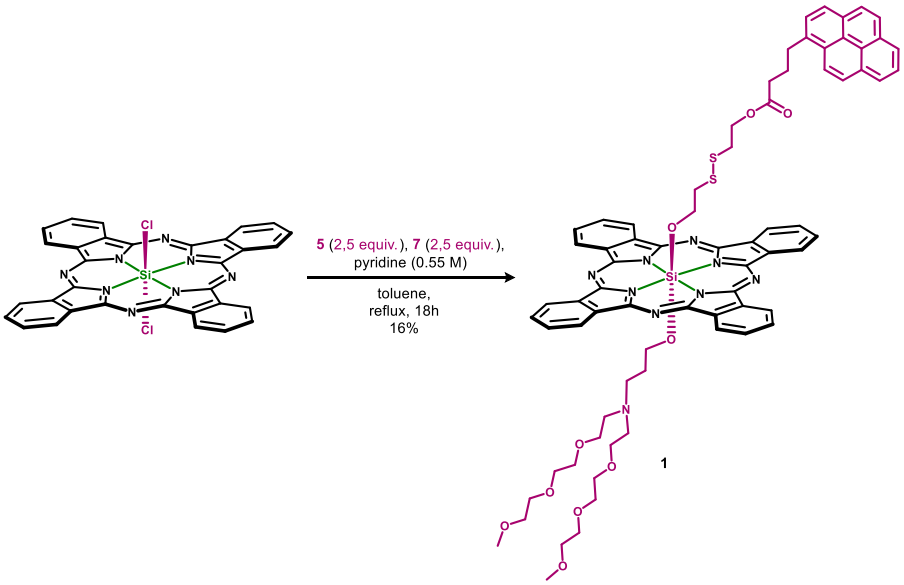

Scheme 11. Synthesis of asymmetric SiPc **1**.

Figure 32 shows the ^{1}H-NMR spectrum, recorded in $CDCl_3$, of the building blocks for axial substitution **5** and **7**, and the corresponding symmetrical SiPc **1**, respectively. Again, the signals for the SiPc aromatic protons, at 9.63 pm and 8.32 ppm, are well resolved, and the ring current effect exerted by the π-electron cloud of the SiPc macrocycle greatly effects the chemical shift of the nearby protons of both axial substituents. Although it resulted significantly more difficult than in the case of the symmetrical Pcs, with the help of two-dimensional NMR techniques, such as COSY, TOCSY, HSQC and HMBC, all proton signals could be unquestionably assigned. However, due to the complicity of the spectrum, unambiguous assignment of the ^{13}C-NMR spectrum was in this case not possible for all signals.

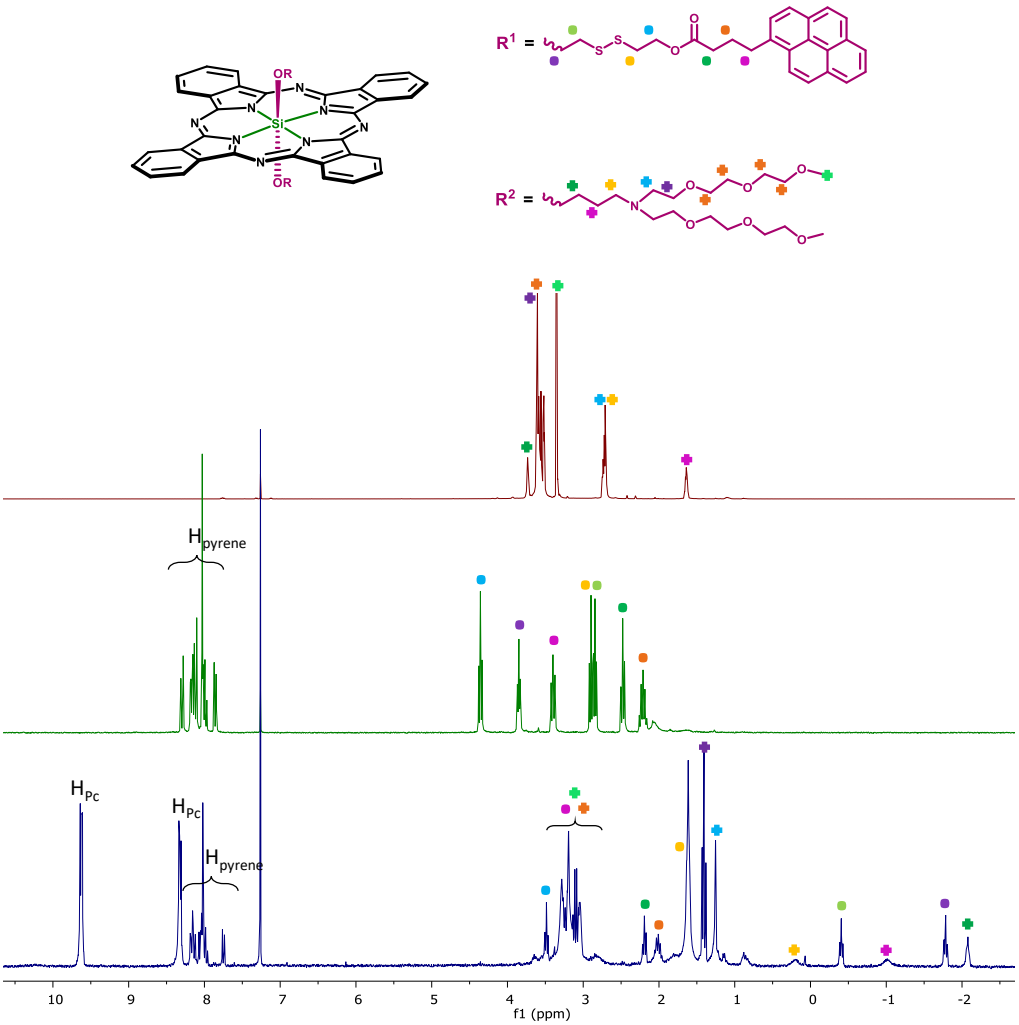

Figure 32. ^{1}H-NMR spectrum of building blocks for axial substitution **7** (top), **5** (middle) and asymmetrical SiPc **1** bearing **5** and **7** as axial substituents (bottom) in $CDCl_3$, showing the effect of the ring current on the protons of the axial substituents: the closer the protons to ring, the greater the upfield displacement of their chemical shift.

1.2.3 Spectral features and photophysical properties

The UV-Vis spectra of **1-4** in DMF show the Q- and Soret bands characteristic of SiPc (Figure 33). Additionally, **1** and **2** exhibit a band at 344 nm, assigned to pyrene. Further, a summation of the spectral features recorded for reference compounds **10** and **4**, in a 1:1 or 2:1 stoichiometry, closely resemble the spectra of the corresponding pyrene-containing SiPc derivatives **1** and **2**, respectively.

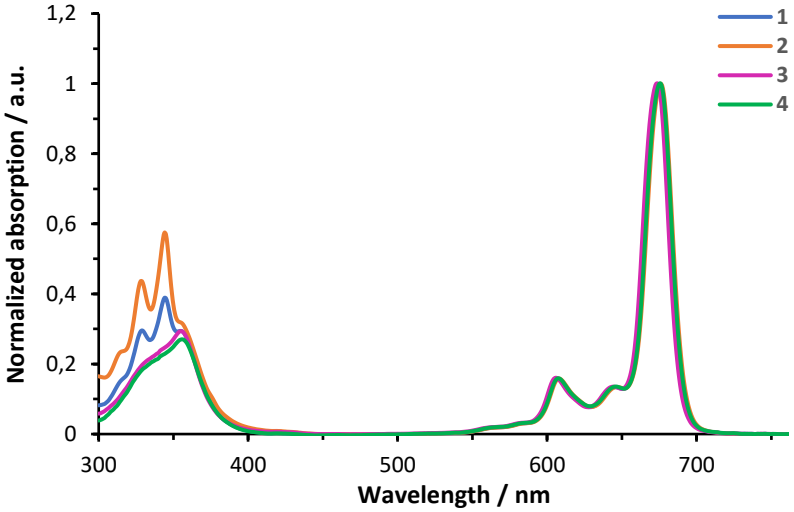

Figure 33. Electronic absorption spectra of SiPcs **1-4** in DMF.

Fluorescence quantum yields (ϕ_F) were measured in DMF by exciting compounds **1-4** at 345 nm (Table 5 and Figure 36), a wavelength coinciding with both pyrene absorption and the SiPc Soret band.

$^1O_2$ quantum yields (ϕ_Δ) were also measured in DMF, by the *relative method*,[127] using 1,3-diphenylisobenzofuran (DPBF, Figure 34) as a chemical scavenger and excitation with visible light filtered below 530 nm ($h\nu_{>530}$).

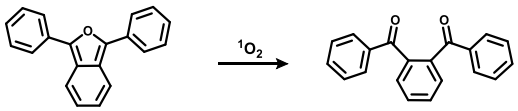

Figure 34. Photoinduced decomposition of DPBF upon reaction with $^1O_2$.

The concentration of the scavenger (DPBF) is monitored spectroscopically at 414 nm in function of the irradiation time of the PS, from which the values of ϕ_Δ can be determined. An example of the spectroscopic data for this measurements for SiPc **1** can be seen in

[127] S. Makhseed, A. Tuhl, J. Samuel, P. Zimcik, N. Al-Awadi, V. Novakova, *Dyes Pigments* **2012**, *95*, 351–357.

Figure 35. Importantly, the decrease of the absorption of DPBF is completely linear (R^2=0.9998) and at the same time no change in the absorption of **1** is observed throughout the measurement, indicating its stability and confirming it is non-aggregated.

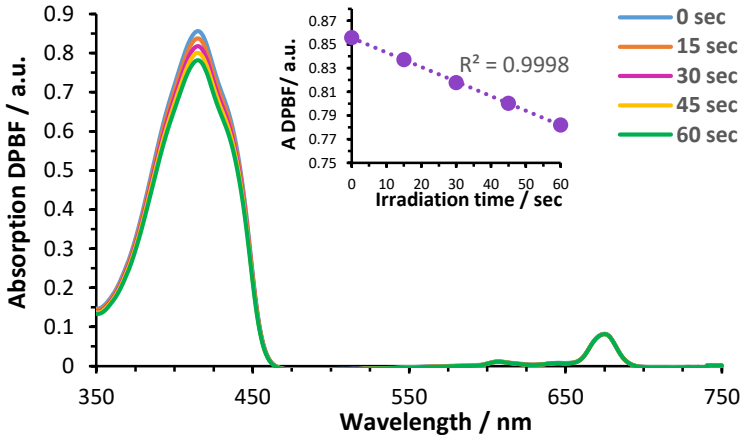

Figure 35. Time dependent photobleaching of DPBF-absorption in the presence of SiPc **1** in DMF, which is directly related to the photoinduced generation of $^1O_2$ by the PS. Inset: detail of DPBF absorption decrease.

An overview of al measured electronic absorption and photophysical data for SiPcs **1**-**4** and reference compound **10** in DMF can be seen in Table 5. ϕ_F and ϕ_Δ are furthermore schematically represented in Figure 36.

Table 5. Electronic absorption and photophysical data for SiPcs **1**-**4** and reference compound **10** in DMF.

Compound	λ_{max} (nm)	λ_{em} (nm)[a]	ϕ_{F377} (%)[b]	ϕ_{F680} (%)[c]	ϕ_Δ (%)[d]
1	678	680	1.6	4.0	4.7
2	676	681	2.1	23.4	19.7
3	676	681	-[f]	2.1	3.5
4	679	684	-[f]	37.1	36.2
10	344	377	59.6	-[e]	-[e]

[a] Excited at 345 nm. [b] Excited at 345 nm. Using anthracene in cyclohexane as the reference (ϕ_F = 0.36). [c] Excited at 610 nm. Using ZnPc in DMF as the reference (ϕ_F = 0.28). [d] Using ZnPc in DMF as the reference (ϕ_Δ = 0.56). [e] Not applicable because the compound does not contain any SiPc moiety. [f] Not applicable because the compound does not contain any pyrene moiety.

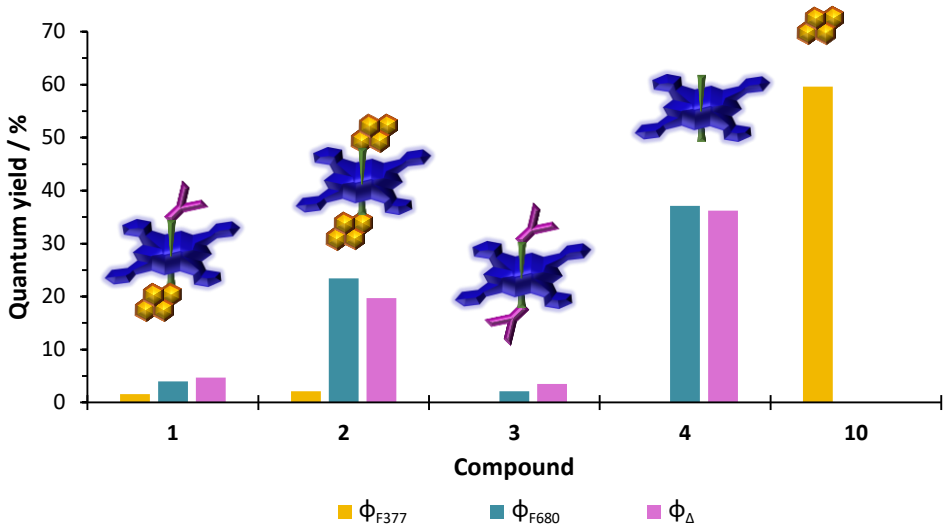

Figure 36. Φ_{F377} (yellow bars), Φ_{F680} (blue bars) and Φ_{Δ} (purple bars) of SiPcs **1**-**4** and reference compound **10**.

Compared to reference derivatives **4** and **10**, the three output signals are significantly deactivated in compounds **1** and **3**, while for compound **2** the reduction in F_{680} intensity and $^1O_2$ production is less than 50%, revealing an inefficient quenching by the pyrene unit. Excitation of the SiPc Soret band, which leads its second singlet excited state, could be the reason for such a decrease in quenching efficiency. The level of SiPc Φ_F and Φ_{Δ} quenching in **1** and **3** actually appears to be further correlated with the number of pendant amino groups, suggesting the stronger quenching capacity of the amino functionality in comparison to pyrene. In compounds **1** and **2**, F_{377} remains nearly fully deactivated, likely as a result of an EET process in which the pyrene emission band and the SiPc Soret band significantly overlap,[121] yet we cannot exclude PET as the quenching mechanism.

1.3 Dependence of fluorescence and $^1O_2$ generation of SiPc 1 on different chemical inputs

To investigate the effect of chemical inputs on the photochemical properties of **1** in physiologically relevant medium, its absorption and fluorescence spectra were monitored for 24 h in phosphate buffered saline (PBS) solutions with varying pH and/or DTT concentrations. Adequate solubility was achieved by adding 0.5% Cremophor EL (v/v), a pharmaceutically approved surfactant.[128]

In general, samples were prepared as following: **1** was dissolved in spectroscopic grade DMF to give a 1 mM solution, which was diluted to 0.4 µM with buffer solution (PBS with 0.5% Cremophor EL). To evaluate the dependence on the DTT-concentration, DTT was dissolved in deionized water to give a 1 M solution and mixtures of **1** (25 mL, 0.4 µM) with DTT (2 µM, 5 mM, 10 mM, 20 mM or 50 mM) or without DTT in 25 mL of buffer solution were prepared and stirred continuously. For pH-dependence experiments, mixtures of **1** (25 mL, 0.4 µM) were adjusted to pH 7.4, pH 6.8 or pH 5 by adding concentrated HCl (0, 6 or 16 µL, respectively) and stirred continuously.

1.3.1 Dependence of fluorescence

(i) DTT-dependence

At neutral pH, there were no significant changes in the absorption features of **1** with varying DTT concentrations (Figure 37). Importantly, once oxidized, DTT forms a stable six-member ring with an internal disulfide bond which absorbs at 283 nm.[129] Due to the high excess of DTT in **c)** and **d)**, the absorption peak of its oxidation product causes a 'lift' of the spectrum between 400-300 nm. Nevertheless, it is clear that the sharp Q-band remains unchanged at all DTT concentrations, indicating that the compound remains intact and non-aggregated, and assuring that any changes in fluorescence must be a consequence of quenching relaxation upon reductive cleavage of the disulfide linker rather than a change in the compound aggregation.

[128] H. Gelderblom, J. Verweij, K. Nooter, A. Sparreboom, *Eur. J. Cancer* **2001**, *37*, 1590–1598.
[129] A. Seo, J. L. Jackson, J. V. Schuster, D. Vardar-Ulu, *Anal. Bioanal. Chem.* **2013**, *405*, 6379–6384.

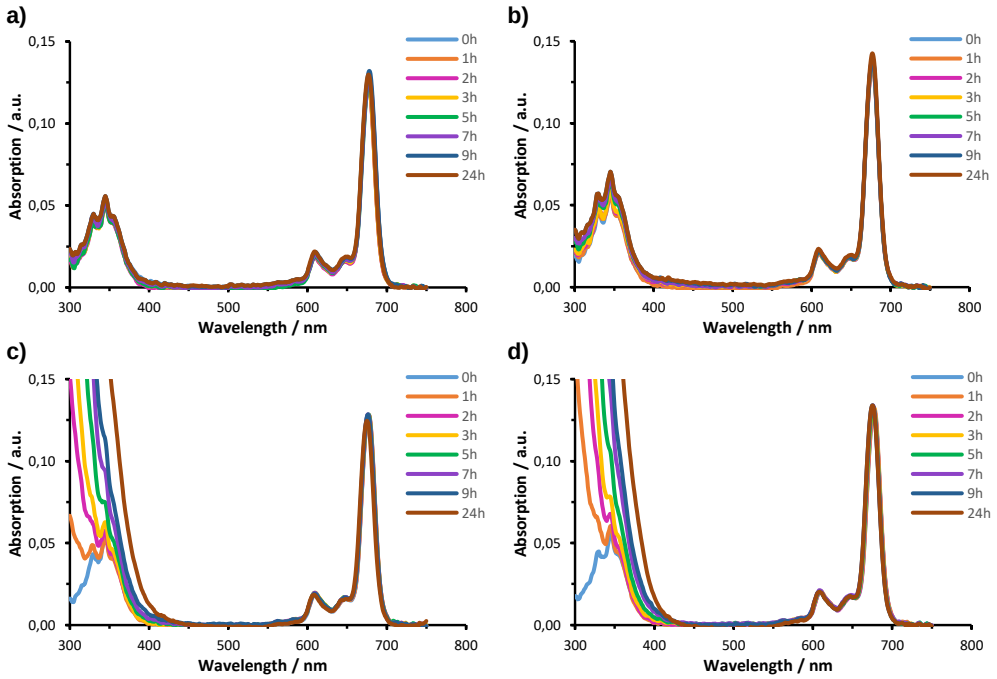

Figure 37. UV-Vis spectra of **1** in PBS (0.5% Cremophor EL) with a) 0 µM DTT, b) 2 µM DTT, c) 20 mM DTT and d) 50 mM DTT, from t = 0 h to t = 24 h.

On the contrary, the intensity of F_{377} exhibited a 2-, 3-, 5- and 6.5-fold increment in the presence of 5, 10, 20 and 50 mM DTT, respectively. The increase in F_{377} intensity reflects that pyrene emission is recovered upon disulfide cleavage (Figure 38). At 50 mM DTT, F_{377} reaches a plateau after 8 h and thus is taken as an indication that at this concentration, all of the disulfide bonds have been cleaved (Figure 39). In the absence of DTT, there is no F_{377} enhancement, which reflects the need of a reducing environment to promote activation via disulfide cleavage.

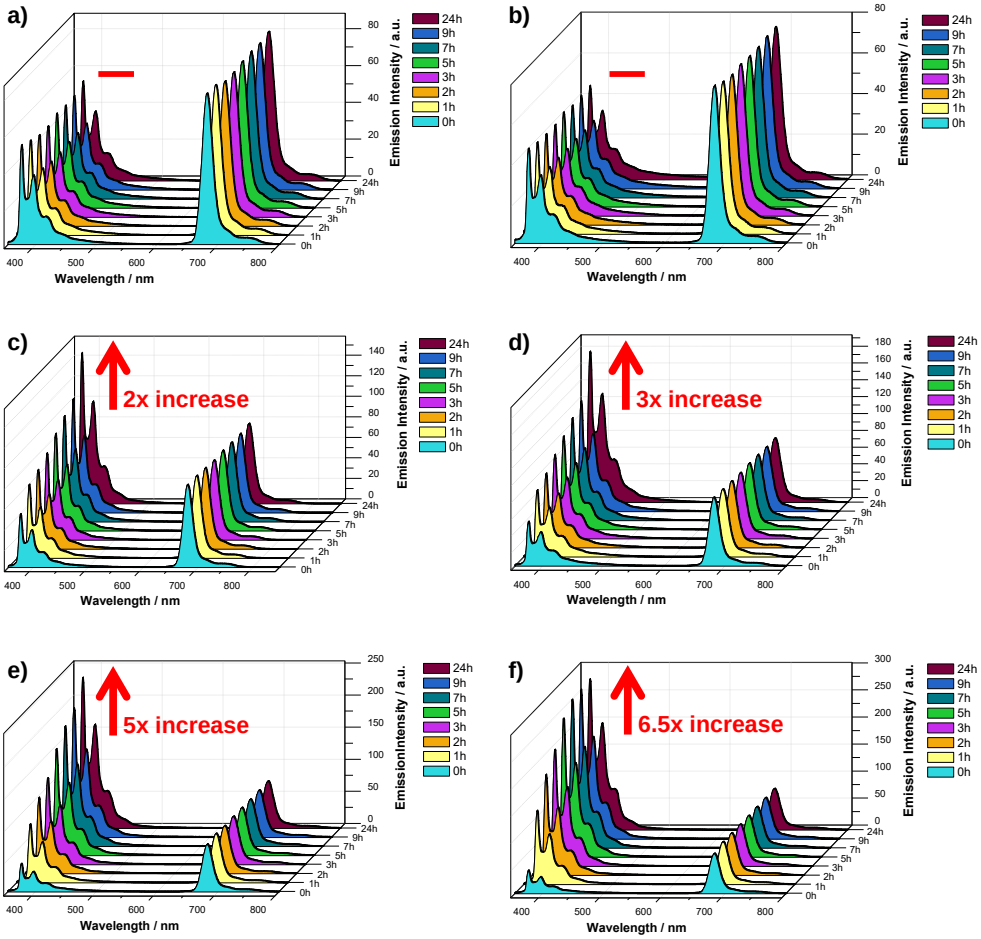

Figure 38. 3D representation of the fluorescence spectra of **1** in PBS (0.5% Cremophor EL) with a) 0 µM DTT, b) 2 µM DTT, c) 5 mM DTT, d) 10 mM DTT, e) 20 mM DTT and f) 50 mM DTT, from t = 0 h to t = 24 h.

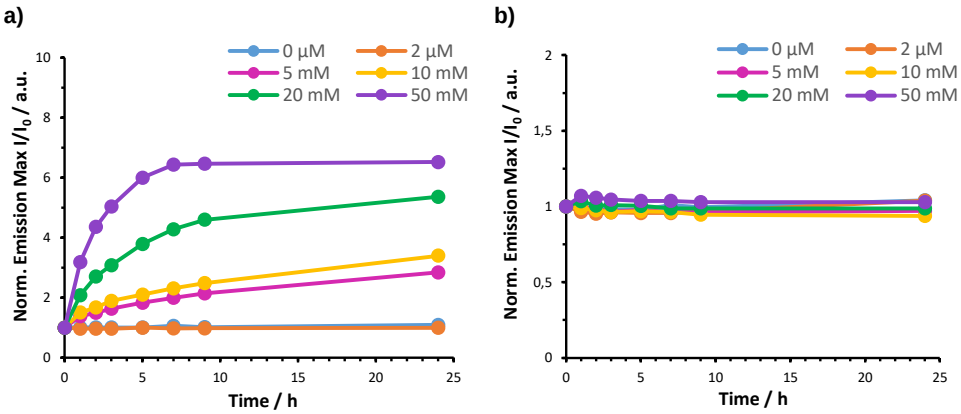

Figure 39. Normalized emission maximum of **1** in PBS (0.5% Cremophor EL) in function of time for a) the pyrene unit (F_{377}) and b) the SiPc (F_{680}). λ_{exc} = 345 nm.

(ii) pH-dependence

The UV-Vis and fluorescence spectra of **1** in PBS buffer were also monitored at decreasing pH values. As can be seen in Figure 40, the absorption bands of **1** remain unchanged at the three different pH values, indicating that the compound is stable and that there is no protonation of the Pc meso nitrogens at all experiment conditions. The same conclusion could be drawn from ^{1}H-NMR data, the spectrum not showing any significant change when set at pH=5.

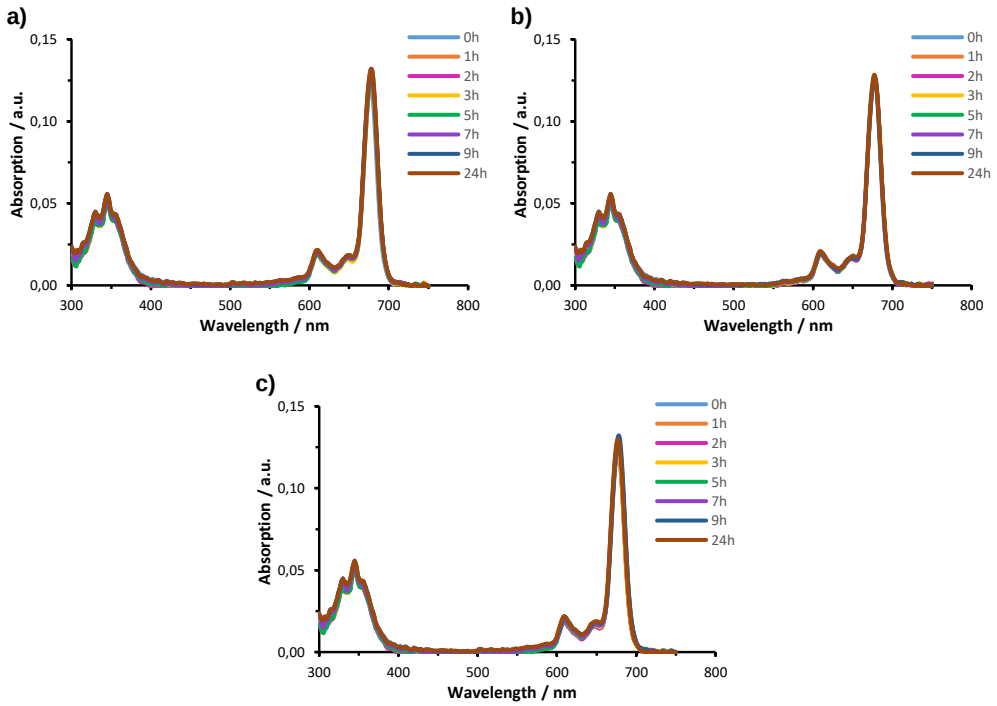

Figure 40. UV-Vis spectra of **1** in PBS (0.5% Cremophor EL) at a) pH = 5, b) pH = 6.8 and c) pH = 7.4, from t = 0 h to t = 24 h.

In contrast to disulfide cleavage, protonation of the amino group is instantaneous. The F_{680} signal is recuperated immediately after sample preparation, and remains unchanged over the whole experiment (Figure 41). Thus, the degree of fluorescence recovery depends directly on the acidity of the medium, reaching a maximum effect at the slightly acidic pH of 5 (Figure 42).

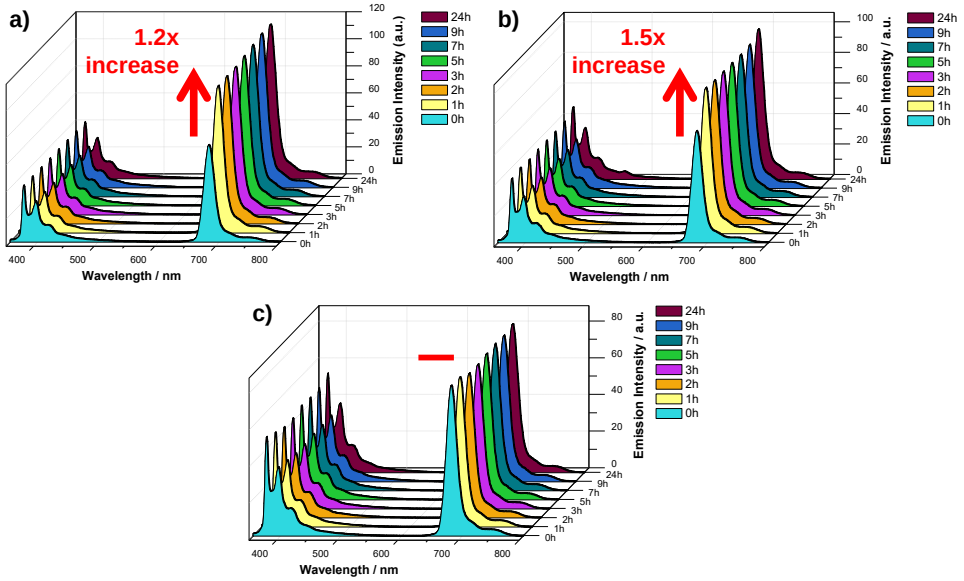

Figure 41. 3D representation of the fluorescence spectra of **1** in PBS (0.5% Cremophor EL) at a) pH = 5, b) pH = 6.8 and c) pH = 7.4, from t = 0 h to t =24 h.

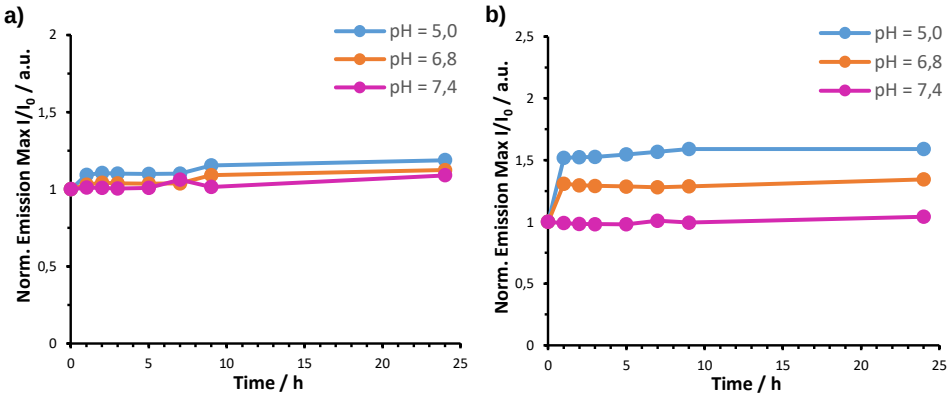

Figure 42. Normalized emission maximum of **1** in PBS (0.5% Cremophor EL) in function of time for a) the pyrene unit (F_{377}) and b) the SiPc (F_{680}). λ_{exc} = 345 nm.

(iii) Combined DTT- and pH-dependence

Finally, the combined effect of DTT and pH on F_{680} and F_{377} was evaluated (Figure 43). At pH 5, a complete recovery of F_{680} is observed, independent of the DTT concentration. Conversely, no significant changes in this peak were recorded at neutral pH (Figure 44b). F_{377} shows no increases in the absence of DTT or at low (2 µm) concentration, at both pH 5 and 7.4. With stronger reducing conditions and at pH 5, a moderate increase of F_{377} was noted, while samples at pH 7.4 present a pronounced F_{377} enhancement, up to 6.5-fold for 50 mM DTT.

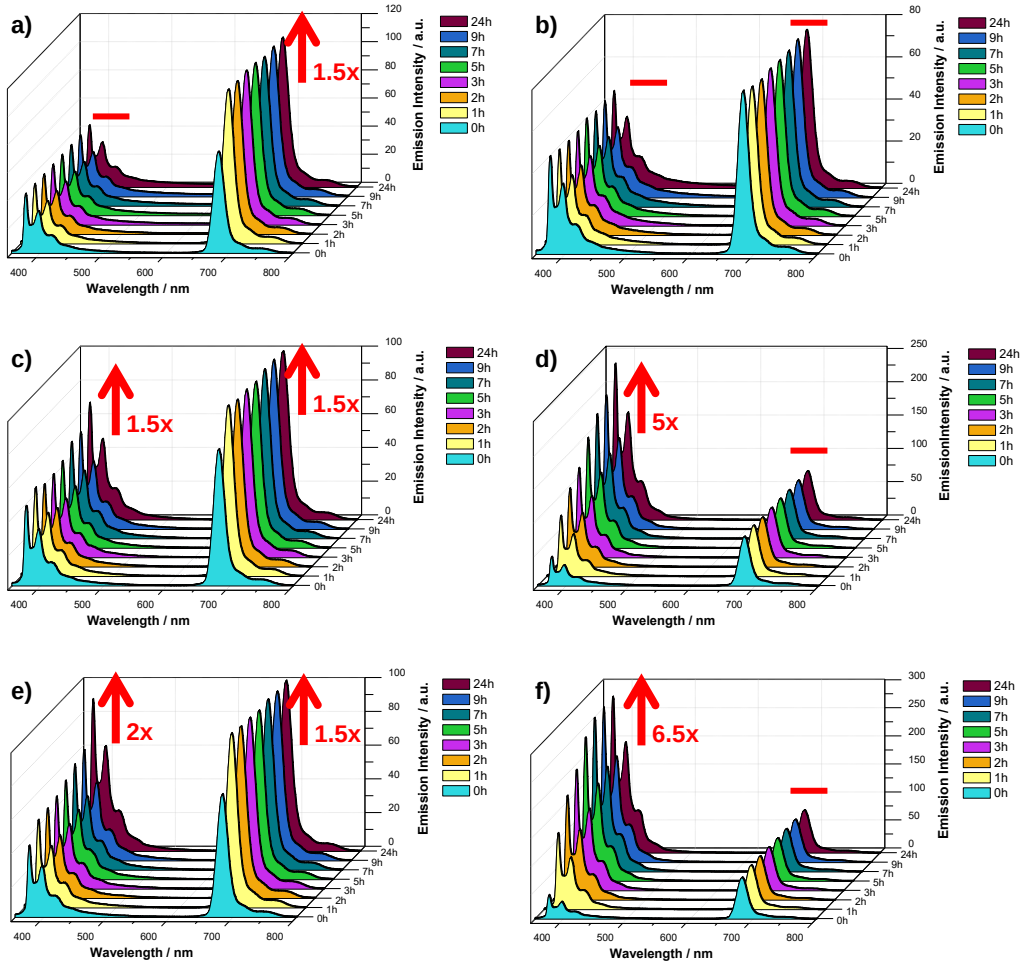

Figure 43. 3D representation of the fluorescence spectra of **1** in PBS (0.5% Cremophor EL) with a) 2 µM DTT – pH 5, b) 2 µM DTT – pH 7.4, c) 20 mM DTT – pH 5, d) 20 mM DTT – pH 7.4, e) 50 mM DTT – pH 5 and f) 50 mM DTT – pH 7.4, from t = 0 h to t = 24 h.

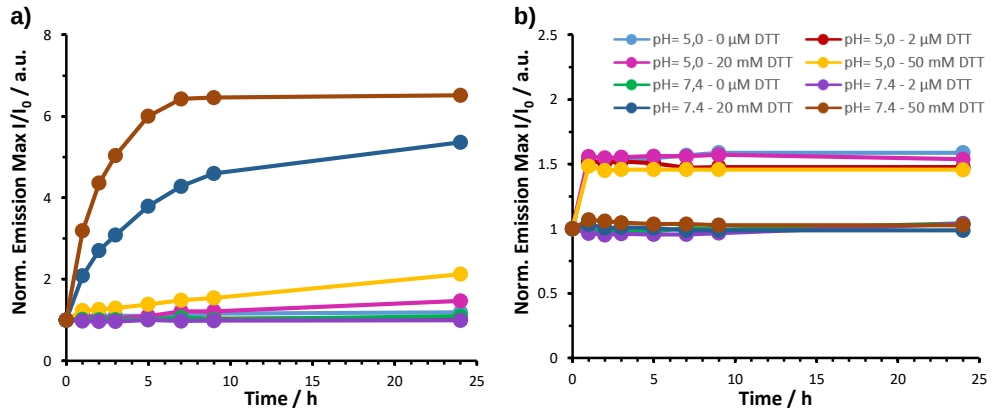

Figure 44. Normalized emission maximum of **1** in PBS (0.5% Cremophor EL) in function of time for a) the pyrene unit (F_{377}) and b) the SiPc (F_{680}). λ_{exc} = 345 nm.

1.3.2 Dependence of singlet oxygen generation

In order to activate $^1O_2$ production, $h\nu_{>530}$ needs to be considered as a third (physical) input, in combination with the two previous chemical ones. $^1O_2$ studies were performed in the same buffer conditions, measuring the rate of DPBF photodegradation, which is proportional to the amount of $^1O_2$ formation. Figure 45a shows the scavenger absorption decay at 414 nm for three DTT concentrations (i.e., 0, 2 µM and 20 mM), sensitized by **1** upon $h\nu_{>530}$ illumination, demonstrating that more efficient $^1O_2$ generation results from samples exposed to a higher concentration of DTT. Similar experiments were performed to examine the effect of pH on $^1O_2$ production (Figure 45b), showing that at lower pH $^1O_2$ production is more efficient. We attribute this to the higher degree of amino protonation. To complete the photochemical study of **1**, Figure 45c shows the combined effect of DTT and pH. Importantly, all concentrations of DTT (including 0 µM DTT) at pH 5, generated $^1O_2$ at a faster rate than even the most concentrated (20 mM DTT) solution at pH 7.4. From these results we conclude that although $^1O_2$ sensitization is effected by the concentration of DTT, the most important factor to obtain a high response is low pH. Moreover, dark control experiments confirm that, under all conditions, **1** is unable to produce $^1O_2$ without $h\nu_{>530}$ illumination.

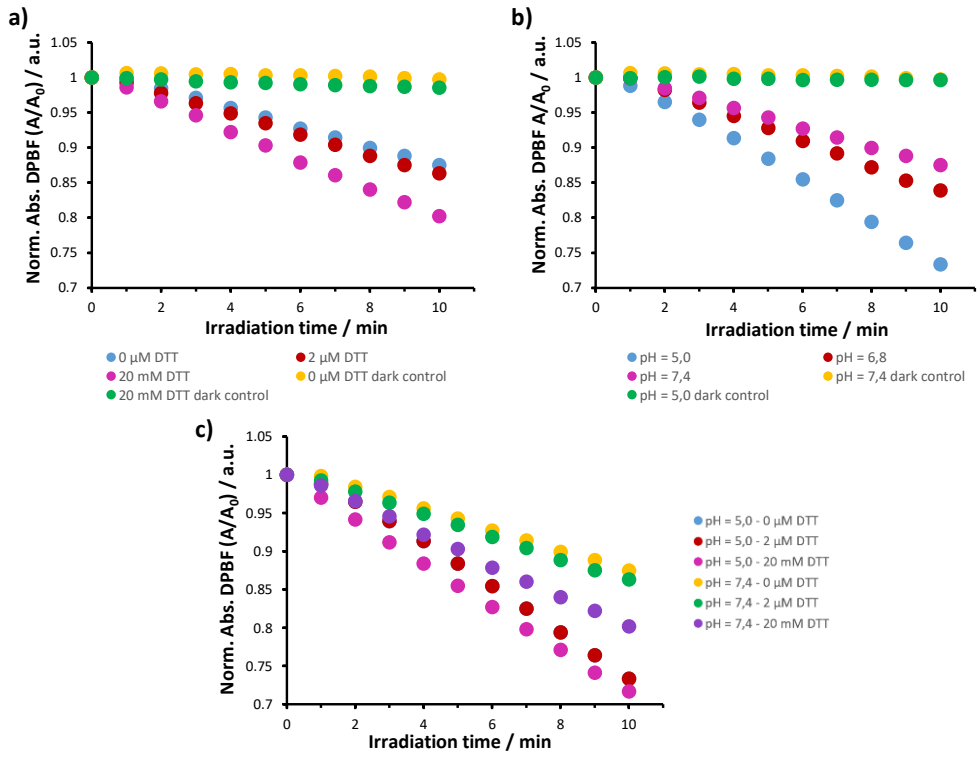

Figure 45. Normalized absorption (A/A_0) of DPBF over time, which shows its photodegradation rate sensitized by **1** upon excitation with light with wavelengths above 530 nm, at a) different DTT concentrations, b) different pH values, and c) the combined effect of DTT and pH.

1.4 Multifunctional logic in a photosensitizer with triple-mode fluorescent and photodynamic activity

In an effort to utilize the above photochemical pathways for the development of multimodal cellular imaging and PDT applications, a logical analysis of the interrelations between different input and output functions shown in Figure 30 is beneficial. Inputs and outputs can be encoded as binary digits (i.e., off = 0, on = 1), following positive logic conventions.[130] DTT is considered as input A, with 0 and 20 mM assigned to the 0 and 1 states. The pH stimulus is input B, for which pH 7.4 and 5, correlating with low and high proton concentrations, respectively, correspond to the 0 and 1 states. Finally, $h\nu_{>530nm}$ irradiation represents input C, for which "off" and "on" correspond to the 0 and 1 states. Importantly, this input should not be confused with the excitation light required for fluorescence measurements (i.e., at 345 nm). The corresponding outputs are F_{377} (output A), F_{680} (output B) and $^1O_2$ generation (output C), which can each be non-activated or activated, corresponding to 0 or 1 states.

With these conventions in mind, and with the goal of fabricating a system that can selectively activate the three different imaging and/or therapeutic functions, the output signals of the PS should evolve from complementary logic operations with different input combinations. To evaluate such differential responses, we first analyzed the three outputs upon applying binary stimuli combinations, with the third input in the "0" state (Figure 46).

[130] J. Andréasson, U. Pischel, *Chem. Soc. Rev.* **2015**, *44*, 1053–1069.

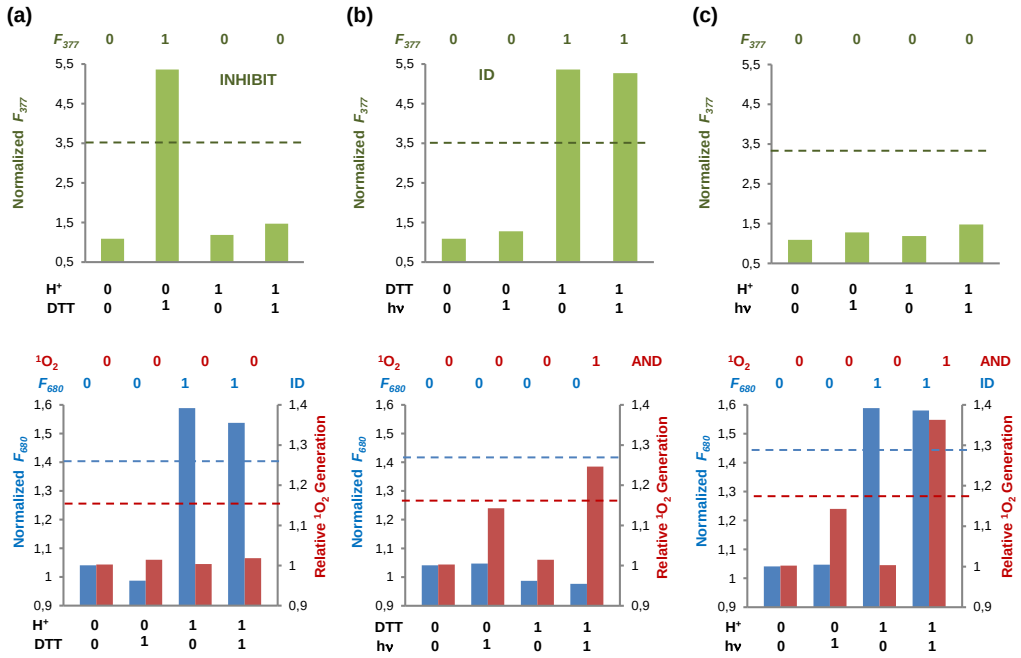

Figure 46. Performance of logic gate functions based on F_{377} (green data), F_{680} (blue) and $^1O_2$ (red) upon applying different stimuli pairs: (a) H^+ and DTT, hν = 0; (b) DTT and hν, H^+ = 0; (c) H^+ and hν, DTT = 0; hν meaning light above 530 nm. Input combinations and output responses (off = 0, on = 1) are shown at the bottom and top of each graph, respectively. The bars show output values for each gate as the Y-axis label, with respect to threshold values indicated by dashed lines. Emission data are normalized as I/I_0, while relative $^1O_2$ generation is given by DPBF absorption decay normalized as A_0/A. Due to normalization, a value of 1 in any Y-axis means zero response of the system.

The first conclusion that can be drawn from this analysis is that F_{680} and F_{377} can be selectively activated. In the absence of input C (Figure 46a), **1** always outputs F_{680} as 1 in acidic pH and 0 in neutral pH, independent of DTT concentration (Figure 46a, blue bars). This is consistent with an *identity* (ID) gate that identifies F_{680} to the logic input of protons. F_{377}, in turn, is sensitive to DTT; yet acidic pH quenches the DTT-mediated disulfide cleavage reaction (Figure 46a, green bars).[131] This leads to an INHIBIT logic operation of pH on the F_{377} response to DTT. Taken in concert, these fluorescent responses are complementary to one another and could find use in bioimaging applications.

In both of the other two dual-input scenarios, input C ($h\nu_{>530}$) does not affect the fluorescence output signals. As expected, F_{377} and F_{680} operate as ID logic gates that identify with DTT (Figure 46b, green bars) and protons (Figure 46c, blue bars), respectively. In turn, $h\nu_{>530}$ irradiation leads to $^1O_2$ sensitization by **1**, providing an alternative output signal, and enabling the construction of two AND logic gates based on the positive

[131] P. T. Corbett, J. Leclaire, L. Vial, K. R. West, J.-L. Wietor, J. K. M. Sanders, S. Otto, *Chem. Rev.* **2006**, *106*, 3652–3711.

dependence of $^1O_2$ production with either pH or DTT and light (Figure 46b-c, red bars). The threshold value in this case was set according to Figure 46c, because the effect of pH on $^1O_2$ production is much more relevant than DTT. Indeed, the $^1O_2$ response at pH 5 more than doubles that at neutral pH.

Now that threshold values for each output have been established, the three different output signals can separately be represented in function of all three inputs, which combine in eight possible ternary input combinations (Figure 47).

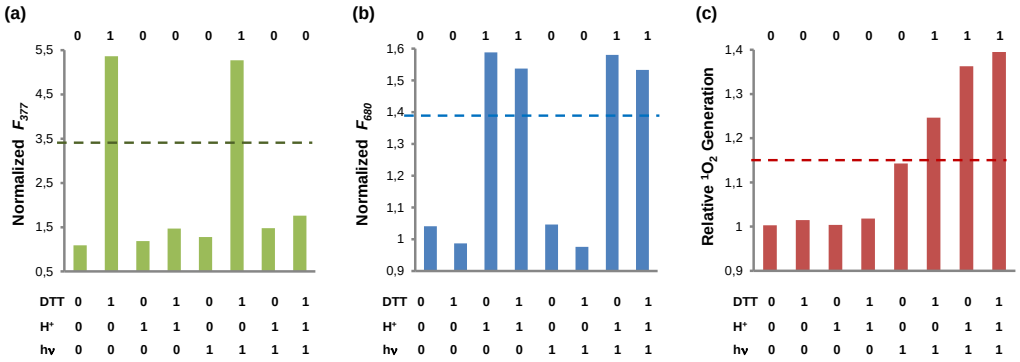

Figure 47. Performance of logic functions based on a) F_{377} (green data), b) F_{680} (blue) and c) $^1O_2$ (red) upon applying different ternary combination of H^+, DTT and hv input stimuli. Input combinations and output responses (off = 0, on = 1) are shown at the bottom and top of each graph, respectively. The graph bars show output values for each function as the Y-axis label, with respect to threshold values indicated by dashed lines. Emission data are normalized as I/I_0, while relative $^1O_2$ generation is given by DPBF absorption decay normalized as A_0/A. Due to normalization, a value of 1 in any Y-axis means zero response of the system.

As can be concluded from the above graphs, the eight possible ternary input combinations lead to the logic system depicted in Figure 48, and its corresponding truth table (Table 6).

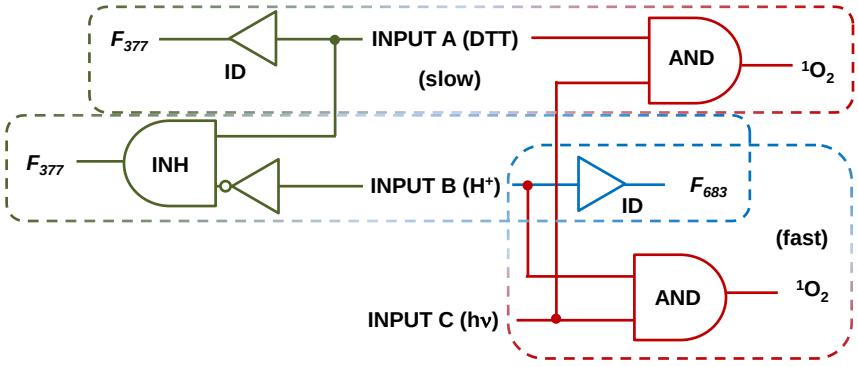

Figure 48. Logic circuit for SiPc **1**. Dashed rectangles represent combinations of logic operations that allow the selective and sequential activation of two different output signals through different dual combinations of input stimuli: F_{377} / $^1O_2$ (green/red), F_{377} / F_{680} (green/blue) or F_{680} / $^1O_2$ (blue/red).

Table 6. Truth table for the three-input-dependent molecular logic system SiPc **1**.

Entry	Input A (DTT)	Input B (H^+)	Input C (hv)	Output A (F_{377})	Output B (F_{680})	Output C ($^1O_2$)
1	0	0	0	0	0	0
2	1	0	0	1	0	0
3	0	1	0	0	1	0
4	1	1	0	0	1	0
5	0	0	1	0	0	0
6	1	0	1	1	0	1
7	0	1	1	0	1	1
8	1	1	1	0	1	1

Most notably, there are combinations of inputs that activate only one output fluorescence signal (entries 2 for F_{377} and 3/4 for F_{680}) with no $^1O_2$ response. In turn, $^1O_2$ production can be switched on with three input combinations, together with either F_{377} (entry 6) or F_{680} (entries 7/8). Taken together, this setup would allow for the application of a stimuli sequence that first activates imaging at either of the emission wavelengths, followed by PDT treatment upon $h\nu_{>530}$ irradiation, and finally re-imaging of the target at the alternative emission wavelength in a separate spectral region. In practice, because the kinetics of amino protonation is in the range of seconds and disulfide cleavage in the range of hours, while $^1O_2$ sensitization takes minutes, the most favourable situation for biomedical studies would be to monitor F_{680}, followed by PDT via irradiation, and monitoring F_{377} at the post-treatment imaging stage.

1.5 *In vitro* photodynamic activity of selected silicon phthalocynines

Subcellular localization and PDT efficacy experiments for the selected SiPc PS have been performed in the research group of Prof. Ángeles Juarranz de la Fuente, in collaboration with Alicia Zamarrón Moreno.

For the in *vitro* studies, cultured Hep-2 cells (a human larynx carcinoma cell line), SCC-13 cells (a human squamous cell carcinoma cell line) and HeLa cells (a human cervical carcinoma cell line) were used. The choice for these cell lines is well-reasoned, since they all represent types of cancer that are easily accessible for irradiation and PDT treatment. For the SiPcs on the other hand, it was chosen to study SiPc **1**, SiPc **3** and SiPc **4**, since they are the most activatable SiPc, the most hydrophilic SiPc, and the SiPc with the highest ϕ_Δ, respectively. Stock solutions of the SiPcs were prepared in DMSO, whereas work solutions for cell incubations were prepared from the stock solutions using cell medium, making sure the final concentration of DMSO was always lower than 0.5% (v/v).

1.5.1 Subcellular localization

In order to analyse the localization of the SiPcs inside the cells, Hep-2, SCC-13 and HeLa cells were incubated with SiPc **1**, SiPc **3**, or SiPc **4** ($2*10^{-6}$ M) for 18 h at 37°C, in the dark. Afterwards, cells were washed with PBS, and observed *in vivo* with a fluorescence microscope (Figure 49 - Figure 51).

The red fluorescence of SiPc **1** and SiPc **3** could be detected in all cell lines. In the case of SiPc **4**, on the other hand, no fluorescent signal could be observed inside the cells, from which it could be deduced that it was not taken up effectively. Furthermore, since the intracellular red fluorescence of SiPc **3** was higher than that of SiPc **1**, the amount of cell uptake could be directly correlated to the hydrophilicity of the PS structure, since SiPc **3**, bearing four triethylene glycol chains, is the most amphiphilic SiPc, followed by SiPc **1**, bearing only two triethylene glycol chains. SiPc **4** is purely hydrophobic in nature, which could explain the lack of cell uptake. With regards to the subcellular localization of SiPc **1** and **3**, no colocalization with the blue autofluorescence of the mitochondria was observed, and a nuclear localization can be ruled out because the nuclei (as seen by phase contrast) do not show any red fluorescence. The observed juxtanuclear red fluorescence indicates a possible uptake in the Golgi apparatus or endoplasmic reticulum,[132] although this should be confirmed in subsequent experiments, by the use of well-known markers for the endoplasmic reticulum (ER-Tracker®) and the Golgi apparatus (NBD®).

[132] E. Deni, A. Zamarrón, P. Bonaccorsi, M. Carmen Carreño, Á. Juarranz, F. Puntoriero, M. T. Sciortino, M. Ribagorda, A. Barattucci, *Eur. J. Med. Chem.* **2016**, *111*, 58–71.

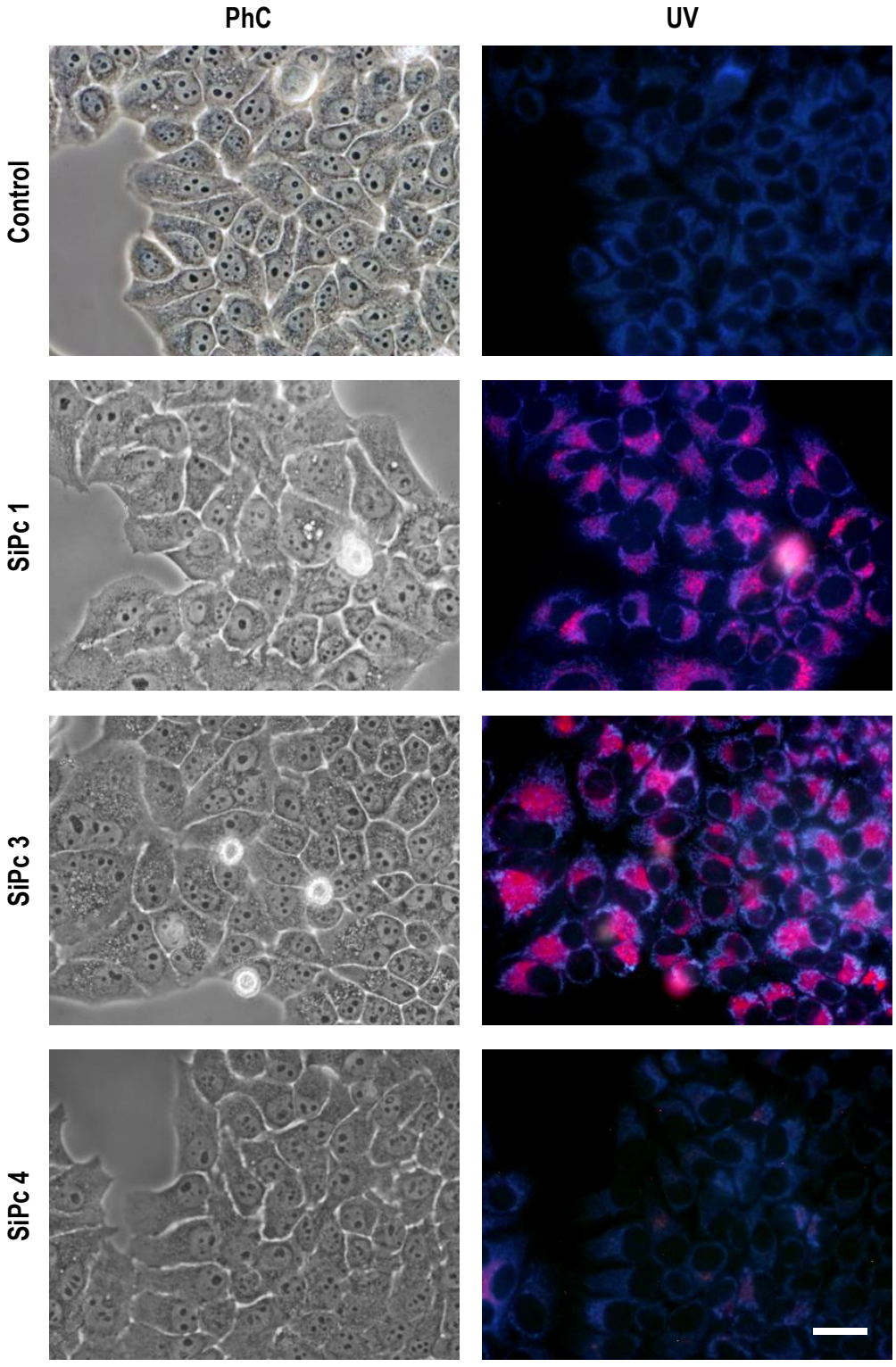
PhC
UV
Control
SiPc 1
SiPc 3
SiPc 4

Figure 49. Subcellular localization of SiPc **1**, SiPc **3** and SiPc **4** in HEp-2 cells. SiPc concentration: $2 \cdot 10^{-6}$ M. Scale bar: 20 µM.

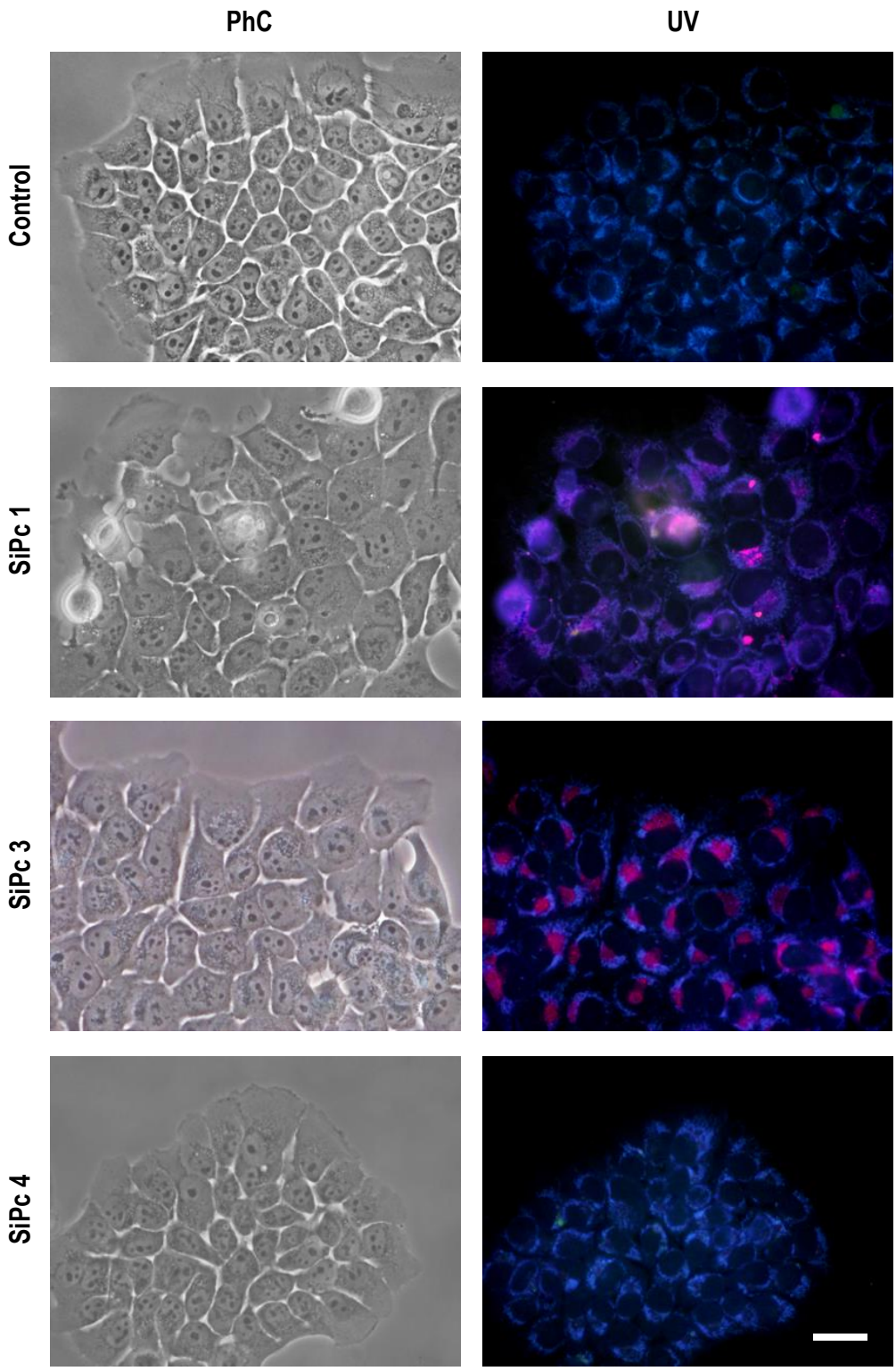

Figure 50. Subcellular localization of SiPc **1**, SiPc **3** and SiPc **4** in SCC-13 cells. SiPc concentration: $2*10^{-6}$ M. Scale bar: 20 µM.

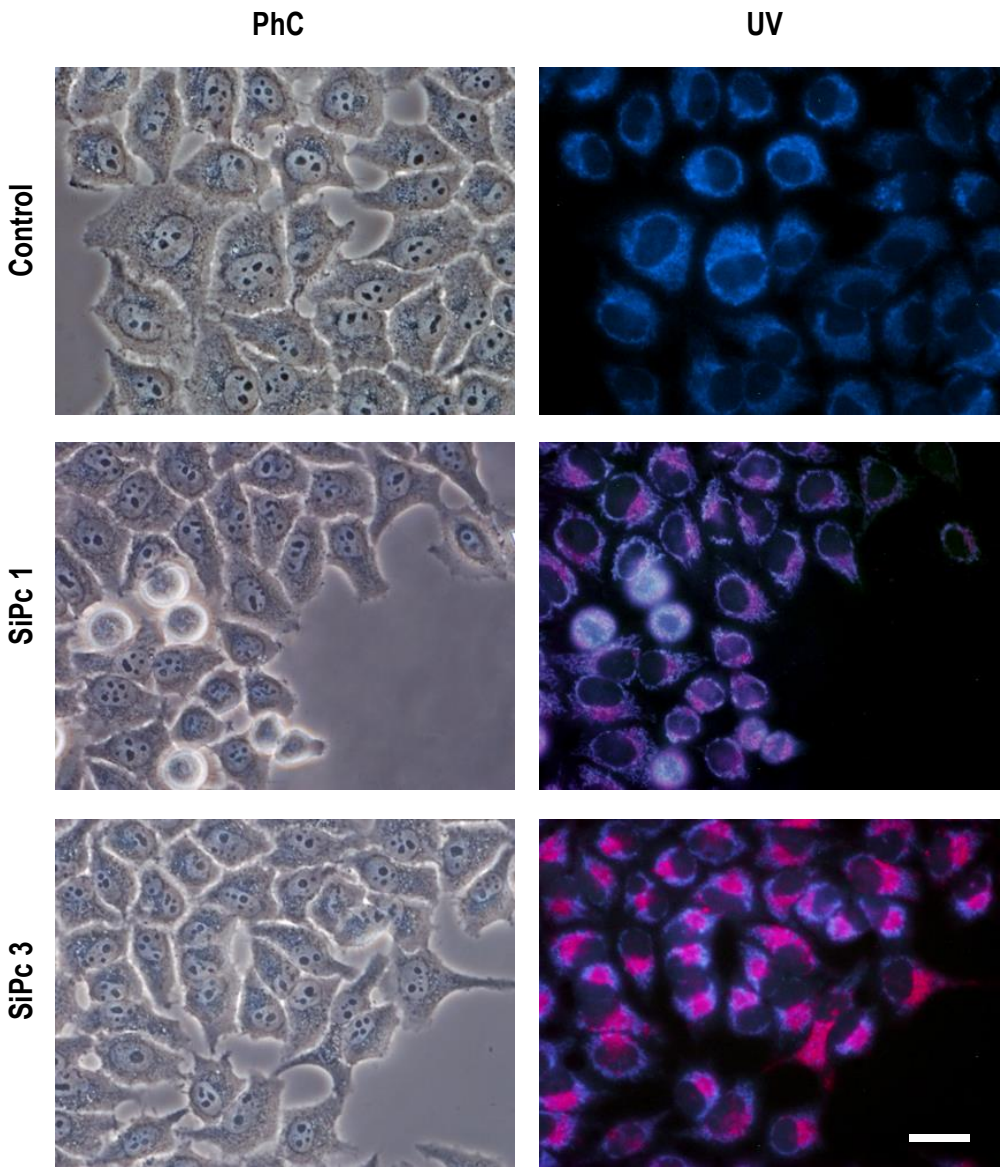

Figure 51. Subcellular localization of SiPc **1** and SiPc **3** in HeLa cells. SiPc concentration: $2*10^{-6}$ M. Scale bar: 20 µM.

1.5.2 Effects of PDT on cell morphology and cell survival

For photodynamic treatment, HeLa, SCC-13 and Hep-2 cells were incubated with different concentrations of SiPcs and irradiated with a red light emitting diode source.[133]

Changes in cell morphology after photodynamic treatment were analysed *in vivo* by phase contrast microscopy. As a result of the photodynamic treatment, cells treated by SiPc **1** and SiPc **3** revealed different morphological changes, whereas untreated cells showed spread morphology and homogeneous nuclei. For cells treated with SiPc **1**, a significant increase of unbound cells can be observed, with characteristics that indicate an apoptotic cell death, such as cell rounding and blebbing (Figure 52a - Figure 54a). Furthermore, for those cells that remained bound to the surface, a gradual cytoplasmic cell retraction can be observed. The observed results are similar in all treated cell lines, and their extend clearly depends on the SiPc concentration and the applied light dose. Photodynamic treatment with SiPc **3** resulted more harmful than in the case of SiPc **1**, in all the studied cell lines, which is in correspondence with their higher cell uptake results observed earlier. In general, almost all cells are now unbound to the surface, and show characteristics that indicate a necrotic cell death, such as loss of integrity of the plasma membrane (Figure 55a - Figure 57a). For SiPc **4** on the other hand, no significant effect of the photodynamic treatment could be observed. Furthermore, in the phase contrast images, some blue precipitates can be clearly observed, explaining the low to non-existing cell uptake results mentioned earlier (Figure 58a and Figure 59a).

The cellular toxicity induced by the different concentrations of the SiPcs **1**, **3** and **4** on HEp-2, SCC-13 and HeLa cells was evaluated by the MTT (3-(4,5-dimethylthiazol-2-yl)-2,5-diphenyltetrazolium bromide) assay,[134] and the results obtained are mean values and standard deviations from three independent experiments. Dark control experiments were carried out in parallel, incubating the cells with the same concentrations of SiPc, for 18h, in the dark. For both SiPc **1** and SiPc **3**, this resulted in the observation of a low toxicity in the absence of light towards Hep-2 cells, at both 1µM and 2µM of PS, whereas in SCC-13 and HeLa cells the dark cytotoxicity was negligible at both concentrations (Figure 52b - Figure 57b). This low dark toxicity in Hep-2 cells is however not problematic, since the toxicity upon irradiation of the PS by red light (RL) irradiation for 1 min (0,45 J/cm^2) or 2 min (0,90 J/cm^2) was significantly higher in both cases. In the case of SiPc **1,** at a concentration of 2 µM, a cell survival of only 21.30 ± 2.00% was observed after applying a light dose of 0,45 J/cm^2 in Hep-2 cells (Figure 52b). For SiPc **3** the cell survival was even lower, with values as low as 10.16 ± 0.17% being obtained at the lowest concentration (1 µM) and light dose (0,90 J/cm$^{2)}$ in Hep-2 cells (Figure 55b). Similar results were obtained

---

[133] For more information on the irradiation system, developed by Sega Invex at Universidad Autónoma de Madrid: http://www.uam.es/ss/Satellite/es/1242671166041/1242677464473/UAM_Desarrollo_FA/Desarrollo/Irradiadores_de_LEDs_para_Terapia_Fotodinamica_(TFD).htm

[134] T. Mosmann, *J. Immunol. Methods* **1983**, *65*, 55–63.

for SCC-13 (Figure 53b and Figure 56b) and HeLa cells (Figure 54b and Figure 57b). In conclusion, SiPc **3** is an extremely efficient PS at low light doses and concentrations, accompanied by a negligible dark cytotoxicity. As expected, for SiPc **4** no difference in toxicity can be observed before or after photodynamic treatment (Figure 58b and Figure 59b), since it was shown above that is was not effectively taken up by the cells.

a)

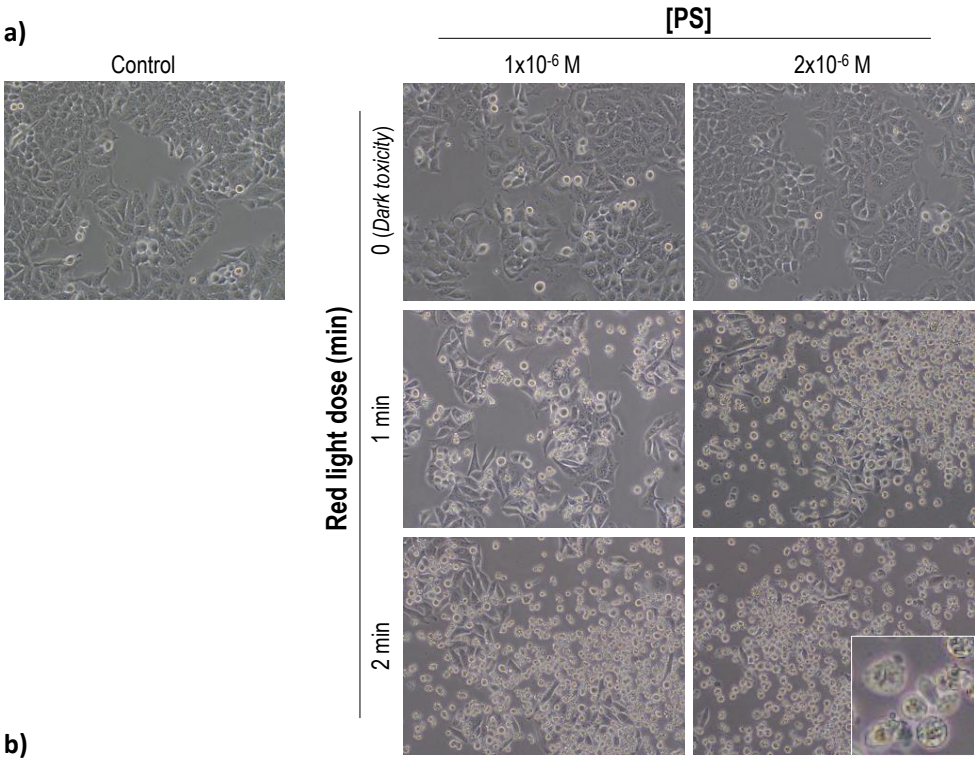

b)

Treatment conditions	Relative cell survival (%)
SiPc **1** 1 µM	75.23 ± 2.90
SiPc **1** 2 µM	73.41 ± 3.29
SiPc **1** 1 µM + 1 min RL	44.70 ± 1.95
SiPc **1** 1 µM + 2 min RL	42.61 ± 1.54
SiPc **1** 2 µM + 1 min RL	29.43 ± 3.89
SiPc **1** 2 µM + 2 min RL	21.30 ± 2.00

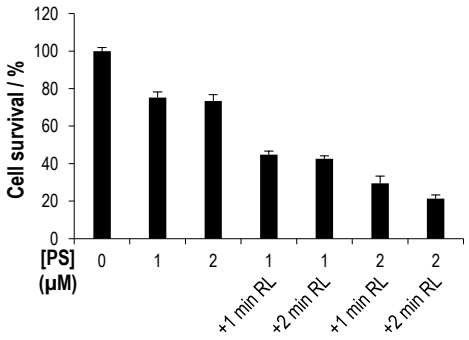

Figure 52. PDT effect of SiPc **1** on a) cell morphology and b) cell survival of HEp-2 cells upon irradiation for 1 or 2 min, corresponding to light doses from 0,45 to 0,90 J/cm^2, at different concentrations of SiPc (1 µM or 2 µM).

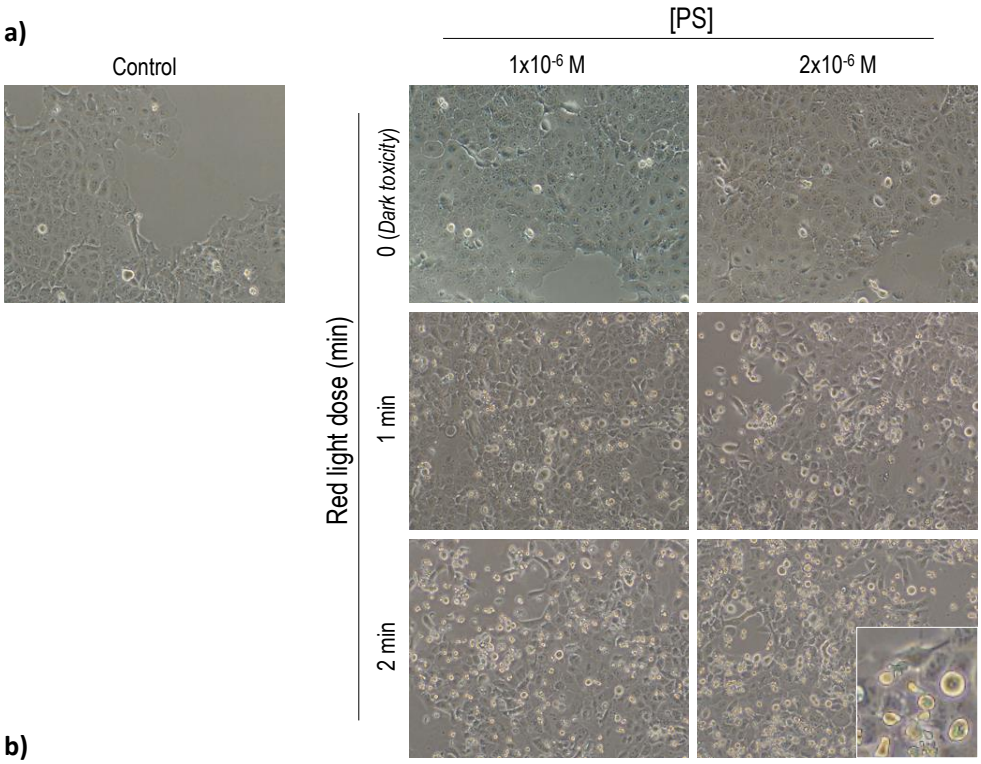

b)

Treatment conditions	Relative cell survival (%)
SiPc **1** 1 µM	94.85 ± 2.45
SiPc **1** 2 µM	93.49 ± 2.52
SiPc **1** 1 µM + 1 min RL	68.26 ± 1.95
SiPc **1** 1 µM + 2 min RL	63.64 ± 2.48
SiPc **1** 2 µM + 1 min RL	56.78 ± 3.52
SiPc **1** 2 µM + 2 min RL	45.79 ± 4.11

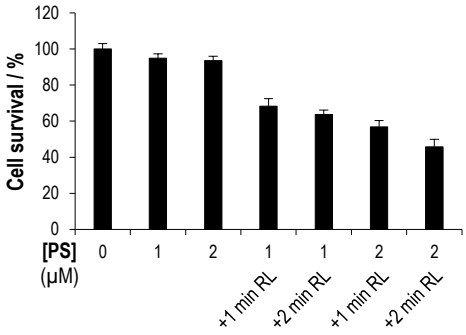

Figure 53. PDT effect of SiPc **1** on a) cell morphology and b) cell survival of SCC-13 cells upon irradiation for 1 or 2 min, corresponding to light doses from 0,45 to 0,90 J/cm^2, at different concentrations of SiPc (1 µM or 2 µM).

a)

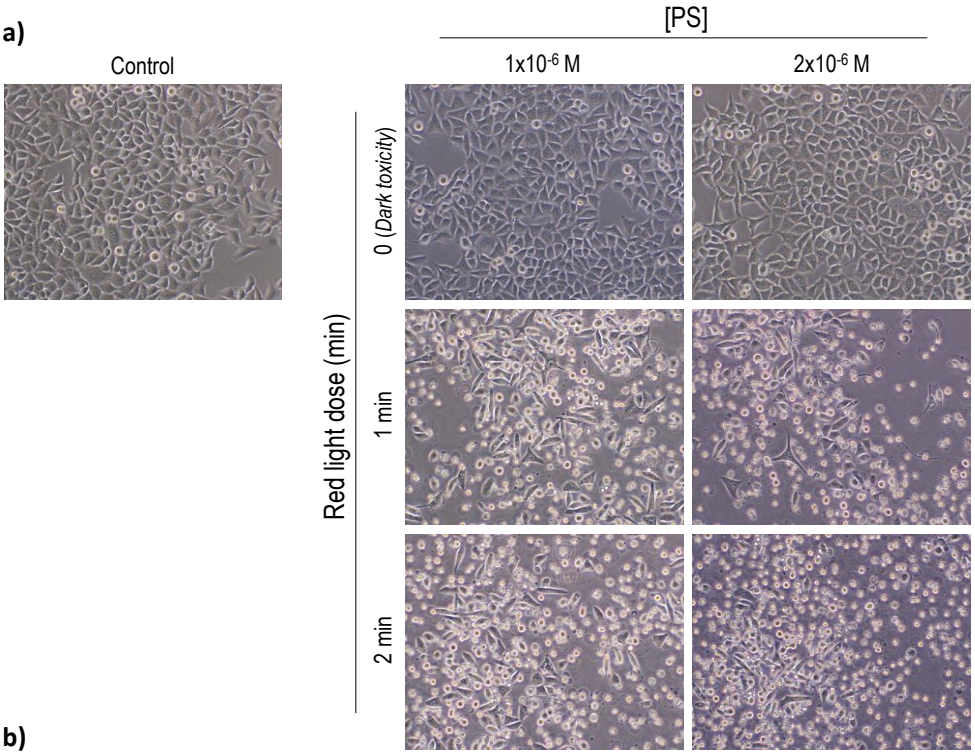

b)

Treatment conditions	Relative cell survival (%)
SiPc **1** 0.5 µM	96.58 ± 4.78
SiPc **1** 1 µM	90.30 ± 1.71
SiPc **1** 2 µM	87.43 ± 4.34
SiPc **1** 0.5 µM + 1 min RL	42.33 ± 3.99
SiPc **1** 0.5 µM + 2 min RL	30.22 ± 3.84
SiPc **1** 1 µM + 1 min RL	24.19 ± 5.81
SiPc **1** 1 µM + 2 min RL	15.93 ± 1.06
SiPc **1** 2 µM + 1 min RL	15.21 ± 0.94
SiPc **1** 2 µM + 2 min RL	12.15 ± 0.78

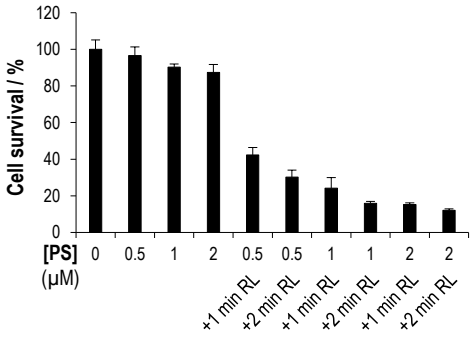

Figure 54. PDT effect of SiPc **1** on a) cell morphology and b) cell survival of HeLa cells upon irradiation for 1 or 2 min, corresponding to light doses from 0,45 to 0,90 J/cm^2, at different concentrations of SiPc (0.5 µM, 1 µM or 2 µM).

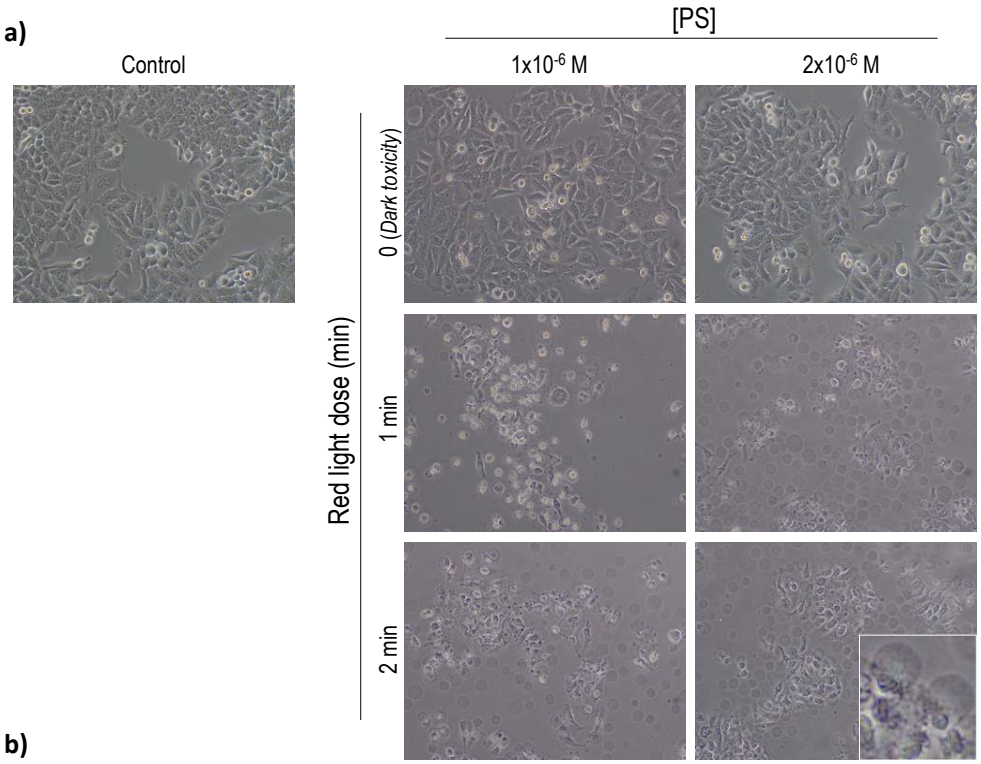

b)

Treatment conditions	Relative ell survival (%)
SiPc **3** 1 µM	75.20 ± 2.03
SiPc **3** 2 µM	70.83 ± 1.71
SiPc **3** 1 µM + 1 min RL	10.16 ± 0.17
SiPc **3** 1 µM + 2 min RL	9.63 ± 0.12
SiPc **3** 2 µM + 1 min RL	9.78 ± 0.32
SiPc **3** 2 µM + 2 min RL	9.21 ± 0.05

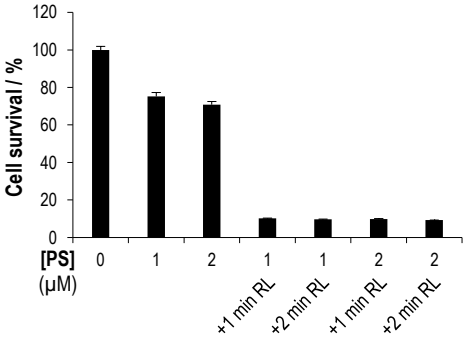

Figure 55. PDT effect of SiPc **3** on a) cell morphology and b) cell survival of HEp-2 cells upon irradiation for 1 or 2 min, corresponding to light doses from 0,45 to 0,90 J/cm^2, at different concentrations of SiPc (1 µM or 2 µM).

a)

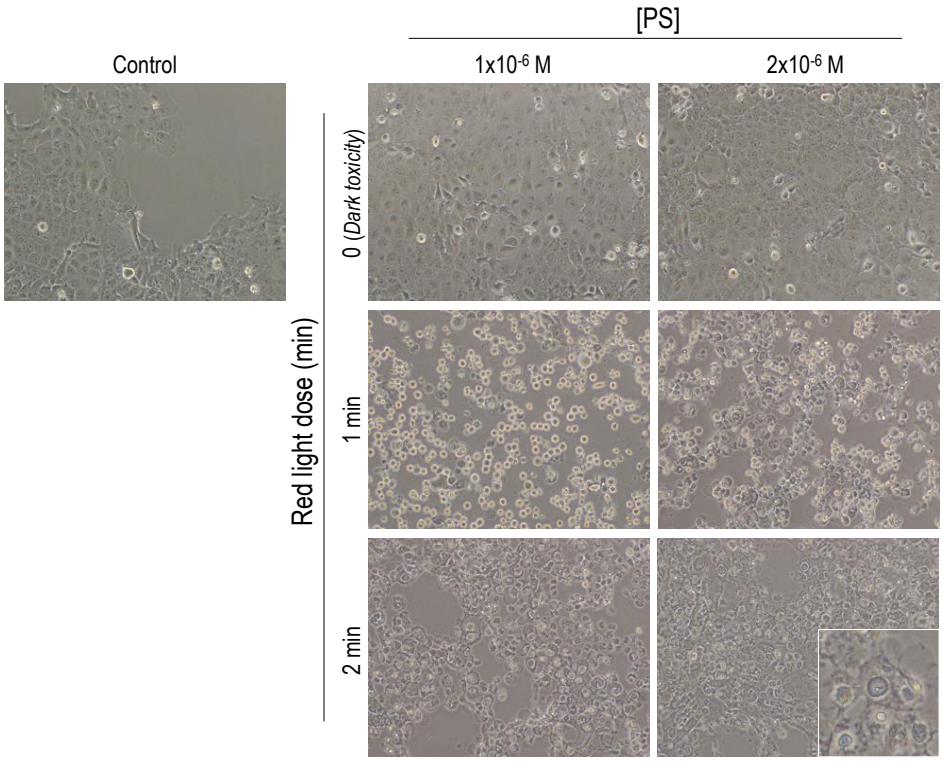

b)

Treatment conditions	Relative cell survival (%)
SiPc **3** 1 µM	99.10 ± 3.97
SiPc **3** 2 µM	98.93 ± 4.16
SiPc **3** 1 µM + 1 min RL	38.20 ± 4.26
SiPc **3** 1 µM + 2 min RL	14.75 ± 5.27
SiPc **3** 2 µM + 1 min RL	16.48 ± 3.07
SiPc **3** 2 µM + 2 min RL	15.87 ± 3.23

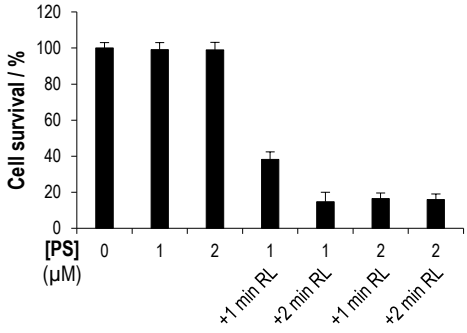

Figure 56. PDT effect of SiPc **3** on a) cell morphology and b) cell survival of SCC-13 cells upon irradiation for 1 or 2 min, corresponding to light doses from 0,45 to 0,90 J/cm^2, at different concentrations of SiPc (1 µM or 2 µM).

a)

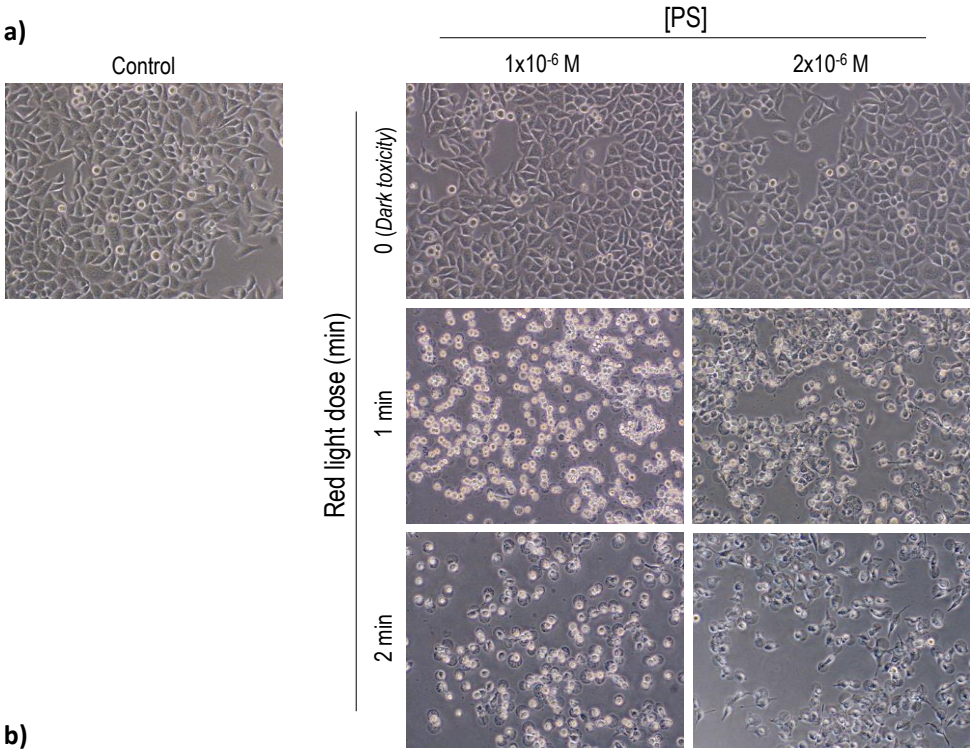

b)

Treatment conditions	Relative cell survival (%)
SiPc **3** 0.5 µM	89.49 ± 4.47
SiPc **3** 1 µM	82.82 ± 4.40
SiPc **3** 2 µM	77.76 ± 2.88
SiPc **3** 0.5 µM + 1 min RL	15.94 ± 1.19
SiPc **3** 0.5 µM + 2 min RL	11.49 ± 0.80
SiPc **3** 1 µM + 1 min RL	12.14 ± 0.52
SiPc **3** 1 µM + 2 min RL	11.23 ± 0.27
SiPc **3** 2 µM + 1 min RL	11.33 ± 1.02
SiPc **3** 2 µM + 2 min RL	10.22 ± 0.79

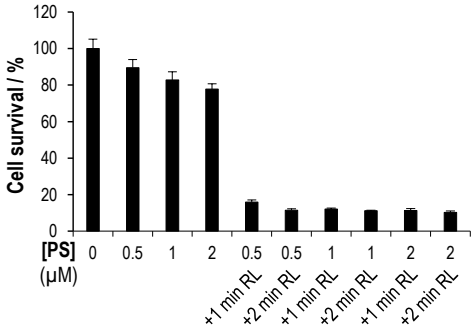

Figure 57. PDT effect of SiPc **3** on a) cell morphology and b) cell survival of HeLa cells upon irradiation for 1 or 2 min, corresponding to light doses from 0,45 to 0,90 J/cm^2, at different concentrations of SiPc (0.5 µM, 1 µM or 2 µM).

a)

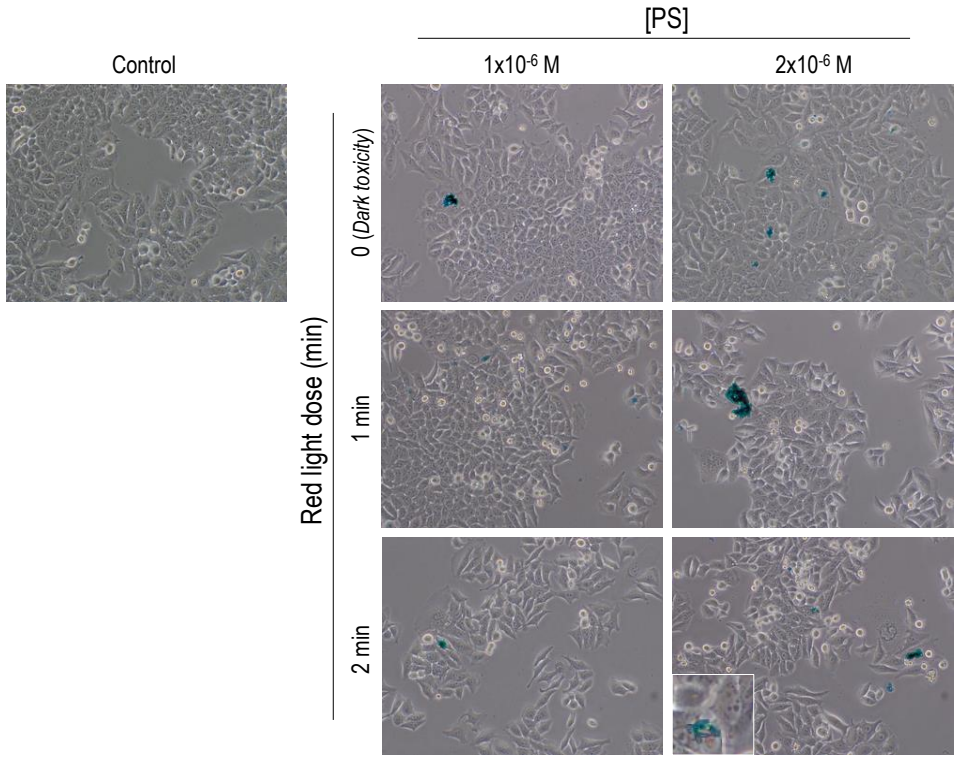

b)

Treatment conditions	Relative cell survival (%)
SiPc **4** 1 µM	80.15 ± 2.12
SiPc **4** 2 µM	79.67 ± 4.28
SiPc **4** 1 µM + 1 min RL	76.66 ± 1.79
SiPc **4** 1 µM + 2 min RL	75.91 ± 0.62
SiPc **4** 2 µM + 1 min RL	69.79 ± 5.16
SiPc **4** 2 µM + 2 min RL	66.96 ± 2.02

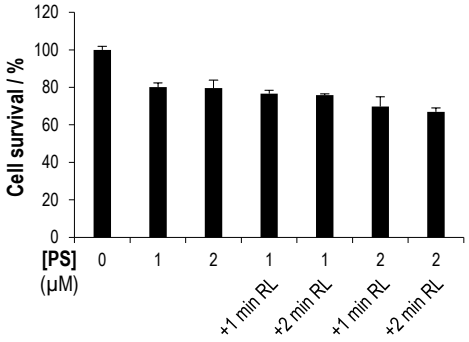

Figure 58. PDT effect of SiPc **4** on a) cell morphology and b) cell survival of HEp-2 cells. upon irradiation for 1 or 2 min, corresponding to light doses from 0,45 to 0,90 J/cm^2, at different concentrations of SiPc (1 µM or 2 µM).

a)

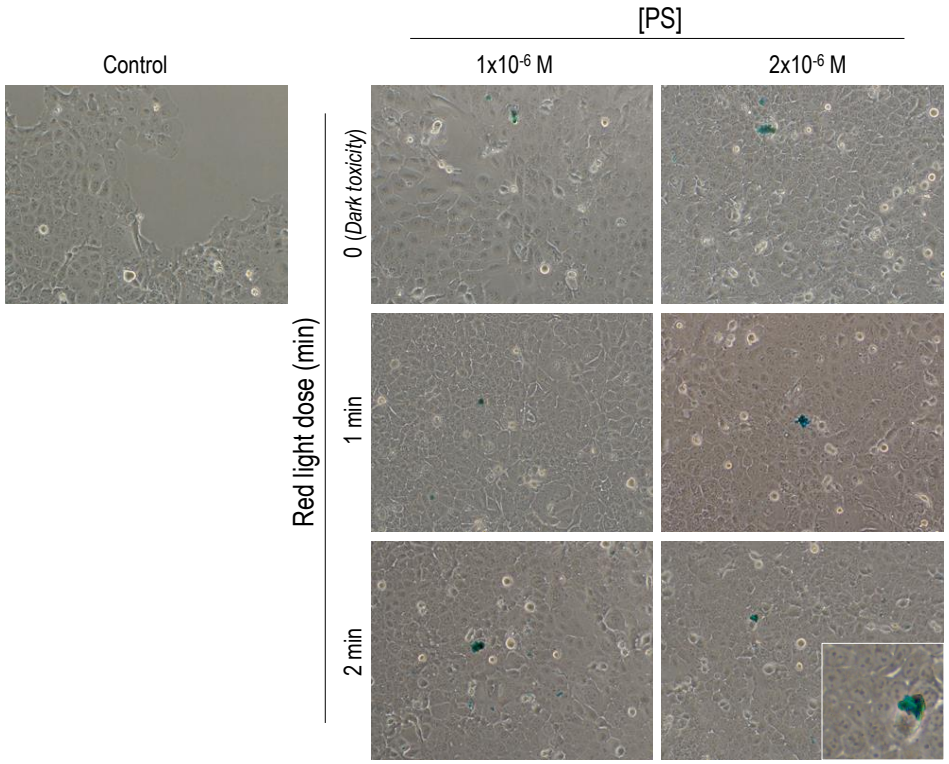

b)

Treatment conditions	Relative cell survival (%)
SiPc **4** 1 µM	96.59 ± 3.26
SiPc **4** 2 µM	95.70 ± 5.30
SiPc **4** 1 µM + 1 min RL	95.44 ± 2.55
SiPc **4** 1 µM + 2 min RL	94.66 ± 4.85
SiPc **4** 2 µM + 1 min RL	94.42 ± 4.50
SiPc **4** 2 µM + 2 min RL	93.14 ± 3.23

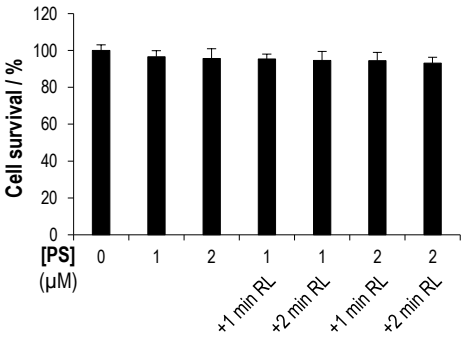

Figure 59. PDT effect of SiPc **4** on a) cell morphology and b) cell survival of SCC-13 cells. upon irradiation for 1 or 2 min, corresponding to light doses from 0,45 to 0,90 J/cm^2, at different concentrations of SiPc (1 µM or 2 µM).

2

Neutral subphthalocyanines as photosensitizers for photodynamic therapy

2.1 State of the art

Apart from some cationic SubPc derivatives, which will be discussed in their appropriate chapter (Chapter 2 – Subchapter 2), there has been little mention in literature about SubPcs in PDT. The early impetus for research into SubPcs stemmed from their use in ring expansion reactions to prepare unsymmetrical A_3B-type Pcs, which could in principle be useful indirectly for PDT since the consequent monofunctionalization of the obtained PS would allow them to be coupled with tumor specific antibodies or other target selective groups.[135] Later on, the focus has shifted towards their technological applications, for example, as octupolar non-linear optical materials,[136] photovoltaic devices[137] and photosynthetic models for the study of photoinduced electron and energy transfer

[135] a] N. Kobayashi, R. Kondo, S. Nakajima, T. Osa, *J. Am. Chem. Soc.* **1990**, *112*, 9640–9641; b) R. G. Senz, R. Herter, *Proc. SPIE* **1995**, *2325*, 349–350; c] P. M. R. Pereira, B. Korsak, B. Sarmento, R. J. Schneider, R. Fernandes, J. P. C. Tomé, *Org. Biomol. Chem.* **2015**, *13*, 2518–2529.

[136] a] A. Sastre, T. Torres, M. A. Díaz-García, F. Agulló-López, C. Dhenaut, S. Brasselet, I. Ledoux, J. Zyss, *J. Am. Chem. Soc.* **1996**, *118*, 2746–2747; b) B. del Rey, U. Keller, T. Torres, G. Rojo, F. Agulló-López, S. Nonell, C. Martí, S. Brasselet, I. Ledoux, J. Zyss, *J. Am. Chem. Soc.* **1998**, *120*, 12808–12817; c] D. Dini, S. Vagin, M. Hanack, V. Amendola, M. Meneghetti, *Chem. Commun.* **2005**, 3796–3798.

[137] K. L. Mutolo, E. I. Mayo, B. P. Rand, S. R. Forrest, M. E. Thompson, *J. Am. Chem. Soc.* **2006**, *128*, 8108–8109.

processes.[138] Reports on the bio-medical applications of this class of functional dyes, however, remain extremely rare.

Nevertheless, the use of SubPcs in PDT could be of great interest, as they display various beneficial characteristics. First, SubPcs are intrinsically cone-shaped, which hinders π-π stacking, resulting in a low aggregation tendency and high solubility. Low aggregation is very beneficial in PDT, as it results in less quenching of $^1O_2$ generation. Second, the absorption maximum of SubPcs lies around 560-600 nm, close to the optimal therapeutic window, so that only a small proportion of the irradiation light would be absorbed by the surrounding tissue and the irradiation would be more effective. Finally, preliminary photophysical studies have shown that SubPcs can exhibit high ϕ_t and ϕ_Δ,[139] making them potentially useful as PS for PDT and other photosensitizing applications.

The use of SubPcs in PDT was reported for the first time in 2007, when Ng and co-workers, published the synthesis, characterization and photophysical properties of a series of axially substituted SubPcs and their *in vitro* photodynamic activity (Figure 60).[140]

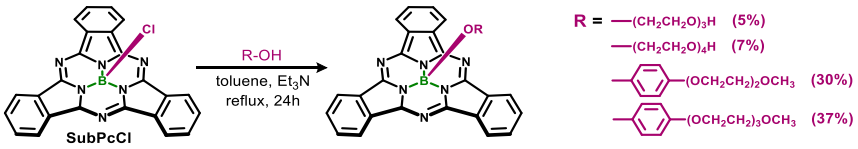

Figure 60. Series of SubPcs substituted axially with an oligoethylene glycol chain or a *p*-phenoxy oligoethylene glycol methyl ether chain, as synthesized by Ng. and co-workers.[140]

As axial substituents, Ng and co-workers chose for a series of oligoethylene glycol chains, to increase the solubility and biocompatibility of the SubPc compounds. They carried out the substitution starting from the commercially available SubPc chloride (SubPcCl) with the corresponding alcohols, in the presence of triethylamine in toluene, obtaining the alkoxy analogues with very low yields and the phenoxy analogues with slightly higher yields. These yields are in accordance to results previously described when using these reaction conditions, however better alternatives are now available, especially for the substitution with aliphatic alcohols.[141] The photodynamic activity of the resulting SubPcs was investigated against two different cell lines, namely HepG2 human hepatocarcinoma cells and HT29 human colon adenocarcinoma cells. All molecules showed a substantial cell

---

138 a] D. González-Rodríguez, T. Torres, D. M. Guldi, J. Rivera, L. Echegoyen, *Org. Lett.* **2002**, *4*, 335–338; b) D. González-Rodríguez, T. Torres, D. M. Guldi, J. Rivera, M. A. Herranz, L. Echegoyen, *J. Am. Chem. Soc.* **2004**, *126*, 6301–6313; c] R. S. Iglesias, C. G. Claessens, T. Torres, G. M. A. Rahman, D. M. Guldi, *Chem. Commun.* **2005**, 2113–2115; d) D. González-Rodríguez, T. Torres, M. M. Olmstead, J. Rivera, M. Á. Herranz, L. Echegoyen, C. A. Castellanos, D. M. Guldi, *J. Am. Chem. Soc.* **2006**, *128*, 10680–10681.

139 S. Nonell, N. Rubio, B. del Rey, T. Torres, *J. Chem. Soc. Perkin Trans. 2* **2000**, 1091–1094.

140 H. Xu, X.-J. Jiang, E. Y. M. Chan, W.-P. Fong, D. K. P. Ng, *Org. Biomol. Chem.* **2007**, *5*, 3987–3992.

141 J. Guilleme, D. González-Rodríguez, T. Torres, *Angew. Chem. Int. Ed.* **2011**, *123*, 3568–3571.

uptake, with localization in the cell cytoplasm. However, there was a discrepancy in the phototoxicity and in particular that of the alkoxy analogues, who had a higher ϕ_Δ as compared to the phenoxy analogues but showed almost no phototoxicity. Further tests revealed that the alkoxy analogues were highly unstable upon irradiation in the cell medium, whereas for the phenoxy analogues the photostability was a lot better, resulting in a higher phototoxicity with IC_{50} values down to 0.02 μM.

2.2 Molecular design, synthesis and characterization of a series of neutral subphthalocyanine photosensitizers

In view of the lack of examples about the use of SubPcs in PDT, this is a mostly unexplored research field. However, as previously mentioned, the interesting characteristics of SubPcs deserve that some more investigation is done in the area. Therefore, the specific objective of this subchapter is the design and synthesis of a series of axially substituted SubPc derivatives. Taking into account the positive results obtained in the previous subchapter, with a series of building blocks for axial substitution designed to impart enhanced fluorescence and photodynamic properties in SiPcs, we decided to incorporate the same building blocks at the axial positions of SubPcs (Figure 61). Furthermore, we aim to investigate the photophysical properties of the obtained SubPcs, and study their *in vitro* photodynamic activity towards a series of tumoral cell lines, including Hep-2, SCC-13 and HeLa, enabling in this way a comparison of the *in vitro* photodynamic behaviour of the obtained SubPcs with their SiPc counterparts.

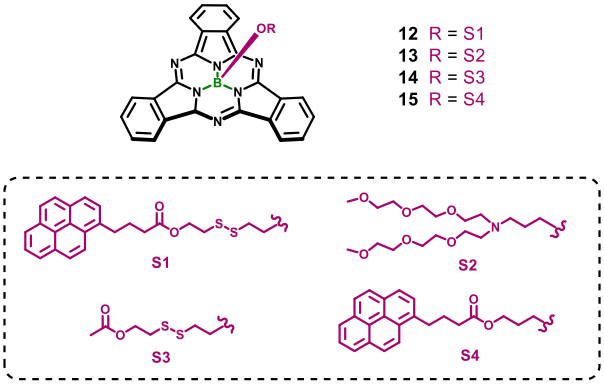

Figure 61. Target compounds of Chapter 1 - Subchapter 2: A series of axially substituted SubPcs bearing different axial substituents.

It is well known that the axial substitution of SubPcs in standard reaction conditions has certain limits, since the tetracoordinated boron atom (in which the vacant p orbital is occupied by formation of a dative bond with one of the nitrogens in the macrocycle) is rather unreactive. Most often, the standard axial reaction with primary alcohols is not selective enough and requires high temperatures, which may ultimately lead to SubPc ring opening and decomposition. In our research group, a new and versatile strategy was developed to this end, which revolutionized the possibilities of axial substitution in SubPcs, using triflate-SubPc as a reactive intermediate which readily reacts with a variety of nucleophiles (Scheme 12).[141] Therefore we decided to follow this methodology, instead of the methodology employed by Ng and co-workers, obtaining in this way axially substituted alkoxy-SubPcs with much higher yields. The detailed synthesis of compounds **12**-**15** is described in the next sections.

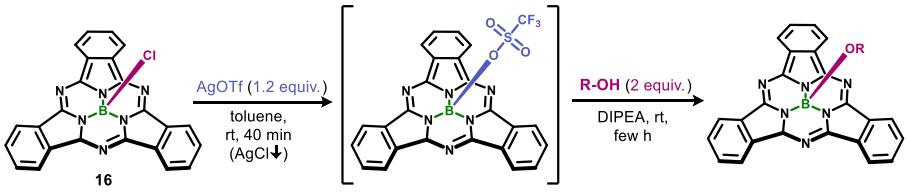

Scheme 12. New methodology for axial substitution of SubPcs, developed in our research group.

2.2.1 Synthesis of target neutral subphthalocyanines

Although SubPcCl is commercially available, it is quite pricy. However, it is easy to synthesize starting from 1,2-dicyanobenzene (also known as phthalonitrile) and boron trichloride solution 1.0 M in *p*-xylene, which despite the low yield of this reaction proves to be a lot cheaper (Scheme 13).[86c]

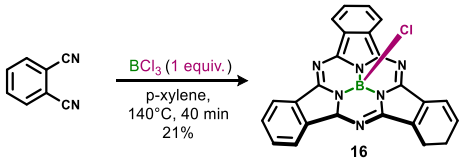

Scheme 13. Synthesis of SubPcCl (**16**).

Once we obtained a reasonable quantity of SubPcCl (**16**), we continued with the incorporation of the series of building blocks for axial substitution that were synthesized previously (Subchapter 1 of this chapter). To this end, **16** was first dissolved in dry toluene and treated with 1.2 equivalents of silver triflate, to irreversibly remove the axial chlorine atom and to obtain a "SubPcB^{+}" species with a weakly coordinating triflate anion. The formation of this triflate intermediate was followed by thin layer chromatography (TLC) and usually completes after ca. 40 min of reaction at rt. The activated triflate-SubPc intermediate shows considerable reactivity towards nucleophilic attack at the boron atom, and can be easily reacted with a variety of nucleophiles. Therefore, upon completion of the formation of the triflate intermediate, 2 equivalents of the corresponding building block for axial substitution were added to the reaction mixture, in the presence of 1.2 equivalents of recently distilled DIPEA in order to neutralize the triflic acid generated in this step, which could promote unwanted secondary reactions. The reaction has to be performed under strictly anhydrous conditions. Otherwise, the

presence of traces of water would immediately lead to a mixture of hydroxy-SubPc and the μ-oxo dimer.[141,142]

The resulting SubPcs (**12**-**15**) could be easily purified by column chromatography, generally using toluene/THF mixtures of various polarity as the eluent. A second purification step by SEC, with Bio-Beads as the stationary phase and toluene as the eluent, was performed to remove any traces of free alcohol or μ-oxo dimer. In this way, the resulting SubPcs were obtained with reasonable to high yields (ranging from 43% to 64%, Scheme 14).

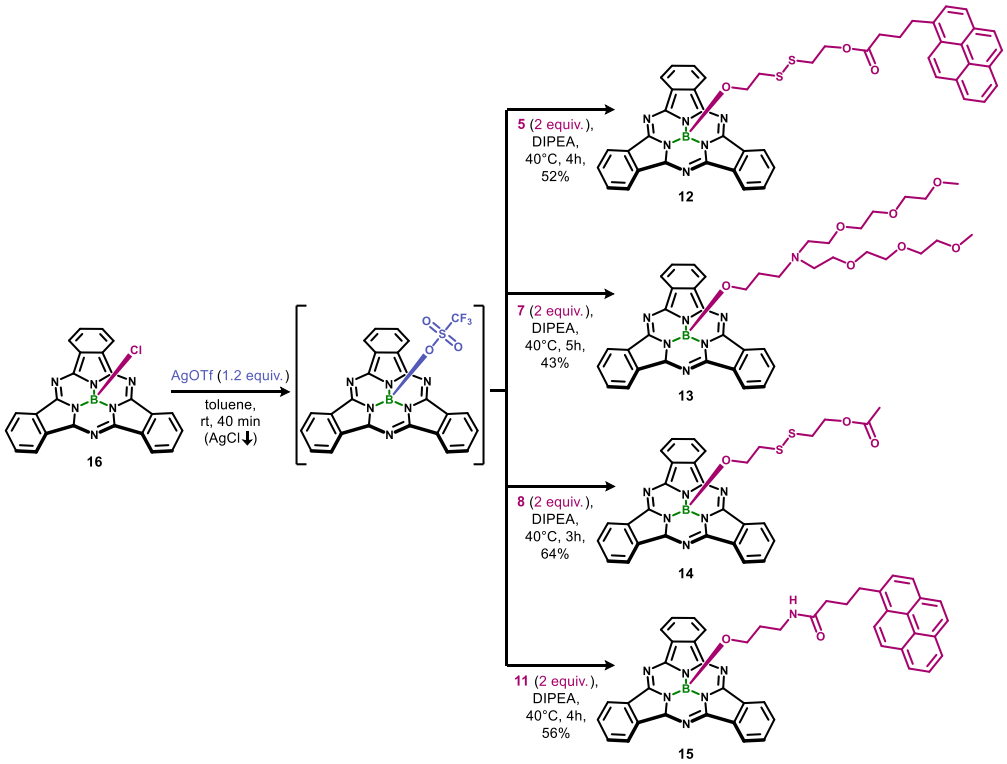

Scheme 14. Synthesis of SubPcs **12-15.**

As mentioned before, due to their cone-shaped 3D geometry, SubPcs are known to show little or no aggregation, leading to an easy and straightforward characterization of SubPcs **12-15** by ^{1}H- and ^{13}C-NMR spectroscopy. As an example, the ^{1}H-NMR of substituent **5** and the corresponding SubPc **12**, recorded in $CDCl_3$, are depicted in Figure 62. Just like for the SiPcs, the SubPc aromatic protons are well resolved, indicating the complete absence of aggregation. Furthermore, the ring current also affects the nearby protons of the axial substituent, though to a smaller extent than in the case of SiPcs.

[142] a] M. Geyer, F. Plenzig, J. Rauschnabel, M. Hanack, B. del Rey, A. Sastre, T. Torres, *Synthesis* **1996**, *1996*, 1139–1151; b) N. Kobayashi, T. Ishizaki, K. Ishii, H. Konami, *J. Am. Chem. Soc.* **1999**, *121*, 9096–9110.

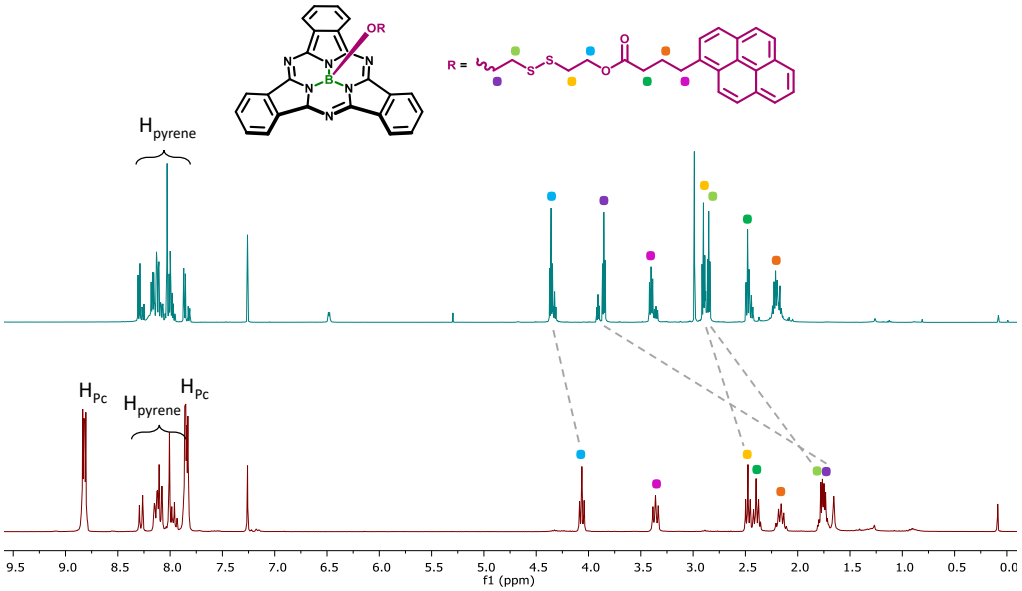

Figure 62. ^{1}H-NMR spectrum of substituent **5** (top) and the SubPc **12** bearing **5** in the as axial substituent (bottom) in $CDCl_3$, showing the effect of the ring current on the protons of the axial substituent: the closer the protons to the ring, the greater the upfield displacement of their chemical shift.

2.2.2 Spectral features and photophysical properties

The normalized absorption spectra of SubPcs **12-16** were measured in DMF, and they all present the typical and intense Q-band, at 566 nm for SubPcBCl **16** and at 562 nm for the axially substituted SubPcs **12-15** (Figure 63). Furthermore, they all present the typically broad B- or Soret-band with a maximum around 305 nm. For SubPcs **12** and **15**, additional absorption bands at 329 and 345 nm can be distinguished, characteristic of the pyrene moiety they bear at the axial position. Exact values of the electronic absorption features for each SubPc can be found in Table 7.

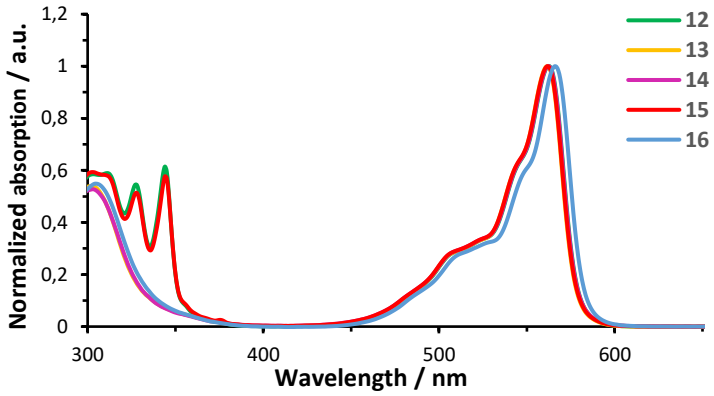

Figure 63. Electronic absorption spectra of SubPcs **12-16** in DMF.

Upon excitation at 345 nm, all the SubPcs showed a fluorescence emission around 571 nm (F_{571}), varying in intensity, with the pyrene-bearing compounds also showing its characteristic fluorescence with maximums around 377 nm (F_{377}). In contrast to Pcs, SubPcs tend to display larger Stokes shifts. For SubPcs **12-16**,the Stokes shift resulted to be between 9-10 nm (Figure 64) (for SiPcs **1-4** the Stokes shift was between 1-5 nm). ϕ_F of both the pyrene and SubPc moieties were determined in DMF, relative to F_{12}SubPcCl in benzonitrile DMF (ϕ_F = 0.58) and anthracene in cyclohexane (ϕ_F = 0.36), exciting at 520 nm or 345 nm, respectively. All results are represented in Table 7.

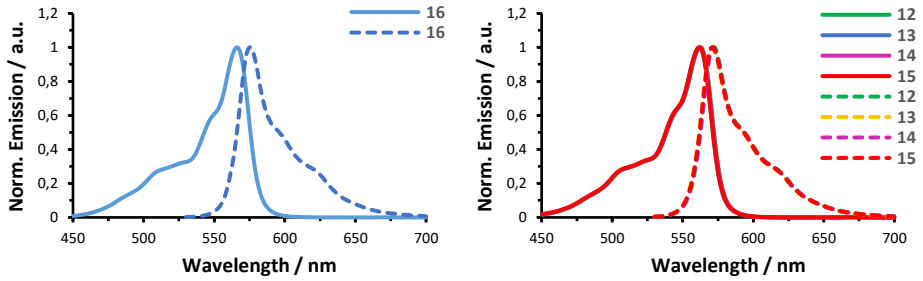

Figure 64. Normalized absorption (full lines) and emission (dashed lines) for SubPcBCl **14** and SubPcs **15**-**18**, indicating their Stokes shift.

The photosensitizing efficiency of SubPcs **12**-**16** was determined in the same way as that of the SiPcs **1-4**, determining their ϕ_Δ in DMF following the well-known relative method based on the photoinduced decomposition of the chemical scavenger DPBF, which reacts readily with $^1O_2$.[127] The resulting ϕ_Δ are resumed in Table 7.

Table 7. Electronic absorption and photophysical data in DMF for the reference compound **10** and SubPcs **12-16.**

Compound	λ_{max} (nm)	λ_{em} (nm)[a]	ϕ_{F377} (%)[b]	ϕ_{F571} (%)[c]	ϕ_Δ (%)[d]
10	344	377	59.6	-[e]	-[e]
12	562	571	1.7	38.1	55.6
13	562	571	-[f]	29.2	37.1
14	562	571	-[f]	35.9	49.0
15	562	571	1.0	36.7	50.2
16	566	575	-[f]	55.1	47.3

[a] Excited at 345 nm. [b] Excited at 345 nm. Using anthracene in cyclohexane as the reference (ϕ_F = 0.36). [c] Excited at 520 nm. Using ClSubPcF_{12} in benzonitrile DMF (ϕ_F = 0.58) as the reference. [d] Using ZnPc in DMF as the reference (ϕ_Δ = 0.56). [e] Not applicable because the compound does not contain any SubPc moiety. [f] Not applicable because the compound does not contain any pyrene moiety.

From the resulting ϕ_F and ϕ_Δ of SubPcs **12-16** two conclusions can be drawn. First, the quenching of F_{377}, probably caused by EET between the pyrene moiety and the SubPc core, is extremely effective in both SubPcs bearing a pyrene group (SubPc **12** and **15**), much better than was the case for the corresponding SiPc bearing two of these pyrene groups (SiPc **2,** see Table 5 and Figure 36). This more effective EET process can probably be

explained by the fact that the emission of the pyrene moiety not only overlaps with the Soret-band of the SubPcs (as in case of the SiPcs), but also partially overlaps with the Q-band of the SubPcs. As a consequence ϕ_{F377} is reduced from almost 60% in reference compound **10** to less than 2% in SubPcs **12** and **15**. Second, the quenching of the SubPc emission (F_{571}) and the $^1O_2$ generation is only effective for SubPc **13**, which bears the amino-containing substituent which can quench the singlet excited state of the SubPc by PET. For SiPcs **1** and **3**, a similar tendency was appreciated, the degree of quenching of both F_{680} and the $^1O_2$ generation depending on the number of pendant amino groups.

As a result of this ineffective quenching of the $^1O_2$ generation for the majority of SubPcs in this series, these SubPcs cannot be classified as activatable PS. Therefore, no studies of their behaviour in function of DTT and/or pH have been undertaken. Nevertheless, although activatable PS are desirable, selectivity in PDT can also obtained by selectively irradiating the malicious tissues, without irradiating healthy tissue. In this way, SubPcs **12**-**16** could be outstanding candidates for PS in PDT, since they display extraordinary high ϕ_Δ values. Furthermore, these excellent ϕ_Δ are companied by high ϕ_{F571} values, which could aid in the visualization of the treatment area. For these reasons, the efficiency in PDT of different cancer cell lines of selected SubPcs will be tested *in vitro*.

2.3 *In vitro* photodynamic activity of selected subphthalocyanines

Subcellular localization and PDT efficacy experiments for the selected SiPc PS are currently being performed in the research group of Prof. Ángeles Juarranz de la Fuente, in collaboration with Alicia Zamarrón Moreno.

3

A SiPc-$(SubPc)_2$ triad as potential photosensitizer for photodynamic therapy

3.1 State of the art

Ever since the fundamental energy exchange processes occurring in multipoprhyrin-quinone assemblies during natural photosynthesis were discovered, a great deal of research has been focussed on the understanding of the mutual interplay between energy- and electron-transfer processes.[143] For this, a large number of systems based on electron-donor and electron-acceptor units, linked by a well-defined spacer, have been synthesized. Although extensive work has been dedicated to the study of Por-quinone dyads[144] mimicking the processes occurring in natural photosynthesis, other photo- or electroactive moieties may be employed in such artificial photosynthetic systems. Both Pcs and SubPcs are interesting electron-donor and/or electron-acceptor candidates, since they both display aromatic delocalization, which gives rise to exceptional optical and electronical properties. Therefore, it is of no surprise that many examples of dyads and

---

[143] a] R. Huber, *Angew. Chem. Int. Ed.* **1989**, *28*, 829–847; b) J. Deisenhofer, H. Michel, *Angew. Chem. Int. Ed.* **1989**, *28*, 829–847; c] R. E. Blankenship, *Molecular Mechanisms of Photosynthesis*, Wiley-VCH, Weinheim, **2001**.

[144] a] M. R. Wasielewski, *Chem. Rev.* **1992**, *92*, 435–461; b) D. Gust, T. A. Moore, A. L. Moore, *Acc. Chem. Res.* **1993**, *26*, 198–205; c] H. Kurreck, M. Huber, *Angew. Chem. Int. Ed.* **1995**, *34*, 849–866; d) D. Gust, T. A. Moore, A. L. Moore, *Acc. Chem. Res.* **2001**, *34*, 40–48; e] M. Huber, *Eur. J. Org. Chem.* **2001**, *2001*, 4379–4389.

triads containing Pcs[145] or SubPcs[146] have been described in the literature, mostly in combination with other chromophores such as fullerenes, BODIPYS, etc.[147] Furthermore, a substantial amount of covalent and non-covalent tetrapyrollic dyads or triads consisting of Pcs and Pors have been reported,[148] but SubPcs covalently conjugated with tetrapyrrole derivatives remain extremely rare, and only few covalent SubPc-Pc dyads have been reported in the literature so far.[149]

In 2005, Gonzalez-Rodriguez *et al.* synthesized a series of SubPc-Pc dyads, prepared by means of Pd-catalyzed cross-coupling reactions between monoalkynyl-Pc and different monoiodo-SubPc derivatives.[149a] Electronic coupling between the two photoactive units is in this way ensured by a rigid and π-conjugated alkynyl linker. Photoinduced energy- and electron -transfer events were precisely studied and tuned by the introduction of different peripheral substituents in the SubPc moiety, varying its electronic characteristics (Figure 65a). Around the same time, Tolbin *et al.* synthesized a SubPc-Pc dyad, incorporating a ZnPc unit at the axial position of the SubPc *via* a peripheral alcohol at the ZnPc unit (Figure 65b).[149b] More recently, two related alkynyl-linked SubPc–Pc dyad were prepared through a Pd(II)-catalyzed Sonogashira coupling between a peripheral ethynyl moiety at the Pc and the *p*-iodo-functionalized position of an axial phenoxy ligand at the SubPc moiety (Figure 65d).[149d]

---

145 a] Y. Rio, W. Seitz, A. Gouloumis, P. Vázquez, J. L. Sessler, D. M. Guldi, T. Torres, *Chem. Eur. J.* **2010**, *16*, 1929–1940; b) G. Rotas, J. Ranta, A. Efimov, M. Niemi, H. Lemmetyinen, N. Tkachenko, N. Tagmatarchis, *ChemPhysChem* **2012**, *13*, 1246–1254; c] C. B. KC, K. Stranius, P. D'Souza, N. K. Subbaiyan, H. Lemmetyinen, N. V. Tkachenko, F. D'Souza, *J. Phys. Chem. C* **2013**, *117*, 763–773; d) S. Zhou, M. Yamamoto, G. A. D. Briggs, H. Imahori, K. Porfyrakis, *J. Am. Chem. Soc.* **2016**, *138*, 1313–1319.

146 a] D. González-Rodríguez, T. Torres, D. M. Guldi, J. Rivera, L. Echegoyen, *Org. Lett.* **2002**, *4*, 335–338; b) D. González-Rodríguez, T. Torres, D. M. Guldi, J. Rivera, M. A. Herranz, L. Echegoyen, *J. Am. Chem. Soc.* **2004**, *126*, 6301–6313; c] R. S. Iglesias, C. G. Claessens, T. Torres, G. M. A. Rahman, D. M. Guldi, *Chem. Commun.* **2005**, 2113–2115; d) D. González-Rodríguez, T. Torres, M. M. Olmstead, J. Rivera, M. Á. Herranz, L. Echegoyen, C. A. Castellanos, D. M. Guldi, *J. Am. Chem. Soc.* **2006**, *128*, 10680–10681; e] L. C. Kasi Viswanath, L. D. Shirtcliff, S. Krishnan, N. V. Handa, K. Darrell Berlin, *Tetrahedron Lett.* **2014**, *55*, 4199–4202; f) E. Maligaspe, M. R. Hauwiller, Y. V. Zatsikha, J. A. Hinke, P. V. Solntsev, D. A. Blank, V. N. Nemykin, *Inorg. Chem.* **2014**, *53*, 9336–9347.

147 a] G. Bottari, G. de la Torre, D. M. Guldi, T. Torres, *Chem. Rev.* **2010**, *110*, 6768–6816; b) G. de la Torre, G. Bottari, M. Sekita, A. Hausmann, D. M. Guldi, T. Torres, *Chem. Soc. Rev.* **2013**, *42*, 8049–8105; c] G. Bottari, G. de la Torre, T. Torres, *Acc. Chem. Res.* **2015**, *48*, 900–910.

148 P.-C. Lo, X. Leng, D. K. P. Ng, *Coord. Chem. Rev.* **2007**, *251*, 2334–2353.

149 a] D. González-Rodríguez, C. G. Claessens, T. Torres, S. Liu, L. Echegoyen, N. Vila, S. Nonell, *Chem. Eur. J.* **2005**, *11*, 3881–3893; b) A. Y. Tolbin, M. O. Breusova, V. E. Pushkarev, L. G. Tomilova, *Russ. Chem. Bull.* **2005**, *54*, 2083–2086; c] Z. Zhao, A. N. Cammidge, M. J. Cook, *Chem. Commun.* **2009**, 7530–7532; d) N. Shibata, B. Das, E. Tokunaga, M. Shiro, N. Kobayashi, *Chem. Eur. J.* **2010**, *16*, 7554–7562.

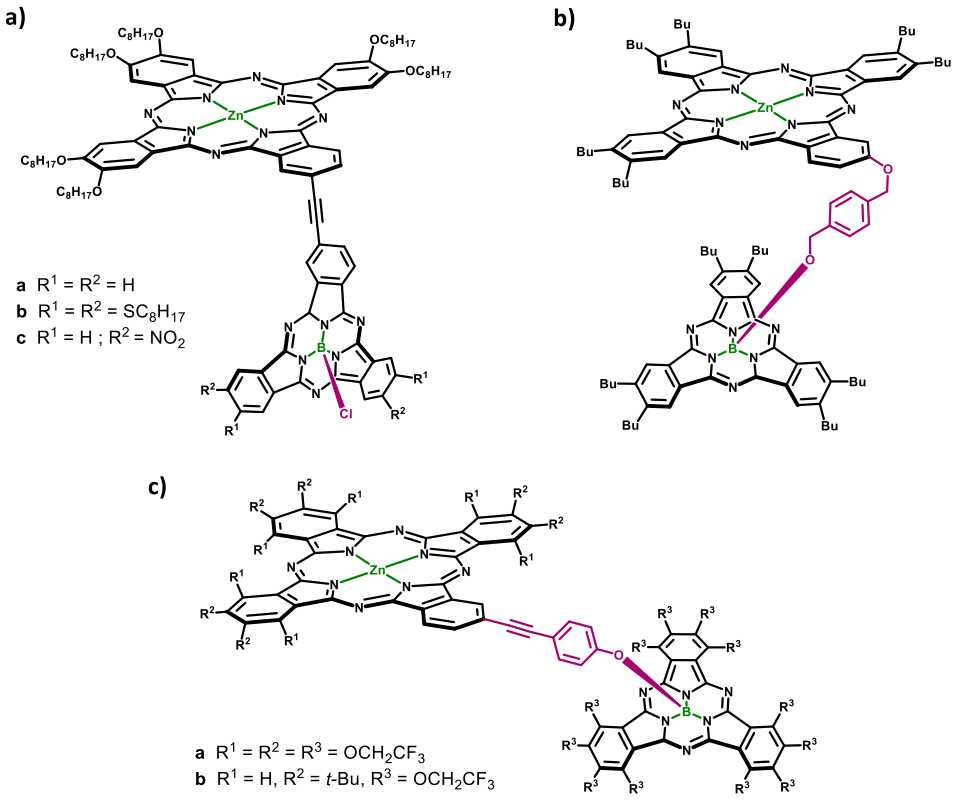

Figure 65. An overview of covalently linked SubPc-Pc dyads, synthesized by a) Gonzalez-Rodriguez *et al.,*[149a] b) Tolbin *et al*.,[149b] and c) Shibata *et.al.*[149d]

The first, and, to the best of our knowledge, the only, SubPc-Pc triad containing two SubPc units, was reported in 2008 by Cook and co-workers (Figure 66).[149c] They parted from dihydroxy silicon octakis(hexyl) Pc and reacted it with SubPcCl to obtain the μ-oxo-linked SubPc-SiPc dyad and triad, expectedly with low yields. The authors indicate the use of these systems as antenna molecules for solar photon collection as most foreseen application, as a result of their absorbance over the whole visible spectrum.

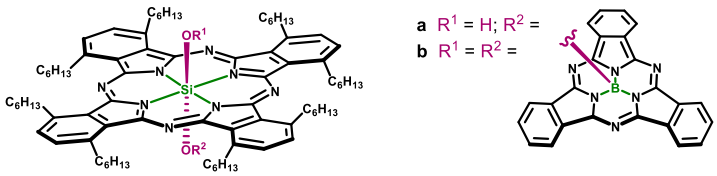

Figure 66. The first and only reported SubPc-Pc-SubPc triad so far, synthesized by Cook and co-workers.[149c]

Apart from these covalent dyads, Ng and co-workers also synthesized a series of non-covalent SubPc-Pc dyads, based on axial complexation of a zinc (II) and ruthenium (II) Pc

with two different SubPcs with an axial pyridyl group.[150] The complexation processes were studied by ^{1}H-NMR and fluorescence spectroscopy methods, indicating a 1:1 stoichiometry in both cases, which was also confirmed by X-ray diffraction analysis.

Up to now, all synthesized Pc-SubPc dyads and triads have been designed and studied for their exceptional optical and electronical properties, with their use as solar light collectors in photovoltaic devices as the ultimate goal. However, apart from their energy- and electron-transfer features, these dyads and triads are also of interest due to their extraordinary absorptive cross section, displayed across the whole UV-Vis spectrum, making them model candidates for application in situations where broadband light sources are necessary. In this way, they could serve as exceptional PS in PDT with wavelength-independent ϕ_Δ, although no research in this direction has been undertaken so far.

[150] H. Xu, D. K. P. Ng, *Inorg. Chem.* **2008**, *47*, 7921–7927.

3.2 Molecular design, synthesis and characterization of the SiPc-(SubPc)$_2$ triad

The specific objective of the present Subchapter is the design and synthesis of the first SubPc-SiPc-SubPc triad (compound **17**, Figure 67a), for use as a PS in PDT. Its ability to generate $^1O_2$ and fluorescence emission have been designed as tumor responsive (Figure 67b). More specifically, the PS consists of a SiPc core, axially substituted with two SubPc units, covalently linked by a cleavable disulfide linker.

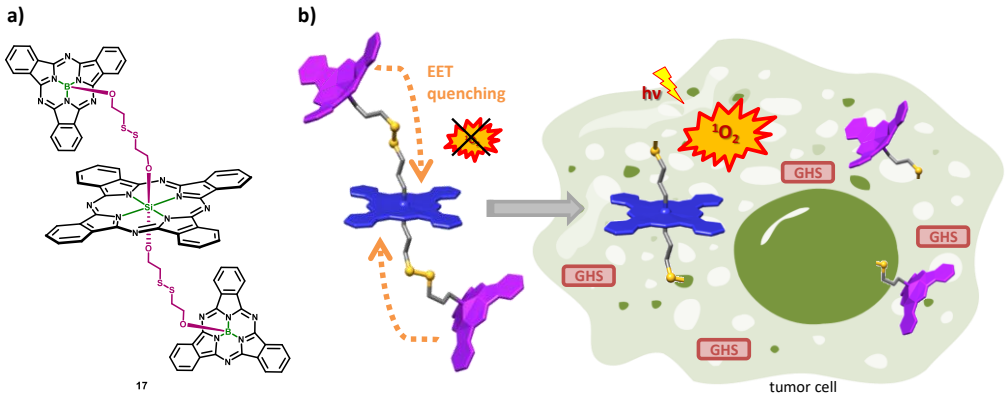

Figure 67. a) Chemical structure of **17**. B) Schematic representation of the possible mechanism of action of PS **17** upon entering a tumor cell. GHS being glutathione, indicating the characteristic reducing environment of tumor cells, responsible for the cleavage of the disulfide linker of **17** and consequent activation of its $^1O_2$ generation and fluorescence.

The design comes as a logical advance on the previously discussed SiPc derivative bearing a pyrene unit as activatable chromophore at the axial position, also linked by the same cleavable disulfide linker (Subchapter 1 of this Chapter). This PS presented three output signals (fluorescence at 377 and 680 nm, and $^1O_2$ production), potentially enabling multifunctional theranostics. However, the fluorescence and $^1O_2$ generation quenching before the PS activation was only moderate, mainly due to inefficient EET from the pyrene unit to the SiPc core, limiting its practical application. In the present case, it is expected that the quenching caused by the SubPc units will be more effective, since the SubPc emission band partially overlaps with the SiPc Q-band, increasing the possible use of the PS in PDT (Figure 68). Furthermore, as SubPcs are lower homologues of Pcs with absorption bands appearing at regions of low SiPc absorption (ca. around 550 nm), their conjugation may enable a panchromatic photosensitization that should in principle maximize $^1O_2$ generation. Indeed, SubPcs are also able to generate $^1O_2$, and having two SubPc units on the SiPc can contribute to the overall ϕ_Δ of this PS system upon activation.

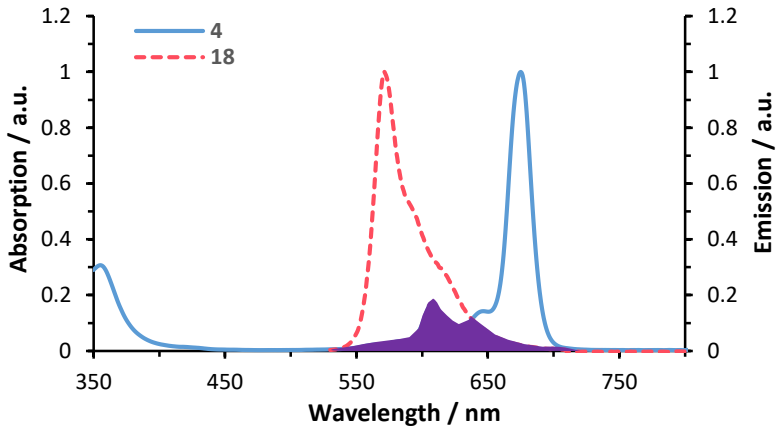

Figure 68. Cross-section (purple) of the normalized emission of SubPc **18** (red) and absorption of SiPc **4** (blue), in DMF, resulting in an EET in SiPc-SubPc triad **17**.

3.2.1 Synthesis of the SubPc building block for axial substitution

The idea behind the synthesis of the new SiPc-SubPc triad is similar as that used by Cook and co-workers, in the way that the SubPc units will be introduced at the axial positions of the SiPc.[149c] However, instead of parting from a dihydroxy SiPc, we wanted to part from the commercially available $SiPcCl_2$, to be able to follow our previously applied methodology for the axial substitution of the SiPcs. Therefore, the SubPc units must bear a primary alcohol available for conjugation. In this respect, the same linker as that used in Subchapter 1 of this Chapter could be used.

SubPcCl **16** was prepared as before[86c] and its axial chloride substituent replaced by 2-hydroxyethyl disulfide following the axial substitution procedure developed in our group (Scheme 15).[141] The progress of the substitution reaction was followed by TLC, and in this case the reaction was completed after 6 h. The crude was then subjected to column chromatography on silica gel using toluene/THF with a gradient from 30:1 to 10:1 as the eluent. Subsequent trituration in water yielded the desired SubPc **18** with a 56% yield.

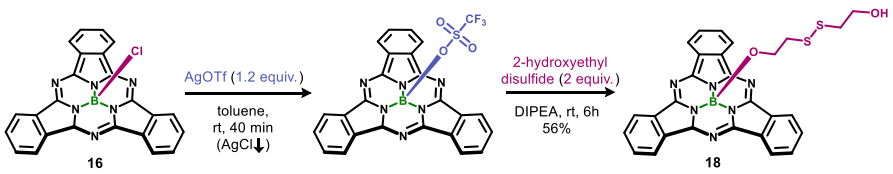

Scheme 15. Synthesis of the axial SubPc units bearing the appropriate linker for incorporation in the $SiPcCl_2$.

3.2.2 Synthesis of the target SiPc-(SubPc)$_2$ triad

The next step involved the nucleophilic displacement of the chlorine atoms in $SiPcCl_2$ with the primary alcohol **18**. To this end, $SiPcCl_2$ and 5 equivalents of **18** were dissolved in pyridine, and DIPEA was added as a base. After refluxing the reaction mixture overnight, the SiPc-SubPc triad **17** was formed (Scheme 16).

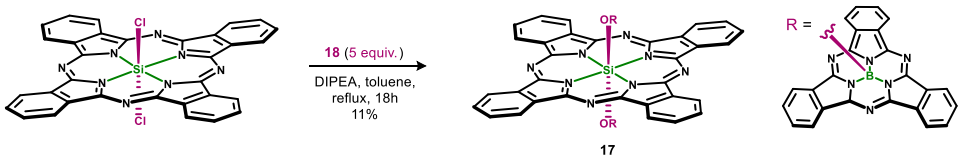

17

Scheme 16. Incorporation of SubPc **18** at the axial positions of $SiPcCl_2$, following the standard procedure, resulting in formation of SiPc-SubPc triad **17**.

The purification of **17** was difficult and tedious because of the inherent instability problems in both standard silica (which is slightly acidic) or silica previously neutralised with Et_3N. In both cases, the compound decomposed rapidly, probably because the Pc unit is acid-sensitive while SubPcs are known to be base-sensitive. Part of the crude reaction mixture could finally be purified by SEC with Bio-Beads as the stationary phase and $CHCl_3$ as the eluent, yielding triad **17** as a dark purple solid. However only a fraction of the compound elutes as pure compound, the remaining part eluting together with the starting products $SiPcCl_2$ and SubPc **18**, and/or decomposition products, for which an estimated yield of the product is reported. Because of this inherent instability of the molecule, it was not possible to detect the molecular ion by mass spectrometry, yet ^{1}H-NMR characterization is conclusive about the purity and identity of the purified fraction of the product (see Figure 69).

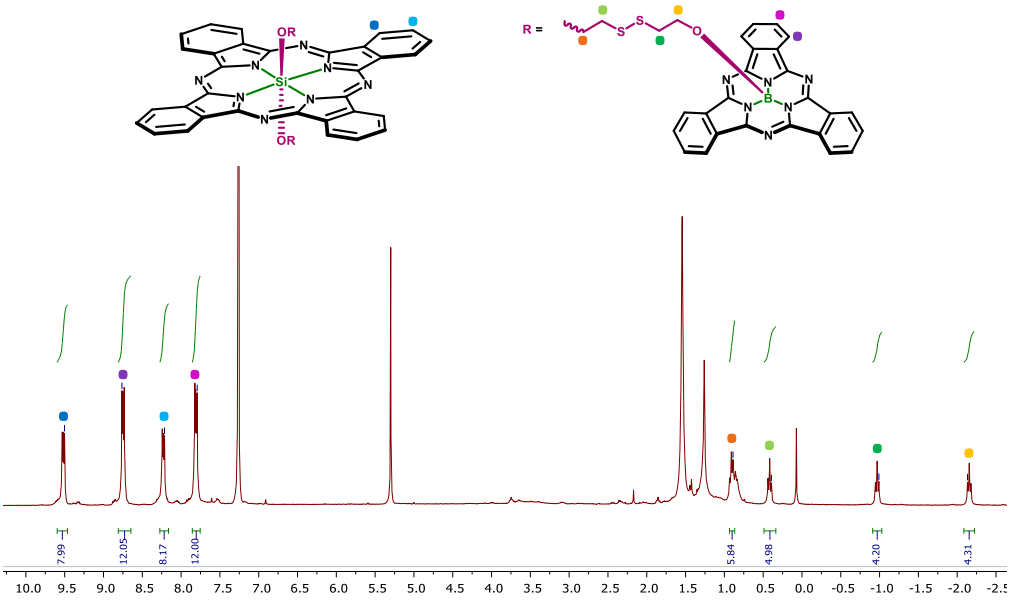

Figure 69. ^{1}H-NMR of SiPc-(SubPc)$_2$ triad **17**, recorded in $CDCl_3$.

3.2.3 Spectral features and photophysical properties

The absorption and photochemical properties of the SiPc-SubPc triad **17**, SubPc **18** and reference SiPc **4** were measured in DMF (Table 8).

Table 8. Electronic absorption and photophysical data for SiPc **4**, SubPc **18** and SiPc-(SubPc)$_2$ triad **17**.

Compound	λ_{max} (nm)	λ_{em} (nm)[a]	ϕ_{F571} (%)[b]	ϕ_{F680} (%)[c]	ϕ_{Δ} (%)[d]
4	679	684	-[d]	37.1	36.2
17	675, 562	680, 571	2.4	5.2	11.7
18	562	571	38.3	-[e]	49.0

[a] Excited at 520 nm. [b] Excited at 520 nm, using $ClSubPcF_{12}$ in benzonitrile as the reference (ϕ_F = 0.58). [c] Excited at 610 nm, using ZnPc in DMF as the reference (ϕ_F = 0.28). [d] Not applicable because the compound does not contain any SubPc moiety. [e] Not applicable because the compound does not contain any Pc moiety.

The UV-Vis spectra of SubPc **18** and SiPc **4** show their typical broad Soret band (at 300-400 nm) and sharp Q band (at 562 and 675 nm, respectively). Accordingly, the UV-Vis spectrum of the SiPc-SubPc triad **17** shows a broad Soret band at 300-400 nm and two Q-bands, the first one originating from the two axial SubPc units (at 562 nm) and the second one from the SiPc unit (at 675 nm), in an expected 2:1 stoichiometrical ratio (Figure 70).

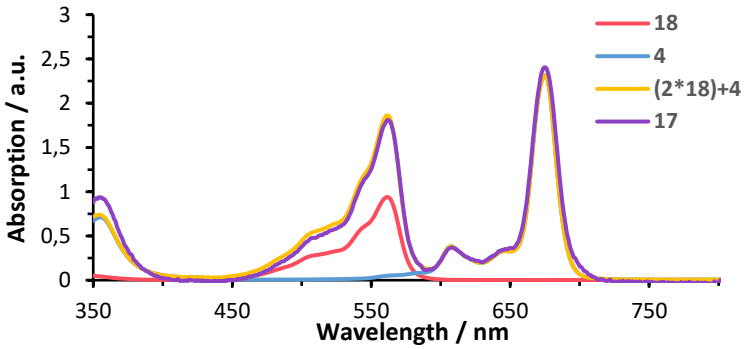

Figure 70. The sum of spectral features in DMF for the reference compounds **18** and **4**, in the right stoichiometry (2:1), matches the spectrum of the SubPc-SiPc triad **17**.

ϕ_F were measured by exciting the compounds at 520 nm (for SubPcs) or 610 nm (for Pcs). ϕ_Δ, in turn, were again measured by the relative method, using DPBF as a chemical scavenger and excitation with visible light filtered below 455 nm (hv > 455 nm). As expected, compared to the reference SiPc **4** and the SubPc **18**, the SiPc-SubPc triad **17** shows a significant deactivation of its fluorescence and $^1O_2$ generation, probably as a result of an electronic energy transfer process in which the SubPc emission band and the SiPc Q-band partially overlap (Figure 68).

3.3 Proposed tumor responsive activation of the SiPc(SubPc)$_2$ triad

According to the design of the molecule (Figure 67b), initially the fluorescent and $^1O_2$-generating properties of **17** are quenched, most probably by electronic energy transfer between the SubPc units and the Pc core. Upon entering a reducing environment, e.g., like that in tumor cells, the disulfide linker would be cleaved and the quenching would be undone, resulting in a sudden generation of $^1O_2$ and a strong fluorescence of both the SiPc and SubPc units. In the following subsections, this behavior has been probed in a physiologically relevant medium, by means of using DTT as a strong reducing agent to achieve the PS activation. In this way we hope to gain understanding of how both the fluorescence and $^1O_2$ generation of **17** would be influenced in a tumor like environment.

3.3.1 Effect of DTT concentration on the fluorescence properties of the SiPc(SubPc)$_2$ triad

To investigate the influence of intratumor-like disulfide cleavage on the fluorescence properties of **17**, its emission spectrum was monitored for 24 h in PBS buffer solutions with varying DTT concentrations (Figure 71).

Sample preparation was as follows: **17** is dissolved in DMF to give a 1 mM solution, which was diluted to 0.4 µM with PBS (with 0.5% Cremophor EL). DTT was dissolved in deionized water to give a 1 M solution. Mixtures of **17** (0.4 µM) with DTT (2 µM, 5 mM, 10 mM, 20 mM or 50 mM) or without DTT in PBS (25 mL) were prepared and stirred continuously.

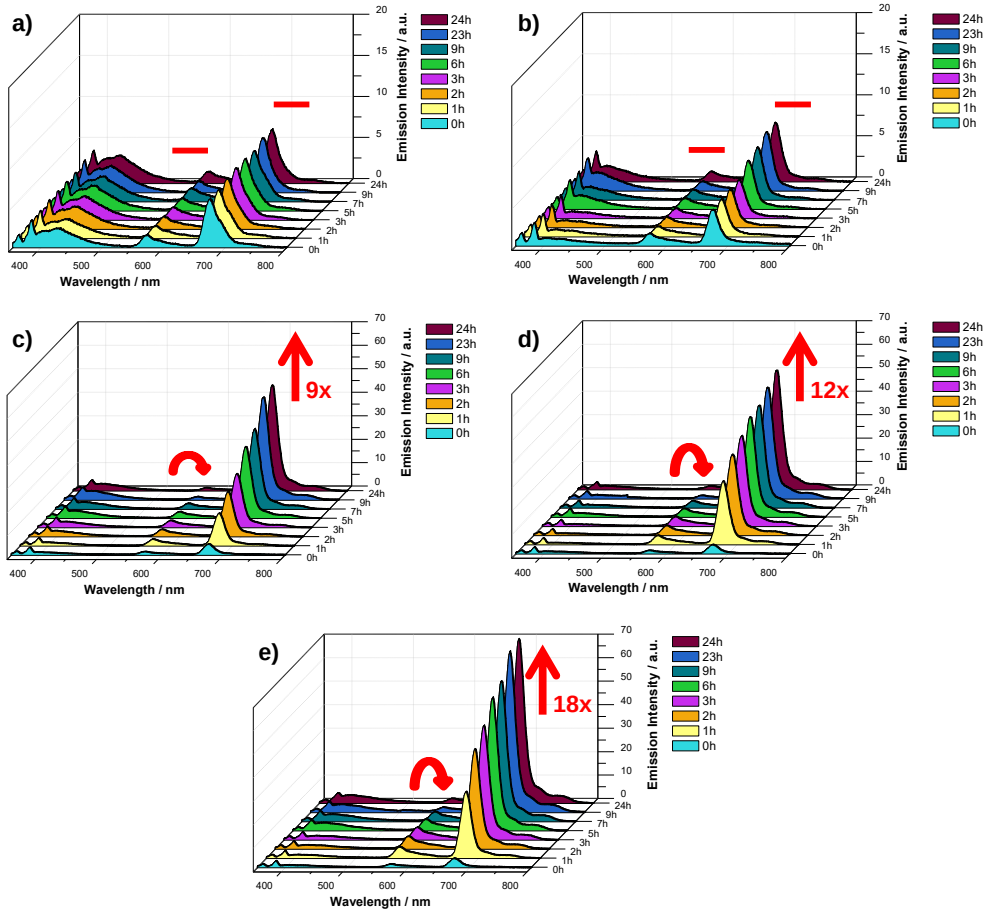

Figure 71. Representation of the fluorescence spectra of **17** in PBS (0.5% Cremophor EL) with a) 0 µM DTT, b) 2µM DTT, c) 5 mM DTT, d) 20 mM DTT and e) 50 mM DTT, from t = 0 h to t = 24 h.

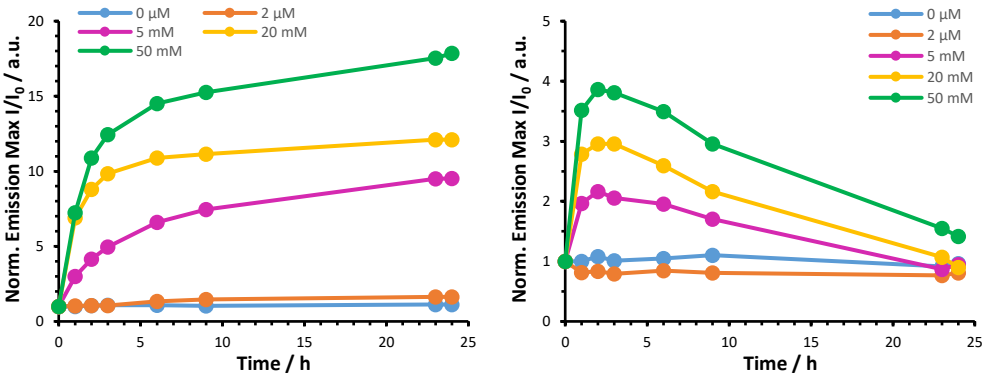

Figure 72. Normalized emission maximum of **17** in PBS (0.5% Cremophor EL) in function of time for a) the SubPc units (F_{571}) and b) the phthalocyanine unit (F_{680}).

As can be seen in Figure 72a, the fluorescence intensity of the SiPc unit (at 674 nm - λ_{ex} = 345 nm) exhibits approximately a 9-, 12- and 18-fold increment in the presence of 5, 20 and 50 mM of DTT respectively, while in the absence of DTT or in the presence of only 2 µM of DTT there is no SiPc fluorescence enhancement. This increase in fluorescence intensity reflects that the SiPc emission is recovered upon disulfide cleavage. On the other hand, the fluorescence intensity of the SubPc unit (at 571 nm - λ_{ex} = 345 nm) displays a similar initial recovery, but reaches a maximum recovery around 2 hours, after which the fluorescence intensity starts decreasing again (Figure 72b).

To explain this unexpected result, the influence of DTT on the absorption of **17** was studied (Figure 73). From this experiment, it became clear that **17** was unstable to the strong reducing environment, indicated by a decrease of the SubPc absorption at 562 nm in function of time, the extent of the decrease being greater at higher concentrations of DTT. This instability, although unexpected and in principle undesired, does not necessarily urge to discard the use of **17** as an activatable tumor responsive and theranostic PS for PDT, however, as the outcome caused by the actual decomposition of the SubPc unit or by the foreseen cleavage of the disulfide linker is the same with respect to both its $^1O_2$ generation and the fluorescence of the SiPc unit. Indeed, both outcomes would be activated once **17** enters the strong reducing environment of a tumor cell, just as they are in solution.

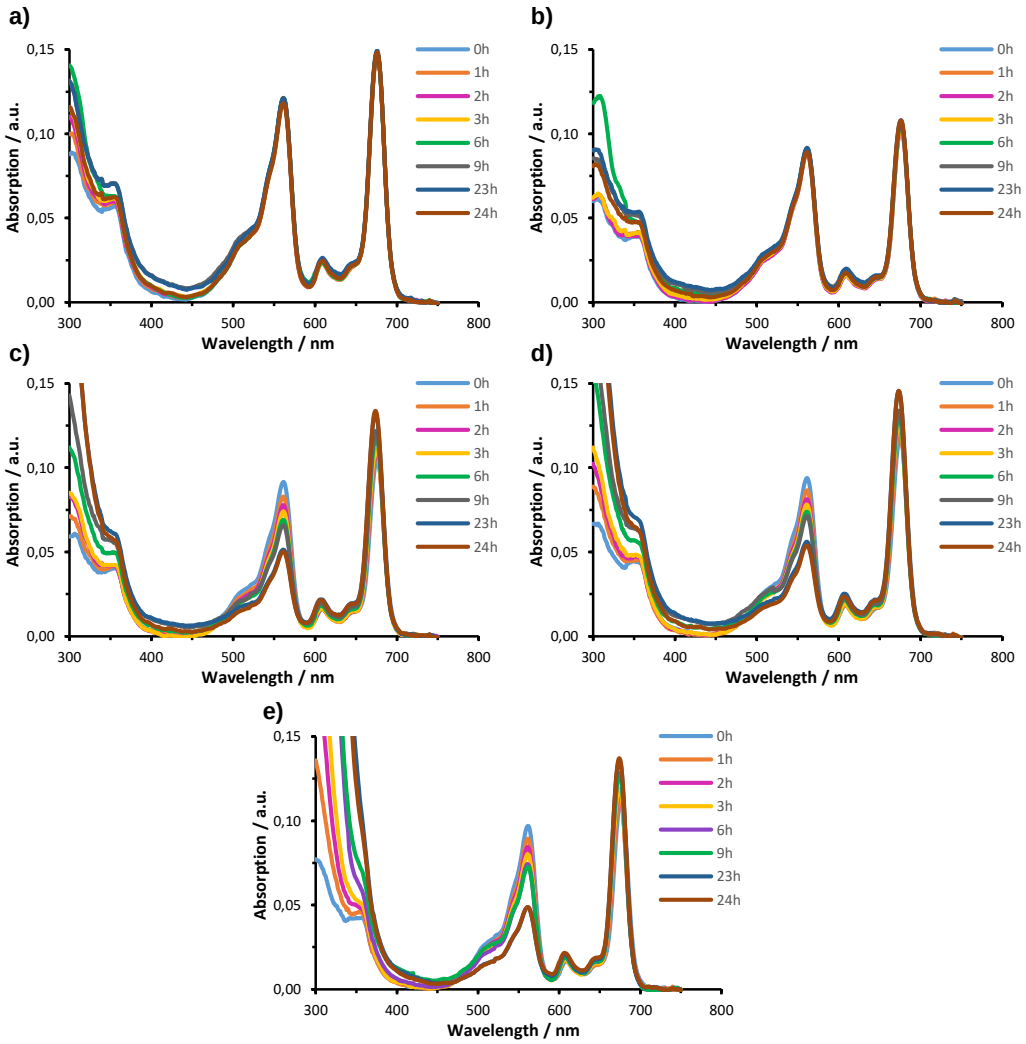

Figure 73. UV-Vis spectra of **17** in PBS (0.5% Cremophor EL) with a) 0 µM DTT, b) 2 µM DTT, c) 5 mM DTT, d) 20 mM DTT and e) 50 mM DTT, from t = 0 h to t = 24 h.

3.3.2 Effect of DTT concentration on $^1O_2$ generation of the SiPc(SubPc)$_2$ triad

To investigate the effect of a reducing environment (as in tumor cells) on the capacity of triad **17** for $^1O_2$ generation in physiologically relevant medium, $^1O_2$ studies were performed in the same buffer solutions with varying DTT concentrations. The rate of DPBF photodegradation upon irradiation of the SiPc-SubPc triad **17**, which is proportional to the amount of $^1O_2$ formation, is measured in combination with 0 µM, 2 µM, 5 mM, 20 mM and 50 mM of DTT and represented in Figure 74.

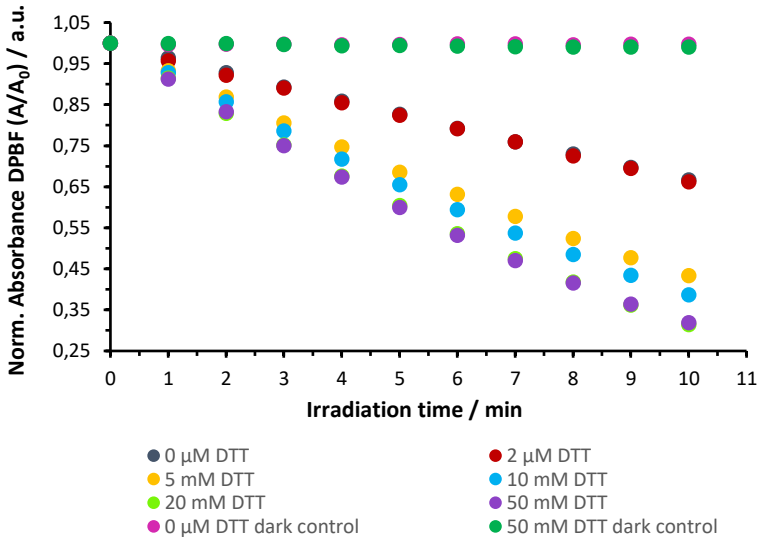

Figure 74. Effect of DTT on the capacity of **17** for $^1O_2$ generation: normalized absorption (A/A_0) of DPBF at various concentrations of DTT over time, showing its photodegradation rate sensitized by **17** upon excitation with light above 455 nm.

A clear trend can be deduced from this data, demonstrating that more efficient $^1O_2$ generation results from samples exposed to a higher concentration of DTT. Thus, the degree of disulfide cleavage seems to be directly correlated to the $^1O_2$ generation efficiency of **17**. In the absence of DTT or in the presence of only 2 µM of DTT (corresponding to the extracellular glutathione concentration) there is no enhancement of the $^1O_2$ generation, which reflects the need of a strong reducing environment to promote such activation via disulfide cleavage. Moreover, dark control experiments confirm that, under all conditions, compound **17** is unable to produce $^1O_2$ without $h\nu_{>455nm}$ illumination.

In summary, SiPc-SubPc triad **17** is a PS with the ability to generate $^1O_2$, the main reactive species in PDT, in a substantially higher amount once entered in a reducing environment simulating that of tumor cells. However, due to the difficulty in the preparation and purification of the SiPc-SubPc triad, and the inherent instability problems, no *in vitro* tests of PDT efficacy are performed for this PS.

4

Summary and conclusions

In the present chapter, the synthesis of different neutral SiPc and SubPc derivatives, including SiPc-SubPc triad, has been explored, with their use as PS in PDT of different oncological treatments as the final goal.

Regarding SiPcs, we have synthesized a series of neutral derivatives bearing different substituents at the axial positions of the central silicon atom. It was our aim to make use of axial substituents that can actively quench the singlet excited state of the PS, and therefore their $^1O_2$ generation efficiency and fluorescence, in a reversible way. To this end, activation studies of these quenching processes in function of different external stimuli were undertaken. The most interesting SiPc derivative (SiPc **1**), bears two different of such quenching groups that can each selectively be activated, and consequently displays the ability to perform multiple logic operations based on three input and three output signals. This multi-input/multi-output nature enables single-, double- and triple-mode activation pathways of its different molecular functions, through the interplay of various interrelated AND, ID and INHIBIT gates. Moreover, the three outputs elicit a high biomedical value considering $^1O_2$ is the main reactive species in PDT, while dual fluorescence emissions are potentially useful for orthogonal optical imaging protocols. The applied stimuli are also relevant from the medical point of view, as low pH and reducing conditions are characteristic of tumor tissues. Finally, for selected SiPcs, their efficacy as PS was studied *in vitro* against various tumour cell lines, such as HEp-2 (from a human larynx carcinoma), SCC-13 (from a human squamous cell carcinoma of the skin) and HeLa (from a human cervical carcinoma), SiPc **1** and SiPc **3** giving rise to excellent results in all studied cell lines.

SubPcs are equally interesting PS molecules as compared to Pcs, but research in directed at the use of SubPcs in PDT is lacking. In view of the interesting results obtained in the first subchapter, the same substituents as those used in SiPcs were also incorporated at the axial position of the boron atom in SubPcs, and their influence on various properties such as fluorescence and $^1O_2$ generation was studied in detail. However, in this case both the EET and PET quenching processes resulted less effective than in the case of SiPcs.

Nevertheless, it could be noted that all synthesized SubPc derivatives presented high to very high $\phi_{\Delta,}$ which is promising for their use as PS in PDT. Therefore, for selected SubPcs their efficacy as PS will be studied *in vitro* against HEp-2, SCC-13 and HeLa, enabling the comparison of their results with those obtained for their SiPc counterparts.

Finally, both macrocycles were combined in one single molecule, in the synthesis of a SiPc-$(SubPc)_2$ triad, consisting of a SiPc core axially substituted with two SubPc units. Its ability to generate $^1O_2$ and fluorescence emission were designed as tumor responsive, and selective activation experiments depending on different external stimuli have been undertaken in this direction. Furthermore, since SiPcs and SubPcs possess complementary absorption maxima, the SiPc-$(SubPc)_2$ triad displayed a panchromatic photosensitization, which contributed to the overall ϕ_Δ of this PS system upon activation, outperforming that of both of its PS parts.

5

Experimental section

5.1 Materials and methods

All reagents were used as purchased from commercial sources without further purification. Solvents were dried using standard techniques prior to use. The starting materials silicon phthalocyanine dichloride ($SiPcCl_2$), 1-pyrene butyric acid, 2-hydroxyethyl disulfide, triethylene glycol monomethyl ether, and 3-amino-1-propanol were commercially available. All reactions were performed in standard glassware under inert argon atmosphere. Reactions were monitored by TLC, using TLC plates pre-coated with silica gel 60-F254 (Merck). Column chromatography was carried out on Merck silica gel 60, 40-63 µm (230-400 mesh). Size Exclusion Chromatography (SEC) was performed using Biorad Biobeads SX-1 (200-400 mesh).

^{1}H and $^{13}C\{1H\}$ NMR spectra were recorded using Bruker AC-300 (^{1}H: 300 MHz; ^{13}C: 75 MHz) instruments, unless mentioned otherwise. Spectra were referenced internally by using the residual solvent (^{1}H: δ = 7.26 for $CDCl_3$, δ = 2.49 for DMSO-d_6) or solvent resonances (^{13}C: δ = 77.0 for $CDCl_3$, δ = 39.5 for DMSO-d_6) relative to $SiMe_4$, respectively.

UV-Vis and fluorescence spectra were recorded with a JASCO V-660 and a JACSO FP-8600 spectrophotometer, respectively. The logarithm of the molar absorption coefficient ε is expressed in between parentheses.

Matrix-assisted laser desorption/ionization time of flight (MALDI-TOF) MS and high-resolution (HR-MS) mass spectra were recorded with a Bruker Ultrareflex III spectrometer. Fast atom bombardment (FAB) mass spectra were recorded with a VG AutoSpec of Waters instrument. All MS experiments were carried out at the Servicio Interdepartmental de

Investigación (SIdl) of the Universidad Autónoma de Madrid. All the data are expressed with the intensity in percentage between parentheses.

IR spectra (IR) were recorded on a FTIR IFS66v (Bruker) spectrophotometer using KBr disks, in the Servicio Interdepartmental de Investigación (SIdl) of the Universidad Autónoma de Madrid (in Subchapter 1) or on a FTIR Cary 630 (Agilent Technologies) using the ATR technique (in Subchapter 2 and 3). Spectra intensity were corrected by ATR algorithm and subsequent baseline correction.

Melting points (Mp) were determined in a Buchi 504392-S equipment, in the Department of Organic Chemistry of the Universidad Autónoma de Madrid.

5.1.1 Fluorescence and singlet oxygen quantification

Fluorescence quantum yields

ϕ_F were measured in DMF using the *comparative method* of Williams *et al*,[127] in which ϕ_F is determined by the equation:

$$\phi_F^S = \phi_F^R \left(\frac{Grad_S}{Grad_R}\right)\left(\frac{\eta_S^2}{\eta_R^2}\right)$$

where subscripts *R* and *S* denote reference and sample, respectively, ϕ_F is the fluorescence quantum yield, *Grad* the gradient from the plot of the integrated fluorescence intensity (at the specified wavelength) *versus* the absorption (at the same wavelength), and η the refractive index of the solvent. Non-substituted zinc (II) phthalocyanine (ZnPc) in DMF (ϕ_F = 0.28),[151] ClSubPcF$_{12}$ in benzonitrile DMF (ϕ_F = 0.58),[152] and anthracene in cyclohexane (ϕ_F = 0.36)[153] were used as references for the SiPc, SubPc and pyrene emissions, respectively. Excitation took place at 610 nm for SiPcs, at 520 nm for SubPcs, and at 310 nm for pyrene moieties.

$^1O_2$ quantum yields

ϕ_Δ were measured in DMF following the well-known *relative method*, based on the photoinduced decomposition of a chemical scavenger (i.e., DPBF) that reacts readily with

[151] I. Scalise, E. N. Durantini, *Bioorg. Med. Chem.* **2005**, *13*, 3037–3045.

[152] C. R. Nieto, J. Guilleme, C. Villegas, J. L. Delgado, D. González-Rodríguez, N. Martin, T. Torres, D. M. Guldi, *J. Mater. Chem.* **2011**, *21*, 15914–15918.

[153] I. B. Berlman, *Handbook of Fluorescence Spectra of Aromatic Molecules*, Academic Press, New York, **1971**.

$^1O_2$. Non-substituted ZnPc was used as reference compound (ϕ_Δ(DMF) = 0.56).[154] In detail, the procedure was as follows: 2.5 mL of a stock solution of DPBF (with an absorption of ca. 1) in DMF was transferred into a 10 x 10 mm quartz optical cell and bubbled with $^3O_2$ for 1 min. A concentrated stock solution of the PS in the same solvent was then added, in a defined amount to reach a final Q-band absorbance value of about 0.1. The solution was stirred and irradiated for defined time intervals, using a halogen lamp (300 W). The duration of these intervals are tuned in each experiment, in order to get a decrease in DPBF absorption of about 3-4%. Incident light was filtered through a water filter (6 cm) and an additional filter to remove light under 530 nm (Newport filter FSQ-OG530) or 455 nm (Newport filter 20CGA-455), for SiPcs and SubPcs respectively. Additional neutral density filters (FBS-ND03 or FB-ND10) were used when necessary. The decrease of DPBF absorbance with irradiation time was monitored at 414 nm. ϕ_Δ was calculated through the following equation:

$$\phi_\Delta^S = \phi_\Delta^R \frac{k^S I_{aT}^R}{k^R I_{aT}^S}$$

where *R* and *S* indicate reference and sample, respectively. *k* is the slope of a plot of ln(A_0/A_t) *versus* irradiation time *t*, with A_0 and A_t being the absorbance of scavenger at the monitoring wavelength before and after irradiation time t, respectively. I_{aT} is the total amount of light absorbed by the dye and is calculated as the sum of intensities of the absorbed light I_a from wavelength 530 up to 800 nm. I_a at given wavelength is calculated using Beer's law:

$$I_a = I_0(1 - e^{-2.3A})$$

where I_0 is the transmittance of the filter at a given wavelength and *A* the absorbance of the dye at this wavelength. All experiments are performed three times and the obtained data represent mean values of those three experiments.

Fluorescence studies in PBS

Samples were prepared as following: the corresponding SiPc was dissolved in spectroscopic grade DMF to give a 1 mM solution, which was diluted to 0.4 µM with buffer solution (PBS with 0.5% Cremophor EL®). DTT was dissolved in deionized water to give a 1 M solution. Mixtures of the SiPc (25 mL, 0.4 µM) with DTT (2 µM, 5 mM, 10 mM, 20 mM or 50 mM) or without DTT in PBS buffer, and adjusted to pH = 7.4, pH = 6.8 or pH = 5 by adding concentrated HCl (0, 6 or 16 µL, respectively), were prepared and stirred

[154] W. Spiller, H. Kliesch, D. Wöhrle, S. Hackbarth, B. Röder, G. Schnurpfeil, *J. Porphyr. Phthalocyanines* **1998**, *2*, 145–158.

continuously. Their absorption and fluorescence spectra (λ_{exc} = 345 nm, λ_{em} = 355-850 nm) were recorded over time, from t = 0h up until t = 24h.

$^1O_2$ generation studies in PBS

Samples were prepared as following: DPBF was first dissolved in DMF to give a 10 mM solution. The corresponding SiPc was dissolved in spectroscopic grade DMF to give a 1 mM solution, which was diluted to 0.4 μM with buffer solution (PBS with 0.5% Cremophor EL®). Mixtures of the SiPc (25 mL, 0.4 μM) and DTT (0, 2 μM or 20 mM) in PBS, adjusted to pH = 7.4, pH = 6.8 or pH = 5 by adding concentrated HCl (0, 6 or 16 μL, respectively) were stirred continuously for 24 h after which 3 mL of these solutions were mixed with the DPBF solution (10 mM, 21 μL) followed by illumination with $h\nu_{>530nm}$. The decay of the absorbance of DPBF at 414 nm was monitored over time.

5.1.2 *In vitro* photodynamic therapy experiments

Cell Cultures

For the in *vitro* studies, cultured Hep-2 cells (a human larynx carcinoma cell line), SCC-13 cells (a human squamous cell carcinoma cell line) and HeLa cells (a human cervical carcinoma cell line) were used. All cell types were routinely grown as a monolayer in F25 flasks (Costar, Corning, NY, USA) on culture dishes with or without glass coverslips placed inside the dishes. In the case of SCC-13 and HeLa, Dulbecco's modified Eagle's medium (DMEM) supplemented with 10% (v/v) fetal bovine serum (FBS), 50 units/mL penicillin, and 50 μg/mL streptomycin was used. In the case of Hep-2, Roswell Park Memorial Institute medium (RPMI), also supplemented with 10% (v/v) fetal bovine serum (FBS), 50 units/mL penicillin, and 50 μg/mL streptomycin was used. Cells were grown in a HERA cell incubator (Heraeus, Kendro, Germany) with a 5% CO_2 atmosphere, a 95% relative humidity and a constant temperature of 37°C.

Preparation of SiPcs and Incubation of Cells

Stock solutions of the SiPcs (1.5×10^{-3} M) were prepared in DMSO. Work solutions for cell incubations were prepared from the stock solutions using DMEM or RPMI with 10% FBS. The final concentration of DMSO was always lower than 0.5% (v/v), and the lack of toxicity of this DMSO concentration for Hep-2, SCC-13 and HeLa cells was tested and confirmed.

Subcellular Localization of SiPcs

In order to analyse the localization of the SiPcs inside the cells, Hep-2, SCC-13 and HeLa cells were grown on coverslips. When cells reached around 80% of confluence, they were incubated with SiPc **1**, SiPc **3**, or SiPc **4** (diluted in cellular medium (DMEM or RPMI) with 1% FBS, to a final concentration of 2×10^{-6} M) for 24 h at 37°C, in the dark. Then, cells were washed with PBS, mounted on slides, and observed *in vivo* with a fluorescence microscope (Olympus BX61) using an excitation light with a wavelength of 365 nm (excitation filter: UG-1).

Photodynamic Treatments

HeLa, SCC-13 or Hep-2 cells were seeded in 24-well plates on cover slips until they reached around 80% of confluence. They were then incubated with different concentrations of SiPcs, ranging from 0.5×10^{-6} M to 2×10^{-6} M (diluted in cellular medium (DMEM or RPMI)), for 6 h. After incubation, cells were washed with PBS and then irradiated in complete media at 7.5 mW/cm^2 for variable times (1 or 2 min, corresponding to light doses from 0,45 to 0,90 J/cm^2) with a red light emitting diode source[133] with an emission peak at λ = 635 nm, as measured with a spectrophotometer. After irradiation, the cells were incubated in complete medium in the incubator at 37°C for 24 h. Dark control experiments were carried out in parallel, incubating the cells with the same concentrations of SiPc, for 18h, in the dark.

Cellular Toxicity

Toxicity of the different concentrations of SiPcs on HEp-2, SCC-13 and HeLa cells was evaluated 24 h after photodynamic treatment by the MTT (3-(4,5-dimethylthiazol-2-yl)-2,5-diphenyltetrazolium bromide, Sigma, St Louis, MI, USA) assay. This method is widely accepted as a quantitative colorimetric assay for mammalian cell toxicity[134] based on active cell metabolism. A stock MTT solution (1 mg/mL) in PBS was prepared immediately prior to use. Then, a solution of MTT with DMEM (10% FBS) was prepared (1 mL MTT-PBS/10 mL DMEM) and added to the culture dishes to obtain a final concentration of 50 µg/mL. After incubation at 37°C for 4 h, the culture medium was removed, and the precipitated formazan was dissolved in 500 µL of DMSO per well. The absorption was measured at 542 nm in a spectrophotometer (Espectra Fluor 4, Tecan). Cellular toxicity was expressed as a percentage of formazan absorption from PS-treated cells compared to control cells (which received neither PS nor PDT) (cell survival (%) = (mean OD value of PDT-treated cells / mean OD value of control cells) x 100%). The results obtained are mean values and standard deviations from three independent experiments.

Morphological Studies

HeLa, SCC-13 or Hep-2 cells were grown in coverslips until 80% confluence. Changes in cell morphology after photodynamic treatment (SiPc concentration of 1 x 10^{-6} M or 2 x 10^{-6} M for 6 h and a light dose of 0.45-0.90 J/cm^2) were analysed in vivo by phase contrast microscopy (Olympus BX61).

Optical and Electron Microscopy

Microscopic observations were carried out using an Olympus BX61 epifluorescence microscope equipped with filter sets for fluorescence microscopy: ultraviolet (UV, 365 nm, exciting filter UG-1), blue (450−490 nm, exciting filter BP 490), and green (545 nm, exciting filter BP 545). Photographs were obtained with the digital camera Olympus DP50 and processed using the Adobe PhotoShop CS5 extended version 12.0 software (Adobe Systems Inc, USA).

5.2 Experimental details synthesis

5.2.1 Synthesis of building blocks for axial substitution

1-Pyrenebutanoic acid, 2-[(2-hydroxyethyl)dithio]ethyl ester (**5**):

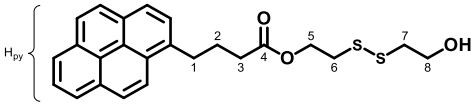

1-Pyrene butyric acid (2.00 g, 7 mmol), 2-hydroxyethyl disulfide (1.28 g, 8 mmol) and DMAP (cat.) were dissolved in dry DCM (300 mL) under argon atmosphere. EDC (0.595 g, 8 mmol) was separately dissolved in dry DCM (50 mL) and added. The solution was stirred at rt overnight, after which it was washed with water to remove the water-soluble EDC side-product. The organic phases were collected and dried on anhydrous $MgSO_4$. The solvent was removed under reduced pressure and the crude product purified by column chromatography using chloroform/methanol (100:1) as the eluent to yield **5** (2.30 g, 77%) as a light yellowish oil.

^{1}H-NMR (300 MHz, $CDCl_3$): δ(ppm) 8.39 – 7.76 (m, 9H, H_{py}), 4.36 (t, *J* = 6.6 Hz, 2H, H_5), 3.85 (t, *J* = 5.8 Hz, 2H, H_8), 3.40 (t, 2H, H_3), 2.87 (dt, *J* = 14.9, 6.2 Hz, 4H, H_6, H_7), 2.48 (t, *J* = 7.2 Hz, 2H, H_1), 2.21 (quin, *J* = 7.3 Hz, 2H, H_2).

^{13}C-NMR (75 MHz, $CDCl_3$): δ(ppm) 173.43 (C_4), 135.68 (C_{py}), 131.55 (C_{py}), 131.02(C_{py}), 130.14 (C_{py}), 128.88 (C_{py}), 127.60 (C_{py}), 127.55 (C_{py}), 127.49 (C_{py}), 126.88 (C_{py}), 125.99 (C_{py}), 125.23 (C_{py}), 125.11 (C_{py}), 125.08 (C_{py}), 124.94 (C_{py}), 124.92 (C_{py}), 123.41 (C_{py}), 62.43 (C_5), 60.37 (C_8), 41.76 (C_7), 37.17 (C_6), 33.88 (C_1), 32.84 (C_3), 26.81 (C_2).

MS (FAB, m-NBA): *m/z* = 424.1 $[M]^+$ (100), 215 $[pyrene+CH_3]^+$ (35).

HR-MS (FAB, m-NBA): $[M]^+$ Calcd. for $C_{24}H_{24}O_3S_2$: 424.1167; Found: 424.1156.

FT-IR (neat) ν (cm^{-1}): 3608 (O-H), 3045, 2947, 2878, 1732 (C=O), 1603, 1587, 1458, 1416, 1384, 1184, 1161, 1056, 848.

Triethylene glycol monomethyl ether tosylate (**6**):[155]

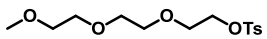

Triethylene glycol monomethyl ether (15.0 g, 0.091 mol) and NaOH (5.09 g, 0.127 mol) were dissolved in a mixture of THF (23 mL) and water (27 mL) under argon atmosphere. At 0°C, a solution of *p*-toluenesulfonyl chloride (15.6 g, 0.082 mol) in THF (27 mL) was added dropwise and the mixture was stirred for 3h at 0°C. The crude was poured into ice-water (90 mL) and the aqueous phase extracted several times with DCM and diethyl ether. The organic phases were collected

[155] D. A. Sheik, L. Brooks, K. Frantzen, S. Dewhurst, J. Yang, *ACS Nano* **2015**, *9*, 1829–1836.

and washed once with HCl 1 M and once with brine. The organic phase was dried on anhydrous $MgSO_4$ and the solvent removed under reduced pressure to yield the tosylate **6** (23.77 g, 82%) as a colorless oil. Characterization as reported in literature.

^{1}H-NMR (300 MHz, $CDCl_3$): δ(ppm) 7.75 (d, *J* = 8.2, 2H), 7.30 (d, 2H), 4.12 (t, *J* = 6.1 Hz, 2H), 3.64 (t, *J* = 6.1 Hz, 2H), 3.60 – 3.52 (m, 6H), 3.49 (t, *J* = 6.4 Hz, 2H), 3.33 (s, 3H), 2.41 (s, 3H).

^{13}C-NMR (75 MHz, $CDCl_3$): δ(ppm) 144.76, 133.07, 129.80, 127.96, 71.91, 70.75, 70.55, 69.22, 68.68, 59.01, 21.62.

3-[bis(methoxy(diethylenoxy)ethyl)amino]-1-propanol (**7**):

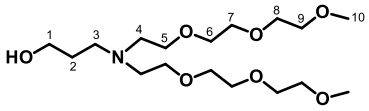

3-amino-1-propanol (0.50 g, 6.6 mmol), **6** (6.33 g, 19.9 mmol), Et_3N (3.2 mL, 2.66 mmol) and molecular sieves (3Å) were heated in acetonitrile (33 mL) under reflux and argon atmosphere for 36h. The solvent was removed under reduced pressure, the residue dissolved in $CHCl_3$, washed with a saturated solution of $NaHCO_3$ and extracted with DCM. The organic phase was dried on anhydrous $MgSO_4$, the solvent removed under reduced pressure and the crude purified by column chromatography using DCM/methanol (20:1) as the eluent to yield **7** (1.15 g, 61%) as a colorless oil.

^{1}H-NMR (300 MHz, $CDCl_3$): δ(ppm) 3.73 (t, *J* = 8.1 Hz, 2H, H_1), 3.66 – 3.50 (m, 20H, $H_{5\text{-}9}$), 3.35 (s, 6H, H_{10}), 2.77 – 2.66 (m, 6H, $H_{3\text{-}4}$), 1.64 (quin, *J* = 4.8 Hz, 2H, H_2).

^{13}C-NMR (75 MHz, $CDCl_3$): δ(ppm) 72.00 (C_9), 70.67 ($C_{6\text{-}8}$), 70.58 ($C_{6\text{-}8}$), 70.48 ($C_{6\text{-}8}$), 69.47 (C_5), 63.87 (C_1), 59.09 (C_{10}), 55.41 (C_3), 53.94 ($C_{5,6}$), 28.56 (C_2).

MS (FAB, m-NBA): *m/z* = 368.4 $[M]^+$ (100), 143.3 (30), 133.0 (30), 59.1 (40).

HR-MS (FAB, m-NBA): $[M]^+$ Calcd. for $C_{17}H_{38}NO_7$: 368.2648; Found: 368.2641.

FT-IR (neat) ν (cm^{-1}): 3448 (O-H), 2882, 1456, 1351, 1277, 1199, 1105 (C-O), 850.

2-[(2-hydroxyethyl)disulfanyl]ethyl acetate (**8**):[156]

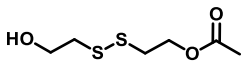

2-Hydroxyethyl disulfide (1.0 g, 6.5 mmol) was dissolved in dry DCM (50 mL) and triethylamine (1.36 mL, 9.7 mmol) was added under argon atmosphere. The reaction mixture was cooled to 0°C and acetyl chloride (0.46 mL, 6.5 mmol) was added dropwise. The solution was allowed to warm up to rt and the reaction was followed by TLC. Upon completion of the reaction (30 min), the reaction mixture was quenched with a saturated solution of $NaHCO_3$ and extracted with DCM. The

[156] A. K. Jain, M. G. Gund, D. C. Desai, N. Borhade, S. P. Senthilkumar, M. Dhiman, N. K. Mangu, S. V. Mali, N. P. Dubash, S. Halder, A. Satyam, *Bioorganic Chem.* **2013**, *49*, 40–48.

organic phases were collected and dried on anhydrous $MgSO_4$. The solvent was removed under reduced pressure and the crude purified by column chromatography using DCM/methanol (100:1) as the eluent. **8** was isolated as a colorless oil (0.43 g, 33%). Characterization as reported in literature.

^{1}H-NMR (300 MHz, $CDCl_3$): δ(ppm) 4.32 (t, *J* = 6.6 Hz, 2H), 3.86 (q, *J* = 5.7 Hz, 2H), 2.99 – 2.81 (m, 4H), 2.06 (s, 3H).

^{13}C-NMR (75 MHz, $CDCl_3$): δ(ppm) 58.88, 24.06, 19.70, 13.64.

3-aminopropyl (tert-butyl)dimethylsilyl ether (**9**):[157]

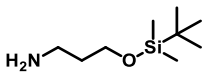

3-amino-1-propanol (8.4 mL, 0.11 mol) and *tert*-butyldimethylsilyl chloride (18.2 g, 1.12 mol) were dissolved in dry DCM (200 mL) under argon atmosphere. Triethylamine (23 mL) was added and the cloudy mixture was vigorously stirred at rt for 12 h. The resulting clear solution was washed with water and the organic layer dried on anhydrous MgSO4, filtered and concentrated to yield compound **9** as colorless oil (20.4 g, 98%). Characterization as reported in literature.

^{1}H-NMR (300 MHz, $CDCl_3$): δ(ppm) 3.67 (t, *J* = 6.1 Hz, 2H), 2.76 (t, *J* = 6.8 Hz, 2H), 1.62 (quin, *J* = 6.71 Hz, 2H), 0.86 (s, 8H), 0.02 (s, 6H).

^{13}C-NMR (75 MHz, $CDCl_3$): δ(ppm) 61.35, 39.48, 36.26, 26.04, 18.39, -5.26.

1-Pyrenebutanoic acid, N-(3-((tert-butyldimethylsilyl)oxy)propyl) amide (**10**):

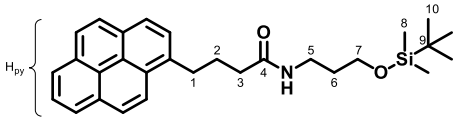

1-Pyrene butyric acid (2.000 g, 7 mmol), **9** (1.576 g, 8 mmol) and DMAP (cat.) were dissolved in dry DCM (400 mL) under argon atmosphere. EDC (1.595 g, 8 mmol) was separately dissolved in dry DCM (50 mL) and added. The solution was stirred at rt overnight, after which it was washed with water to remove the water-soluble EDC side-product. The organic phases were collected and dried on anhydrous $MgSO_4$. The solvent was removed under reduced pressure and the crude product purified by column chromatography using chloroform/methanol (100:1) as the eluent to yield **10** (3.517 g, 96%) as a light yellowish oil.

[157] D. F. Middleton, Analogues of Bredinin: Synthesis of 5-Hydroxyimidazoles from Acyclic Precursors, The University of Hull, **2008**.

^{1}H-NMR (300 MHz, $CDCl_3$): δ(ppm) 8.64 – 7.70 (m, 9H, H_{py}), 3.70 (t, *J* = 5.6 Hz, 2H, H_7), 3.44 – 3.31 (m, 4H, H_1, H_5), 2.28 – 2.13 (m, 4H, H_3, H_2), 1.70 (quin, *J* = 11.8 Hz, 2H, H_6), 0.81 (s, 9H, H_{10}), -0.01 (s, 6H, H_8).

^{13}C-NMR (75 MHz, $CDCl_3$): δ(ppm) 172.38 (C_4), 136.10 (C_{py}), 131.57 (C_{py}), 131.08 (C_{py}), 130.08 (C_{py}), 128.93 (C_{py}), 127.61 (C_{py}), 127.49 (C_{py}), 126.80 (C_{py}), 125.94 (C_{py}), 125.26 (C_{py}), 125.16 (C_{py}), 124.99 (C_{py}), 124.92 (C_{py}), 124.87 (C_{py}), 123.58 (C_{py}), 62.87 (C_7), 38.56 (C_5), 36.33 (C_3), 33.00 (C_1), 31.59 (C_6), 27.70 (C_2), 25.96 (C_{10}), 18.25 (C_9), -5.36 (C_8).

MS (FAB, m-NBA): *m/z* = 460.4 $[M + H]^+$ (30), 402.3 $[M - t\text{-Bu}]^+$ (30), 73.1 $[M - TBDMS]^+$ (100).

HR-MS (FAB, m-NBA): $[M+H]^+$ Calcd. for $C_{29}H_{38}NO_2Si$: 460.2672; Found: 460.2661.

FT-IR (neat) ν (cm^{-1}): 2955, 2931, 2857, 1666 (C=O), 1516, 1092, 848.

1-Pyrenebutanoic acid, N-(3-hydroxypropyl) amide (**11**):

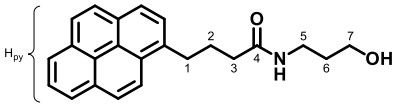

10 (3.517 g, 0.007 mol) is added to a dry flask flushed with argon. Dry methanol (30 mL) is added and the reaction mixture is cooled to 0°C. Acetyl chloride (0.001 mol, 0.082 mL) is added dropwise under vigorous stirring. Completion of the reaction is followed by TLC. After 2h, the reaction is complete and the solvent is evaporated. The residue is dissolved in DCM and washed with water. The organic phases are collected and dried on anhydrous $MgSO_4$. The solvent is removed under reduced pressure and the crude product purified by column chromatography using a gradient of Chloroform to chloroform/methanol (10:1) as the eluent to yield **11** (1.899 g, 69%) as viscous brown oil.

^{1}H-NMR (300 MHz, $CDCl_3$): δ(ppm) 8.44 – 7.55 (m, 9H, H_{py}), 6.01 (s, 1H, NH), 3.55 (t, *J* = 5.6 Hz, 2H, H_7), 3.37 – 3.19 (m, 4H, H_1, H_5), 2.27 – 2.05 (m, 4H, H_2, H_3), 1.57 (p, *J* = 5.8 Hz, 2H, H_6).

^{13}C-NMR (75 MHz, $CDCl_3$): δ(ppm) 173.99 (C_4), 135.70 (C_{py}), 131.38 (C_{py}), 130.86 (C_{py}), 129.93 (C_{py}), 128.72 (C_{py}), 127.45 (C_{py}), 127.38 (C_{py}), 127.29 (C_{py}), 126.71 (C_{py}), 125.87 (C_{py}), 125.05 (C_{py}), 124.93 (C_{py}), 124.78 (C_{py}), 123.29 (C_{py}), 59.29 (C_7), 36.28 (C_5), 35.90 (C_3), 32.70 (C_1), 32.18 (C_6), 27.46 (C_2).

MS (FAB, m-NBA): *m/z* = 691.3 $[2M]^+$ (20), 346.2 $[M+H]^+$ (100), 154 [matrix] (40), 137 [matrix] (30).

HR-MS (FAB, m-NBA): $[M]^+$ Calcd. for $C_{23}H_{24}NO_2$: 346.1807; Found: 346.1804.

FT-IR (neat) ν (cm^{-1}): XXX

5.2.2 Synthesis of silicon phthalocyanines

Silicon (IV) phthalocyanine **1**:

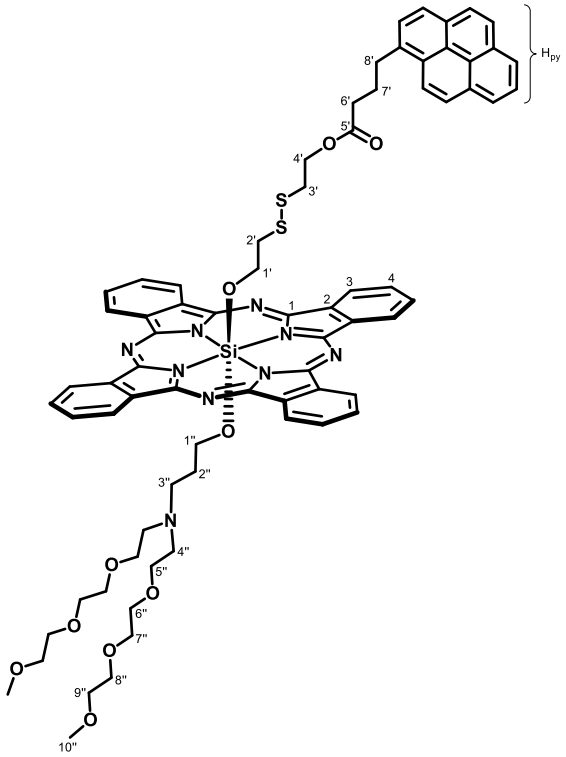

$SiPcCl_2$ (0.100 g, 0.164 mmol), alcohol **5** (0.174 g, 0.409 mmol), alcohol **7** (0.150 g, 0.409 mmol) and pyridine (0.3 mL) in dry toluene (15 mL) were heated under reflux and argon atmosphere for 18 h. The solvent was removed under reduced pressure and the crude purified by column chromatography using silica gel, previously neutralized with triethylamine, and DCM/methanol (50:1) as the eluent. After further SEC with Bio-Beads in DCM, **1** (0.030 g, 16%) was obtained as a dark blue sticky paste.

^{1}H-NMR (300 MHz, $CDCl_3$): δ(ppm) = 9.64 (dd, *J* = 5.7, 3.1 Hz, 8H, H_3), 8.34 (dd, *J* = 5.7, 2.9 Hz, 8H, H_4), 8.21 – 7.77 (m, 9H, H_{py}), 3.49 (t, *J* = 6.2 Hz, 2H, $H_{4'}$), 3.35 (t, 2H, $H_{8'}$), 3.33 – 3.01 (m, 22H, $H_{6''\text{-}10''}$), 2.19 (t, *J* = 6.7 Hz, 2H, $H_{6'}$), 2.01 (quin, *J* = 7.8 Hz, 2H, $H_{7'}$), 1.63 (t, 2H, $H_{3'}$), 1.44 – 1.38 (m, 4H, $H_{5''}$), 1.25 (s, 4H, $H_{4''}$), 0.19 (br s, 2H, $H_{3''}$), -0.41 (t, *J* = 6.3 Hz, 2H,$H_{2'}$), -1.01 (br s, 2H, $H_{2''}$), -1.78 (t, *J* = 7.2 Hz, 2H, $H_{1'}$), -2.08 (t, *J* = 5.5 Hz, 2H, $H_{1''}$).

^{13}C-NMR (75 MHz, $CDCl_3$): δ(ppm) = 173.36 ($C_{5'}$), 149.86 (C_1), 136.45 (C_2), 131.61 (C_4), 129.26 (C_{py}), 128.05 (C_{py}), 127.87 (C_{py}), 127.28 (C_{py}), 126.40 (C_{py}), 125.48 (C_{py}), 125.34 (C_{py}), 124.31 (C_{py}), 123.82 (C_3), 72.29, 70.77, 70.38, 62.21, 59.44, 54.46, 53.99, 51.46, 39.55, 39.32, 36.81, 33.17, 30.17, 23.26, 11.98.

MS (MALDI-TOF, DCTB): *m/z* = 1352.4 $[M+Na]^+$ (40), 963.3 $[M\text{-}L_{axial(S3)}]^+$ (100).

HR-MS (MALDI-TOF, DCTB): $[M+Na]^+$ Calcd. for $C_{73}H_{75}N_9O_{10}S_2SiNa$: 1352.4740; Found: 1352.4708.

UV-VIS (DMF): λ_{max} (nm) (log ε): 675 (5.30), 645 (sh), 607 (4.50), 356 (sh), 344 (4.77), 328 (4.77).

FT-IR (neat) ν (cm^{-1}): 2929, 2880, 2361, 2340, 1733 (C=O), 1334, 1291, 1123, 1081, 911, 848.

Silicon (IV) phthalocyanine **2**:

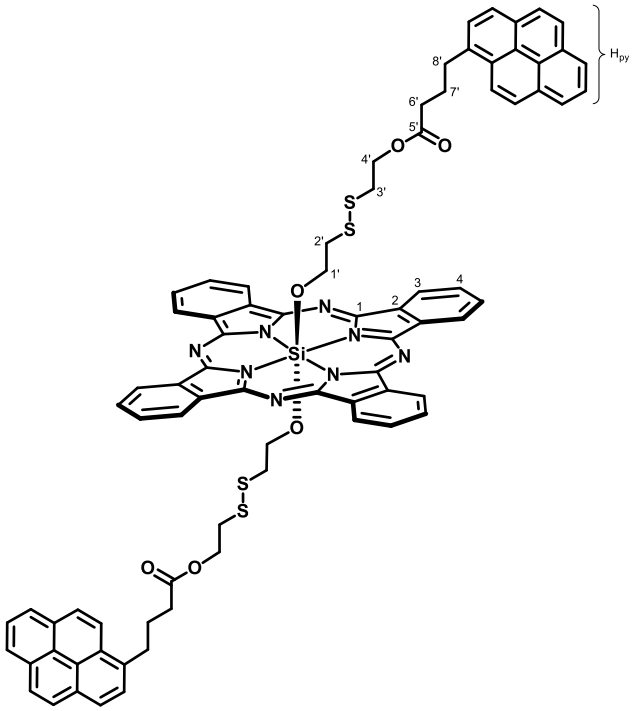

$SiPcCl_2$ (0.100 g, 0.164 mmol), alcohol **5** (0.347 g, 0.817 mmol) and pyridine (0.3 mL) in dry toluene (15 mL) were heated under reflux and argon atmosphere for 18 h. The solvent was removed under reduced pressure and the crude purified by column chromatography using silica gel, previously neutralized with triethylamine, and DCM as the eluent. After trituration in methanol and recrystallization from toluene, **2** (0.061 g, 32%) was obtained as a dark blue solid.

^{1}H-NMR (300 MHz, $CDCl_3$): δ(ppm) 9.65 (dd, *J* = 5.7, 3.1 Hz, 8H, H_3), 8.30 (dd, *J* = 6.0, 2.8 Hz, 8H, H_4), 8.24 – 7.75 (m, 18H, H_{py}), 3.52 (t, *J* = 6.5 Hz, 4H, $H_{4'}$), 3.28 (t, *J* = 7.7 Hz, 4H, $H_{8'}$), 2.23 (t, *J* = 7.2 Hz, 4H, $H_{6'}$), 2.04 (q, *J* = 7.2 Hz, 4H, $H_{7'}$), 1.64 (t, *J* = 6.5 Hz, 4H, $H_{3'}$), -0.38 (t, *J* = 6.5 Hz, 4H, $H_{2'}$), -1.75 (t, *J* = 6.5 Hz, 4H, $H_{1'}$).

^{13}C-NMR (75 MHz, $CDCl_3$): δ(ppm) 172.82 ($C_{5'}$), 149.38 (C_1), 135.98 (C_2), 135.62 (C_{py}), 131.42 (C_{py}), 130.95 (C_4), 130.88 (C_{py}), 129.96 (C_{py}), 128.70 (C_{py}), 127.49 (C_{py}), 127.36 (C_{py}), 127.32 (C_{py}), 126.72 (C_{py}), 125.84 (C_{py}), 125.08 (C_{py}), 124.98 (C_{py}), 124.92 (C_{py}), 124.78 (C_{py}), 123.70 (C_3), 123.27 (C_{py}), 53.91 ($C_{1'}$), 50.93 ($C_{4'}$), 38.70 ($C_{2'}$), 36.27 ($C_{3'}$), 33.53 ($C_{6'}$), 32.62 ($C_{8'}$), 26.58 ($C_{7'}$).

MS (MALDI-TOF, DCTB): *m/z* = 1387.3 $[M+H]^+$ (24), 963.2 $[M-L_{axial}]^+$ (100).

HR-MS (MALDI-TOF, DCTB): $[M]^+$ Calcd. for $C_{80}H_{62}N_8O_6S_4Si$: 1386.3425; Found: 1386.3439.

UV-VIS (DMF): λ_{max} (nm) (log ε ($dm^3\ mol^{-1}\ cm^{-1}$)): 676 (5.38), 644 (sh), 607 (4.58), 356 (sh), 344 (5.14), 328 (5.02).

FT-IR (neat) ν (cm^{-1}): 2929, 2880, 2361, 2340, 1733 (C=O), 1334, 1291, 1123, 1081, 911, 848.

Mp: 282°C.

Silicon (IV) phthalocyanine **3**:

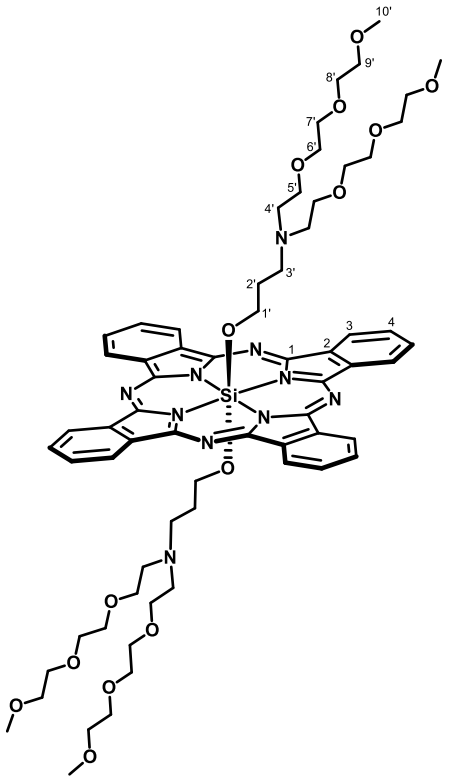

$SiPcCl_2$ (0.100 g, 0.164 mmol), alcohol **7** (0.293 g, 0.817 mmol) and pyridine (0.3 mL) in dry toluene (15 mL) were heated under reflux and argon atmosphere for 18 h. The solvent was removed under reduced pressure and the crude purified by column chromatography using silica gel, previously neutralized with triethylamine, and DCM/methanol (20:1) as the eluent. After further SEC with Bio-Beads in DCM, **3** (0.041 g, 24%) was obtained as a dark blue solid.

^{1}H-NMR (300 MHz, $CDCl_3$): δ(ppm) = 9.64 (dd, *J* = 5.6, 2.7 Hz, 8H, H_3), 8.35 (dd, *J* = 5.6, 3.0 Hz, 8H, H_4), 3.46 – 3.38 (m, 12H, $H_{4'\text{-}10'}$), 3.35 – 3.26 (m, 16H, $H_{4'\text{-}10'}$), 3.09 (t, *J* = 4.8 Hz, 8H, $H_{4'\text{-}10'}$), 2.51 (br s, 8H, $H_{4'\text{-}10'}$), 1.49 (br s, 8H, $H_{4'\text{-}10'}$), -0.39 (br s, 4H, $H_{3'}$), -1.48 (br s, 4H, $H_{2'}$), -2.11 (t, *J* = 5.8 Hz, 4H, $H_{1'}$).

^{13}C-NMR (75 MHz, $CDCl_3$): δ(ppm) = 149.35 (C_1), 136.08 (C_2), 131.06 (C_4), 123.84 (C_3), 72.10 ($C_{4'\text{-}10'}$), 71.96 ($C_{4'\text{-}10'}$), 70.69 ($C_{4'\text{-}10'}$), 70.47 ($C_{4'\text{-}10'}$), 70.04 ($C_{4'\text{-}10'}$), 68.70 ($C_{4'\text{-}10'}$), 59.20 ($C_{4'\text{-}10'}$), 59.09 ($C_{4'\text{-}10'}$), 52.81 ($C_{1'}$), 49.88 ($C_{3'}$), 29.86 ($C_{2'}$).

MS (MALDI-TOF, DCTB): *m/z* = 1318.6 $[M+2Na]^+$ (50), 1295.6 $[M+Na]^+$ (60), 929.4 $[M\text{-}L_{axial}+Na]^+$ (100), 906 $[M\text{-}L_{axial}]^+$ (95).

HR-MS (MALDI-TOF, DCTB): $[M+Na]^+$ Calcd. for $C_{66}H_{88}N_{10}O_{14}SiNa$: 1295.6143, Found: 1295.6108.

UV-VIS (DMF): λ_{max} (nm) (log ε): 673 (5.35), 644 (sh), 605 (4.56), 355 (4.82).

FT-IR (neat) ν (cm^{-1}): 2933, 2882, 2357, 2342, 1334, 1123, 1081 (C-O), 568.

Silicon (IV) phthalocyanine **4**:

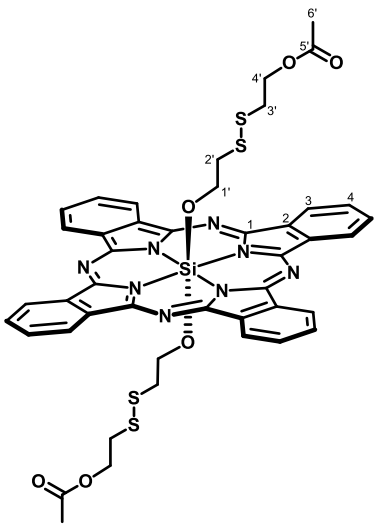

$SiPcCl_2$ (0.100 g, 0.164 mmol), alcohol **8** (0.160 g, 0.817 mmol) and pyridine (0.3 mL) in dry toluene (15 mL) were heated under reflux and argon atmosphere for 18 h. The solvent was removed under reduced pressure and the crude purified by column chromatography using silica gel, previously neutralized with triethylamine, and DCM/methanol (100:1) as the eluent. After recrystallization from methanol, compound **4** (0.036 g, 28%) was obtained as a dark blue solid.

^{1}H-NMR (300 MHz, $CDCl_3$): δ(ppm) 9.67 (dd, *J* = 5.7, 3.1 Hz, 8H, H_3), 8.37 (dd, J = 5.7, 3.1 Hz, 8H, H_4), 3.46 (t, *J* = 6.9 Hz, 4H, $H_{4'}$), 1.81 (s, 6H, $H_{6'}$), 1.61 (t, J = 6.6 Hz, 4H, $H_{3'}$), -0.40 (t, *J* = 6.5 Hz, 4H, $H_{2'}$), -1.77 (t, *J* = 6.4 Hz, 4H, $H_{1'}$).

^{13}C-NMR (75 MHz, $CDCl_3$): δ(ppm) 170.55 ($C_{5'}$), 149.52 (C_1), 136.16 (C_2), 131.11 (C_4), 123.88 (C_3), 61.91 ($C_{4'}$), 54.06 ($C_{1'}$), 38.87 ($C_{2'}$), 36.39 ($C_{3'}$), 20.80 ($C_{6'}$).

MS (MALDI-TOF, DCTB): *m/z* = 930.2 $[M]^+$ (46), 735.2 $[M\text{-}L_{axial}]^+$ (100).

HR-MS (MALDI-TOF, DCTB): $[M]^+$ Calcd. for $C_{44}H_{38}N_8O_6S_4Si$: 930.1561; Found: 930.1554.

UV-VIS (DMF): λ_{max} (nm) (log ε): 675 (5.34), 644 (sh), 607 (4.54), 356 (4.77).

FT-IR (neat) ν (cm^{-1}): 1738 (C=O), 1612, 1520, 1380, 1348, 1334, 1292, 1271, 1258, 1123, 1081, 911, 572.

Mp: 212°C.

5.2.3 Synthesis of subphthalocyanines

Boron subphthalocyanine chloride **16**:[86]

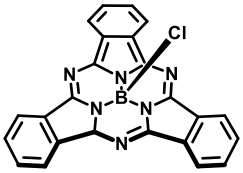

BCl_3 in *p*-xylene 1 M (7.8 mL, 0.0078 mmol) was added to 1,2-dicyanobenzene (1.0 g, 0.0078 mmol) under argon atmosphere and the resulting reaction mixture was immediately brought to reflux and stirred vigorously at this temperature for 40 min. The reaction mixture was then allowed to cool down to rt, after which heptane was added to precipitate the resulting SubPc. The solid obtained was washed extensively with heptane and methanol, until the filtrate remained completely colorless, yielding SubPcCl **16** (0.235 g, 21%) as a dark brown solid. Characterization as reported in literature.

^{1}H-NMR (300 MHz, $CDCl_3$): δ(ppm) 8.72-8.63 (dd, J = 5.7, 3.1 Hz, 6H, H_3), 7.88-7.78 (dd, J = 5.8, 3.2 Hz, 6H, H_4).

UV-VIS ($CHCl_3$): λ_{max} (nm) (log ε): 565 (4.4), 529 (h), 308 (4.1), 273 (4.1).

Mp: >250°C.

Subphthalocyanine **12**:

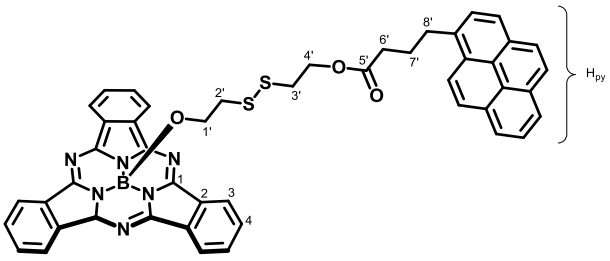

SubPcCl **16** (0.080 g, 0.190 mmol) and silver triflate (0.060 g, 0.230 mmol) were dissolved anhydrous toluene (3 mL) and the mixture was stirred at rt under argon atmosphere for 40 min until **16** was consumed. Once the SubPcBOTf is generated, the nucleophile **5** (0.158 g, 0.380 mmol) and DIPEA (40 µL, 0.230 mmol) were added. The mixture was stirred at 40°C for 4h until the reaction was completed. The solvent was removed by evaporation under reduced pressure and the product was directly purified by column chromatography on silica gel using toluene/THF (10:1) as the eluent. After further SEC with Bio-Beads in toluene, **12** (0.081 g, 52%) was obtained as a dark pink solid.

^{1}H-NMR (300 MHz, $CDCl_3$): δ(ppm) 8.75 – 8.57 (dd, *J* = 5.9, 3.2 Hz, 6H, H_3), 8.16 – 7.74 (m, 9H, H_{py}), 7.70 – 7.61 (dd, *J* = 5.8, 3.2 Hz, 6H, H_4), 3.94 (t, *J* = 6.5 Hz, 2H, $H_{4'}$), 3.21 (t, *J* = 7.6 Hz, 2H, $H_{8'}$), 2.35 (t, *J* = 6.5 Hz, 2H, $H_{3'}$), 2.26 (t, *J* = 7.1 Hz, 2H, $H_{6'}$), 2.09 – 1.96 (m, 2H, $H_{7'}$), 1.70 – 1.59 (m, 4H, $H_{1'\text{-}2'}$).

^{13}C-NMR (75 MHz, $CDCl_3$): δ(ppm) 172.71 ($C_{5'}$), 151.07 (C_1), 135.31 (C_{py}), 130.83 (C_{py}), 130.60 (C_2), 129.57 (C_4), 129.41 (C_{py}), 129.34 (C_{py}), 128.66 (C_{py}), 128.36 (C_{py}), 127.84 (C_{py}),

127.09 (C_{py}), 127.02 (C_{py}), 126.99 (C_{py}), 126.29 (C_{py}), 125.38 (C_{py}), 124.56 (C_{py}), 124.45 (C_{py}), 124.35 (C_{py}), 122.96 (C_{py}), 121.73 (C_3), 61.78 ($C_{4'}$), 57.32 ($C_{1'}$), 39.37 ($C_{2'}$), 36.67 ($C_{3'}$), 33.36 ($C_{6'}$), 32.37 ($C_{8'}$), 26.36 ($C_{7'}$).

MS (MALDI-TOF, DCTB): *m/z* = 1104.3 (2), 1068.4 (2), 966.2 (2), 894.2 (2), 818.3 $[M]^+$ (100), 471.2 $[M\text{-}C_{3'\text{-}16''}]^+$ (5), 412.2 $[M\text{-}L_{axial}\text{+OH}]^+$ (2), 395.2 $[M\text{-}L_{axial}]^+$ (2)

HR-MS (MALDI-TOF, DCTB): $[M]^+$ Calcd. for $C_{48}H_{37}BN_6O_3S_2$: 818.2308; Found: 818.2316.

UV-VIS (DMF): λ_{max} (nm) (log ε): 562 (4.78), 544 (sh), 505 (sh), 344 (4.57), 327 (4.52), 311 (4.55).

FT-IR (neat) ν (cm^{-1}): 1726 (C=O), 1455, 1381, 1285, 1171, 1128, 843, 731.

Mp: >250°C.

Subphthalocyanine **13**:

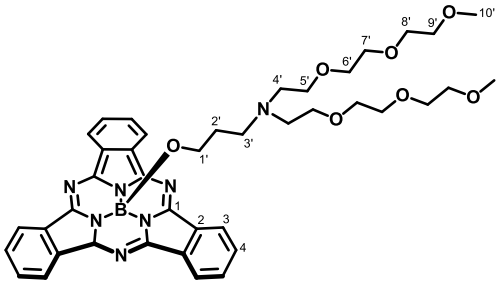

SubPcCl **16** (0.080 g, 0.190 mmol) and silver triflate (0.060 g, 0.230 mmol) were dissolved in anhydrous toluene (3 mL) and the mixture was stirred at rt under argon atmosphere for 40 min until **16** was consumed. Once the SubPcBOTf is generated, the nucleophile **7** (0.137 g, 0.380 mmol) and DIPEA (40 µL, 0.230 mmol) were added. The mixture was stirred at 40°C for 5h until the reaction was completed. The solvent was removed by evaporation under reduced pressure and the product was directly purified by column chromatography on silica gel using toluene/THF (10:1 to 1:1) as the eluent. After further SEC with Bio-Beads in toluene, **13** (0.062 g, 43%) was obtained as a dark pink sticky paste.

^{1}H-NMR (300 MHz, $CDCl_3$): δ(ppm) 8.89 – 8.79 (dd, *J* = 5.7, 3.1 Hz, 6H, H_3), 7.93 – 7.84 (dd, *J* = 5.8, 3.2 Hz, 6H, H_4), 3.72 – 3.35 (m, 20H, $H_{5'\text{-}9'}$), 3.31 (br s, 6H, $H_{10'}$), 2.56 (br s, 4H, $H_{4'}$), 2.04 (s, 2H, $H_{3'}$), 1.49 (t, *J* = 6.0 Hz, 2H, $H_{1'}$), 0.77 (br s, 2H, $H_{2'}$).

^{13}C-NMR (75 MHz, $CDCl_3$): δ(ppm) 151.60 (C_1), 131.04 (C_2), 129.94 (C_4), 122.25 (C_3), 71.87 ($C_{5'\text{-}9'}$), 70.33 ($C_{5'\text{-}9'}$), 70.30 ($C_{5'\text{-}9'}$), 70.14 ($C_{5'\text{-}9'}$), 59.05 ($C_{10'}$), 57.11 ($C_{1'}$), 53.43 ($C_{4'}$), 51.55 ($C_{3'}$), 26.88 ($C_{2'}$).

MS (MALDI-TOF, DCTB): *m/z* = *m/z* = 784.4 $[M+Na]^+$ (24).

HR-MS (MALDI-TOF, DCTB): $[M]^+$ Calcd. for $C_{41}H_{48}BN_7O_7$: 761.3708; Found: 761.3712.

UV-VIS (DMF): λ_{max} (nm) (log ε): 562 (4.97), 544 (sh), 506 (sh), 303 (4.70).

FT-IR (neat) ν (cm^{-1}): 2871, 1725, 1465, 1376, 1284, 1249, 1090, 1028, 846, 744.

Mp: >250°C.

Subphthalocyanine **14**:

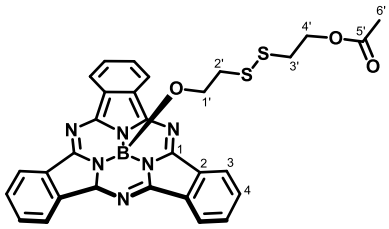

SubPcCl **16** (0.080 g, 0.190 mmol) and silver triflate (0.060 g, 0.230 mmol) were dissolved in anhydrous toluene (3 mL) and the mixture was stirred at rt under argon atmosphere for 40 min until **16** was consumed. Once the SubPcBOTf is generated, the nucleophile **8** (0.073 g, 0.380 mmol) and DIPEA (40 µL, 0.230 mmol) were added. The mixture was stirred at 40°C for 3h until the reaction was completed. The solvent was removed by evaporation under reduced pressure and the product was directly purified by column chromatography on silica gel using toluene/THF (30:1 to 10:1) as the eluent. After further SEC with Bio-Beads in toluene, **14** (0.072 g, 64%) was obtained as a dark pink solid.

^{1}H-NMR (300 MHz, $CDCl_3$): δ(ppm) 8.92 – 8.77 (dd, *J* = 5.8, 3.1 Hz, 6H, H_3), 7.94 – 7.81 (dd, J = 5.9, 3.1 Hz, 6H, H_4), 4.02 (t, *J* = 6.6 Hz, 2H, $H_{4'}$), 2.47 (t, J = 6.6 Hz, 2H, $H_{3'}$), 1.99 (s, 3H, $H_{6'}$), 1.81 – 1.70 (m, 4H, $H_{1'\text{-}2'}$).

^{13}C-NMR (75 MHz, $CDCl_3$): δ(ppm) 170.80 ($C_{5'}$), 151.63 (C_1), 131.12 (C_2), 129.89 (C_4), 122.26 (C_3), 62.34 ($C_{4'}$), 57.79 ($C_{1'}$), 39.83 ($C_{2'}$), 37.08 ($C_{3'}$), 20.97 ($C_{6'}$).

MS (MALDI-TOF, DCTB): *m/z* = 590.2 $[M]^+$ (100), 471.2 $[M\text{-}(CH_2)_2OCOCH_3]^+$ (10), 395.2 $[M\text{-}L_{axial}]^+$ (5).

HR-MS (MALDI-TOF, DCTB): $[M+Na]^+$ Calcd. for $C_{30}H_{23}BN_6O_3S_2$: 590.1366 ; Found: 590.1385.

UV-VIS (DMF): λ_{max} (nm) (log ε): 562 (4.86), 545 (sh), 507 (sh), 303 (4.59).

FT-IR (neat) ν (cm^{-1}): 1734 (C=O), 1638, 1455, 1430, 1379, 1323, 1287, 1226, 1193, 1129, 1027, 738.

Mp: >250°C.

Subphthalocyanine **15**:

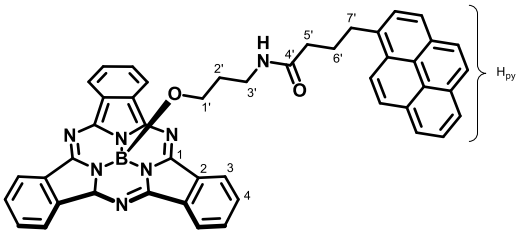

SubPcCl **16** (0.080 g, 0.190 mmol) and silver triflate (0.060 g, 0.230 mmol) were dissolved in anhydrous DCM (3 mL) and the mixture was stirred at rt under argon atmosphere for 40 min until **16** was consumed. Once the SubPcBOTf was generated, the nucleophile **11** (0.128 g, 0.380 mmol) and DIPEA (40 µL, 0.230 mmol) were added. The mixture was stirred at 40°C for 4h until the reaction was completed. The solvent was removed by evaporation under reduced pressure and the product was directly purified by column chromatography on silica gel using toluene/THF (10:1) as the eluent. After trituration in heptane **15** (0.079 g, 56%) was obtained as a dark pink solid.

^{1}H-NMR (300 MHz, $CDCl_3$): δ(ppm) 8.87 – 8.75 (dd, *J* = 5.8, 3.2 Hz, 6H, H_3), 8.28 – 7.92 (m, 9H, H_{py}), 7.89 – 7.79 (dd, *J* = 5.9, 3.2 Hz, 6H, H_4), 5.19 (s, 1H, $H_{4'}$), 3.31 – 3.16 (m, 2H, $H_{6'}$), 2.68 – 2.54 (m, 2H, $H_{3'}$), 2.05 – 1.89 (m, 4H, $H_{7'-8'}$), 1.60 (t, *J* = 5.6 Hz, 2H, $H_{1'}$), 0.82 – 0.68 (m, 2H, $H_{2'}$).

^{13}C-NMR (75 MHz, $CDCl_3$): δ(ppm) 172.08 ($C_{4'}$), 151.55 (C_1), 136.14 (C_{py}), 131.54 (C_{py}), 131.07 (C_2), 131.02 (C_4), 130.01 (C_{py}), 129.93 (C_{py}), 128.87 (C_{py}), 127.65 (C_{py}), 127.46 (C_{py}), 127.42 (C_{py}), 126.73 (C_{py}), 125.87 (C_{py}), 124.92 (C_{py}), 124.83 (C_{py}), 123.65 (C_{py}), 122.24 (C_3), 58.48 ($C_{1'}$), 37.84 ($C_{3'}$), 36.27 ($C_{7'}$), 32.95 ($C_{5'}$), 29.38 ($C_{2'}$), 27.44 ($C_{6'}$).

MS (MALDI-TOF, DCTB): *m/z* = 762.3 $[M+Na]^+$ (2), 739.4 $[M]^+$ (100), 628.3 (2), 395.2 $[M-L_{axial}]^+$ (2).

HR-MS (MALDI-TOF, DCTB): $[M]^+$ Calcd. for $C_{47}H_{34}BN_7O_2$: 739.2869; Found: 739.2874.

UV-VIS (DMF): λ_{max} (nm) (log ε): 562 (4.78), 543 (sh), 506 (sh), 344 (4.54), 328 (4.49), 303 (4.56).

FT-IR (neat) ν (cm^{-1}): 2954, 2868, 2359, 1724, 1643 (C=O), 1456, 1431, 1287, 1230, 1177, 1130, 845, 742.

Mp: >250°C.

5.2.4 Synthesis of SiPc-(SubPc)$_2$ triad

Subphthalocyanine **18**:

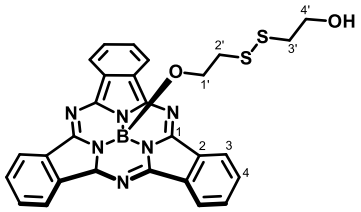

SubPcCl **16** (0.080 g, 0.190 mmol) and silver triflate (0.060 g, 0.230 mmol) were dissolved in anhydrous toluene (3 mL) and the mixture was stirred at rt under argon atmosphere for 40 min until **16** was consumed. Once the SubPcBOTf is generated, 2-hydroxyethyl disulfide (0.058 g, 0.380 mmol) and DIPEA (40 µL, 0.230 mmol) were added. The mixture was stirred at 40°C for 6h until the reaction was completed. The solvent was removed by evaporation under reduced pressure and the product was directly purified by column chromatography on silica gel using toluene/THF (30:1 to 10:1) as the eluent. After trituration in water, **18** (0.063 g, 56%) was obtained as a dark pink solid.

^{1}H-NMR (300 MHz, $CDCl_3$): δ(ppm) 8.90 – 8.78 (dd, *J* = 5.8, 3.3 Hz, 6H, H_3), 7.96 – 7.81 (dd, *J* = 5.9, 3.2 Hz, 6H, H_4), 3.62 (t, *J* = 5.8 Hz, 2H, $H_{4'}$), 2.43 (t, *J* = 5.8 Hz, 2H, $H_{3'}$), 1.76 (dt, *J* = 9.8, 4.9 Hz, 4H, $H_{1'\text{-}2'}$).

^{13}C-NMR (75 MHz, $CDCl_3$): δ(ppm) 151.61 (C_1), 131.11 (C_2), 129.96 (C_4), 122.29 (C_3), 60.22 ($C_{4'}$), 58.04 ($C_{1'}$), 41.50 ($C_{2'}$), 39.92 ($C_{3'}$).

MS (MALDI-TOF, DCTB): *m/z* = 564.2 (5), 548.2 $[M]^+$ (100), 498.2 (5), 471.2 $[M\text{-}(CH_2)_2OH]^+$ (15), 412.2 $[M\text{-}L_{axial}\text{+}OH]^+$ (10), 242.3 (20).

HR-MS (MALDI-TOF, DCTB): $[M]^+$ Calcd. for $C_{28}H_{21}BN_6O_2S_2$: 548.1260 ; Found: 548.1261.

UV-VIS (DMF): λ_{max} (nm) (log ε): 562 (4.95), 544 (sh), 507 (sh) 302 (4.68).

FT-IR (neat) ν (cm^{-1}): 2872, 1725, 1669, 1576, 1455, 1377, 1284, 1250, 1029, 847, 744.

Mp: >250°C.

SiPc-(SubPc)$_2$ triad **17**:

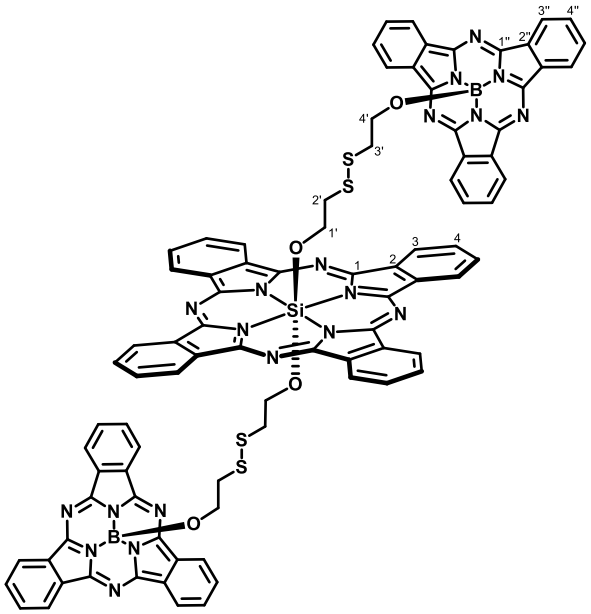

$SiPcCl_2$ (0.027 g, 0.044 mmol), **18** (0.121 g, 0.222 mmol) and DIPEA (0.081 mL) in anhydrous toluene (4.1 mL) were heated under reflux and argon atmosphere for 18 h. The solvent was removed under reduced pressure and the crude purified by SEC with Bio-Beads in Chloroform, to yield **17** (0.008 g, estimated yield 11%)[158] as a dark purple solid.

^{1}H-NMR (300 MHz, $CDCl_3$): δ(ppm) 9.52 (dd, J = 5.8, 3.0 Hz, 8H, H_3), 8.75 (dd, *J* = 5.9, 3.1 Hz, 12H, $H_{3''}$), 8.23 (dd, *J* = 5.7, 3.0 Hz, 8H, H_4), 7.81 (dd, *J* = 5.9, 3.1 Hz, 12H, $H_{4''}$), 0.98 – 0.69 (m, 4H, $H_{4'}$), 0.42 (t, *J* = 6.6 Hz, 4H, $H_{3'}$), -0.97 (t, *J* = 6.6 Hz, 4H, $H_{2'}$), -2.16 (t, J = 6.7 Hz, 4H, $H_{1'}$).

^{13}C-NMR (75 MHz, $CDCl_3$): δ(ppm) 151.37 ($C_{1''}$), 149.27 (C_1), 136.01 (C_2), 130.97 (C_4, $C_{2''}$), 129.75 ($_{C4''}$), 123.75 (C_3), 122.13 ($C_{3''}$), 57.24 ($C_{4'}$), 53.57 ($C_{1'}$), 29.86 ($C_{2'}$), 22.85 ($C_{3'}$).

UV-VIS (DMF): λ_{max} (nm) (log ε): 675 (5.36), 646 (sh), 608 (4.54), 562 (5.23), 544 (sh) , 508 (sh), 354 (4.95).

[158] An estimated yield of the product is reported due to the difficulty of purification (after SEC with Bio-Beads as the stationary phase and chloroform as the mobile phase, only a fraction of the **17** elutes as pure compound, the remaining part eluting together with the starting products **$SiPcCl_2$** and **18**, and/or decomposition products). For the same reason (low stability), it was not possible to detect the molecular ion by mass spectrometry, yet ^{1}H-NMR characterization is conclusive about the purity and identity of the product.

CHAPTER 2

Design, synthesis and *in vitro* evaluation of positively charged (sub)phthalocyanines for use in photodynamic inactivation of microorganisms

1

Cationic silicon phthalocyanines as photosensitizers for photodynamic inactivation

1.1 State of the art

Several photosensitizing agents have proven to induce an efficient inactivation of different classes of microbial pathogens. Antimicrobial PS should generally display the same characteristics as PS used in PDT, including high extinction coefficients in the NIR region of the electromagnetic spectrum, a long-lived triplet state and high ϕ_Δ. On the basis of biochemical and morphological features of microbial cells, and striving for a broad spectrum of action on bacteria, fungi, yeasts and parasitic protozoa, the most effective PS in PDI have found to be the cationic ones. To this end, parallel to our series of neutral SiPcs synthesized in Chapter 1 – Subchapter 1, which serve as PS for PDT of different cancer types, we took up the idea to synthesize a series of cationic SiPcs that could serve as broad spectrum PS for PDI of different microorganisms.

1.1.1 The necessity of positively charged photosensitizers

As mentioned in the Introduction of this Thesis, the PDI of microorganisms is based on causing photoinduced damage to their cytoplasmic membrane, which rapidly results in cell death. Therefore, in the search for a general PS that can effectively inactivate a wide range of microorganisms, one must take into account that Gram negative bacteria are the hardest ones to inactivate. The reason for this is that their cytoplasmic membrane is protected by the presence of an impermeable outer cell membrane, which hinders the PS to reach the site of action (Figure 75a). On contrary, the cytoplasmic membrane of Gram-

positive bacteria is surrounded by a relatively porous cell wall composed of peptidoglycan that allows for an easy crossing of PS molecules (Figure 75b).

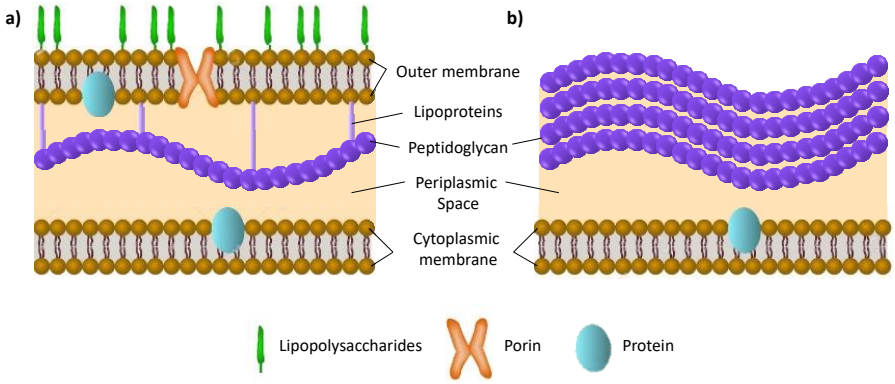

Figure 75. Structure of the cell wall of Gram-negative (left) vs. Gram-positive (right) bacteria.

To be able to permeabilize this outer membrane in Gram-negative bacteria, PS for PDI were initially applied in combination with permeabilizing agents such as EDTA, PMNP and $CaCl_2$.[159] Later, in the 1990s, it was discovered that cationic PS were effective in the eradication of both Gram-positive and Gram-negative bacteria, without the necessity of additives.[160] This can be explained by the fact that the cytoplasmic membrane of both Gram-positive and Gram-negative bacteria bears negatively charged carboxylate functions,[161] and the positive charge on the PS molecule appears to promote a tight electrostatic interaction with these negatively charged sites at the outer surface of the bacterial cells. As a consequence of these electrostatic interactions, the outer membrane of Gram-negative bacteria is disturbed, opening a way for the PS to reach the site of action. On the other hand, neutrally or negatively charged PS will never be able to cross this barrier and, although they might be able to inactivate Gram positive bacteria, yeast and viruses, they will not function for the PDI of Gram negative bacteria.[162] Importantly, the use of cationic PS has a second highly beneficial property, since it has been demonstrated both *in vitro* and *in vivo* that cationic charges target for microbial cells selectively over host mammalian cells that will also be present in an infected lesion.[163]

---

159 F. F. Sperandio, Y.-Y. Huang, M. R. Hamblin, *Recent Patents Anti-Infect. Drug Disc.* **2013**, *8*, 108–120.

160 Z. Malik, H. Ladan, Y. Nitzan, *J. Photochem. Photobiol. B* **1992**, *14*, 262-266.

161 L. Bourré, F. Giuntini, I. M. Eggleston, C. A. Mosse, A. J. Macrobert, M. Wilson, *Photochem. Photobiol. Sci.* **2010**, *9*, 1613–1620.

162 S. George, M. R. Hamblin, A. Kishen, *Photochem. Photobiol. Sci.* **2009**, *8*, 788-795.

163 a) T. N. Demidova, M. R. Hamblin, *Int. J. Immunopathol. Pharmacol*. **2004**, 17, 245-254; b) L. Huang, Y. Y. Huang, P. Mroz, G. P. Tegos, T. Zhiyentayev, S. K. Sharma, Z. Lu, T. Balasubramanian, M. Krayer, C. Ruzie, E. Yang, H. L. Kee, C. Kirmaier, J. R. Diers, D. F. Bocian, D. Holten, J. S. Lindsey, M. R. Hamblin, *Antimicrob. Agents Chemother*. **2010**, 54, 3834-3841; c) V. Mantareva, V. Kussovski, I. Angelov, D. Wöhrle, R. Dimitrov, E. Popova, S. Dimitrov, *Photochem. Photobiol. Sci.* **2011**, 10, 91-102.

1.1.2 Approaches towards cationic phthalocyanines

Cationic Pc derivatives can be obtained by quaternization of aliphatic or aromatic nitrogen atoms in their substituents. The quaternization reaction usually takes place as the last step in the synthetic route, due to the experimental inconvenience of working with pH-independent charged species. It is worth noting that all methylating agents are recognized as carcinogenic, as they are likely to methylate DNA. For this reason, extreme precautions must be taken when they are handled. Some of the most commonly used quaternizing agents are iodo- or bromomethane, dimethyl sulfate, dimethyl carbonate, and tetramethylammonium chloride. Less common but more powerful (and more dangerous) methylating reagents include methyl triflate, diazomethane, and methyl fluorosulfonate (magic methyl). Iodoalkanes of various chain lengths and iodo-oligo(ethylene glycol) have also been employed as quaternizing agents, aiming to modulate the amphiphilicity of the resulting cationic compounds. Below, some of the most common cationic functional groups employed for the design of cationic Pcs will be discussed, and are summarized in Figure 76.

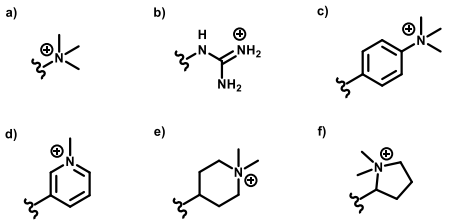

Figure 76. Cationic moieties frequently incorporated in the periphery or axial positions of cationic Pcs. a) trimethylammonium moiety, b) guanidinium moiety, c) anilinium moiety, d) pyridinium moiety, e) piperidinilium moiety, and f) pyrrolidinium moiety.

(i) Ammonium moieties

Different Pcs have been functionalized with trimethylammonium groups (Figure 76a), either bearing the ammonium moiety directly bound to the Pc core, connected by a linker in the periphery or at the axial positions. Trimethylammonium-functionalized Pcs, bearing the ammonium moiety directly bound to the Pc core, have been described very recently, after dealing with solubility issues of the precursors. This kind of Pcs show strong π-π stacking interactions, despite the "a priori" intense cation-cation repulsion,[164] and have been employed as DNA-labelling molecules and PDI agents.[165] Functionalized Pc tertiary amines and their hydrochloride salts have been commonly achieved by grafting 2-

[164] a) W. Duan, Z. Wang and M.J. Cook, *J. Porphyrins Phthalocyanines*, **2009**, *13*, 1255-1261; b) H. Yang, L. Chen, M. Guo, Y. Deng, P. Huang and D. Li, *Anal. Sci.*, **2015**, *31*, 543-549.

[165] D.M.G.C. Rocha, N. Venkatramaiah, M.C. Gomes, A. Almeida, M.A.F. Faustino, F.A.A. Paz, A. Cunha and J.P.C. Tomé, *Photochem. Photobiol. Sci.*, **2015**, *14*, 1872-1879.

(dimethylamino)ethanethiol,[166] 2-(diethylamino)ethanethiol,[167] 1,3-bis(dimethylamino)-2-propanol,[168] 2-(dimethylamino)ethanol,[169] or 3-aminothiophenol,[170] either by ether or thioether linkages, resulting in α and/or β mono- and disubstituted phthalonitriles, which are subsequently subjected to cyclotetramerization and quaternization reactions.[171] Furthermore, trimethylammonium moieties have also been successfully incorporated at the axial positions of SiPcs.[112b,172] More complex spacers such as 2,4,6-tris(*N,N,N*-trimethylaminomethyl)-phenol have been employed, enabling the inclusion of a higher number of ammonium moieties and reducing, at the same time, the natural trend of these compounds to aggregate.[173] Guanidinium-substituted Pcs (Figure 76b), on the other hand, have been synthesized since they demonstrate high specificity in G-quadruplex binding.[174] Methoxy(oligoethylenoxy) spacers have been used in some case, resulting in an increased amphiphilicity[175] or the possibility to prepare cationic Pc dimers.[176]

(ii) Anilinium moieties

Anilinium moieties bear a quaternized nitrogen atom directly bound to an aromatic ring, conjugating its lone pair with the cycle (Figure 76c). Despite this particularity, this functional group is suitable to be quaternized in similar conditions as for ammonium derivatives. Following such strategy, a Suzuki-Miyaura reaction between 4-(dimethylamino)phenylboronic acid and 4-iodo- or 4,5-dibromophthalonitrile, and subsequent cyclotetramerization and quaternization reactions, led to rigid tetra- and

---

166 a) S. Dabak, G. Gümus, A. Gül and Ö. Bekaroglu, *J. Coord. Chem.*, **1996**, *38*, 287-293; b) S. Gürsoy, A. Cihan, M.B. Koçak and Ö. Bekaroglu, *Monatsh. Chem.*, **2001**, *132*, 813-819; c) Y. Arslanoglu and E. Hamuryudan, *Dyes Pigments*, **2007**, *75*, 150-155; d) B. Manisova, S. Binder, L. Malina, J. Jiravova, K. Langova and H. Kolarova, *Anticancer Res.*, **2015**, *35*, 3943-3951.

167 a) M. Idowu and T. Nyokong, *Polyhedron*, **2009**, *28*, 416-424; b) M. Machacek, A. Cidlina, V. Novakova, J. Svec, E. Rudolf, M. Miletin, R. Kucera, T. Simunek and P. Zimcik, *J. Med. Chem.*, **2015**, *58*, 1736-1749.

168 a) M.P. De Filippis, D. Dei, L. Fantetti and G. Roncucci, *Tetrahedron Lett.*, **2000**, *41*, 9143-9147; b) M. Soncin, C. Fabris, A. Busetti, D. Dei, D. Nistri, G. Roncucci and G. Jori, *Photochem. Photobiol. Sci.*, **2002**, *1*, 815-819.

169 a) K. Kasuga, K. Ohmori, H. Tanaka, M. Handa, T. Sugimori, *Inorg. Chem. Commun.*, **2006**, *9*, 1019-1022; b) Y. Arslanoglu, E. Hayran and E. Hamuryudan, *Dyes Pigments*, **2013**, *97*, 340-346.

170 F. Giuntini, D. Nistri, G. Chiti, L. Fantetti, G. Jori and G. Roncucci, *Tetrahedron Lett.*, **2003**, *44*, 515-517.

171 L. Zhang, J. Huang, L. Ren, M. Bai, L. Wu, B. Zhai and X. Zhou, *Bioorg. Med. Chem.*, **2008**, *16*, 303-312.

172 a] S. Rywkin, E. Ben-Hur, Z. Malik, A. M. Prince, Y. S. Li, M. E. Kenney, N. L. Oleinick, B. Horowitz, *Photochem. Photobiol.* **1994**, *60*, 165–170; b) E. Ben-Hur, N. E. Geacintov, B. Studamire, M. E. Kenney, B. Horowitz, *Photochem. Photobiol.* **1995**, *61*, 190–195; c] P.-C. Lo, J.-D. Huang, D. Y. Y. Cheng, E. Y. M. Chan, W.-P. Fong, W.-H. Ko, D. K. P. Ng, *Chem. Eur. J.* **2004**, *10*, 4831–4838.

173 a) S.B. Sesalan, A. Koca and A. Gül, *Dyes Pigments*, **2008**, *76*, 259-264; b) X.-S. Li, J. Guo, J.-J. Zhuang, B.-Y. Zheng, M.-R. Ke and J.-D. Huang, *Bioorg. Med. Chem. Lett.*, **2015**, *25*, 2386-2389.

174 a) J. Alzeer, B.R. Vummidi, P.J.C. Roth and N.W. Luedtke, *Angew. Chem. Int. Ed.,* **2009**, *48*, 9362-9365. b) A. Membrino, M. Paramasivam, S. Cogoi, J. Alzeer, N.W. Luedtke and L.E. Xodo, *Chem. Commun.*, **2010**, *46*, 625-627. c) J. Alzeer and N.W. Luedtke, *Biochemistry.*, **2010**, *49*, 4339-4348.

175 Z. Biyiklioglu, M. Durmus and H. Kantekin, *J. Photochem. Photobiol. A*, **2011**, *222*, 87-96.

176 E. Yabas, E. Bagda and E. Bagda, *Dyes Pigments*, **2015**, *120*, 220-227.

octacationic Pc derivatives, respectively.[177] A range of spacers have been employed between the aniline unit and the Pc core, such as ether moieties,[178] methoxy(oligoethylenoxy),[179] and more complex conjugated bridges.[180] Furthermore, anilinium moieties have been incorporated at the axial positions of SiPcs[181] or other axial substituent bearing Pcs.[182] Nonetheless, the anilinium moiety is not a broadly employed functionality, since it requires more challenging synthetic routes and shows no remarkable advantages in comparison to the synthetically more accessible ammonium derivatives.

(iii) Pyridinium moieties

By far the most common cationic moieties encountered in the periphery of Pcs are the pyridinium type moieties (Figure 76d), due to their synthetic versatility and accessibility. This heterocycle provides a lone nitrogen pair not conjugated within the aromatic ring, presenting aromaticity even after quaternization. In particular, the linkage of pyridines to phthalonitriles is usually achieved through a ether or thioether bond, by nucleophilic substitution of 3- or 4-nitrophthalonitrile (for monosubstituted derivatives), or 4,5-dichlorophthalonitrile (for disubstituted ones), with 4- hydroxypyridine,[151,183] 3-hydroxypyridine,[163c,184] 2-hydroxypyridine,[185] 4-mercapto-pyridine[183d,186] or 2-mercaptopyridine.[187] Alternatively, alkynylpyridines can be reacted with halogen bearing

---

177 T. Sugimori, J. Nojima, T. Ozawa, M. Handa and K. Kasuga, *Chem. Lett.*, **2004**, *33*, 1014-1015.

178 B.G. Ongarora, B. Hu, H. Li, F.R. Fronczek and M.G.H. Vicente, *Med. Chem. Comm.*, **2012**, *3*, 19-194.

179 a) D. Çakir, V. Çakir, Z. Biyiklioglu, M. Drumus and H. Kantekin, *J. Organomet. Chem.*, **2013**, *745-746*, 423-431; b) Z. Biyiklioglu, *J. Organomet. Chem.*, **2014**, *752*, 59-66.

180 G.K. Karaoglan, G. Gümrükçü, A. Koca and A. Gül, *Dyes Pigments*, **2011**, *88*, 247-256.

181 a] Z. Bıyıklıoğlu, *Dyes Pigments* **2013**, *99*, 59–66; b) *Polyhedron* **2013**, *63*, 1–8.

182 Z. Bıyıklıoğlu, V. Çakır, F. Demir, A. Koca, *Synth. Met.* **2014**, *196*, 166–172.

183 a) S. Banfi, E. Caruso, L. Buccafurni, R. Ravizza, M. Gariboldi and E. Monti, *J. Organomet. Chem.*, **2007**, *692*, 1269-1276; b) M.B. Spesia, D.A. Caminos, P. Pons and E.N. Durantini, *Photodiagn. Photodyn. Ther.*, **2009**, *6*, 52-61; c) T.T. Tasso, Y. Yamasaki, T. Furuyama and N. Kobayashi, *Dalton Trans.*, **2014**, *43*, 5886-5892; d) O.J. Achadu, I. Uddin and T. Nyokong, *J. Photochem. Photobiol. A*, **2016**, *317*, 12-25.

184 a) S. Gaspard and T.T. Thi, *J. Chem. Soc., Perkin Trans. II*, **1989**, 383-389; b) G. Schneider, D. Wöhrle, W. Spiller, J. Stark and G. Schulz-Ekloff, *Photochem. Photobiol.*, **1994**, *60*, 333-342; c) V. Mantareva, D. Petrova, L. Avramov, I. Angelov, E. Borisova, M. Peeva and D. Wöhrle, *J. Porphyrins Phthalocyanines*, **2005**, *9*, 47-53; d) M. Durmus and T. Nyokong, *Inorg. Chem. Commun.* **2007**, *10*, 332-338; e) M. Durmus and T. Nyokong, *Photochem. Photobiol. Sci.*, **2007**, *6*, 659-668; f) H. Li, T.J. Jensen, F.R. Fronczek and M.G.H. Vicente, *J. Med. Chem.*, **2008**, *51*, 502-511.

185 a) W. Chidawanyika, A. Ogunsipe and T. Nyokong, *New. J. Chem.*, **2007**, *31*, 377-384; b) N. Masilela and T. Nyokong, *J. Lumin.*, **2010**, *130*, 1787-1793; c) R. Zugle and T. Nyokong, *J. Mol. Catal. A*, **2012**, *358*, 49-57.

186 a) N. Masilela and T. Nyokong *Dye Pigm.*, **2010**, *84*, 242-248; b) J.B. Pereira, E.F.A. Carvalho, M.A.F. Faustino, R. Fernandes, M.G.P.M.S. Neves, J.A.S. Cavaleiro, N.C.M. Gomes, A. Cunha, A. Almeida and J.P.C. Tomé, *Photochem. Photobiol.*, **2012**, *88*, 537-547.

187 a) N. Sehlotho, M. Durmus¸ V. Ahsen and T. Nyokong, *Inorg. Chem. Commun*. **2008**, *11*, 479-483; b) F. Matemadombo, M. Durmus, V. Escriou, S. Griveau, D. Scherman, F. Bedioui and T. Nyokong, *Curr. Anal. Chem.*, **2009**, *5*, 330-338; c) N. Saydan, M. Durmus, M.G. Dizge, H. Yaman, A.G. Gürek, E. Antunes, T. Nyokong and V. Ahsen, *J. Porphyrins Phthalocyanines*, **2009**, *13*, 681-690; d) M. Durmus and V. Ahsen, *J. Inorg. Biochem.*, **2010**, *104*, 297-309; e) M. Durmus, H. Yaman, C. Göl, V. Ahsen and

phthalonitriles or Pcs using the Sonogashira coupling reaction,[188] and subsequently be quaternized to obtain the cationic Pc derivatives.[189]

(iv) Piperidinilium moieties

Although a few Pcs with piperidinyl groups in the periphery have been reported,[190] none of these have been methylated/alkylated to obtain cationic Pcs. The only example until now of the use of a piperidinilium moiety (Figure 76e) to introduce a positive charge in a Pc is one of a SiPc with two such moieties at its axial positions.[191] To this end, $SiPcCl_2$ was reacted with 4-hydroxypiperidine using standard axial substitution conditions, and the resulting axially substituted SiPc was consequently subjected to methylation.

(v) Pyrrolidinium moieties

Examples of Pcs with pyrrolidine or pyrrolidinium moieties (Figure 76f) are even less common, and to the best of our knowledge only reported by Uslan *et al.*,[192] who incorporated these moieties at the axial positions of SiPcs. Preparation however is straightforward, incorporating (1-methylpyrrolidin-2-yl)methanol in $SiPcCl_2$ followed by subsequent methylation using standard procedures.

1.1.3 Cationic silicon phthalocyanines for photodynamic inactivation

Although various cationic SiPcs have been synthesized,[172,181,182,184f,185b,191,192] their PDI efficacy has been investigated only for few of them. Early on, in 1994, Horowitz and co-workers studied the use of a cationic SiPc bearing a trimethylammonium moiety as PS for the PDI of viruses in blood samples.[172a,b] The virus sterilization of red blood cells is an important issue in improving the safety of blood transfusion. To avoid the loss of irradiation due to hemoglobin absorption, the absorption maximum of the PS should be greater than 600 nm, which makes SiPcs ideal PS candidates for this purpose. The cationic SiPc depicted in Figure 77 resulted in complete inactivation of viruses after 20 min of irradiation with red light (30 J/cm^2) when applying a PS dose of 6.5 µM in the blood.

T. Nyokong, *Dyes Pigments*, **2011**, *91*, 153-163; f) M.A. Idowu, Y. Arslanoglu and T. Nyokong, *Cent. Eur. J. Chem.*, **2014**, *12*, 403-415.

188 T. Ikeuchi, S. Agrawal, M. Ezoe, S. Mori, M. Kimura, *Chem. Asian J.* **2015**, *10*, 2347–2351.

189 W. M. Sharman, J. E. van Lier, *J. Porphyr. Phthalocyanines* **2005**, *9*, 651–658.

190 a] K. Kassab, C. Fabris, M. P. Defilippis, D. Dei, L. Fantetti, G. Roncucci, E. Reddi, G. Jori, *J. Photochem. Photobiol. B* **2000**, *55*, 128–137; b) A. Fedotova, Y. Zhuravleva, V. Maizlish, G. Shaposhnikov, *Russ. J. Gen. Chem.* **2013**, *83*, 757–761.

191 B.-Y. Zheng, X.-J. Jiang, T. Lin, M.-R. Ke, J.-D. Huang, *Dyes Pigments* **2015**, *112*, 311–316.

192 C. Uslan, K. T. Oppelt, L. M. Reith, B. Ş. Sesalan, G. Knör, *Chem. Commun.* **2013**, *49*, 8108–8110.

Importantly, this SiPc is particularly attractive because there is no inhibition of virus inactivation in the presence of plasma.

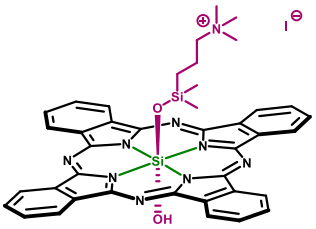

Figure 77. A monocationic SiPc that is an effective PS in the PDI of viruses in blood samples.[172a,b]

Wöhrle and co-workers synthesized a cationic SiPc bearing four pyridinium moieties, one on each isoindole unit (Figure 78a).[192a] They investigated its uptake and PDI efficacy on *Candida albicans*, a fungus commonly present in infections in the oral cavity, in the planktonic phase and in biofilm cultures. Fungal cells in suspension were completely inactivated with a PS dose of 1.8 µM and a soft light radiation of 50 J/cm^2. Fungal biofilm, which is harder to inactivate due to limited penetration depth, could be efficiently inactivated using fractionated light irradiation.

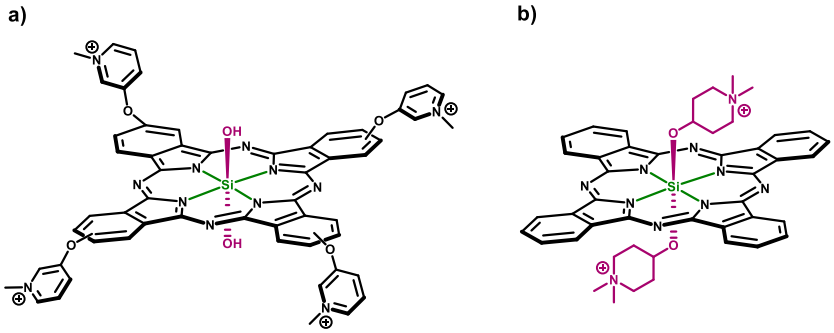

Figure 78. a) A tetracationic SiPc as PS for the PDI of *C. albicans* cultures.[192a] b) A dicationic SiPc with PDI activity against *C. albicans*. Iodide counterions are not represented for clarity.[191]

More recently, Huang and co-workers have synthesized a cationic SiPc containing piperidinilium moieties at the axial positions (Figure 78b).[191] They compared its antifungal photoactivity towards *C. albicans* with that of an analogue di-substituted with cyclohexyl groups instead of piperidinilium moieties. As a result, they found that the cationic derivative showed the highest photodynamic activity, causing a 4 log CFU (colony forming unit) reduction of this fungus at concentrations of 100 µM of PS in combination with a light dose of 27 J/cm. This could be attributed to its high ϕ_Δ, low aggregation in aqueous media, and relatively efficient cellular uptake in comparison to the neutral PS analogue.

1.2 Molecular design, synthesis and characterization of a series of cationic silicon(IV) phthalocyanine photosensitizers

The optimization of the synthesis and characterization of the SiPcs described in this chapter has been performed in collaboration with Marta Moreno Simoni, a master student under my guidance from October 2015 until June 2016.

As mentioned above, the specific objective of this subchapter is the synthesis of a series of cationic SiPcs for use in PDI (Figure 79). Since SiPcs require axial substituents, we aim to utilize those employed in Chapter 1 – Subchapter 1, which gave good results in a series of neutral SiPcs designed for PDT against cancer cells. To this end, in the present Subchapter, the required cationic moieties will be introduced at the peripheral positions of the macrocycle, following a strategy which is similar to that applied by Vicente and co-workers, who synthesized a series of cationic SiPcs for use in PDT.[184f] In particular, eight pyridyloxy groups will be introduced at the β-positions of the SiPc isoindoles. Upon axial substitution with the previously synthesized primary alcohol building blocks (**5**, **7**, **8** and **11**), and subsequent methylation of the pyridyloxy groups, the cationic SiPcs **19a-d,** bearing eight pyridinium oxy moieties, would be obtained.

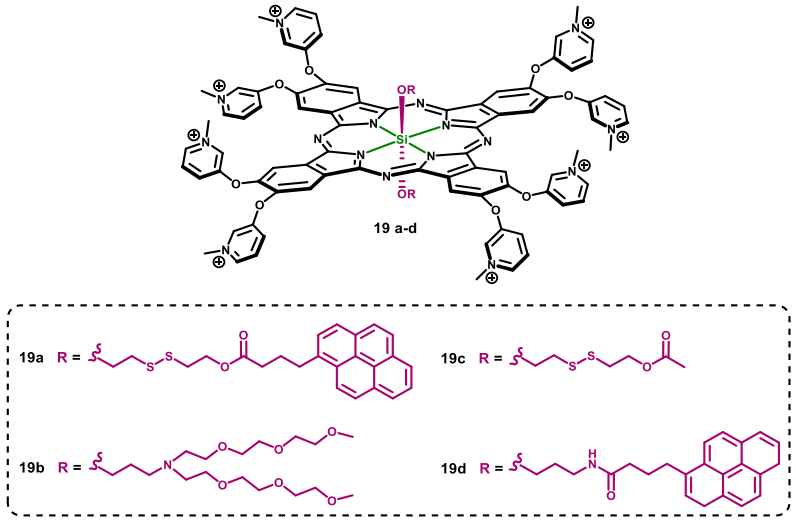

Figure 79. Molecular structure of target SiPcs **19a-d**, a series of cationic SiPcs bearing the same axial substituents as those used in Chapter 1 of this thesis. Iodide counterions are not represented for clarity.

1.2.1 Synthesis of octa(3-pyridyloxy)silicon(IV) phthalocyanine dichloride

The preparation of 4,5-bis(3-pyridyloxy)phthalonitrile (**24**) and the corresponding SiPc (**26**) is a multistep synthesis that has been previously reported in the literature (Scheme 17).[184f,193] Noteworthy, it is completely chromatography-free. This is important, as column chromatography is often a drawback in pyridinyl Pc compounds, since they tend to aggregate and stick to the silica gel, making purification cumbersome and resulting in a decrease of yield.

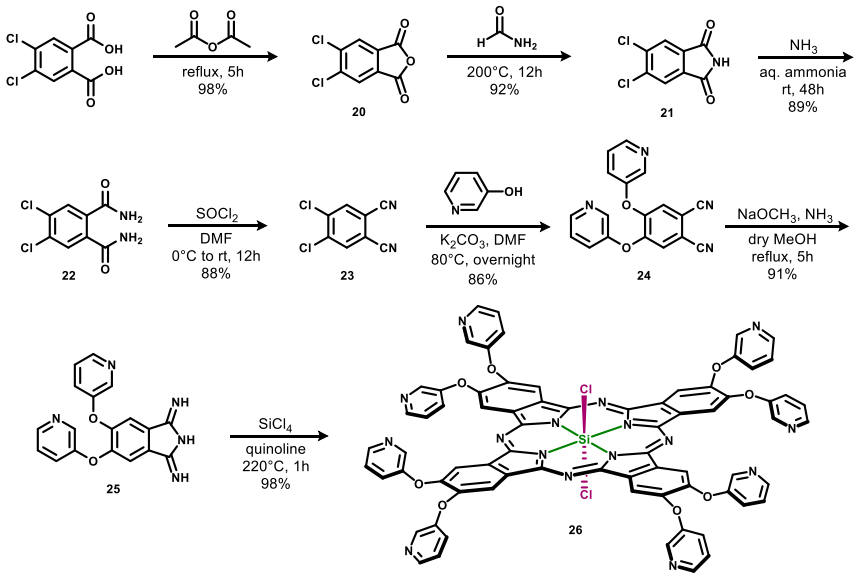

Scheme 17. Synthesis of 4,5-bis(3-pyridyloxy)phthalonitrile (**24**) and its corresponding SiPc (**26**).

The synthesis started from the commercially available and inexpensive 4,5-dichlorophthalic acid, which was refluxed in acetic anhydride. This resulted in the formation of 4,5-dichlorophthalic anhydride (**20**), which was in turn reacted with formamide to yield 4,5-dichlorophthalimide (**21**). Next, a suspension of **21** was stirred for 48h in aqueous ammonia, resulting in the precipitation of 4,5-dichlorophthalamide (**22**), which can be transformed into 4,5-dichlorophthalonitrile (**23**) by reaction with freshly distilled thionyl chloride.[193] **23** was then reacted with 3-hydroxypyridine in dry DMF, in the presence of anhydrous potassium carbonate, yielding 4,5-bis(3-pyridyloxy) phthalonitrile (**24**) *via* a nucleophilic aromatic substitution reaction.[184f] Purification was performed by recrystallization in EtOH.

4,5-bis(3-pyridyloxy)-1,3-diiminoisoindoline (**25**), the precursor for the formation of our target SiPc (**26**), was formed upon reaction of **24** with ammonia gas in the presence of

[193] D. Wöhrle, M. Eskes, K. Shigehara, A. Yamada, *Synthesis* **1993**, 194–196.

sodium methoxide, in freshly distilled methanol.[184f] Finally, standard reaction conditions for formation of SiPc dichloride compounds were followed for the formation of **26**, by refluxing the corresponding 1,3-diiminiosoindoline (**25**) in freshly distilled quinoline in the presence of $SiCl_4$, in which the tetravalent silicon atom acts as a template for the formation of the SiPc dichloride. The formation of $SiPcCl_2$ derivatives generally proceeds fast and with high yields. Furthermore, due to their low solubility, they can be easily precepitated by lowering the temperature of the reaction mixture to rt, avoiding cumbersome column chromatography.

1.2.2 Axial substitution

In order to obtain the axially substituted SiPcs **27a-d** (Scheme 18), various reaction conditions were tried (Table 9, Entry 1-5).

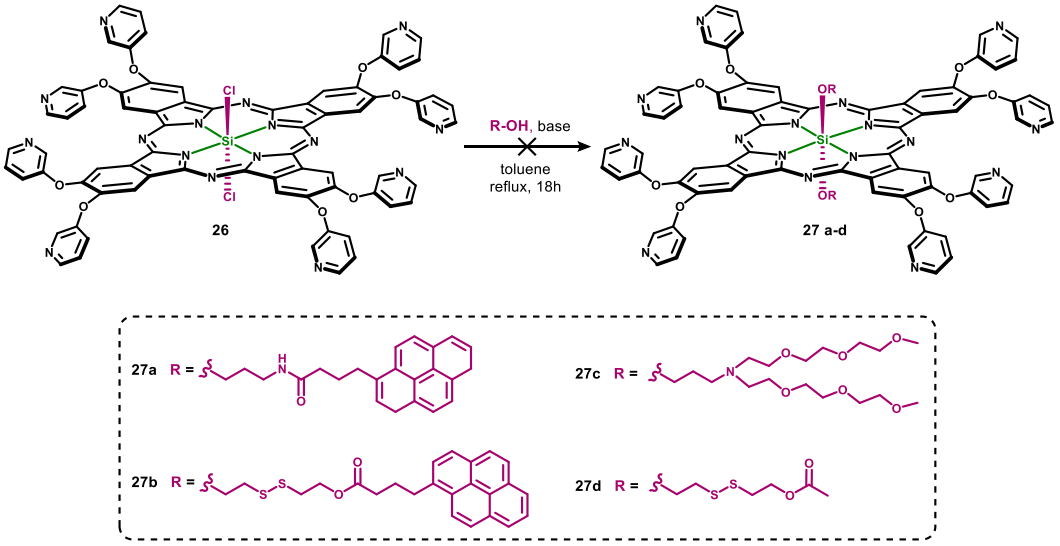

Scheme 18. Intended axial substitution of the SiPc **26** with the previously synthesized primary alcohol building blocks **5**, **7**, **8** and **11**.

Table 9. Various reaction conditions tested for the incorporation of axial substituents in the SiPc **26**.

Entry	Solvent[a]	Base[a] (v/v%)	Temp.	Building block	Yield
1	Toluene	Pyridine (2)	111°C	**5**	0%
2	Toluene	DIPEA (2)	111°C	**5**	0%
3	Toluene	Pyridine (50)	111°C	**5**	0%
4	Toluene	Pyridine (2)	111°C	**8**	0%
5	Toluene	Pyridine (50)	111°C	**8**	0%
6	2-methoxy ethylether	-	162°C	4-tert-butyl benzoic acid	0%

[a] Anhydrous

Since no axial substitution could be observed when employing the standard reaction conditions (Table 9, Entries 1 and 4), the use of a stronger base such as DIPEA was considered (Table 9, Entry 2), however without any positive result. At this point, the solubility of **26** in the reaction medium was questioned. Since no significant solubility could be observed in a series of high-boiling point organic solvents, the proportion of pyridine in the reaction mixture was increased (Table 9, Entries 3 and 5). Nevertheless, a green precipitate could still be observed in the reaction mixture.

In all of the aforementioned trials, the remaining green precipitate upon overnight reaction was filtered off and confirmed to be the starting product (**26**) by ^{1}H-NMR spectroscopy. The filtrate, which showed a slight green color in some case, was purified by column chromatography using DCM/methanol (20:1) as the eluent, to verify if any axial substitution had taken place. Surprisingly, the same product was obtained in all cases, namely a SiPc derivative with methoxy groups at the axial positions, as characterized by ^{1}H-NMR (Figure 80).

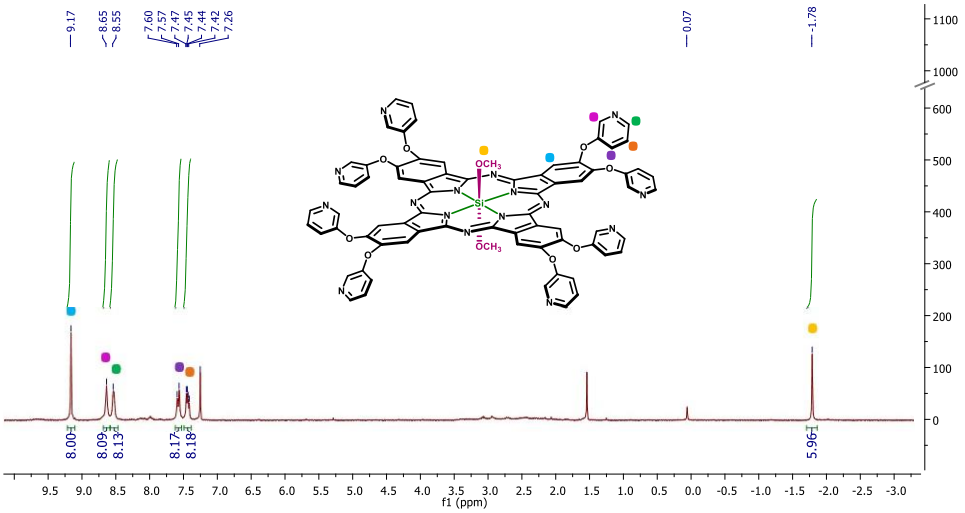

Figure 80. ^{1}H-NMR of the side product obtained by column chromatography of the axial substitution reactions detailed in Table 9.

Upon literature research, it has been found that bulky axial alkoxide substituents can be exchanged by other nucleophiles.[172b,194] The relative lability of the alkoxide substituent decreases with the decreasing bulkiness, with methoxide resulting as the most stable axial substituent. In our case, such exchange must have taken place during the column chromatography purification, in which methanol was present in the eluent. This indicates that during the reaction some axial substitution with the desired ligand had taken place, however the resulting Si-alkoxide bond must have been very labile and prone to exchange with methanol.

As a final test another well-known type of axial substitution of SiPcs was tested, by reacting the $SiPcCl_2$ (**26**) with a benzoic acid in an appropriate solvent, like 2-methoxyethyl ether, following a procedure described in the literature (Table 9, Entry 6).[125] This would result in a more stable axial substituent, unable to undergo the aforementioned exchange with methanol. However, also in this case no axial substitution could be achieved, probably due to the insolubility and low reactivity of compound **26**.

1.2.3 Hydrolysis of 26 and subsequent axial substitution

Since the SiPc **26** unfortunately seemed to be unreactive towards nucleophilic displacement of its chlorine atoms, another strategy for axial functionalization had to be considered. In their publication, in the approach of SiPc systems for PDT of cancer, Vicente and co-workers hydrolyse this SiPc dichloride to obtain the SiPc dihydroxy variant, which can be reacted with various trialkylchlorosilanes in refluxing pyridine. Therefore, we then

[194] Z. Li, M. Lieberman, *Inorg. Chem.* **2001**, *40*, 932–939.

undertook this route, and in an attempt to study the influence of the axial substituent on the aggregation behaviour and/or PDI efficacy of the resulting octacationic SiPcs, various commercial trialkylchlorosilanes of different bulkiness and different chemical nature (e.g., aromatic versus aliphatic) were introduced (Scheme 19). To this end, **26** was dissolved in a mixture of water and ethanol (5:1) in the presence of sodium methoxide. The reaction mixture was refluxed for 5h and **28** could be easily isolated, with 80% yield, by precipitation upon addition of water. Importantly, **28** was vacuum dried for 48h in a vacuum oven, before using it in the next step. For the axial substitution reaction, **28** was refluxed in recently distilled pyridine, and the corresponding trialkylchlorosilane was added in two portions with 8h of difference, and in a high excess. Upon overnight reaction, the reaction mixture was evaporated to dryness. The remaining solid was washed extensively with chloroform, and the filtrate evaporated to dryness and triturated in heptane, yielding in this way the pure SiPcs **29a-d**, with yields between 20 and 40 %.

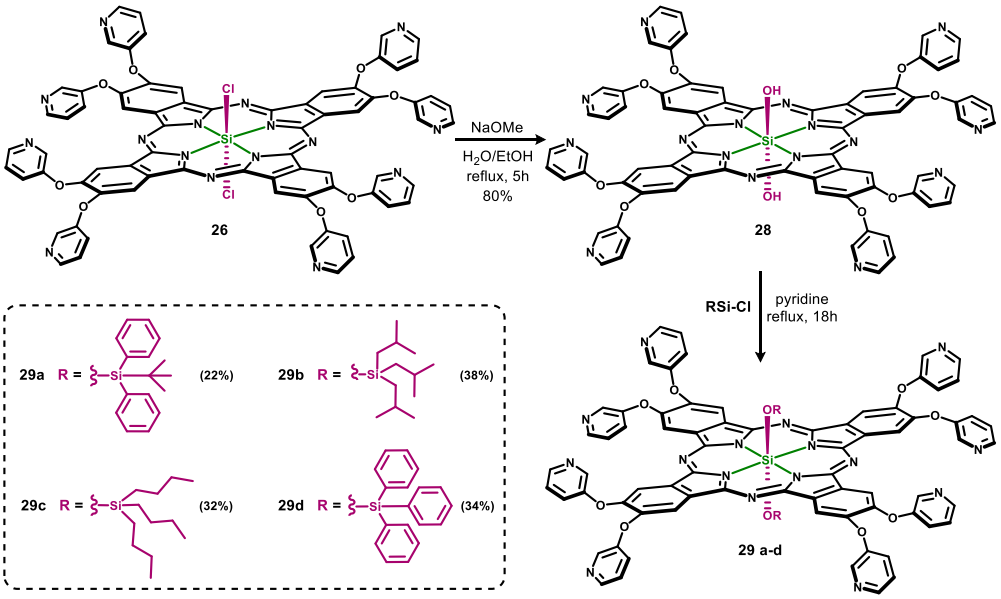

Scheme 19. Hydrolysis of SiPc **26** to obtain the dihydroxy SiPc **28** and consequent axial substitution of its hydroxyl groups by different trialkylchlorosilanes, resulting in the axially substituted SiPcs **29a-d**.

1.2.4 Quaternization reactions

The last step in the synthetic route to obtain the octacationic SiPcs **31a-d** was the methylation of the eight pyridyloxy groups of SiPcs **29a-d** (Scheme 20). Methylation was carried out using methyl iodide as methylating agent and DMF as the solvent, in order to avoid precipitation of partially methylated products. This would result in a complex mixture of products with various degrees of methylation, very hard to purify, and should therefore be avoided at all cost.

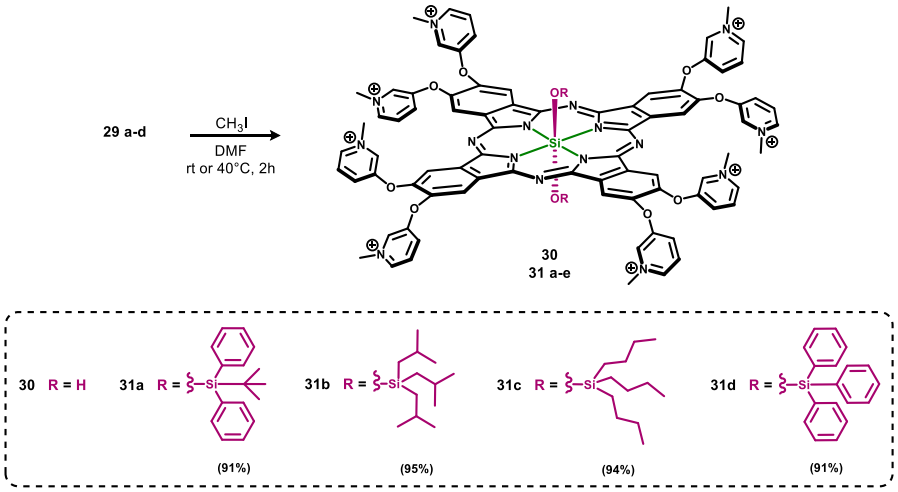

Scheme 20. Quaternization of the SiPcs **29a-d**, resulting in the octamethylated SiPcs **30** and **31a-d**. Iodide counterions are not represented for clarity.

Noteworthy, the procedure published by Vicente and co-workers consisted in methylation of the SiPcs in methyl iodide, without any solvent, which in our case resulted in a premature precipitation of products. Furthermore, they left the reaction for 1 day at 40°C, conditions which in our hands resulted in the removal of the axial ligands and their consequent substitution by hydroxyl groups, yielding the SiPc **30**. This process can be easily followed by ^{1}H-NMR spectroscopy and, based on this, the ideal methylation conditions were determined for each SiPc, yielding SiPcs **31a-d** in very good yields (Table 10).

Table 10. Methylation conditions for obtaining the SiPcs **31a-d**.

Compound	Reaction time	Temperature	Yield
31a	2h	40°C	91%
31b	2h	rt	95%
31c	2h	rt	94%
31d	2h	40°C	91%

1.3 Spectral features and photophysical properties

The normalized absorption spectra of the SiPcs **28** and **29a-d** were measured in DMF (Figure 81a). They all represent the typical spectra of non-aggregated Pcs, with an intense and sharp Q-band around 675 nm and a broad Soret band with a maximum around 360 nm. Furthermore, two typical vibronic bands can be seen around 610 and 643 nm. The normalized absorption spectra of the octacationic SiPcs **30** and **31a-d**, on the other hand, were recorded in Milli-Q water (Figure 81b). They all present nearly identical absorption features to that of their non-quaternized precursors. Upon excitation at 345 nm, all the SiPcs showed a fluorescence emission around 680 nm (F_{680}), varying in intensity (Table 11).

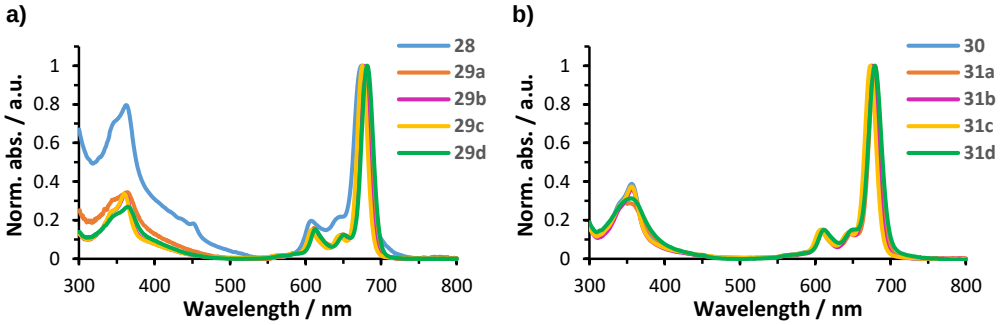

Figure 81. Electronic absorption spectra of a) the SiPcs **28** and **29a-d** in DMF, and b) the quaternized SiPcs **30** and **31a-d** in Milli-Q water.

Since for efficient $^1O_2$ generation it is absolutely indispensable that the PS is non-aggregated in the cellular medium, the solubility of the cationic SiPcs **30** and **31a-d** in a physiologically relevant medium, such as PBS, was assessed by UV-Vis spectroscopy (Figure 82). This analysis was conducted in a range of concentrations between 2 and 10 µM, achieved by the sequential addition of aliquots of stock solutions of each SiPc. For the verification of the Lambert-Beer law, an analysis of linear regression between the intensity of the Q-band and the concentration of the SiPcs was conducted. As can be seen from the insets in Figure 82, the Lambert-Beer was fulfilled for all of the cationic SiPcs, with R^2 values of 0.98 or greater. Hence, SiPcs **30** and **31a-d** seem to be non-aggregated in PBS at the concentration range studied, and are therefore potential good PS candidates, to be tested in cellular medium.

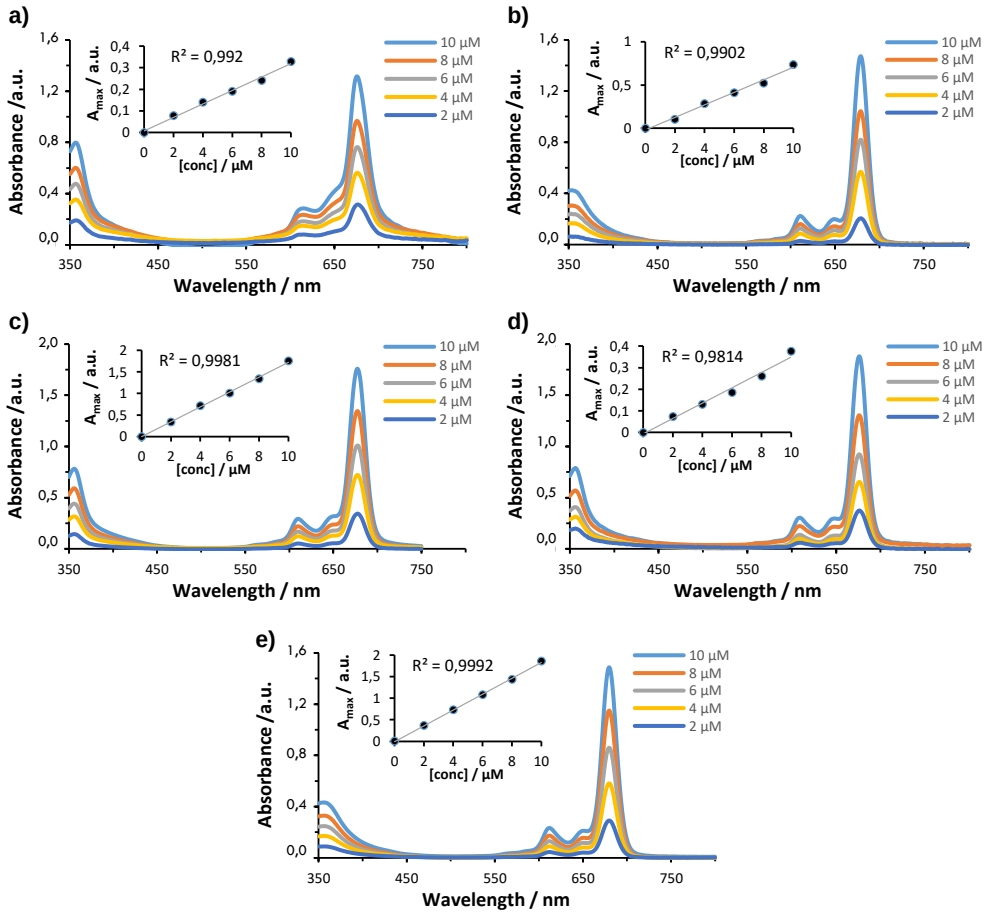

Figure 82. UV-Vis dilution studies of the octacationic SiPcs a) **30**, b) **31a**, c) **31b**, d) **31c**, e) **31d** in physiologically relevant medium (PBS).

For all SiPcs, ϕ_F were determined in DMF and/or water, and the results are represented in Table 11 and Table 12. As a general observation, the ϕ_F values for the cationic SiPcs **30** and **31a-d** are slightly higher (about 5%) than those of their neutral precursors, **28** and **29a-d**. Furthermore, for the cationic SiPcs, ϕ_F presented almost the same values when measured in DMF or in water.

The ϕ_Δ of the neutral precursor SiPcs **28** and **29a-d** has been determined in DMF using the *relative method*, as explained in Chapter 1 and in the Experimental Section, and are also represented in Table 11. During the experiments, decrease in the SiPc Q-band intensity or appearance of new absorption bands were not observed in any case, ensuring the PS integrity. As can be observed, all neutral SiPcs display similar, and reasonably high, ϕ_Δ values, ranging from 30 to 50%.

Table 11. Electronic absorption and photophysical data for the SiPcs **28** and **29a-d** in DMF.

Compound	λ_{max} (nm)	λ_{em} (nm)[a]	ϕ_F (%)[a,b]	ϕ_Δ (%)[c]
28	673	681	20.8	32.2
29a	680	685	24.5	43.6
29b	676	682	26.7	47.0
29c	675	680	33.9	50.7
29d	681	687	23.3	50.0

[a] Excited at 610 nm. [b] Using ZnPc in DMF as the reference (ϕ_F = 0.28). [c] Using ZnPc in DMF as the reference (ϕ_Δ = 0.56).

Table 12. Electronic absorption and photophysical data for the octacationic SiPcs **30** and **31a-d** in water, unless stated otherwise.

Compound	λ_{max} (nm)	λ_{em} (nm)[a]	$\phi_{F(DMF)}$ (%)[a,b]	$\phi_{F(H2O)}$ (%)[a,b]
30	675	681	38.1	40.2
31a	679	682	30.2	29.9
31b	675	681	30.9	30.4
31c	673	679	37.1	38.5
31d	679	685	29.1	28.2

[a] Excited at 610 nm. [b] Using ZnPc in DMF as the reference (ϕ_F = 0.28).

To confirm the positive photosensitizing features of this series of SiPcs, the $^1O_2$ generation ability of the cationic SiPcs **30** and **31a-d** in cellular medium needed to be assessed. To this end, their relative $^1O_2$ generation efficiency in PBS buffer was determined and compared with that of the SiPcs **28** and **29a-d**, by the qualitative method in which DPBF is degraded by $^1O_2$, as explained in Section 1.3 of Chapter 1. The results are depicted in Figure 83a and Figure 83b for the neutral precursor SiPcs **28** and **29a-d**, and the quaternized derivatives **30** and **31a-d**, respectively. The measurement conditions were the same for both series of SiPcs, for which they can be directly compared, even though they are represented in different graphs for clarity.

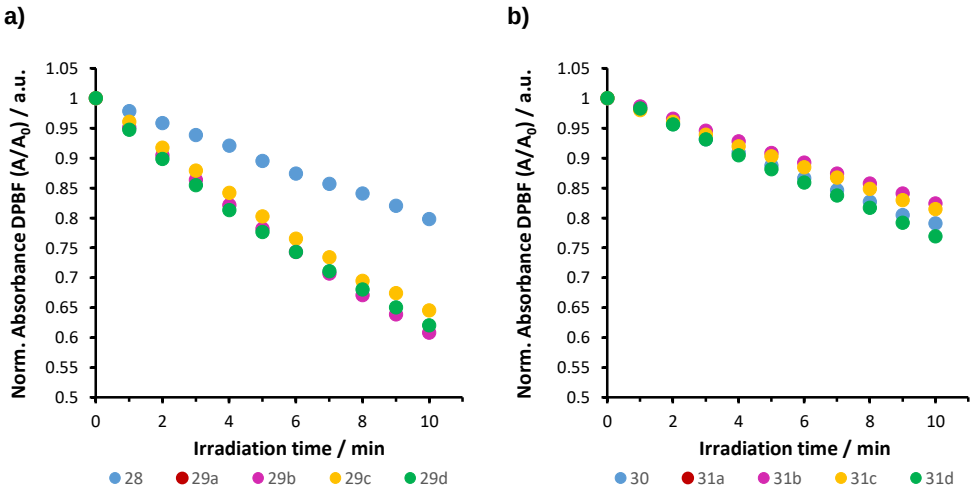

Figure 83. Decay of the absorbance of DPBF at 414 nm, sensitized by a) SiPcs **28** and **29a-d** and b) octacationic SiPcs **30** and **31a-d**, in function of irradiation time (min).

As a general observation, the $^1O_2$ generation efficiency of the octacationic SiPcs **30** and **31a-d** is slightly lower than that of their neutral precursors, the SiPcs **28** and **29a-d**. This may be due to the fact that they possess lower LUMO levels, due to the increased electron acceptor character of their peripheral substituents. Importantly, the $^1O_2$ generation efficiency of the neutral SiPcs **30** and **31a-d** (Figure 83a) is in perfect concordance with their ϕ_Δ previously measured in DMF (Table 11), being very similar for SiPcs **29a-d** and significantly lower for SiPc **28**. This might be explained by the fact that the SiPc **28**, lacking axial substituents, might display some kind of aggregation which hinders $^1O_2$ generation, or by the different electronical characteristics it displays (also indicated by its absorption features in Figure 81). Once quaternized, it shows a similar $^1O_2$ generation efficiency as the other cationic SiPcs. Notably, it is now completely lacking aggregation due to electrostatic repulsion.

1.4 *In vitro* photodynamic inactivation of microorganisms

*PDI experiments with the cationic SiPcs **30** and **31a-d** have been performed in the research group of Prof. Ângela Cunha at the Department of Biology of the University of Aveiro (Portugal), in collaboration with José Antonio Gonzalez Delgado and Bruna David.*

The microorganisms used in this study were the Gram-positive bacteria *Staphylococcus aureus* and methicillin-resistant *Staphylococcus aureus* (MRSA), and the Gram-negative bacterium *Escherichia coli*. They are often used model organisms, since they are easy to grow in laboratory conditions and present an optimal incubation temperature of 37°C and heat resistance. Furthermore, Methicillin-resistant *S. aureus* is a term used to refer to bacteria of any strain of *S. aureus* that have developed resistance to a variety of antibiotics.[195] Such resistance makes MRSA infections more difficult to treat with standard types of antibiotics than normal *S. Aureus* infections, and they are thus more dangerous.

For the PDI treatment, fresh bacterial cultures with a concentration of 10^7 CFU mL^{-1} were irradiated with red light, coinciding with the maximum absorption of the SiPcs, for different time intervals, in the presence of the corresponding SiPc. Experiments are performed in triplicate and the concentration of viable cells was calculated as the average number of colonies. Generally, a PS is considered as an effective antimicrobial in PDI if the inactivation results in at least 4 logs of CFU reduction, corresponding to a cell survival of lower than 0.01%. Dark toxicity must be lower than 1 log of CFU reduction, corresponding to a cell survival of higher than 10%.

Since no significant difference in $^1O_2$ generation efficiency can be observed for the octacationic SiPcs, all of them (except for **31a**, which has been published previously) were tested *in vitro* for their PDI efficiency against *Staphylococcus aureus*, initially, after which the best performing SiPcs were selected for further inactivation experiments. First, the SiPcs **30** and **31b-d** were tested against *S. aureus* at a concentration of 20 µM, applying different light doses to investigate their efficiency (Figure 84). As a first observation, from the light-only studies (without addition of any SiPc) it can be concluded that *S. aureus* is resistant to the light doses used in the experiment, at all irradiation times (Figure 84 – dark green data). Additionally, PS-only experiments (without applying light) were performed to exclude cytotoxicity of the SiPcs. As a result, the SiPcs **30** and **31b** are devoid of any dark toxicity, whereas the cytotoxicity of **31c** and **31d** reaches almost 1 log of CFU reduction (Figure 84 – blue data). Although this level of cytotoxicity is still acceptable, the PDI efficiency of these two SiPcs upon applying different light doses is very low, only reaching 2 logs of CFU reduction (Figure 84c,d – red data). As a result of this combined dark cytotoxicity and low PDI efficiency, the SiPcs **31c** and **31d** are considered ineffective PDI

[195] J. M. Boyce, B. Cookson, K. Christiansen, S. Hori, J. Vuopio-Varkila, S. Kocagöz, A. Y. Öztop, C. M. Vandenbroucke-Grauls, S. Harbarth, D. Pittet, *Lancet Infect. Dis.* **2005**, *5*, 653–663.

agents and are discarded for any further *in vitro* experiments. On the other hand, both **30** and **31b** are effective antimicrobials, with photokilling efficiencies higher than 99,99% and lacking any cytotoxicity. **31b** reaches 4 logs of CFU reduction, and **30** outperforms all the tested SiPcs reaching almost 7 logs of CFU reduction, corresponding to the total eradication of all bacteria present in the sample.

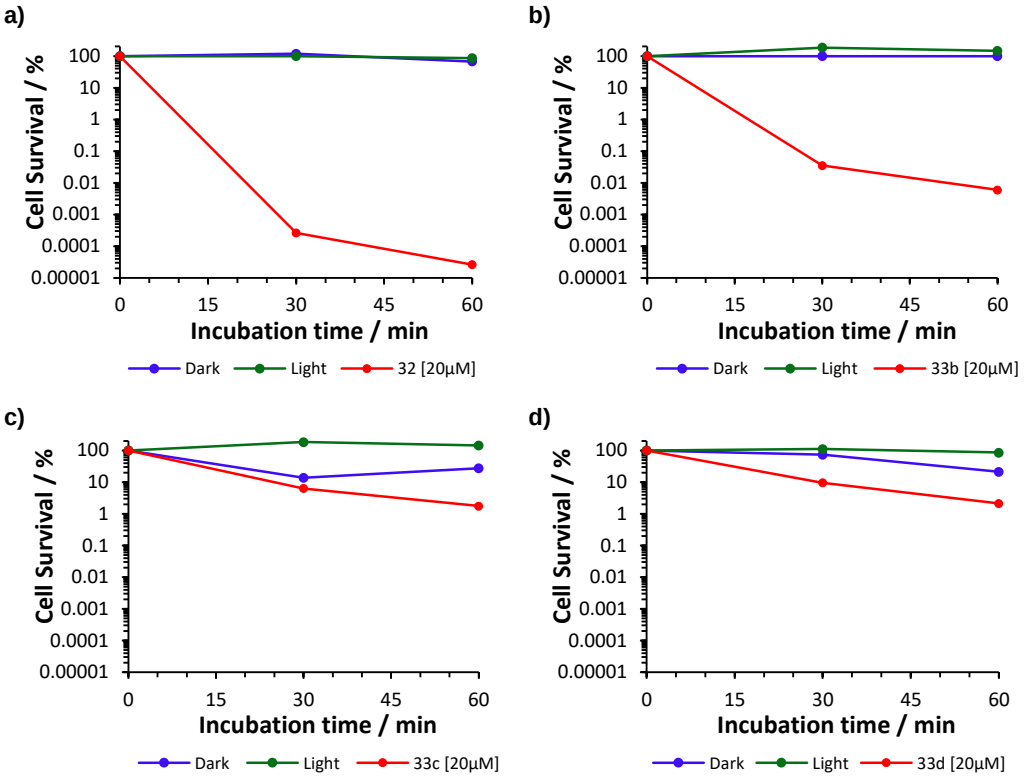

Figure 84. Photoinactivation of *S. aureus* with the SiPcs a) **30**, b) **31b**, c) **31c** and d) **31d**, upon red light irradiation (620–750 nm; 150 mW/cm^2).

Since MRSA is known to be slightly harder to inactivate than *S. aureus*, and the SiPc **30** was the only PS that amply exceeded the 4 log of CFU reduction to be an effective antimicrobial against *S. aureus*, only this PS was tested for its PDI efficiency against MRSA (Figure 85). As expected, in this case **30** shows a slightly lower antimicrobial effect. However, it still reaches 99,99% killing ratios, which is a very good result.

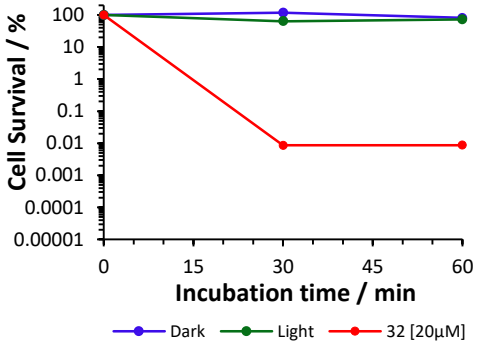

Figure 85. Photoinactivation of *S. aureus* with SiPc **30**, upon red light irradiation (620–750 nm; 150 mW/cm^2).

At the time of writing, the PDI studies of *E. coli* with the SiPc **30** were still ongoing.

2

Cationic subphthalocyanines as photosensitzers for photodynamic inactivation

2.1 State of the art

Just like it was the case for SubPcs as PS in PDT, the use of cationic SubPcs as PS for PDI remains extremely rare. In the last two years, only one paper has been published in which a SubPc was successfully used as a PDI agent.[196] Nevertheless, SubPcs are interesting candidates for use as PS, especially in situations where absorption in the red part of the spectrum is not required. This is the case for example for the inactivation of pathogenic microorganisms grown *in vivo* as localized foci of infection, on skin or on accessible mucous membranes, which can be easily treated by PDI. Therefore, more research on the design of cationic SubPcs as potential PDI agents is warranted.

2.1.1 Approaches towards cationic subphthalocyanines

Unlike Pcs, SubPcs result less versatile with regard to peripheral substitution possibilities, due to the harsh reaction conditions used in their synthesis. When looking at recently published literature concerning SubPcs, most synthetic efforts are directed towards the development of new axial substitution methodologies,[141,197] and much less

[196] I. Roy, D. Shetty, R. Hota, K. Baek, J. Kim, C. Kim, S. Kappert, K. Kim, *Angew. Chem. Int. Ed.* **2015**, *54*, 15152–15155.

[197] a] J. Guilleme, L. Martínez-Fernández, I. Corral, M. Yáñez, D. González-Rodríguez, T. Torres, *Org. Lett.* **2015**, *17*, 4722–4725; b) H. Gotfredsen, M. Jevric, A. Kadziola, M. B. Nielsen, *Eur. J. Org. Chem.* **2016**, *2016*, 17–21; c] H. Gotfredsen, M. Jevric, S. L. Broman, A. U. Petersen, M. B. Nielsen, *J. Org. Chem.* **2016**, *81*, 1–5.

research is focussed on peripheral substitution. Moreover, the peripheral substitution of SubPcs is generally only conducted with an eye on their possible application in dye sensitized solar cells,[198] and not directed towards the investigation of new PS.

Up to now, almost all published cationic SubPcs have exploited the use of alkylated pyridinium substituents, located either at the peripheral or axial positions of the SubPc macrocycle. As mentioned previously in Subchapter 1 of this Chapter, the linkage of pyridines to phthalonitriles can be achieved in various ways, such as by nucleophilic substitution with hydroxy- or mercaptopyridines, or by Sonogashira coupling reactions with alkynylpyridines. Therefore, these have also been until now the methods of choice for their incorporation quaternizable groups into SubPcs.

The first cationic SubPc was published in 2008 by Durantini and co-workers,[199] who synthesised the 4-(4-pyridyloxy)phthalonitrile by nucleophilic substitution of 4-nitrophthalonitrile with 4-hydroxypyridine, and subjected it to boron trichloride induced cyclotrimerization. The resulting SubPc was then methylated, to obtain the corresponding tricationic $SubPc^{3+}$ (Figure 86a). Another tricationic SubPc was obtained in our research group, by subjecting a tri-iodo-SubPc to a triple Heck cross-coupling reaction with 4-vinylpyridine in the presence of catalytic amounts of $PdCl_2$ and tris(*o*-tolyl)phosphine (Figure 86b).[200]

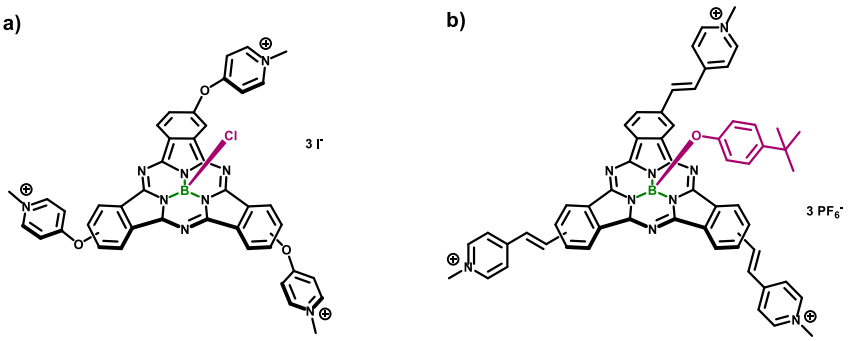

Figure 86. a) The first published tricationic SubPc, as synthesized by Durantini and co-workers.[199] b) Another tricationic SubPc published by I. Sánchez-Molina *et al.*[200]

A more extensive study of the different possibilities for the incorporation of pyridinium substituents at both the periphery and axial position of SubPcs has been conducted in our research group, by Łapok et al.[201] On the one hand, they parted from 4-(3-pyridyloxy)phthalonitrile, to obtain a tricationic SubPc similar to the one depicted above.

---

198 a] M. Urbani, F. A. Sarı, M. Grätzel, M. K. Nazeeruddin, T. Torres, M. Ince, *Chem. Asian J.* **2016**, *11*, 1223–1231; b) C. B. Kc, G. N. Lim, F. D'Souza, *Chem. Eur. J.* **2016**, *22*, 13301–13311.

199 M. B. Spesia, E. N. Durantini, *Dyes Pigments* **2008**, *77*, 229–237.

200 I. Sánchez-Molina, A. Soriano, C. G. Claessens, T. Torres, H. J. Bolink, *J. Porphyr. Phthalocyanines* **2013**, *17*, 1016–1021.

201 Ł. Łapok, C. G. Claessens, D. Wöhrle, T. Torres, *Tetrahedron Lett.* **2009**, *50*, 2041–2044.

On the other hand they made use of another strategy, namely that of grafting pyridylethynyl groups at the periphery of SubPcs by a Sonogashira catalytic cross-coupling reaction between a tri-iodo SubPc and an excess of 3-ethynylpyridine (Figure 87a) or 2-ethynylpyridine (Figure 87b) in Et_3N in the presence of catalytic amounts of $Pd(PPh_3)_2Cl_2$ and CuI. Furthermore they made use of different methylation agents, to assess the influence of the counter anion on the water solubility of the resulting quaternized SubPcs (not depicted in Figure 87). Lastly, they also incorporated a pyridinium moiety at the axial SubPc position (Figure 87c).

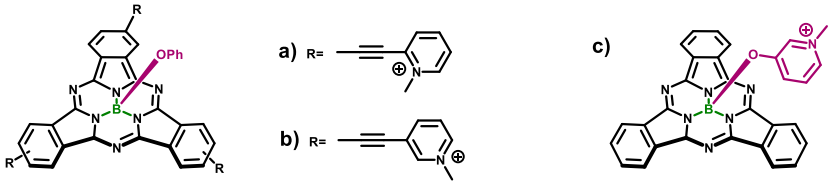

Figure 87. A series of tricationic SubPcs synthesized previously in our research group and published by Łapok *et al.*[201] Counterions are not represented for clarity.

2.1.2 Cationic subphthalocyanines for photodynamic inactivation

Out of the above-mentioned cationic SubPcs, only that reported by of Durantini and co-workers[199] was tested for its possible use as PS in the PDI of microorganisms. In particular, its PDI efficacy was tested *in vitro* against the Gram-negative bacterium *E. coli* and resulted promising. The cationic SubPc was found to bind rapidly to *E. coli* cells, reaching around 2 nmol/10^6 cells after 5 min of incubation with 4 μM of PS in the dark. As a result, PDI treatment lead to a 2.5 log CFU reduction of cell survival, corresponding to 99.7% of cellular inactivation. Furthermore, the growth of *E. coli* cells was completely arrested when cultures were exposed to 8 μM of the cationic SubPc and irradiated, whereas a negligible effect was found in the case of the non-charged SubPc.

More recently, a big advance was made by Kim and co-workers, who synthesized a nanosphere whose shell is composed of covalently linked SubPc units (Figure 88). Upon methylation of the sulphur atoms in the aliphatic chains of the SubPc, the now cationic nanosphere has the ability to target, label and photoinactivate antibiotic-resistant bacteria in a single treatment with more than 99% efficiency, using extremely low light and drug doses.[196] Furthermore, the nanosphere showed a far superior performance compared to that of the corresponding monomers, presumably because of its enhanced water dispersibility and therefore higher efficiency of $^1O_2$ generation and phototoxicity.

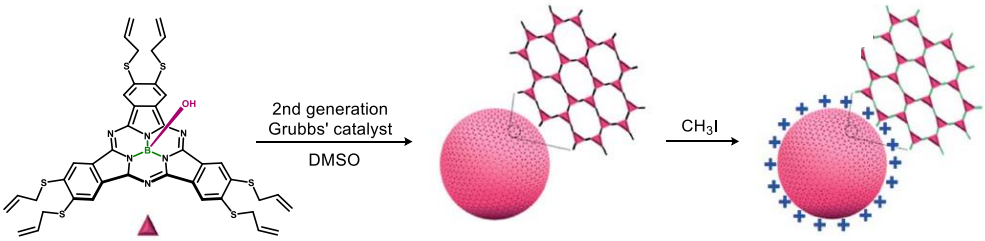

Figure 88. Synthesis of a nanosphere, composed of covalently linked cationic SubPc units, with exceptionally high PDI efficiency.[196]

2.2 Molecular design, synthesis and characterization of a series of cationic subphthalocyanine photosensitizers

The specific objective of this subchapter is to synthesize SubPcs with cationic moieties at the periphery of the macrocycle, similar to our approach used above for cationic SiPcs, and to implement various substituents at the axial positions (Figure 89). As mentioned in the introduction above, in our group, such cationic SubPcs with pyridinium substituents at the periphery of the macrocycle have already been synthesized.[201] In this previous work, macrocyclization of 4-(3-pyridyloxy)phthalonitrile, followed by subsequent methylation, resulted in a tricationic SubPc. In this subchapter, we want to continue with this strategy, and take it to the next level. To this end, we aim to perform the macrocyclization of 4,5-bis(3-pyridyloxy) phthalonitrile in the presence of boron trichloride, in this way obtaining, upon methylation, the first hexacationic SubPc. Next, we want to incorporate the building blocks for axial substitution **5**, **7**, **8** and **11**, synthesized in Chapter 1, at the axial position of this hexacationic SubPc, in this way obtaining a series of axially substituted hexacationic SubPcs with interesting properties for their use in PDT. Importantly, in contrast to the tricationic SubPcs published earlier, the resulting hexacationic SubPcs will not exist as a mixture of regioisomers, but will be isomerically pure molecules, which is advantageous in regard to their possible future use as PS in PDT.

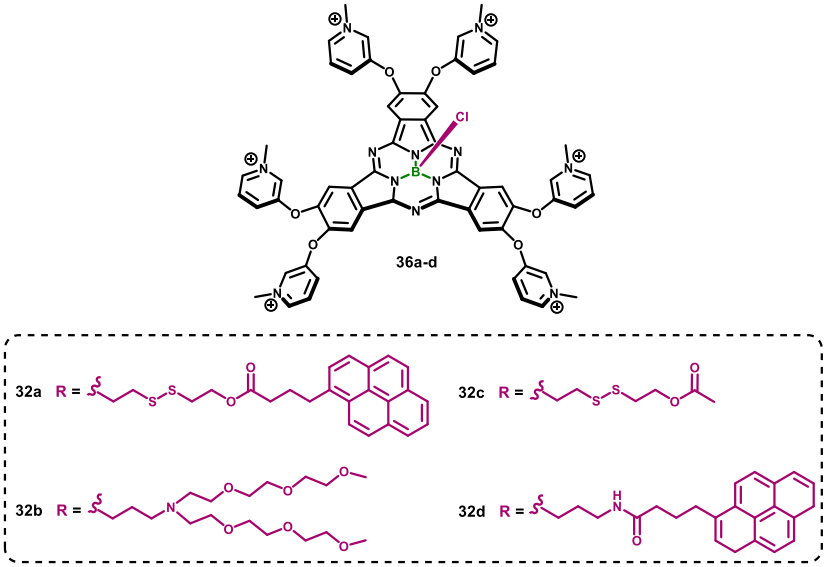

Figure 89. Molecular structure of target SubPcs **32a-d**, a series of hexacationic cationic SiPcs bearing the same axial substituents as those used in Chapter 1 of this thesis. Iodide counterions are not represented for clarity.

2.2.1 Synthesis of hexa(3-pyridyloxy) subphthalocyanine chloride

In the route to hexacationic SubPcs, phthalonitrile **24**, synthesized previously in Subchapter 1 of this Chapter, was subjected to a macrocyclization reaction in the presence of boron trichloride to form SubPc **33** (Scheme 21). Both the starting phthalonitrile and the final SubPc (**33**) display low solubility in various high-boiling point solvents, complicating the synthesis. For this reason, it was found that the ideal reaction conditions consist of a 1:1 mixture of *o*-DCB and *p*-xylene. The macrocyclization reaction proceeded extremely fast and resulted in the immediate precipitation of **33** at the bottom of the flask. This allowed for an easy decantation of the remaining solvent, which remained completely colorless. The crude precipitate was then dissolved in THF and purified by SEC, using Bio-Beads as the stationary phase and THF as the eluent.

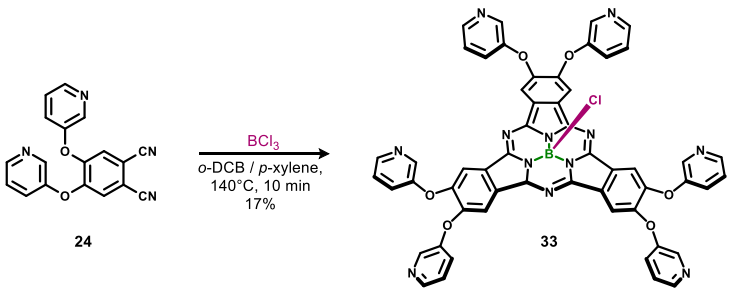

Scheme 21. Macrocyclization reaction of **24** in the presence of BCl_3 in a high-boiling point solvent mixture, resulting in the formation of **33**.

2.2.2 Axial substitution *via* the triflate-subphthalocyanine intermediate

Once we obtained sufficient quantity of SubPc **33**, the axial substitution of its chlorine atom by our previously synthesized building blocks for axial substitution (i.e. the primary alcohols **5**, **7**, **8** and **11**; Chapter 1 – Subchapter 1) was explored. To this end, the same methodology as in Subchapter 2 of Chapter 1 was first applied, namely the use of a triflate-SubPc reactive intermediate that readily reacts with a variety of nucleophiles, including the primary alcohol compounds (Scheme 22). Unfortunately, the treatment of SubPc **33** with AgOTf resulted in the formation of a series of unwanted products, as detected by TLC, and did not lead to formation of the desired triflate-SubPc intermediate. This can be explained by the fact that the silver cation present in silver triflate possibly forms other complexes with **33** by coordinating the pyridine nitrogens, which can act as soft donor groups.[202] Ag^+ usually has a linear bidentate coordination mode but

[202] a] H. Tsukube, S. Shinoda, J. 'ichi Uenishi, T. Hiraoka, T. Imakoga, O. Yonemitsu, *J. Org. Chem.* **1998**, *63*, 3884–3894; b) G. V. Moshorin, G. I. Repkin, V. A. Sharnin, *Russ. J. Coord. Chem.* **2006**, *33*, 368–370.

occasionally forms tridentate or highly coordinated complexes,[203] which might explain the great amount of new spots appearing in the TLC.

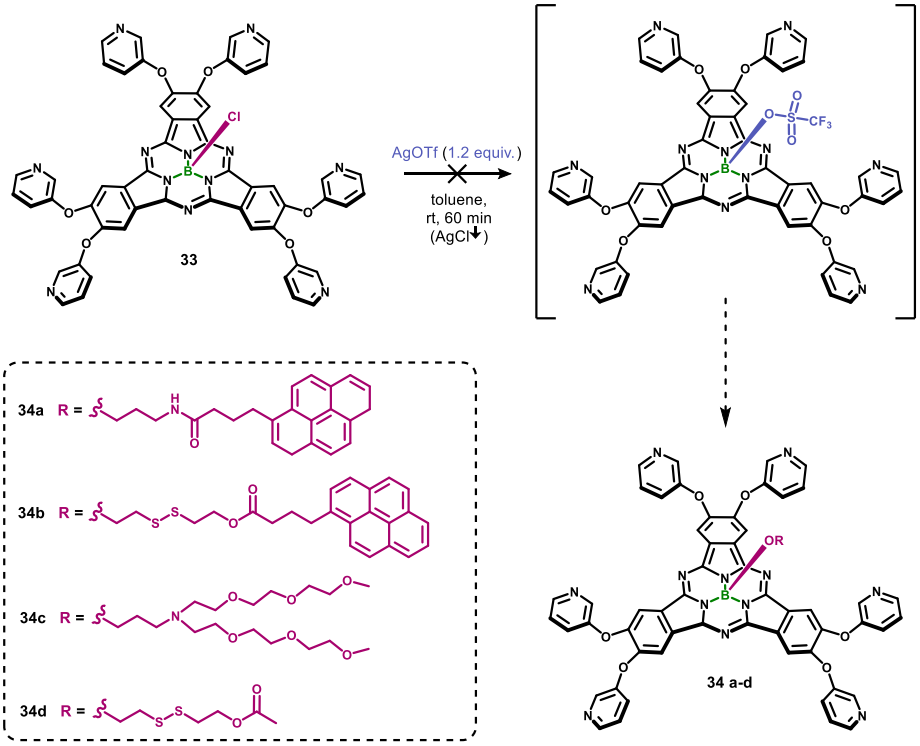

Scheme 22. Intended axial substitution of the SubPc **33**.

2.2.3 Axial substitution with phenols

As possible alternative axial substitution method, it is generally acknowledged that phenols react more efficiently with axial SubPc halides (SubPcX) than aliphatic alcohols, despite their lower nucleophilicity. This suggests the assistance of relatively acidic protons in the weakening of the B–X bond, circumventing the need of activation of the B-X bond by forming the SubPc-triflate intermediate.[83d] As a matter of fact, the reaction with phenols is by far the most widely used approach for the axial functionalization of SubPcs, owing to its simple and relatively high-yielding procedure. Hence, we decided to try this reaction, which is typically carried out by heating a mixture of the SubPc and the desired phenol in a high-boiling point aromatic solvent (toluene, chlorobenzene, etc.), in the presence of a base (Et_3N, pyridine, DIPEA, etc.) in order to neutralize the acidic hydrogen halide released. In this case, we chose to incorporate 3-pyridinol as axial substituent, [201] along to a series of commercially available phenols with different degrees of bulkiness

[203] a] H. C. Kang, A. W. Hanson, B. Eaton, V. Boekelheide, *J. Am. Chem. Soc.* **1985**, *107*, 1979–1985; b) F. R. Heirtzler, H. Hopf, P. G. Jones, P. Bubenitschek, V. Lehne, *J. Org. Chem.* **1993**, *58*, 2781–2784.

(Scheme 23). Various reaction conditions were tested (Table 13), yet none of them led to the formation of the desired product and the starting product was recovered in all cases.

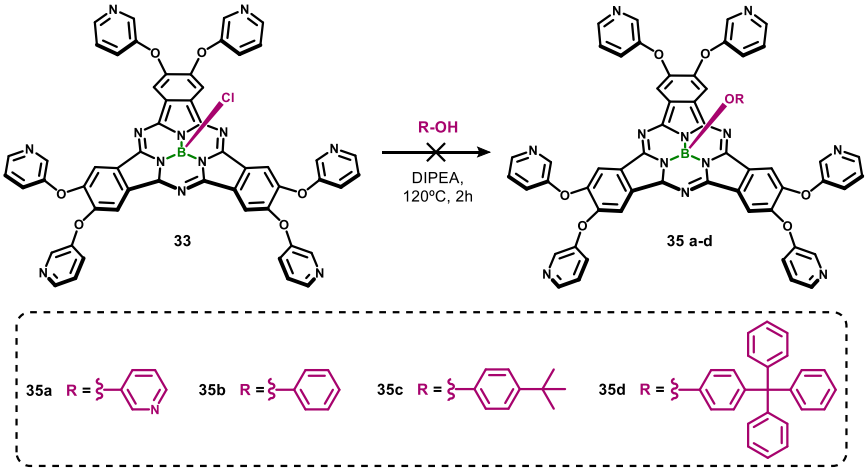

Scheme 23. Intended axial substitution of the SubPc **33** with 3-pyridinol and various phenols with different degrees of bulkiness.

Table 13. Various reaction conditions tested for the axial substitution of the SubPc **33**.

Compound	Solvent	Base	Temperature	Reaction time
36a	THF/toluene 1:1	DIPEA (1,3 equiv.)	120°C	1h
36b	Nitrobenzene	DIPEA (1,3 equiv.)	120°C	2h
36c	THF/toluene 1:1	DIPEA (1,3 equiv.)	120°C	2h
36c	DMF	DIPEA (1,3 equiv.)	120°C	2h
36d	Nitrobenzene	DIPEA (1,3 equiv.)	120°C	2h

2.2.4 Quaternization of hexa(3-pyridyloxy) subphthalocyanine chloride

Since the axial substitution of the SubPc **33** resulted impossible, a new strategy was considered, consisting in primarily quaternizing its pyridine moieties and consequently trying to incorporate the axial ligands. The same standard methylation conditions used for the SiPcs in Subchapter 1 of this Chapter (i.e. an excess of CH_3I in dry DMF) were applied in the present case (Scheme 24).

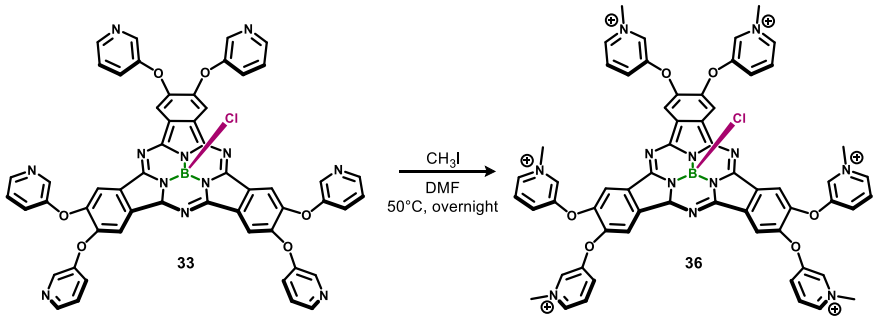

Scheme 24. Quaternization reaction of the SubPc **33**. Iodide counterions are not represented for clarity.

Upon suspected completion of the reaction, the excess of methyl iodide and the solvent were removed by evaporation under reduced pressure. However, during this process, the pink solution slowly started losing its color, until a yellow/orange solid remained. Suspecting **36** is unstable to heating, an alternative work-up was performed, consisting of partitioning the crude reaction mixture between DCM and water, followed by lyophylization of the water phase. During this process, the compound effectively localized preferably in the water phase, confirming that methylation had been effective and rendered the water-soluble hexacationic SubPc. However, during subsequent washing of the water phase the DCM layer kept turning yellow increasingly, while the pink color of the water layer slowly faded. Furthermore, upon lyophylization of the water layer, a yellow/orange solid was again obtained, with no sign of the SubPc.

As a conclusion, the methylated SubPc **36** is highly unstable and although there are indications of its formation (e.g. solubility of the SubPc in water), it has not been possible to isolate and characterize it.

3

Summary and conclusions

In the present chapter, the synthesis of different cationic SiPc and SubPc derivatives has been explored, with their use as broad-spectrum PDI agents for the photoinactivation of various microorganisms as the final goal.

Regarding SiPcs, we have synthesized a series of cationic derivatives, bearing eight positively charged pyridinium units at the macrocycle periphery, while the axial positions remained available for incorporation of different types of axial substituents (compounds **5**, **7** and **8**), enabling the study of the dependence of the PDI activity on the structure of the PS's axial substituents. The resulting SiPcs were carefully characterized, and their electronic and photophysical properties, such as ϕ_F and ϕ_Δ, were studied. Since no significant differences were observed, all of the octacationic SiPc derivatives (except for **31a**, which had been published previously) were tested *in vitro* for their PDI efficiency against *S. aureus*, a Gram-positive bacterium. Importantly, *S. aureus* resulted resistant to the light doses used in the experiment at all irradiation times, whereas dark toxicity experiments showed that the SiPc **30** and **31b** are devoid of any dark toxicity. The cytotoxicity of SiPc **33c** and **33d**, on the other hand, reached 1 log of CFU reduction, which combined with a low PDI efficacy (reaching only 2 logs of CFU reduction) discarded the future use of both PS. **31b** reached 4 logs of CFU reduction, and **30** outperformed all the tested SiPcs reaching almost 7 logs of CFU reduction, corresponding to the total eradication of bacteria present in the sample. Consequently, more resistant bacterial culture lines, such as Methicillin-resistant *S. aureus* (MRSA), were subjected to treatment by SiPc **30**. From this inactivation, **30** showed a slightly lower antimicrobial effect than in the case of *S. aureus*. However, it still reached 99,99% killing ratios, for which it can be considered as an excellent photoantimicrobial agent. At the time of writing, PDI studies with the Gram-negative bacterium *E. coli* were still ongoing.

Regarding SubPcs, our main synthetic objective was to prepare, for the first time, a hexacationic SubPc derivative, bearing pyridinium moieties at the macrocycle periphery, with a potential high efficacy against resistant bacteria. Furthermore, these hexacationic

derivatives would lack the existence of regioisomers, inherently present in the case of all the previously published tricationic systems. In this direction, we first synthesized an unprecedented SubPc with six peripheral quaternizable pyridyloxy groups (**34**). Unfortunately, all attempts for axial substitution of this SubPc, either by treatment with silver triflate to generate a triflate-SubPc intermediate or by the nucleophilic displacement reaction with phenols, were unsuccessful, due to the formation of side products, the absence of reproducibility or the low solubility or reactivity of the starting compound. Quaternization of **33** lead to the hexacationic SubPc **36**, which however resulted too unstable to isolate, for which its possible use as PS in PDI was discarded.

4

Experimental section

4.1 Materials and methods

The materials and methods used in this experimental section are the same as the ones used in that of Chapter 1, except for:

Electrospray Ionization (ESI) mass spectra were recorded with an Applied Biosystems QSTAR (ABSciex) using as injection system HPLC1100 (Agilent Technologies), at the Servicio Interdepartmental de Investigación (SIdI) of the Universidad Autónoma de Madrid. All the data are expressed with the intensity in percentage between parentheses.

IR spectra (IR) were recorded on a FTIR Cary 630 (Agilent Technologies) using the ATR technique. Spectral intensity were corrected by the ATR algorithm and subsequent baseline correction.

4.1.1 Fluorescence and singlet oxygen quantification

The ϕ_F and ϕ_Δ are determined using the same procedures as those used in Chapter 1.

4.1.2 Photodynamic inactivation of bacteria

Preparation of SiPc stock solutions

SiPcs stock solutions used in all the biological experiments were prepared in DMSO at a final concentration of 100 µM.

Solubility

The solubility of the cationic SiPcs was assessed by UV-Visible spectroscopy. Analysis was conducted in a range of concentrations between 1.0 and 10 µM achieved by the sequential addition of aliquots of stock solutions of each SiPc. For the verification of the Beer–Lambert law, an analysis of linear regression between the intensity of the Q-band and the concentration of the Pc was conducted.

Photodynamic inactivation

The microorganisms used in this study were the Gram-positive bacteria *Staphylococcus aureus* and Methicillin-resistant *Staphylococcus aureus* (MRSA) and the Gram-negative bacteria *Escherichia coli*. The bacteria were isolated from Coimbra University Hospitals patients. *E. coli* was isolated from a sample of urine; *S. aureus* and MRSA were isolated from non-surgical wound exudates. Stock cultures in Tryptic Soy Agar (TSA, Merck) were kept at 4°C. Fresh cultures of *S. aureus*, MRSA and *E. coli* were prepared before each assay by inoculating an isolated colony in 30 mL of Tryptic Soy Broth (TSB, Merck). The cultures were incubated for 24 h at 37°C under gentle stirring (120 rpm). From these cultures, aliquots of 100 µL were transferred to 10 mL of fresh TSB. The new cultures were incubated in the same conditions and used as work cultures for the inactivation assays. The work cultures of the yeast were prepared by transferring an aliquot of 100 µL to fresh Yeast Extract Glucose Chloramphenicol Agar (YGCA, Merck) and incubating in the same conditions. Fresh cultures were 10-fold diluted in PBS (pH = 7.4), to a final concentration of 10^7 CFU mL^{-1}. The bacterial suspension was allowed to stabilize at ambient temperature under gentle stirring for 10 min. The suspension was distributed in 12-well plates and appropriate quantities of 100 µM stock solutions of the Pc derivatives were added to obtain the desired PS concentration, in a total volume of 4 mL per well. The suspensions were protected from light with aluminium foil and incubated for 30 min at 37°C, to allow for the adsorption of the PS to cellular material. For the irradiation of the samples with red light (620–750 nm) an illumination system (LC-122-LumaCare, London) containing a halogen/ quartz 250 W lamp was used. The light was delivered at an irradiance of 150 mW cm^{-2}, measured with a Power Meter Coherent FieldMaxII-Top combined with a Coherent PowerSens PS19Q energy sensor. Samples were irradiated for 60 min, under gentle stirring, at ambient temperature. Light and dark controls were included in all experiments. Light controls were prepared and treated exactly as the samples but the PS solution was replaced by PBS. Dark controls were prepared as the samples corresponding to the highest PS concentration (20 µM) but were protected from light during the experiment by wrapping the microplates in aluminium foil. Triplicate aliquots of treatments and controls were collected at times 0, 30, and 60 min and their serial dilutions were pour-plated in TSA. Three independent assays were conducted with each compound. The resulting

culture plates were incubated at 37°C for 24 h. Colonies were counted in the most suitable dilutions and the concentration of viable cells was calculated as the average number of colonies in the most suitable dilution corrected for the dilution factor (CFU mL^{-1}).

4.2 Experimental details synthesis

4.2.1 Synthesis cationic SiPcs

4,5-Dichlorophthalic anhydride (**20**):[193]

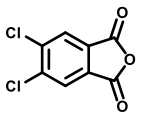

A solution of 4,5-dichlorophthalic acid (15.3 g, 64 mmol) in acetic anhydride (25 mL) was heated to reflux while distilling the acetic acid being formed in the reaction. After 5 h, the remaining acetic acid was eliminated by vacuum distillation. The solid obtained was stirred in heptane over 12 h, obtaining a solid that was filtered and thoroughly washed with the same solvent (3 x 20 mL). The title compound was obtained as a white solid (13.4 g, 98%). Characterization as reported in literature.

^{1}H-NMR (300 MHz, $CDCl_3$): δ(ppm) 8.12 (s, 2H).

^{13}C-NMR (75 MHz, $CDCl_3$): δ(ppm) 160.6, 141.7, 130.0, 127.3.

4,5-Dichlorophthalimide (**21**):[193]

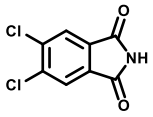

A mixture of **20** (13.5 g, 63 mmol) and formamide (20 mL) was heated to 200°C for 3 h. After cooling to rt, the solid obtained was filtered, washed with water (1 x 20 mL) and vacuum-dried, yielding **21** (12.4 g, 92%) as a white solid. Characterization as reported in literature.

^{1}H-NMR (300 MHz, DMSO-d_6): δ(ppm) 8.10 (s, 2H).

^{13}C-NMR (75 MHz, DMSO-d_6): δ(ppm) 169.7, 137.7, 132.6, 125.3.

4,5-Dichlorophthalamide (**22**):[193]

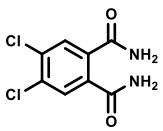

A suspension of **21** (12.4 g, 58 mmol) in 25% aqueous ammonia (173 mL) was stirred at rt for 24 h. At that time, some more 25% ammonium hydroxide solution (58 mL) was added and the mixture was further stirred for 24 h. The white solid obtained was filtered, washed with water (3 x 15 mL) and vacuum-dried, yielding **22** (11.9 g, 89%) as a white solid. Characterization as reported in literature.

^{1}H-NMR (300 MHz, DMSO-d_6): δ(ppm) 7.95 (s, 2H), 7.72 (s, 2H), 7.45 (s, 2H).

^{13}C-NMR (75 MHz, DMSO-d_6): δ(ppm) 169.6, 136.6, 131.9, 129.2.

4,5-Dichlorophthalonitrile (**23**):[193]

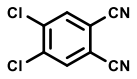

Freshly distilled thionyl chloride (42 mL) was cautiously poured over dry DMF (60 mL) at 0°C and under argon atmosphere. The mixture was vigorously stirred at that temperature for 2 h and then **22** (11.9 g, 51 mmol) was added. After stirring at rt for 12 h, the reaction mixture was poured onto crushed ice (100 mL), resulting in the precipitation of a slightly grey solid which was filtered and washed with water (1 x 20 mL). Recrystallization from methanol yields **23** (8.8 g, 88%) as light yellow needles. Characterization as reported in literature.

^{1}H-NMR (300 MHz, $CDCl_3$): δ(ppm) 7.94 (s, 2H).

^{13}C-NMR (75 MHz, $CDCl_3$): δ(ppm) 138.2, 135.7, 115.0, 114.6, 114.0.

4,5-bis(3-pyridyloxy)phthalonitrile (**24**):[184f]

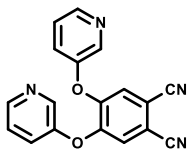

Into a round-bottom flask **23** (2.16 g, 10.9 mmol) and 3-pyridynol (2.52 g, 26.5 mmol) were dissolved in 15 mL of freshly distilled DMF under argon atmosphere. Reaction mixture was warmed up to 40°C and anhydrous potassium carbonate (15.0 g, 110 mmol) was added in small portions every 5 minutes. The reaction mixture is heated overnight, then cooled to rt and poured into 200 mL of ice water. The solid was filtered off and purified by dissolving it in chloroform and adding hot ethanol until appearance of cloudy solution. After the solution is cooled down, filtration yields **24** (2.91 g, 86%) as a white solid. Characterization as reported in literature.

^{1}H-NMR (300 MHz, $CDCl_3$): δ(ppm) 8.54 (dd, *J* = 3.8, 2.2 Hz, 2H), 8.43 (s, 2H), 7.42-7.39 (m, 4H), 7.29 (s, 2H).

^{13}C-NMR (75 MHz, $CDCl_3$): δ(ppm) 151.5, 147.5, 142.2, 127.2, 125.2, 126.8, 115.21, 112.19.

4,5-bis(3-pyridyloxy)diiminoisoindoline (**25**):[184f]

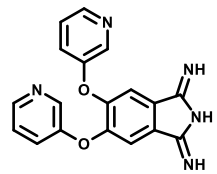

24 (3.0 g, 6.4 mmol) and sodium methoxide (0.5 g, 9.3 mmol) were dissolved in 100 mL of freshly distilled methanol. Ammonia gas was bubbled into the solution for 50 min at rt. The solution was then heated to 65°C and refluxed under ammonia gas atmosphere for 5 h. The solvent was removed under reduced pressure. Water (150 mL) was added to the concentrated residue to precipitate the product. The product was filtered, thoroughly with water and vacuum dried to afford **25** (1.9g, 91%) as light green crystals. Characterization as reported in literature.

^{1}H-NMR (300 MHz, $CDCl_3$): δ(ppm) 8.32–8.16 (m, 3H), 7.42–7.12 (m, 10H).

^{13}C-NMR (75 MHz, $CDCl_3$): δ(ppm) 152.97, 148.32, 144.85, 140.13, 124.95, 124.71, 113.63.

Silicon (IV) phthalocyanine **26**: [184f]

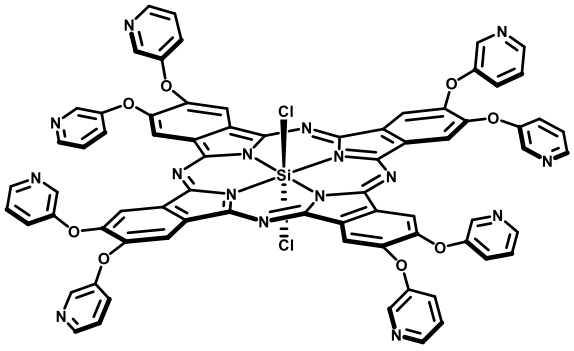

Vacuum dryed **25** (0.500 g, 1.5 mmol) was added to 5 mL of freshly redistilled quinoline. The reaction solution was stirred under argon for 10 min, and then, silicon tetrachloride (0.5mL, 2.2 mmol) was added dropwise to the solution. The temperature was raised to 220°C and maintained for 1 h. The solution was cooled to rt, and the solid was filtered under vacuum and washed successively with water, methanol, and acetone. The title compound **26** (0.5g, 98%) was obtained as a dark green solid. Characterization as reported in literature.

^{1}H-NMR (300 MHz, d-TFA): δ(ppm) 9.66 (s, 8H), 8.98 (d, J=2.7 Hz, 8H), 8.73 (dd, J= 3.5, 1.0 Hz, 8H), 8.58 (m, 8H), 8.21 (m, 8H).

^{13}C-NMR (75 MHz, d-TFA): δ(ppm) 158.95, 152.09, 151.43, 139.324, 137.64, 136.40, 134.08, 131.48, 120.53.

Silicon (IV) phthalocyanine **28**: [184f]

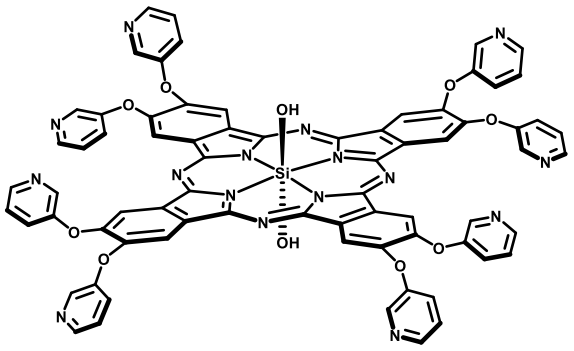

A mixture of **26** (0.450 g, 0.33 mmol) and sodium methoxide (1.5 g, 27 mmol) in 60 mL of water/ethanol (5:1) was heated to reflux for 5h. The solvent was removed under reduced pressure, and the product was isolated by precipitation upon addition of 10mL of water. The slurry solid was filtered and washed with water to yield **28** (0.32 g, 80%) as a dark green solid. Characterization as reported in literature.

^{1}H-NMR (300 MHz, d-TFA): δ(ppm) 9.72 (br s, 8H), 9.03 (br s, 8H), 8.81 (br s, 8H, 8H), 8.64 (br s, 8H), 8.29 (br s, 8H).

^{13}C-NMR (75 MHz, d-TFA): δ(ppm) 159.11, 152.24, 151.58, 139.46, 137.78, 136.55, 134.20, 131.61, 120.67.

Silicon (IV) phthalocyanine **29a**:[184f]

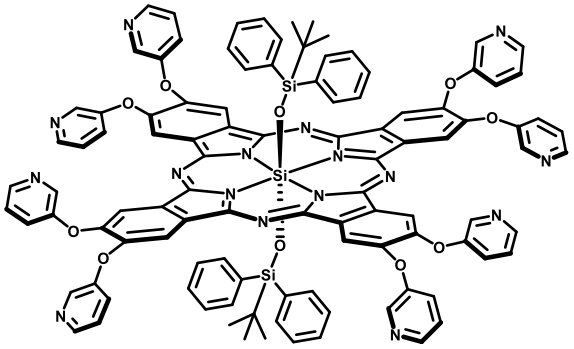

SiPc **28** (0.050 g, 0.038 mmol) was dissolved in 3 mL of dry pyridine at 115°C under an argon atmosphere. *tert*-Butyldiphenylchlorosilane (0.295 mL, 0.947 mmol) was added dropwise to the reaction mixture via syringe. After 8h, another portion of tert-butyldiphenylchlorosilane (0.212 mL, 0.682 mmol) was added. The reaction mixture was refluxed for another 9h, after which the solvent was evaporated to dryness. The remaining solid was washed extensively with chloroform and the filtrate was collected and evaporated to dryness and subjected to a trituration in heptane, in which the solid was collected and washed with heptane and water to obtain the pure compound **29a** (0.015 g, 22%) as a green solid. Characterization as reported in literature.

^{1}H-NMR (300 MHz, DMSO-d_6): δ(ppm) 9.09 (s, 8H), 8.78 (d, J=2.7 Hz, 8H), 8.66 (dd, J= 3.5, 1 Hz, 8H), 7.97 (m, 8H), 7.77–7.70 (m, 8H), 6.93 (t, J= 7.3 Hz, 4H), 6.46 (t, J= 7.4 Hz, 8H), 4.79 (d, J= 7.1 Hz, 8H), -1.30 (s, 18H).

^{13}C-NMR (75 MHz, DMSO-d_6): δ(ppm) 154.44, 151.27, 148.62, 146.13, 141.19, 133.79, 133.30, 133.21, 128.94, 126.94, 126.39, 125.78, 115.95, 24.99, 17.00.

Silicon (IV) phthalocyanine **29b**:

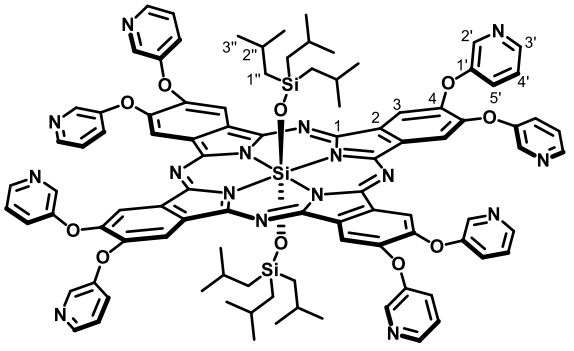

SiPc **28** (0.050 g, 0.038 mmol) was dissolved in 3 mL of dry pyridine at 115°C under an argon atmosphere. Triisobutylchlorosilane (0.254 mL, 0.947 mmol) was added dropwise to the reaction mixture via syringe. After 8h, another portion of triisobutylchlorosilane (0.183 mL, 0.682 mmol) was added. Purified as described above for SiPc **29a,** yielding **29b** (0.025 mg, 38%) as a dark green solid.

^{1}H-NMR (300 MHz, $CDCl_3$): δ(ppm) 9.38 (s, 8H, H_3), 8.66 (d, *J* = 2.7 Hz, 8H, $H_{2'}$), 8.58 (d, *J* = 4.6 Hz, 8H, $H_{3'}$), 7.84 (dd, *J* = 4.9, 1.8 Hz, 8H, $H_{5'}$), 7.68-7.63 (m, 8H, $H_{4'}$), 0.44 (d, 36H, *J* = 6.5Hz, $H_{3''}$), -0.85 (m, 6H, $H_{2''}$), -2.44 (d, 12H, *J* = 7 Hz, $H_{1''}$).

^{13}C-NMR (75 MHz, $CDCl_3$): δ(ppm) 207.40, 154.28, 150.79, 148.59, 145.80, 141.14, 133.59, 125.67, 125.05, 116.04, 78.01, 77.79, 77.58, 77.16, 31.43, 25.77, 25.25, 22.91.

MS (MALDI-TOF, DCTB): *m/z* = 3374.4 $[2M\text{-}iBu]^+$(10), 1715.6 $[M]^+$ (30), 1499.4 $[M\text{-}L_{ax}]^+$ (100).

HR-MS (MALDI-TOF, DCTB): $[M]^+$ Calcd. for $C_{96}H_{94}N_{16}O_{10}Si_3$: 1715.6667; Found: 1715.6561.

UV-VIS (DMF): λ_{max} (nm) (log ε): 676 (5.29), 646 (4.40), 609 (4.46), 361 (4.85).

FT-IR (neat) ν (cm^{-1}): 2950, 1574, 1458, 1418, 1282, 1214, 1087, 1019.

Mp: > 250°C

Silicon (IV) phthalocyanine **29c**:

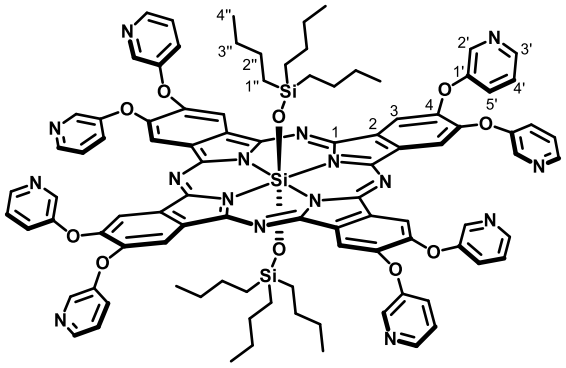

SiPc **28** (0.050 g, 0.038 mmol) was dissolved in 10 mL of dry pyridine at 115°C under an argon atmosphere. n-Butylchlorosilane (0.252 mL, 0.947 mmol) was added dropwise to the reaction solution via syringe. After 8h, another portion of n-butylchlorosilane (0.181 mL, 0.682 mmol) was added. Purified as described above for SiPc **29a,** yielding **29c** (0.021 mg, 32%) as a dark green solid.

^{1}H-NMR (300 MHz, $CDCl_3$): δ(ppm) 9.19 (s, 8H, H_3), 8.64 (d, *J* = 2.7 Hz, 8H, $H_{2'}$), 8.54 (dd, *J* = 3.5, 1.0 Hz, 8H, $H_{3'}$), 7.61 (m, 8H, $H_{5'}$), 7.48-7.44 (m, 8H, $H_{4'}$), 0.13-0.22 (m, 40H, $H_{3''\text{-}4''}$), -1.19 (m, 12H, $H_{2''}$), -2.38 (m, 12H, $H_{1''}$).

^{13}C-NMR (75 MHz, $CDCl_3$): δ(ppm) 153.95, 150.26, 147.98, 144.90, 140.26, 133.14, 125.93, 124.90, 115.66, 77.58, 77.16, 76.73.

MS (MALDI-TOF, DCTB): *m/z* = 3374.4 $[2M\text{-}iBu]^+$(1), 1715.6 $[M]^+$ (100), 1500.4 $[M– L_{ax}+H]^+$ (40), 375,3 (30).

HR-MS (MALDI-TOF, DCTB): $[M]^+$ Calcd. for $C_{96}H_{94}N_{16}O_{10}Si_3$: 1715.6667; Found: 1715.6584.

UV-VIS (DMF): λ_{max} (nm) (log ε): 675 (5.11), 645 (4.28), 608 (4.32), 361 (4.74).

FT-IR (neat) ν (cm^{-1}): 2953, 2919, 2868, 1575, 1459, 1418, 1284, 1214, 1086, 1036, 899, 703.

Mp: > 250°C

Silicon (IV) phthalocyanine **29d**:

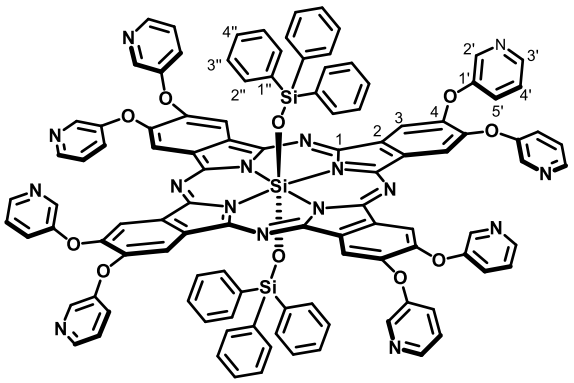

SiPc **28** (0.050 g, 0.038 mmol) was dissolved in 10 mL of dry pyridine at 115°C under an argon atmosphere. Triphenylchlorosilane (0.279 g, 0.947 mmol) was added dropwise to the reaction solution via syringe. After 8h, another portion of triphenylchlorosilane (0.201 g, 0.682 mmol) was added. Purified as described above for SiPc **29a**, yielding **29c** (0.024 mg, 34%) as a dark green solid.

^{1}H-NMR (300 MHz, $CDCl_3$): δ(ppm) 9.04 (s, 8H, H_3), 8.68 (s, Hz, 8H, $H_{2'}$), 8.58 (d, *J* = 2.6 Hz, 8H, $H_{3'}$), 7.65 (dd, *J* = 5.9 ,2.2 Hz, 8H, $H_{5'}$), 7.53 (m, 8H, $H_{4'}$), 6.85 (t, *J* = 7.4 Hz, 6H, $H_{4''}$) , 6.48 (t, *J* = 7.4 Hz, 12H, $H_{3''}$), 4.87 (d, *J* = 7.0 Hz, 12H, $H_{2''}$)

^{13}C-NMR (75 MHz, $CDCl_3$): δ(ppm) 154.00, 149.99, 148.05, 144.68, 139.82, 133.78, 132.93, 132.82, 128.43, 126.51, 126.04, 125.04, 115.74, 77.58, 77.16, 76.74, 31.06.

MS (MALDI-TOF, DCTB): *m/z* = 1835.3 $[M]^+$ (100), 1758.3 $[M\text{-}C_5H_6]^+$ (2) 1560.3 $[M\text{-}L_{ax}]^+$ (10).

HR-MS (MALDI-TOF, DCTB): $[M]^+$ Calcd. for $C_{108}H_{70}N_{16}O_{10}Si_3$: 1835.4790; Found: 1835.4770.

UV-VIS (DMF): λ_{max} (nm) (log ε): 681 (5.10), 649 (4.27), 613 (4.35), 363 (4.26).

FT-IR (neat) ν (cm^{-1}): 3067, 1460, 1428, 1118, 738, 711.

Mp: > 250°C

Silicon (IV) phthalocyanine **30**:

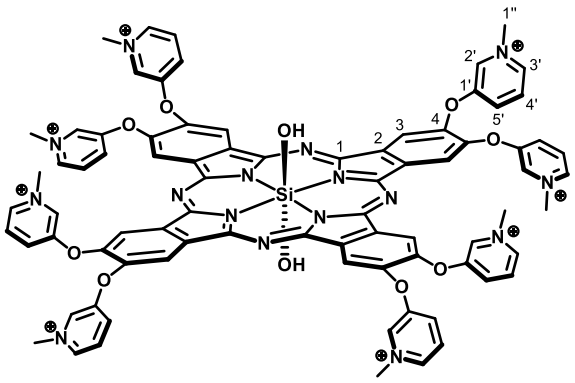

28 (0.017 g, 0.013 mmol) was dissolved in dry DMF (2 mL) under Ar atmosphere and CH_3I (0,5 mL) was added. The mixture was heated at 50°C for 2h. The solvent was evaporated and the crude obtained was triturated and washed with acetone to yield **30** (0.028 g, 87%) as a dark green solid.

^{1}H-NMR (300 MHz, DMSO-d_6): δ(ppm) 9.80 (s, 8H, H_3), 9.37 (s, 8H, $H_{2'}$), 8.96 (d, *J* = 6.0 Hz, 8H, $H_{3'}$), 8.67 (dd, *J* = 6.6 ,1.7 Hz, 8H, $H_{5'}$), 8.31 (m, 8H, $H_{4'}$), 4.43 (s, 24H, $H_{1''}$).

^{13}C-NMR (75 MHz, DMSO-d_6): δ(ppm) 162.20, 155.51, 148.10, 147.45, 141.52, 136.50, 133.71, 133.50, 128.99, 117.02, 48.45, 40.26, 35.68, 34.27, 30.60.

MS (ESI): m/z = 691.10 $[M-3I]^{3+}$, 486.58 $[M-4I]^{4+}$, 364.33 $[M-5I]^{5+}$, 281.32 $[M-6I]^{6+}$, 224.24 $[M-7I]^{7+}$, 179 $[M-8I]^{8+}$

HR-MS (ESI): Calc. for $C_{72}N_{16}SiO_{10}H_{42}I_5C_8H_{24}$: 691.3380, Found: 691.3315
Calc. for $C_{72}N_{16}SiO_{10}H_{42}I_4C_8H_{24}$: 486.7774, Found: 486.7776

UV-VIS (H_2O): λ_{max} (nm) (log ε): 675 (5.25), 646 (4.40), 608 (4.43), 356 (4.84).

FT-IR (neat) ν (cm^{-1}): 3382 (O-H), 1581, 1497, 1451, 1415, 1262, 1083, 844 (Si-O).

Mp: 252°C

Silicon (IV) phthalocyanine **31a**:[184f]

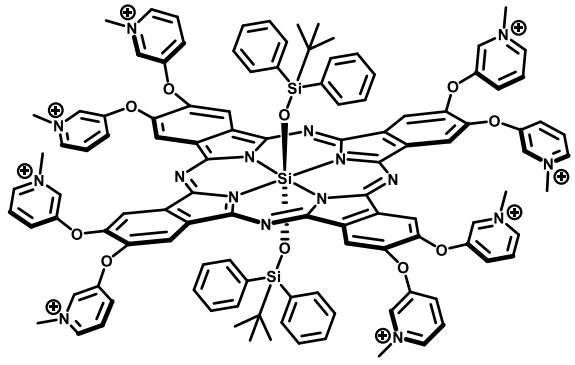

29a (0.025 g, 0.014 mmol) was dissolved in dry DMF (2 mL) under Ar atmosphere and iodomethane (0,5 mL) was added. The mixture was heated at 50°C for 2h. The solvent was evaporated and the crude obtained was triturated and washed with acetone to yield **31a** (0.037 g, 91%) as a dark green solid. Characterization as reported in literature.

^{1}H-NMR (300 MHz, DMF-d_7): δ (ppm) = 9.79 (s, 8H), 9.71 (s, 8H), 9.25 (d, *J* = 5.3 Hz, 8H), 8.88 (d, *J* = 7.8 Hz, 8H), 8.57 (m, 8H), 7.04 (t, *J* = 7.3 Hz, 4H), 6.68 (t, *J* = 7.4 Hz, 8H), 4.89 (d, *J* = 7.0 Hz, 8H), 4.76 (s, 24H), -1.24 (s, 18H).

^{13}C-NMR (75 MHz, DMF-d_7): δ (ppm) = 156.47, 149.87, 148.76, 143.06, 138.95, 135.06, 134.24, 133.70, 133.05, 130.17, 129.32, 127.36, 117.61, 49.61, 25.24, 17.04.

Silicon (IV) phthalocyanine **31b**:

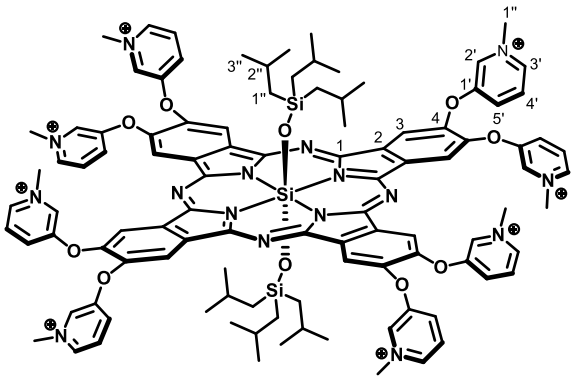

29b 15b (0.025 g, 0.014 mmol) was dissolved in dry DMF (2 mL) under Ar atmosphere and iodomethane (0,5 mL) was added. The mixture was heated at rt for 2h. The solvent was evaporated and the crude obtained was triturated and washed with acetone to yield **31b** (0.038 g, 95%) as a dark green solid.

^{1}H-NMR (300 MHz, DMSO-d_6): δ(ppm) 9.77 (s, 8H, H_3), 9.44 (s, 8H, $H_{2'}$), 9.02 (d, *J* = 5.9 Hz, 8H, $H_{3'}$), 8.59 (d, *J* = 8.8 Hz, 8H, $H_{5'}$), 8.34 (m, 8H, $H_{4'}$), 4.49 (s, 24H, $H_{1''}$) , -0.43 (d, *J* = 6.4 Hz, 36H, $H_{3'''}$), -0.80 (m, 6H, $H_{2'''}$), -2.47 (d, *J* = 7.0 Hz, 12H, $H_{1'''}$).

^{13}C-NMR (75 MHz, DMSO-d_6): δ(ppm) 162.11, 155.49, 147.40, 147.27, 145.47, 143.10, 141.48, 141.02, 136.40, 135.98, 133.39, 128.95, 128.82, 126.05, 125.15, 48.39, 48.34, 35.60, 30.60.

MS (ESI): m/z = 1298.13 $[M-2I]^{2+}$, 823.12 $[M-3I]^{3+}$, 585.62 $[M-4I]^{4+}$, 443.12 $[M-5I]^{5+}$, 349.29 $[M-6I]^{6+}$, 229.49 $[M-8I]^{8+}$

HR-MS (ESI): Calc. for $C_{104}H_{118}N_{16}O_{10}Si_3I_5$: 823.1244, Found: 823.1264
Calc. for $C_{104}H_{118}N_{16}O_{10}Si_3I_4$: 585.6170, Found: 585.6247
Calc. for $C_{104}H_{118}N_{16}O_{10}Si_3I_3$: 443.1126, Found: 443.1228
Calc. for $C_{104}H_{118}N_{16}O_{10}Si_3I_2$: 348.1097, Found: 348.1191
Calc. for $C_{104}H_{118}N_{16}O_{10}Si_3$: 229.3560, Found: 229.3623

UV-VIS (H_2O): λ_{max} (nm) (log ε): 675 (5.34), 646 (4.45), 608 (4.49), 356 (4.90).

FT-IR (neat) ν (cm^{-1}): 1582, 1497, 1452, 1417, 1262, 1083.

Mp: 232°C

Silicon (IV) phthalocyanine **31c**:

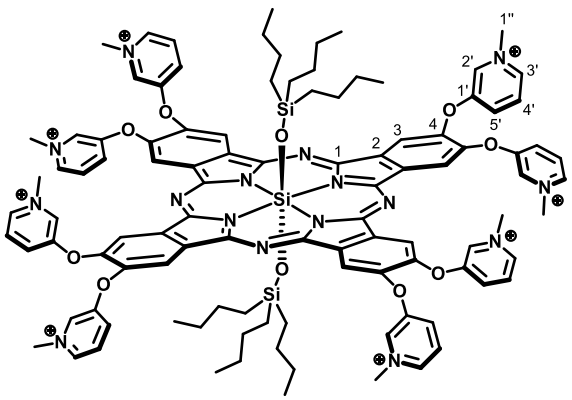

SiPc **29c** (0.025 g, 0.014 mmol) was dissolved in dry DMF (2 mL) under Ar atmosphere and iodomethane (0,5 mL) was added. The mixture was heated at 50°C for 2h. The solvent was evaporated and the crude obtained was triturated and washed with acetone to yield **31c** (0.037 g, 94%) as a dark green solid.

^{1}H-NMR (300 MHz, $CDCl_3$): δ(ppm) 9.64 (s, 8H, H_3), 9.32 (s, 8H, $H_{2'}$), 8.88 (d, *J* = 6.0, 8H, $H_{3'}$), 8.44 (dd, *J* = 7.0, 1.3 Hz, 8H, $H_{5'}$), 8.20 (m, 8H, $H_{4'}$), 4.35 (s, 24H, $H_{1''}$) , -0.01 (m, 30H, $H_{3'''-4'''}$), -1.38 (m, 12H, $H_{2'''}$), -2.56 (m, 12H, $H_{1'''}$).

^{13}C-NMR (75 MHz, DMSO-d_6): δ(ppm) 162.11, 146.11, 142.10, 127.98, 35.62, 34.23, 30.61.

MS (ESI): m/z = 1298.13 $[M-2I]^{2+}$, 823.13 $[M-3I]^{3+}$, 585.62 $[M-4I]^{4+}$, 443.12 $[M-5I]^{5+}$, 348.28 $[M-6I]^{6+}$, 229.48 $[M-8I]^{8+}$

HR-MS (ESI): Calc. for $C_{104}H_{118}N_{16}O_{10}Si_3I_5$: 823.1244, Found: 823.1271
Calc. for $C_{104}H_{118}N_{16}O_{10}Si_3I_4$: 585.6170, Found: 585.6252
Calc. for $C_{104}H_{118}N_{16}O_{10}Si_3I_3$: 443.1126, Found: 443.1231
Calc. for $C_{104}H_{118}N_{16}O_{10}Si_3I_2$: 348.1097, Found: 348.1194
Calc. for $C_{104}H_{118}N_{16}O_{10}Si_3$: 229.3560, Found: 229.3629

UV-VIS (H_2O): λ_{max} (nm) (log ε): 673 (5.34), 643 (4.47), 606 (4.51), 356 (4.91).

FT-IR (neat) ν (cm^{-1}): 2997, 2920, 1584, 1500, 1454, 1419, 1284, 1174, 1085, 1023.

Mp: 230°C

Silicon (IV) phthalocyanine **31d**:

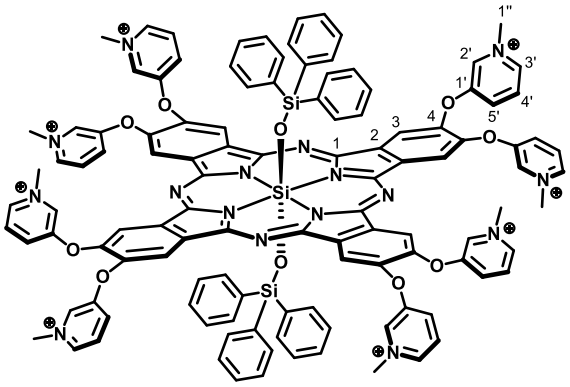

SiPc **29d** (0.025 g, 0.013 mmol) was dissolved in dry DMF (2 mL) under Ar atmosphere and iodomethane (0,5 mL) was added. The mixture was heated at 50°C for 2h. The solvent was evaporated and the crude obtained was triturated and washed with acetone to yield **31d** (0.035 g, 91%) as a dark green solid.

^{1}H-NMR (300 MHz, DMSO-d_6): δ(ppm) 9.65 (s, 8H, H3), 9.48 (s, 8H, $H_{2'}$), 9.05 (d, *J* = 6.0 Hz, 8H, $H_{3'}$), 8,68 (dd, *J* = 6.9 ,2.0 Hz, 8H, $H_{5'}$), 8.40 (m, 8H, $H_{4'}$), 6.92 (t, *J* = 7.4 Hz, 6H, $H_{4'''}$) , 6.55(t, *J* =7.4 Hz, 12H, $H_{3'''}$), 4.72 (d, 6.9 Hz, 12H, $H_{2'''}$), 4.51 (s, 24H, $H_{1''}$).

^{13}C-NMR (75 MHz, DMSO-d_6): δ(ppm) 155.26, 148.91, 147.74, 142.17, 137.75, 133.98, 132.97, 132.05, 129.39, 128.92, 126.96, 116.64, 77.58, 77.16, 76.74, 48.82.

MS (ESI): m/z = 1358.53 $[M-2I]^{2+}$, 863.06 $[M-3I]^{3+}$, 615.82 $[M-4I]^{4+}$.

HR-MS (ESI): $[M-2I]^{2+}$ Calcd. for $C_{108}H_{70}N_{16}O_{10}Si_3I_6C_8H_{24}$: 1358.5458; Found: 1358.5832.

UV-VIS (H_2O): λmax (nm) (log ε): 679 (5.20), 648 (4.38), 611 (4.38), 355 (4.70).

FT-IR (neat) ν (cm^{-1}): 2998, 1582, 1498, 1454, 1418, 1283, 1175, 1085, 1036, 955, 886, 760.

Mp: 207°C

4.2.2 Synthesis cationic SubPcs

Subphthalocyanine **33**:

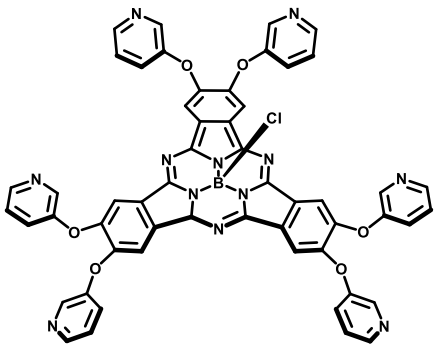

24 (0.100 g, 0.318 mmol) is dried in a vacuum oven and placed in a two neck flask equipped with a reflux cooler together with a stirring bar. The system is subjected to various vacuum cycles, after which *o*-DCB (1 mL) is added and the mixture is heated to 140°C. BCl_3 in DCM (0.382 mL, 0.382 mmol) and another portion of BCl_3 in *p*-xylene (0.382 mL, 0.382 mmol) are quickly added. Formation of SubPc **33** results in its immediate precipitation, and after 10 minutes of reaction the remaining solvent is completely colorless and the reaction is stopped. The mixture is allowed to cool to rt and the colorless solvent is decanted. The remaining solvent is removed by evaporation under reduced pressure and the crude is purified by size-exclusion chromatography (SEC) through Bio-Beads in THF, yielding **33** (0.017 mg, 17%) as a dark pink solid.

^{1}H-NMR: xxx

MS (ESI): m/z = xxx

UV-VIS (H_2O): λ_{max} (nm) (log ε): xxx

FT-IR (neat) ν (cm^{-1}): 2998

Mp: xxx

CHAPTER 3

Design, synthesis and *in vitro* evaluation of (sub)phthalocyanine-based biohybrids for photodynamic therapy and/or inactivation

1

Sub(phthalocyanine)-peptide biohybrid conjugates for improved cellular uptake

1.1 State of the art

Many biologically active compounds, although very effective on their own, require to be conjugated to a site-specific delivery counterpart for intracellular delivery, enabling them to exert their therapeutic action inside the cytoplasm, the nucleus, or other specific organelles such as mitochondria.[204] Similarly, also in the case of PS, conjugation to such a biological site-directing molecule can actually be very beneficial and is widely employed.[18]

1.1.1 Introduction to photosensitizer-based biohybrids

As mentioned in the Introduction of this thesis, Pcs and SubPcs belong to the second generation of PS. In order to obtain better characteristics, such as less aggregation, better solubility in physiological media and selective accumulation within the targeted tissue, second-generation PS are often conjugated to site-specific delivery agents and/or formulated in or on nanostructured delivery platforms. If such delivery agents or platforms are of biological nature, the PS conjugates are classified as biohybrid materials.

PS-based biohybrids can be divided in different groups, based on the nature of the biological unit (Figure 90). Most frequently, the PS is conjugated to a peptidic delivery agent, such as cell penetrating peptides, monoclonal antibodies, antibody fragments,

[204] B. Gupta, T. S. Levchenko, V. P. Torchilin, *Adv. Drug Deliv. Rev.* **2005**, *57*, 637–651.

serum proteins, protein cages or single amino acids (Figure 90a). Additionally, a whole series of other biological delivery agents have been successfully used, such as liposomes, nucleic acids, hormones, folic acid, carbohydrates, etc. (Figure 90b).[18]

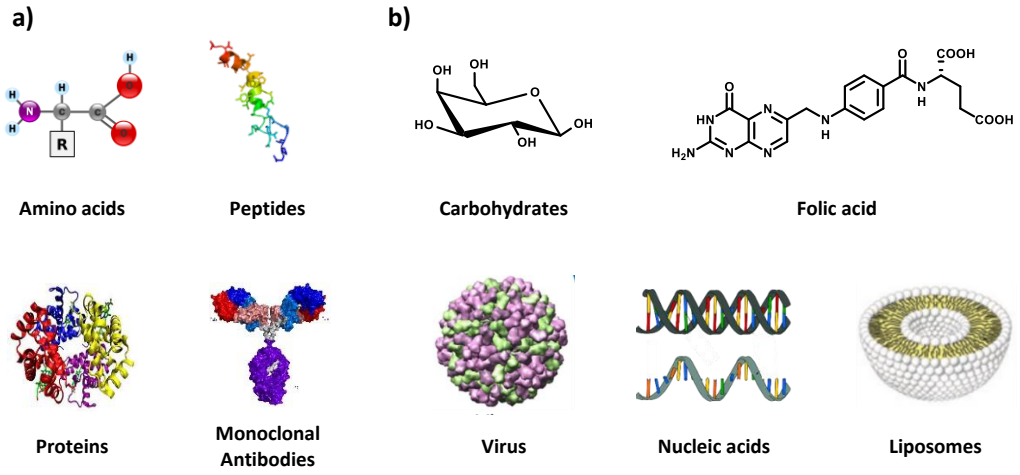

Figure 90. Frequently used biological counterparts for the synthesis of PS-based biohybrids with improved delivery and other characteristics.

Photoactive biohybrids can be obtained either by non-covalent or covalent association of the PS with the different biomolecules:[18,205]

- *Covalent approach:* also known as bioconjugation. The vast majority of publications concerning biohybrid conjugates refer to species where the PS is linked to the biomolecule *via* a covalent bond. In this way, PS have been conjugated to antibodies directed against tumor antigens, sugars, oligonucleotides to enhance photogenotoxicity, aptamers to recognise cell-membrane proteins, hormones, metabolites, cellular signalling species to selectively target an over-expressed enzyme or receptor, and also to peptides and proteins.

- *Non-covalent conjugation:* offers a much wider choice in terms of the nature of the biological partner. As a consequence, it grants the possibility of interaction with a diversity of targets.

In this Chapter, a covalent approach for bioconjugation has been follow in Subchapter 1, while Subchapter 2 deals with a non-covalent strategy.

In the case of covalent conjugation, two different classes can be distinguished based on the type of functional groups involved in the linkage of the PS and the biomolecule.[205] The first class is the most evident one, taking advantage of the amino- or carboxylic groups

[205] F. Giuntini, C. M. A. Alonso, R. W. Boyle, *Photochem. Photobiol. Sci.* **2011**, *10*, 759–791.

naturally present on most biomolecules (e.g. amino acids, peptides, proteins, oligonucleotides, etc.). In this case, the PS must bare one or more complementary carboxylic or amino groups, respectively. A second class of conjugation methods is based on reactions between non-naturally occurring (abiotic) functionalities, which are introduced in the PS and/or the biomolecule especially for this purpose. Examples are the Sonogashira reaction,[206] the Suzuki-Miyaura reaction,[206c] the Buchwald-Hartwig amination,[206c] the Cu-catalyzed Huisgen [3+2] cycloaddition (between an azide and an alkyne)[207] and the thiol-maleimide Michael addition reaction.[160]

Exceptionally popular is the bioconjugation of PS to different kinds of peptides, as it is an expedient method to overcome the issues generally associated with the use of PS, such as scarce water solubility and prominent aggregation. Additionally, the main benefit of the use of natural peptides, peptide analogues and newly designed peptides lies in their high selectivity and affinity for biological targets, for which they are ideal drug delivery vehicles.[208] As they are relatively small in size (<50 amino acid residues) they tend to be non-immunogenic and display good tissue penetration, including the possibility to cross malfunctioning blood-brain barriers. Furthermore, peptides are readily accessible, both from natural sources and by chemical synthesis, and they can be easily modified, allowing alterations in the sequence and straightforward conjugation to other chemical entities.[205] Large peptide libraries containing well-known trafficking sequences (e.g. cell-penetrating peptides), intracellular localisation sequences (e.g. mitochondria or nuclear localisation sequences), receptor binding sequences (e.g. vascular endothelial growth factor) and enzymes substrates (e.g. proteases) are available to choose from, making the use of peptides as delivery unit for small molecule drugs especially attractive.

In this first Subchapter, the covalent bioconjugation of two different PS, a SiPc and a SubPc, to a cell penetrating peptide have been investigated.

---

[206] a] J. L. Sessler, J. Jayawickramarajah, A. Gouloumis, G. Dan Pantos, T. Torres, D. M. Guldi, *Tetrahedron* **2006**, *62*, 2123–2131; b) M. R. Reddy, N. Shibata, Y. Kondo, S. Nakamura, T. Toru, *Angew. Chem.* **2006**, *118*, 8343–8346; c] H. Ali, S. Ait-Mohand, S. Gosselin, J. E. van Lier, B. Guérin, *J. Org. Chem.* **2011**, *76*, 1887–1890; d) E. Ranyuk, N. Cauchon, K. Klarskov, B. Guérin, J. E. van Lier, *J. Med. Chem.* **2013**, *56*, 1520–1534.

[207] a] M. Mudyiwa, M. W. Ndinguri, S. A. Soper, R. P. Hammer, *J. Porphyr. Phthalocyanines* **2010**, *14*, 891–903; b) N. V. Sokolova, T. Schotten, H. J. Berthold, J. Thiem, V. G. Nenajdenko, *Synthesis* **2013**, *45*, 556–561; c] M.-R. Ke, D. K. P. Ng, P.-C. Lo, *Chem. Asian J.* **2014**, *9*, 554–561.

[208] N. Sewald, H.-D. Jaakubke, *Application of Peptides and Proteins*, Wiley-VCH Verlag GmbH & Co. KGaA, Darmstadt, **2009**.

1.1.2 Cell penetrating peptides

Cell penetrating peptides (CPP) are a diverse set of short peptide sequences, usually consisting of 30 or less amino acids, that possess the remarkable property of being able to cross cell membranes and deliver bioactive cargo with molecular weights several times greater than their own.[209]

The first indications that some proteins are capable of crossing the cell membrane were first noted about 30 years ago, when the transcription trans-activating protein (Tat) from HIV-1 was found capable of entering cells and even the cell nucleus.[210] Shortly after, this property of translocation was also found in Antennapedia (Antp), a transcription factor of Drosophila,[211] and in VP22, a herpes virus protein.[212] Later it became clear that their ability to translocate across the plasma membranes is confined to short sequences of less than 20 amino acids, which are highly rich in basic residues. Therefore, CPPs are characterized by those sequences, generally containing multiple arginine (Arg) and Lysine (Lys) residues.

Since their initial discovery, the Tat-peptide and its derivatives are still the most used CPPs, although the discovery and design of new CPPs has been increasing rapidly ever since.[213] As a result, there now exist a great variety of CPPs in terms of amino acid composition and degree of polarity, and CPPs are generally classified into three categories according to their origin (see Table 14). The first group is that of the protein-derived peptides, such as Tat and penetratin, which originate from naturally occurring proteins. They are also called protein-transduction domains. Another group is that of chimeric peptides, where two peptides sequences originating from two different proteins are fused together. The most used example from this category is transportan (TP), containing the peptide sequence from the amino terminus of the neuropeptide galanin, bound *via* the lysine residue with the membrane-interacting wasp venom peptide, mastoparan. The third group consists of synthetic peptides, where the polyarginine family and the model amphipathic peptide (MAP) are the best studied members.

---

209 a] M. Lindgren, M. Hällbrink, A. Prochiantz, U. Langel, *Trends Pharmacol. Sci.* **2000**, *21*, 99–103; b) C. P. Cerrato, K. Künnapuu, Ü. Langel, *Expert Opin. Drug Deliv.* **2016**, 1–11.

210 a] M. Green, P. M. Loewenstein, *Cell* **1988**, *55*, 1179–1188; b) A. D. Frankel, C. O. Pabo, *Cell* **1988**, *55*, 1189–1193.

211 E. Vivès, P. Brodin, B. Lebleu, *J. Biol. Chem.* **1997**, *272*, 16010–16017.

212 W. B. Kauffman, T. Fuselier, J. He, W. C. Wimley, *Trends Biochem. Sci.* **2015**, *40*, 749–764.

213 E. Vives, *J. Controlled Release* **2005**, *109*, 77–85.

Table 14. Sequences of selected CPPs

CPP	Sequence[a]	Origin	Ref
Arg11	RRRRRRRRRRR	Synthetic	[214]
MAP	KLALKLALKALKAALKLAamide	Synthetic	[215]
Penetratin (Antp)	RQIKIWFQNRRMKWKK[b]	Protein-derived	[216]
Tat(48-60)	GRKKRRQRRRPPQ[c]	Protein-derived	[211]
Transportan (TP)	GWTLNSAGYLLGKINLKALAALAKKILamide	Chimeric	[217]
VP22	DAATATRGRSAASRPTERPRAPARSASRPRRVD	Protein-derived	[218]

[a] Peptides are C-terminal free acids unless stated otherwise. [b] Originally synthesized as C-terminal free acids but later also shown to have CPP properties when amidated. [c] This sequence is included in all Tat fragments with known translocation ability [e.g. Tat fragment (37–72) that has been used for intracellular protein delivery]. It should be noted that the Tat protein has a high genetic variability so the exact amino acid sequence might differ depending on the viral strain.

Different CPPs differ in their rate of uptake and efficiency of membrane perturbation, as demonstrated by fluorescence resonance energy transfer (FRET) analysis.[219] Hällbrinck *et al*. found that the membrane disturbing potential of the CPPs is proportional to their hydrophobic moment, which they calculated using the Kyte and Doolitle scale of hydrophobicity, and suggest that future designs of CPPs should aim to minimize their hydrophobic moment in order to increase their membrane-disturbing.[220] In terms of cellular uptake and cargo delivery kinetics, MAP shows the fastest uptake, followed by TP, Tat(48-60) and penetratin. However, MAP is also the most potent inducer of membrane leakage, whereas TP also causes leakage at higher concentrations, but not at concentrations sufficient for cellular uptake and cargo delivery.[221] On the other hand,

[214] J. B. Rothbard, S. Garlington, Q. Lin, T. Kirschberg, E. Kreider, P. L. McGrane, P. A. Wender, P. A. Khavari, *Nat. Med.* **2000**, *6*, 1253–1257.
[215] J. Oehlke, A. Scheller, B. Wiesner, E. Krause, M. Beyermann, E. Klauschenz, M. Melzig, M. Bienert, *BBA - Biomembr.* **1998**, *1414*, 127–139.
[216] D. Derossi, A. H. Joliot, G. Chassaing, A. Prochiantz, *J. Biol. Chem.* **1994**, *269*, 10444–10450.
[217] M. Pooga, M. Hällbrink, M. Zorko, U. Langel, *FASEB* **1998**, *12*, 67–77.
[218] G. Elliott, P. O'Hare, *Cell* **1997**, *88*, 223–233.
[219] R. B. Sekar, A. Periasamy, *J. Cell Biol.* **2003**, *160*, 629–633.
[220] M. Hällbrink, A. Florén, A. Elmquist, M. Pooga, T. Bartfai, Ü. Langel, *BBA Biomembr.* **2001**, *1515*, 101–109.
[221] J. Mueller, I. Kretzschmar, R. Volkmer, P. Boisguerin, *Bioconjug. Chem.* **2008**, *19*, 2363–2374.

there are indications that TP can cause unwanted side effects in biological systems, for which Tat-derivatives result as the most interesting, safe and effective CPPs.[222]

1.1.3 Mechanism of CPP induced cell uptake

Even though the use of CPPs as delivery vectors is now a widely accepted phenomenon, the pathways that CPPs use for cell entry are still subject to debate. The cell uptake mechanism of a specific CPP is influenced by the properties of the CPP (length, charge distribution, etc.), the physiochemical properties of the cargo molecule and the cell type.[221] Based on various experiments that indicate that CPP uptake is unaffected when inhibiting endocytosis (by depletion of the ATP pool and incubation at 4°C),[223] it was proposed that a direct penetration (Figure 91a) of the plasma membrane is in general more likely than an endocytotic pathway.[211,216] However, direct penetration and crack formations in the membrane cannot explain the delivery of large complexes, and are difficult to reconcile with the low cytotoxicity of most CPPs. A proposed non-endocytotic internalization mechanism that has received more attention is the inverted micelle mediated model (Figure 91c), suggested for the uptake of e.g. penetratin.[224] But although this model may explain the translocation of some amphipathic peptides, others like Tat and polyarginines, lacking hydrophobic amino acids, are most likely taken up through other mechanisms. Furthermore, even though the fact that internalization does not involve endocytosis was first generally accepted, it is currently in doubt and an increasing number of studies are showing results in favour of the endocytotic uptake of CPPs (Figure 91b).[225]

---

222 S. El-Andaloussi, T. Holm, U. Langel, *Curr. Pharm. Des.* **2005**, *11*, 3597–3611.

223 U. Langel, *Cell-Penetrating Peptides: Processes and Applications, 1st Edition*, CRC Press, Boca Raton, **2002**.

224 D. Derossi, S. Calvet, A. Trembleau, A. Brunissen, G. Chassaing, A. Prochiantz, *J. Biol. Chem.* **1996**, *271*, 18188–18193.

225 a] J. P. Richard, K. Melikov, E. Vives, C. Ramos, B. Verbeure, M. J. Gait, L. V. Chernomordik, B. Lebleu, *J. Biol. Chem.* **2003**, *278*, 585–590; b) M. Lundberg, S. Wikström, M. Johansson, *Mol. Ther.* **2003**, *8*, 143–150; c] A. Ferrari, V. Pellegrini, C. Arcangeli, A. Fittipaldi, M. Giacca, F. Beltram, *Mol. Ther.* **2003**, *8*, 284–294; d) G. Drin, S. Cottin, E. Blanc, A. R. Rees, J. Temsamani, *J. Biol. Chem.* **2003**, *278*, 31192–31201.

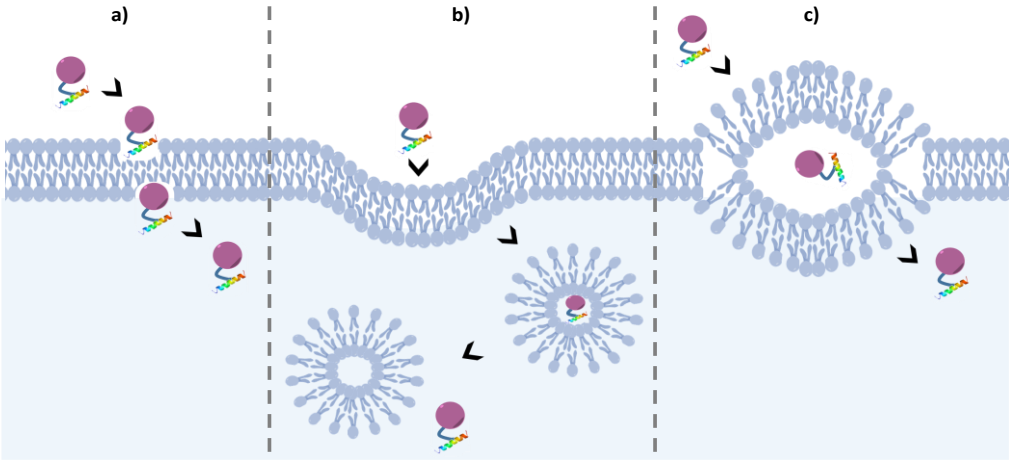

Figure 91. Proposed internalization mechanisms for CPPs and CPP-cargo complexes. a) Direct penetration, b) endocytosis and c) the inverted micelle model.

The Tat-based CPPs are the most extensively studied delivery vectors for different bioactive cargos, and the mechanism for their delivery, and for most CPPs, is now considered to be mediated through temperature dependent endocytosis. However, there are conflicting reports concerning what type of endocytosis is involved: a caveolae-mediated endocytosis,[225c,226] clathrin-mediated endocytosis,[227] or macropinocytosis[228]. In any case, after internalization through endocytosis, the CPP-cargo complexes end up inside endocytic vesicles, allowing for endosomal-lysosomal cargo delivery. If the target of the delivered molecule is outside of the vesicles, it must be able to escape into the cytosol to reach its target.[229]

Even though the exact uptake mechanism of CPPs is still unclear and subject to debate, they have been proven useful in the delivery of many otherwise impermeable, large and hydrophobic macromolecules across plasma membranes, inducing a variety of biological responses independently on the uptake mechanisms.

1.1.4 Photosensitizer-CPP biohybrids

Most existing PS-CPP conjugates described in literature are based on Pors, although some other PS such as two Pcs and a chlorin have also been used. As for the CPP, while there literally exist thousands of different sequences, and possibilities are endless, Tat-derivatives are by far the most popular ones. They are often used by itself or in

---

226 A. Fittipaldi, A. Ferrari, M. Zoppé, C. Arcangeli, V. Pellegrini, F. Beltram, M. Giacca, *J. Biol. Chem.* **2003**, *278*, 34141–34149.

227 P. Säälik, A. Elmquist, M. Hansen, K. Padari, K. Saar, K. Viht, U. Langel, M. Pooga, *Bioconjug. Chem.* **2004**, *15*, 1246–1253.

228 J. S. Wadia, R. V. Stan, S. F. Dowdy, *Nat. Med.* **2004**, *10*, 310–315.

229 E. Koren, V. P. Torchilin, *Trends Mol. Med.* **2012**, *18*, 385–393.

combination with nuclear localizing sequences (NLS), another type of CPP. As expected, most of these conjugates have been applied for PDT applications. Some research groups however have taken benefit of the multiply charged conjugates and have tested them also for PDI applications, with successful outcomes.

Pioneers in the field are Vicente and co-workers, synthesizing and publishing several papers on Por-CPP conjugates early on. First, and based on the fact that most CPP sequences consist mainly of cationic amino acids (such as Lys or Arg), they synthesized a series of Por conjugates containing one to four Lys or Arg residues and investigated their cell uptake.[230] Although the photodynamic efficacy of these conjugates has not been demonstrated, all conjugates showed low dark cytotoxicity and localized mainly in cellular vesicles and lysosomes, the extent of cellular uptake depending significantly on the nature, number and sequence of amino acid residues. As a continuation of this work, they later published the first Por-CPP conjugates using NLS SV40 or the fusogenic peptides HIV-1 Tat (40-60) and octa-Arg.[231] Tat (40-60) and octa-Arg were the most effective in delivering the conjugates to the cells, while subcellular distribution of the conjugates was found to be dependent on the nature of substituents on the Por macrocycle. In an effort to improve this design, they later published a series of Por-CPP conjugates containing a linear bifunctional sequence containing both a CPP and a NLS.[232] Since this approach resulted in improved cell uptake, they continued in this line by synthesizing another series of Por-CPP conjugates bearing bifunctional CPP-NLS or NLS-CPP sequences (Figure 92).[233] Again, the conjugates containing Tat-derivatives were the most promising ones, showing the lowest dark cytotoxicity and highest phototoxicity. *In vivo*, the conjugates accumulated in tumor cells to a higher extent than Hp, which lead to very promising PDT results in the treatment of prostate cancer cells.

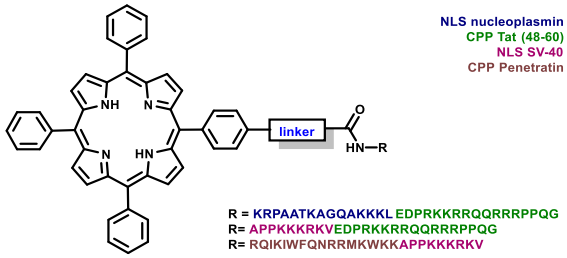

Figure 92. Por-CPP conjugates synthesized by Vicente *et al.*, containing bifunctional CPP-NLS or NLS-CPP sequences.[233] The designation of the sequence is indicated by their corresponding color in the top right legend.

[230] M. Sibrian-Vazquez, T. J. Jensen, F. R. Fronczek, R. P. Hammer, M. G. H. Vicente, *Bioconjug. Chem.* **2005**, *16*, 852–863.
[231] M. Sibrian-Vazquez, T. J. Jensen, R. P. Hammer, M. G. H. Vicente, *J. Med. Chem.* **2006**, *49*, 1364–1372.
[232] M. Sibrian-Vazquez, T. J. Jensen, M. G. H. Vicente, *J. Med. Chem.* **2008**, *51*, 2915–2923.
[233] I. Sehgal, M. Sibrian-Vazquez, M. G. H. Vicente, *J. Med. Chem.* **2008**, *51*, 6014–6020.

All conjugates by Vicente and co-workers were synthesized using the same methodology, that is solid phase synthesis of the desired peptide followed by coupling of the Por (bearing a carboxylic acid group) using standard amide coupling reagents (Figure 93). After cleavage of the conjugate from the solid phase, it was purified by reversed phase HPLC (RP-HPLC).

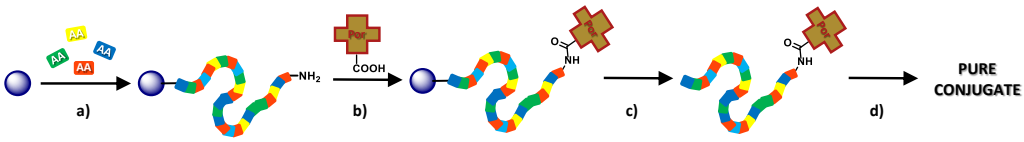

Figure 93. Synthesis of Por-peptide conjugates following the methodology used by Vicente and co-workers. a) Solid Phase Peptide Synthesis (SPPS), b) Solid phase coupling of Por-derivative, c) Cleavage of Por-peptide conjugate from the solid phase resin, d) RP-HPLC purification of Por-peptide conjugate.

Other conjugation methods not requiring solid phase coupling of the Por, which disadvantageously requires the use of a great excess of it, have been used later on. Dmitriev *et al.* made use of the isothiocyanate (NCS) functional group, which reacts with a free amino group on the peptide to form an isothiourea bond (Figure 94a).[234] This method allows for bioconjugation under soft conditions and without formation of intermediates or byproducts. Another promising method is that used by Bourré *et al.*[160] and Wang *et al.*,[235] applying the thiol-maleimide Michael addition reaction. In this methodology, maleimide-substituted PS are conjugated with peptides containing a sulfhydryl reactive group, forming a thioether bond (Figure 94b). In both conjugates, the popular Tat sequence was used as CPP. Bourré *et al.* tested the resulting conjugate as an antimicrobial agent in PDI, a well thought approach since Tat-derivatives, just like most CPP, are cationic and often amphipathic, similar to membrane-active antimicrobial peptides.[236] On the other hand, Wang *et al*. focussed on studying the process of photochemical internalization (PCI), a site-specific technique for improving the cellular delivery of macromolecular drugs. PCI efficacy was tested in combination with various small drug molecules, and a significant reduction in cell viability was measured *versus* the drug or PS treatment alone. This demonstrates that CPP-PS bioconjugation is a promising and versatile approach for enhancing the therapeutic potential of bioactive agents through PCI.

---

[234] R. I. Dmitriev, A. V. Zhdanov, G. V. Ponomarev, D. V. Yashunski, D. B. Papkovsky, *Anal. Biochem.* **2010**, *398*, 24–33.

[235] J. T.-W. Wang, F. Giuntini, I. M. Eggleston, S. G. Bown, A. J. MacRobert, *J. Controlled Release* **2012**, *157*, 305–313.

[236] F. Liu, A. Soh Yan Ni, Y. Lim, H. Mohanram, S. Bhattacharjya, B. Xing, *Bioconjug. Chem.* **2012**, *23*, 1639–1647.

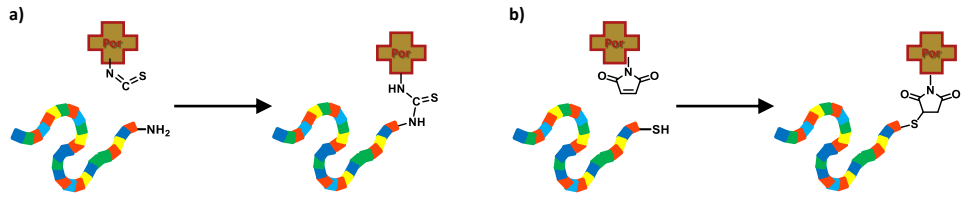

Figure 94. Por-peptide conjugation using a) isothiocyanate functional groups and b) maleimide functional groups.

More recently, Li *et al.* have synthesized a Por-CPP conjugate containing a proteinase-sensitive CPP for tumor targeted PDT, taking the use of CPPs as delivery agents to the next level (Figure 95).[237] The CPP R_9GPLGLAGE$_8$ consists of a polycationic polyarginine (R_9) sequence linked to a polyanionic polyglutamic acid sequence (E_8) by a proteinase-sensitive linker (GPLGLAG). In normal tissues, the cell-penetrating function of polycationic CPP (R_9) is blocked by the presence of the polyanionic peptide (E_8) through intramolecular electrostatic attraction. Once exposed to the proteinases present at the tumor site, proteolysis of the oligopeptide linker (GPLGLAG) between the CPP and the polyanionic peptide dissociates the inhibitory polyanions and releases the CPP-Por conjugate for PDT.

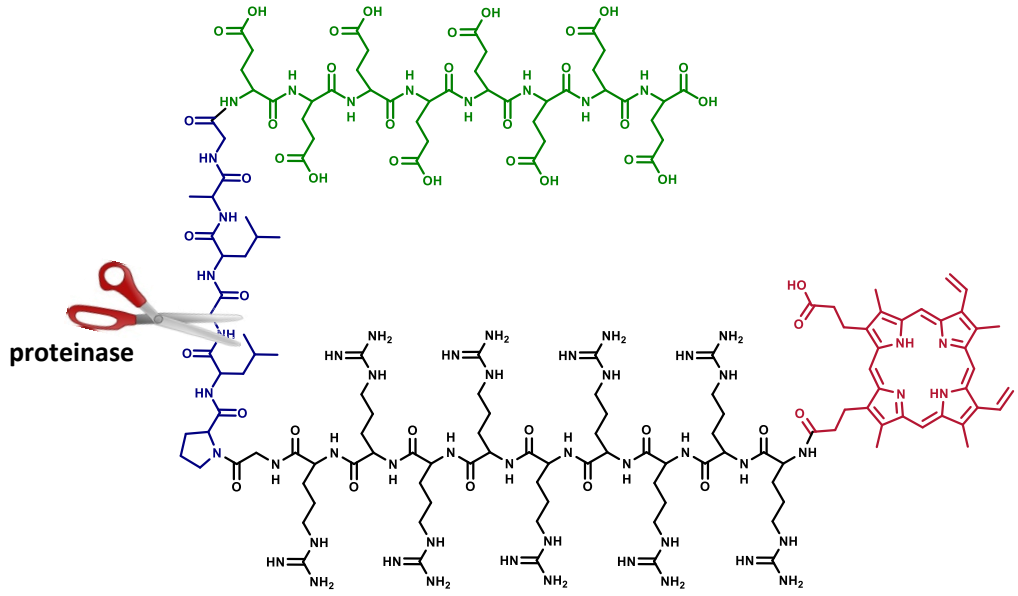

Figure 95. Por conjugated to a CPP by Li *et al.*[237] The CPP consists of a polycationic polyarginine sequence (black) linked to a polyanionic polyglutamic acid sequence (green) by a proteinase-sensitive linker GPLGLAG (blue).

[237] S.-Y. Li, H. Cheng, W.-X. Qiu, L.-H. Liu, S. Chen, Y. Hu, B.-R. Xie, B. Li, X.-Z. Zhang, *ACS Appl. Mater. Interfaces* **2015**, *7*, 28319–28329.

Apart from Pors, CPPs have been successfully conjugated to other dyes and $^1O_2$ generators such as a chlorin,[238] carboxytetramethylrhodamine,[239] and a whole series of strongly fluorescent dyes investigated by Ohtsuki *et al*.[240] With Pcs, only a couple of examples have been described. In the first case, Vicente and co-workers conjugated a bifunctional peptide, consisting of a bipartite NLS nucleoplasmin and a Tat(48-60) peptide, to a zinc phthalocyanine (ZnPc) (Figure 96).[241] The resulting conjugates were highly phototoxic and showed increased cellular uptake, once more proving the concept of using CPP as delivery vector. Just like for most PS-CPP conjugates, they were found to preferentially localize within the cell lysosomes.

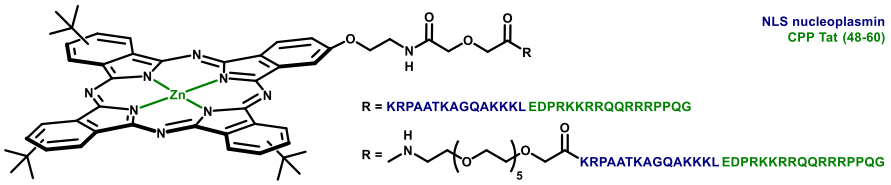

Figure 96. An example of two Pc-CPP conjugate synthesized by Vicente *et al*.[241]

In the second case, published by Yaghini *et al.*, stable nanocomposites of Tat-conjugated quantum dots with disulfonated aluminium Pcs (AlPcs) were formed in aqueous solution and in human breast cancer cells.[242] In cells, the Tat-conjugated quantum dots localize in lysosomes and, upon excitation of the quantum dots, a FRET transfer to the AlPc was observed, resulting in a FRET-induced release of quantum dots from endo/lysosomes. This was attributed to photooxidative damage to the endo/lysosomal membranes mediated by the Pc FRET acceptor.

---

238 Y. Choi, J. R. McCarthy, R. Weissleder, C.-H. Tung, *ChemMedChem* **2006**, *1*, 458–463.

239 D. Srinivasan, N. Muthukrishnan, G. A. Johnson, A. Erazo-Oliveras, J. Lim, E. E. Simanek, J.-P. Pellois, *PloS One* **2011**, *6*, e17732.

240 T. Ohtsuki, S. Miki, S. Kobayashi, T. Haraguchi, E. Nakata, K. Hirakawa, K. Sumita, K. Watanabe, S. Okazaki, *Sci. Rep.* **2015**, *5*, 18577.

241 M. Sibrian-Vazquez, J. Ortiz, I. V. Nesterova, F. Fernandez-Lazaro, A. Sastre-Santos, S. A. Soper, M. G. H. Vicente, *Bioconjug. Chem.* **2007**, *18*, 410–420.

242 E. Yaghini, F. Giuntini, I. M. Eggleston, K. Suhling, A. M. Seifalian, A. J. MacRobert, *Small* **2014**, *10*, 782–792.

1.2 Molecular design, synthesis and characterization of SiPc-CPP and SubPc-CPP biohybrids

From the above paragraph describing the state of the art about PS-CPP conjugates, two conclusions can be drawn. First, in every single example of PS-CPP conjugates already published, the conjugation of the PS to a CPP greatly enhanced its cellular uptake and consequently its photodynamic efficacy. Another promising feature of the conjugates is that none of them showed significant dark cytotoxicity, making them ideal candidates for PDT or PDI treatments. Second, despite the very encouraging results shown above, only few groups have entered in this field and relatively few PS-CPP conjugates have been reported. The specific objective of this subchapter is therefore the synthesis, characterization and *in vitro* evaluation of two new PS-CPP conjugates, more specifically a SiPc-CPP and a SubPc-CPP conjugate (Figure 97). SiPcs are, among Pcs, one of the best candidates for their use as in PS in PDT, and although two Pc-CPP conjugates have been reported, none of these was based on SiPcs. As an additional advantage, SiPcs display two axial positions available for functionalization, for which it is possible to incorporate up to two CPPs, through conjugation with linkers incorporated at the axial positions to this end. For SubPcs, there are no antecedents in literature of conjugation to CPP at all. However, SubPcs display very beneficial PS characteristics in solution, such as high quantum yields and triplet lifetimes (see introduction). Nevertheless, *in vitro* studies of SubPcs in PDT or PDI remain very rare. Furthermore, just like SiPcs, SubPcs allow functionalization at their axial position, which also makes them ideal candidates for conjugation to site specific delivery agents. Importantly, using primary alcohol type linkers, one single linker can be used for incorporation in both SiPcs and the SubPcs, making the synthesis of both conjugates very convergent.

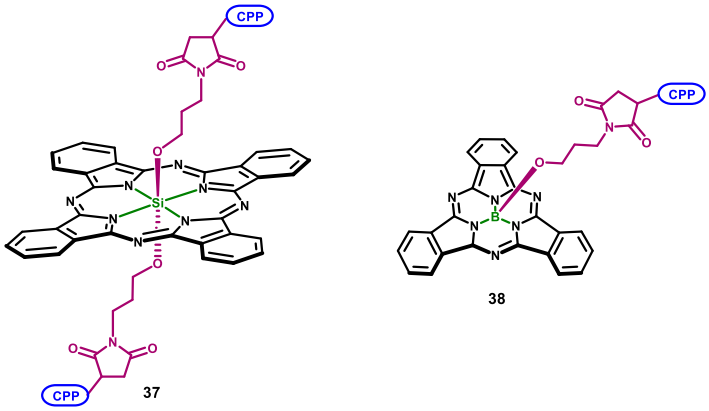

Figure 97. Molecular structure of the target biohybrid PS-CPP conjugates **37** and **38**, based on a SiPc and a SubPc as PS, respectively.

From the state of the art displayed above, it remains clear that the most used CPPs are Tat derivatives. Furthermore, in various cases where more than one CPP was tested, the Tat

sequence was almost always the most effective one, the resulting biohybrid conjugates showing low dark cytotoxicity and high phototoxicity. With this in mind, a 14 amino acid Tat variant (**39**), with sequence GRKKRRQRRRGYKC (from N to C) (Figure 98), was ordered from Biomatik©, a USA-based product and service provider in life sciences and drug discovery. The peptide was assembled on a Rink Amide resin, cleaved of and completely deprotected. A Cys residue was added at the amidated C-terminus of the peptide for easy and straightforward conjugation with the SubPc and SiPc precursors, containing the complementary maleimide functionality.

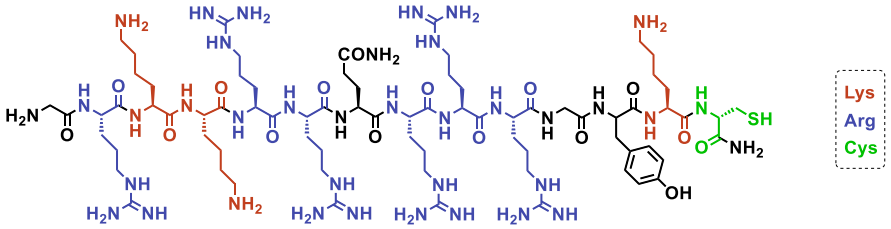

39

Figure 98. Chemical structure of CPP **39**, with sequence GRKKRRQRRRGYKC, a close variant of the Tat sequence.

As can be seen in Figure 98, the peptide contains multiple arginine (blue) and lysine (red) residues, which are fundamental for achieving the desired cell uptake. Furthermore, studies have highlighted the importance of arginines over lysines, since the guanidinium group of arginine seems pivotal for efficient cell uptake.[243]

1.2.1 Synthesis of maleimide-containing silicon phthalocyanine and subphthalocyanine

For the linkage of the SiPc and SubPc cores to the Tat CPP, it has been chosen to make use of the maleimide-thiol type 'click' reaction for various reasons. Desirably, solid phase synthesis is avoided, since large excesses of valuable PS are required. Amide formation, the most widespread conjugation strategy, on the other hand, would require either an amine or a carboxylic acid functionality in the primary alcohol linker, which would greatly complicate its incorporation into the SiPc and SubPc. Furthermore, amide conjugation should be avoided as most peptides contain several NH_2 and COOH groups, which can result in the formation of multiply conjugated products. Using a maleimide

[243] a] P. A. Wender, D. J. Mitchell, K. Pattabiraman, E. T. Pelkey, L. Steinman, J. B. Rothbard, *Proc. Natl. Acad. Sci.* **2000**, *97*, 13003–13008; b) D. J. Mitchell, D. T. Kim, L. Steinman, C. G. Fathman, J. B. Rothbard, *J. Pept. Res.* **2000**, *56*, 318–325.

functionality in the linker, to target a cysteine residue in the CPP, allows circumventing these problems.

Thiol-ene reactions are well-established in peptide synthesis, exploiting the naturally present thiol groups of cysteine-containing peptides. Although thiols can be reacted with a variety of electrophiles, such as isocyanates and epoxides, the nucleophilic Michael addition taking place between a thiol and a maleimide is one of the fastest conjugation reactions and it is therefore also the most popular one.[244] Furthermore, it results in stable thio-ether bonds when aliphatic thiols are used as the nucleophile.

Our synthesis of the axial maleimide-containing linker is based on a peripheral linker used by Liu *et al.*,[236] but using a primary alcohol for incorporation into the SiPc or SubPc (Scheme 25) instead of a primary amine for conjugation with the carboxylic acid functionality of protoporphyrin IX.

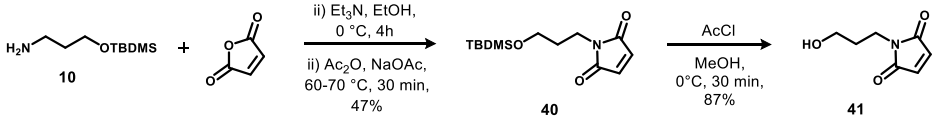

Scheme 25. Synthesis of the maleimide-containing building block for axial substitution.

Maleic anhydride, commercially available,[245] is an ideal stating product if one wants to make use of the maleimide-thiol type click reactions. It can be easily reacted with a primary amine, such as in this case 3-aminopropyl (tert-butyl)dimethylsilyl ether (**10**), synthesized in Chapter 1, to yield the protected precursor **40**. Special caution should be taken during its deprotection and the work-up of the final product (**41**), since the unprotected alcohol can react with the maleimide, resulting in a polymerization reaction. For deprotection of the (tert-butyl)dimethylsilyl group, a catalytic amount of acetyl chloride was added to a mixture of **40** in anhydrous methanol at 0°C, and the reaction was followed by TLC. Upon completion of the reaction, the solvent was evaporated at low pressure without heating of the rotary evaporator bath, to avoid the aforementioned polymerization problems. Furthermore, the incorporation of **41** into the SiPc and SubPc cores must be performed immediately after the isolation **41**, since conservation of this compound, even at -18°C under argon atmosphere, provokes a decrease in purity.

For axial SiPc substitution with **41**, the same conditions as those used in Chapter 1 were first tested (Entry 1 - Table 15). However, the yield was very disappointing, for which various other conditions and reaction times were tested (Entries 2-5 - Table 15). Notably, when trying to dissolve **41** in the reaction mixture prior to adding the $SiPcCl_2$, the yield dropped even further. This can probably be explained by polymerization of **41**. By using

[244] L.-T. T. Nguyen, M. T. Gokmen, F. E. D. Prez, *Polym. Chem.* **2013**, *4*, 5527–5536.

[245] "Maleic anhydride puriss., ≥99.0%," can be found under http://www.sigmaaldrich.com/catalog/, **2016**.

more sterically hindered bases, the yield could be significantly increased from pyridine to Et_3N and DIPEA. Finally, the reaction of $SiPcCl_2$ with 5 equivalents of **41** in anhydrous toluene, with DIPEA as base, resulted in the desired product **42** with an acceptable 51% yield (Scheme 26).

Table 15. Various reaction conditions tested for the reaction of **41** with $SiPcCl_2$.

Entry	Solvent[a]	Base[a]	Reaction time	Yield
1	Toluene	Pyridine	18h[b]	4%
2	Toluene	Pyridine	5h[b]	3%
3	Toluene	Pyridine	18h[c]	0.5%
4	Toluene	Et_3N	18h[b]	18%
5	Toluene	DIPEA	18h[b]	51%

[a] Anhydrous. [b] Standard procedure. [c] Preheating **41** in toluene/pyridine, in order to overcome solubility problems.

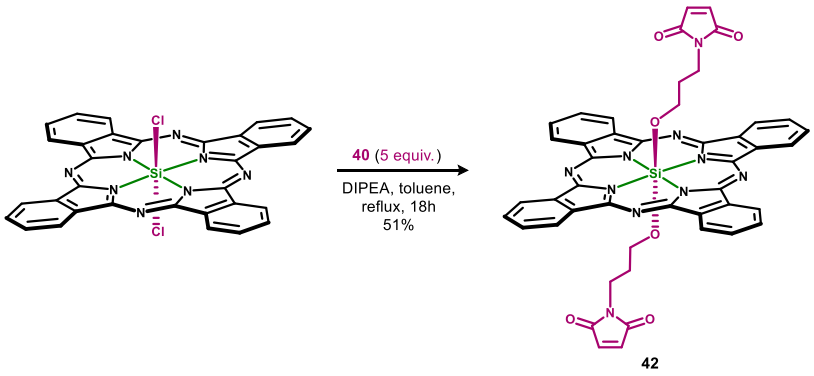

Scheme 26. Incorporation of the axial maleimide-containing linker into the SiPc structure.

Similarly, **41** was reacted with the SubPcCl **16**, under the same conditions for axial substitution as those employed in Chapter 1. This process gave rise to the final product **43** with 38% yield (Scheme 27).

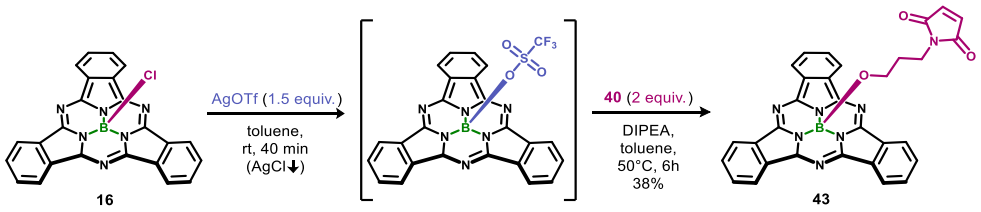

Scheme 27. Incorporation of the axial maleimide-containing linker into the SubPcCl **16** structure.

1.2.2 Synthesis and characterization of the PS-CPP biohybrids

The synthesis of the PS-CPP biohybrid conjugates has been performed during a predoctoral stay in the research group of Prof. Annemieke Madder at the Laboratory for Organic and Biomimetic Chemistry of the University of Ghent (Belgium), in collaboration with Eva Marina Llamas Garcinuño.

For the conjugation of the SiPc **42** and the SubPc **43** with the **39**, a procedure adopted from that used by Bourré *et al.* was followed.[161] In general, the thiol is deprotonated by a tertiary amine catalyst, in this case pyridine, resulting in the formation of a strongly nucleophilic thiolate anion (Figure 99). The anion adds to the double bound of the maleimide, generating an enolate intermediate with a delocalized negative charge. In the last step, the proton is subtracted again from the amine catalyst, resulting in a stable thio-ether adduct.

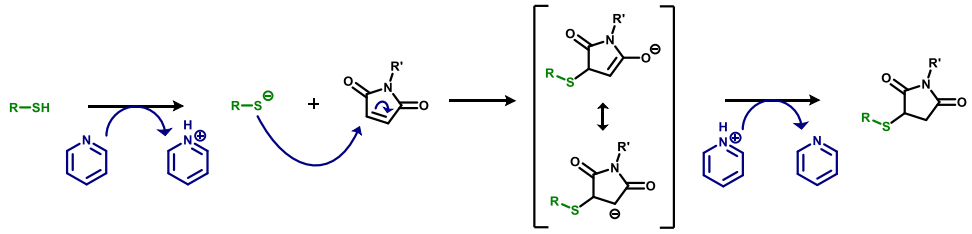

Figure 99. General mechanism of the thiol-maleimide reaction, catalyzed by a tertiary amine (in this case pyridine), with the formation of a thio-ether bond.

Since the conjugation of the SubPc **43** with **39** implies the incorporation of one single peptide, in comparison to two in the case of the SiPc **42**, it represents an easier scenario. For this reason, we decided to explore it prior to tackling the double conjugation of the SiPc **42**.

1.2.2.1 SubPc-CPP conjugate 38

For the conjugation of SubPc **43** with the CPP, both the SubPc and the peptide were dissolved in a small quantity of DMSO. Pyridine was added to the SubPc solution, after which both solutions were mixed, shielded from light, and allowed to stand overnight at rt (Scheme 28). Since **39** is the most costly starting product, a 3 equiv. excess of SubPc **43** was used.

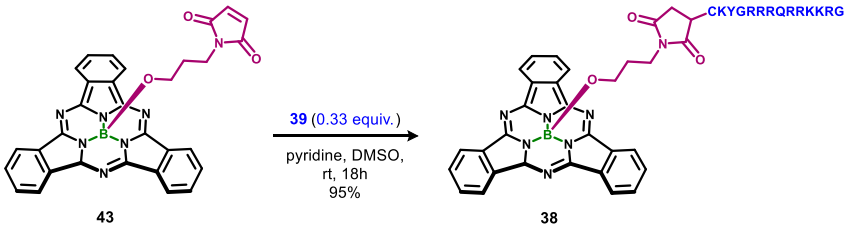

Scheme 28. Synthesis of the SubPc-CPP conjugate **38**.

After reaction, the mixture was partitioned between ethyl acetate and deionised 0.1% aqueous TFA. The non-conjugated free SubPc **43** remained in the organic phase, while the conjugate **37**, which is water soluble, remained in the water phase, together with any non-conjugated peptide. The aqueous layer was then evaporated to a small volume, and applied to a Discovery DSC-18 solid phase extraction cartridge, from which the conjugate was eluted with a gradient (from 5% acetonitrile 0.1% aq. TFA to 20% acetonitrile 0.1% aq. TFA) mobile phase. Finally, the conjugate was lyophilised to give the pure conjugated product **38** in a 95% yield.

The reaction and purification were also followed by RP-HPLC, using a gradient of 0.1% TFA in water and 0.1% TFA in acetonitrile, from 0 to 100%, over 25 min. UV-Vis detection was performed at 214, 254, 280 and 560 nm. The first three wavelengths are used standardly when eluting peptides, visualizing the peptide bond (214 nm) and some aromatic residues such as tyrosine, tryptophan and phenylalanine (254 and 280 nm).[246] The fourth wavelength, hv = 560 nm, coincides with the Q-band of the SubPc and was chosen to visualize the elution of the SubPc-CPP conjugate **38**. Peptides do not absorb at this wavelength. The resulting chromatograms of the peptide, the crude aqueous phase and the DSC-18 purified conjugate **38** can be seen in Figure 100a-c, respectively.

[246] M.-I. Aguilar, *HPLC of Peptides and Proteins: Methods and Protocols*, © Humana Press Inc., **2004**.

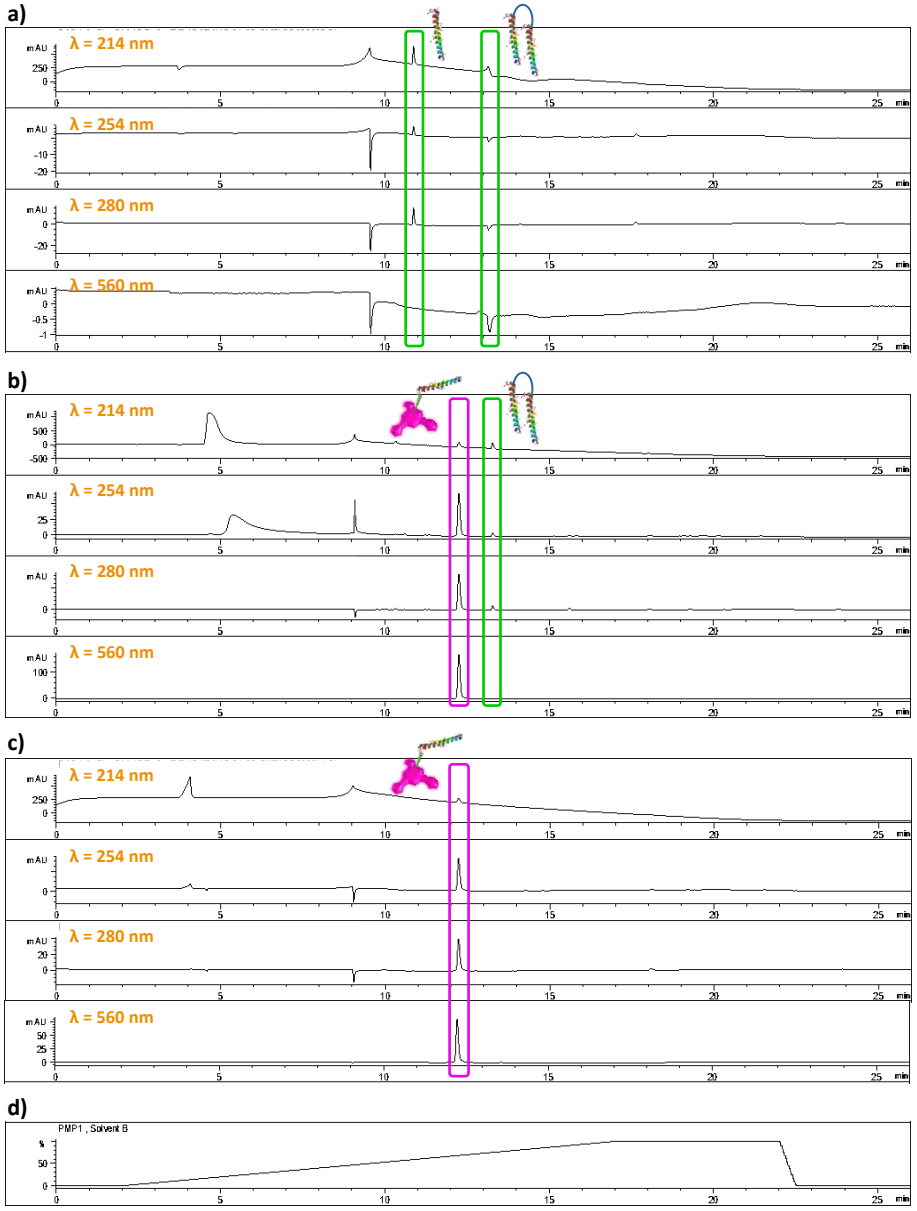

Figure 100. RP-HPLC chromatograms of a) **39**, b) the crude aqueous phase, c) the DSC-18 purified conjugate **38**, and d) the solvent mixture used to elute the compounds, consisting of 0.1% TFA in water (Solvent A) and 0.1% TFA in acetonitrile (Solvent B) with a gradient from 0 to 100%B in 25 min. The elution of all compounds is followed at hv = 214, 254, 280 and 560 nm.

In the chromatogram of **39** (Figure 100a) two peaks can be observed, one at retention time t_r=10,8 min, which is the peptide, and an impurity at t_r=13,2 min. The second peak could probably be the result of dimerization of the peptide, since its free sulfhydryl group could react with that of a second peptide, forming a disulfide bridge between two peptide

moieties. The formation of SubPc-CPP conjugate **38** can clearly be detected in the chromatogram of the aqueous phase obtained by extraction of the crude reaction mixture (Figure 100b), since a new elution peak appears at t_r=12,2 min and absorbs both at the typical peptide wavelengths (i.e. 214, 254 and 280 nm) and at 560 nm, the wavelength of maximal absorption of the SubPc. As desired, no unbound peptide was detected, as a three-fold excess of SubPc **43** was used in order to fully consume the peptide. Notably, the impurity at t_r=13,2 min also present in the chromatogram of the peptide, confirms it could be the peptide dimer, which has no longer a free sulfhydryl group to bind to the SubPc **43**. Finally, in the chromatogram of the DSC-18 purified conjugate **38** (Figure 100c) it is clear that the conjugate is now completely pure.

The mass of conjugate **38** could be confirmed by MALDI-TOF spectrometry (Figure 101), detecting the molecular ion $[M]^+$ as the most intense peak. Besides, two fragments that can from by fragmentation of the molecular ion (i.e. F1 and F2, Figure 102) were also detected.

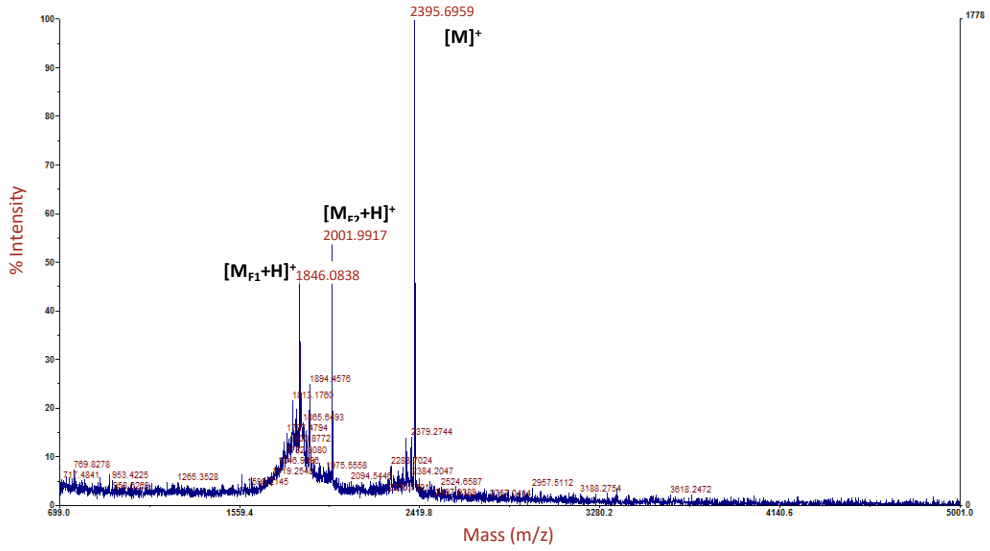

Figure 101. MALDI-TOF spectrum of DSC-18 purified conjugate **38**.

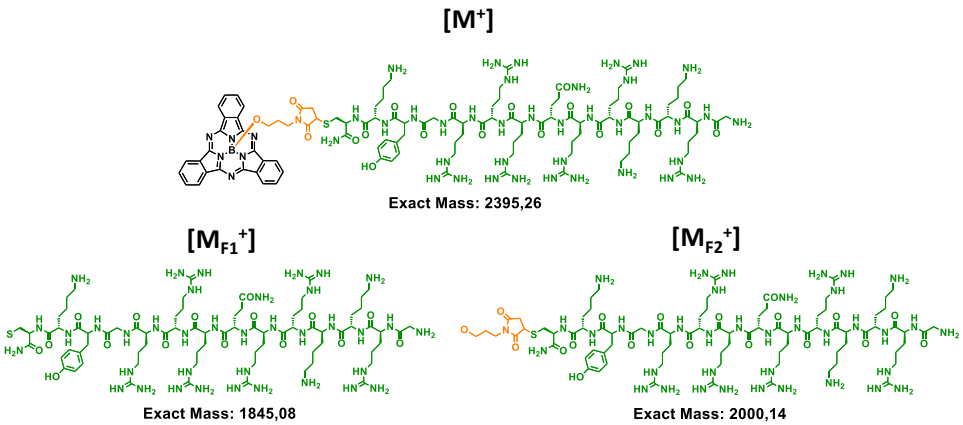

Figure 102. Structural formula and molecular mass corresponding to the molecular ion and its fragments F1 and F2, detected in MALDI-TOF spectrum, of the conjugate **38**.

1.2.2.2 SiPc-CPP conjugate 37

After the successful synthesis of the SubPc-CPP conjugate, the double conjugation of the **39** to SiPc **42** was attempted. In this case, the peptide cannot be used as the limiting reagent, since this would result in a mixture of mono- and di-substituted SiPc-CPP conjugates. Therefore, in a first trial, the same reaction conditions as before, but using a threefold excess of peptide, were tested (Scheme 29, Entry 1 - Table 16). However, due to the large excess of peptide utilized in this case, solubility problems arized and, upon reaction overnight, no conjugate was formed. The process was then repeated in a bigger amount of DMSO (Entry 2 - Table 16), obtaining a better solubility of the starting products.

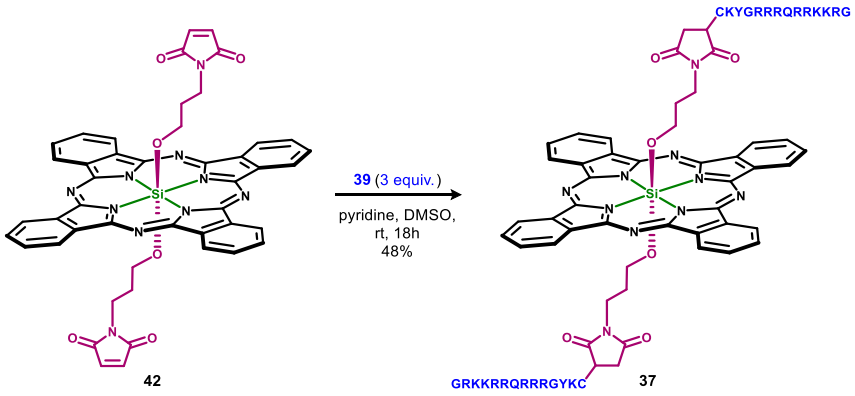

Scheme 29. Synthesis of the SiPc-CPP conjugate **37**.

Table 16. Reaction conditions for the double conjugation of **39** to SiPc **42.**

Entry	Solvent	42 (equiv.)	39 (equiv.)	Base	Conditions
1	DMSO (400 µL)	1	3	Pyridine	rt, overnight
2	DMSO (1000 µL)	1	3	Pyridine	rt, overnight
3	DMSO	1	3	DIPEA	40°C, overnight
4	DMF	1	3	DIPEA	rt, vortex, overnight

The same workup as for the SubPc conjugate was applied in the present case, that is partitioning the reaction mixture between ethyl acetate and deionised 0.1% aqueous TFA. Initially, the water phase turns blue, which would mean conjugation did take place and conjugate **37** is water-soluble. However, upon concentrating the water phase and applying it to a Discovery DSC-18 solid phase extraction cartridge for separation, no conjugate eluted (all blue color remained at the front of the column), even when increasing the gradient of the mobile phase from 5% acetonitrile 0.1% aq. TFA to 100% acetonitrile 0.1% aq. TFA.

The RP-HPLC chromatogram of the water phase was also recorded, using the same parameters as in the previous section but with 676 nm as the fourth wavelength of detection, coinciding with the Q-band of the SiPc, to visualize the elution of SiPc-CPP conjugates (Figure 103b). At 214 nm the formation of a new product with t_R = 18 min can be observed, indicating the formation of some kind of conjugate. However, from the chromatogram recorded at 676 nm, it is clear that some kind of decomposition has taken place, since a mixture of products eluted from t_R = 15 to 20 min.

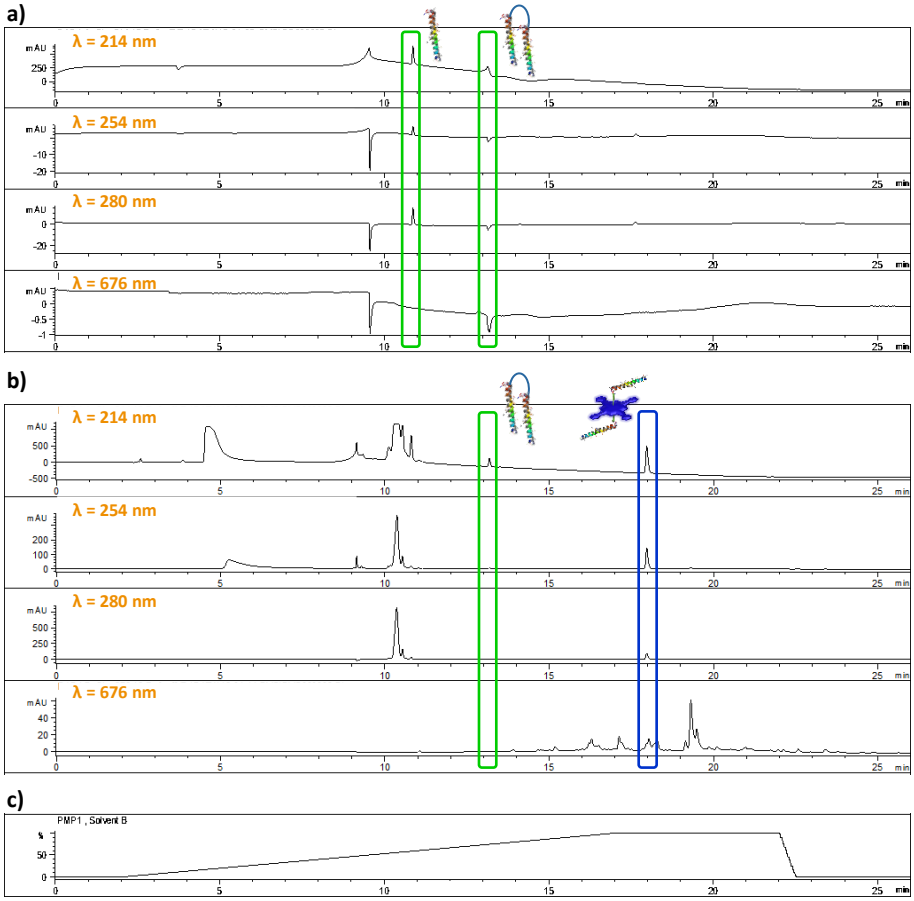

Figure 103. RP-HPLC chromatograms of a) **39**, b) the crude aqueous phase, and c) the solvent mixture used to elute the compounds, consisting of 0.1% TFA in water (Solvent A) and 0.1% TFA in acetonitrile (Solvent B) with a gradient from 0 to 100%B in 25 min. The elution of all compounds is followed at hv= 214, 254, 280 and 676 nm.

Two more reaction conditions were tested (Entries 3 and 4 - Table 16), with the same results: the water phase initially turned blue upon extraction, indicating the formation of some kind of conjugate, but its blue color faded slowly and no conjugate could be detected by RP-HPLC. Both observations indicate that if the conjugate was formed, it decomposed during the work-up and/or during the RP-HPLC measurement. With this in mind, the stability of compound **42** to acids was tested by ^{1}H-NMR spectroscopy (Figure 104), conforming that it doesn't resist even a small 0.1% proportion of TFA.

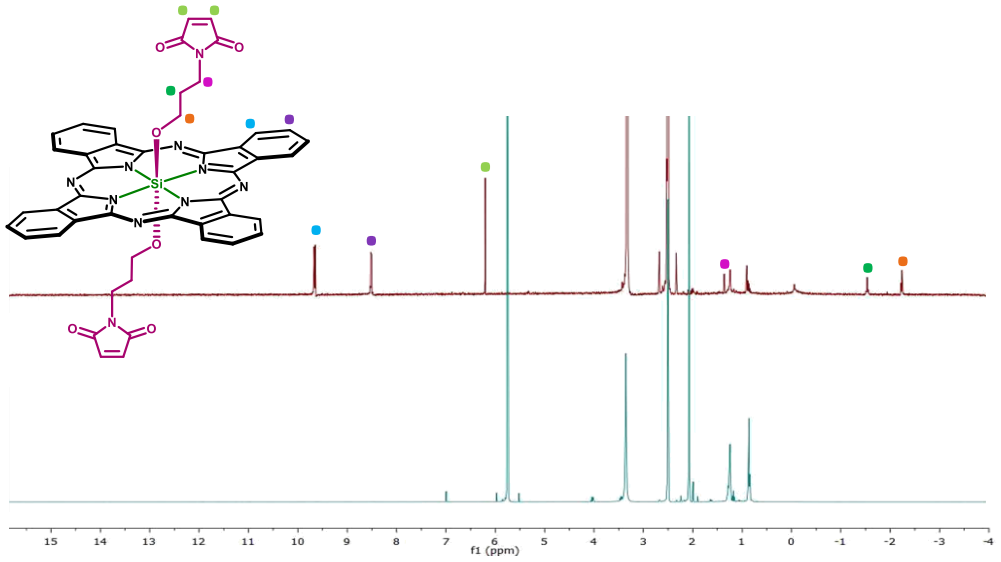

Figure 104. Stability test of compound **42** to slightly acidic (0.1% aq. TFA) conditions. Up: ^{1}H-NMR spectrum of compound **42** in DMSO-d_6. Down: ^{1}H-NMR spectrum of compound **42** after a 5 min treatment with 0.1% aq. TFA, in DMSO-d_6, clearly missing the SiPc aromatic signals.

From this experiment, it became clear that the conjugate had probably been formed in all of the previous trials, but we simply did not detect it because of instability issues. Therefore, for Entry 3 and Entry 4 (Table 15), an alternative work-up was attempted, avoiding the use of 0.1% aq. TFA. Upon reaction overnight, 10 mL of diethyl ether were added to the reaction mixture, resulting in a blue precipitate. After centrifugation, the colorless supernatant was removed and the remaining solid was dissolved in distilled water and extracted with DCM to remove any remaining unreacted SiPc **42**. After this treatment, a MALDI-TOF analysis was performed (Figure 105).

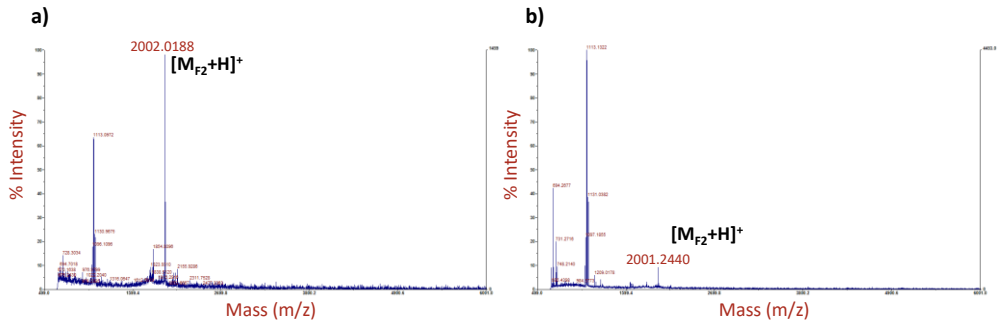

Figure 105. MALDI-TOF analysis of the crude obtained from entries a) 3 and b) 4 of Table 15.

The molecular ion of the conjugate **37** ([M$^+$] = 4540,41) was not observed, yet fragment F2 can be detected in both cases. This fragment was also present in the MALDI-TOF analysis of SubPc-CPP conjugate **38** (Figure 101), and can only exist if conjugation has

effectively taken place. This confirmed our suspicions of the instability of SiPc-CPP conjugate **37** to TFA, and the fact that most likely the molecular ion cannot be observed because of the slightly acidic matrix (α-cyano-4-hydroxycinnamic acid) that is used for the MALDI-TOF analysis.

Although the results obtained from this analysis indicate that some conjugate has been formed, they give no decisive answer about whether there exists a mixture of mono- and bi-conjugated product or only the desired compound **37**. Since an excess of peptide was used and since the thiol-maleimide Michael addition is a fast and efficient reaction,[244] it can be expected that only di-conjugated product has been formed, but this needs to be confirmed. Therefore, a final purification step was performed by SEC using Sephadex beads as the stationary phase and water as the eluent. Since the peptide is large (MW = 1846.07 g/mol), it is expected that the mono- and di-substituted products would have different elution times. However, only one product eluted, either using G10 or G15 size Sephadex beads.

In a last experiment to prove the purity of the conjugate **37**, RP-HPLC analysis was performed under the same conditions as above, but without using 0.1% TFA in the mobile phase. This is normally not done, because TFA serves as ion-pair reagent, both for the stationary phase and the peptide. Without using TFA in the mobile phase it is expected to see broad peaks, unless the column is packed with high purity silica with few metal ion impurities that could lower the resolution.[247] The obtained results can be seen in Figure 106. In the chromatogram of the peptide (Figure 106a), it can be observed that the peptide elutes together with the injection peak, because this peak, at t_R = 2 min, is a lot broader than normal. The injection peak returned to its normal shape in Figure 106b, the chromatogram of conjugate **37**, indicating there was no remaining free peptide. Furthermore, only one more product could be observed, eluting at t_R = 12.5 min. Importantly this product absorbs both at the typical peptide wavelengths (i.e. 214, 254 and 280 nm) and at 676 nm, the wavelength of maximal absorption of the SiPc, confirming this is indeed pure SiPc-CPP conjugate **37**.

[247] D. Carr, *A Guide to the Analysis and Purification of Proteins and Peptides by Reversed-Phase HPLC*, ACE® HPLC Columns, **2010**.

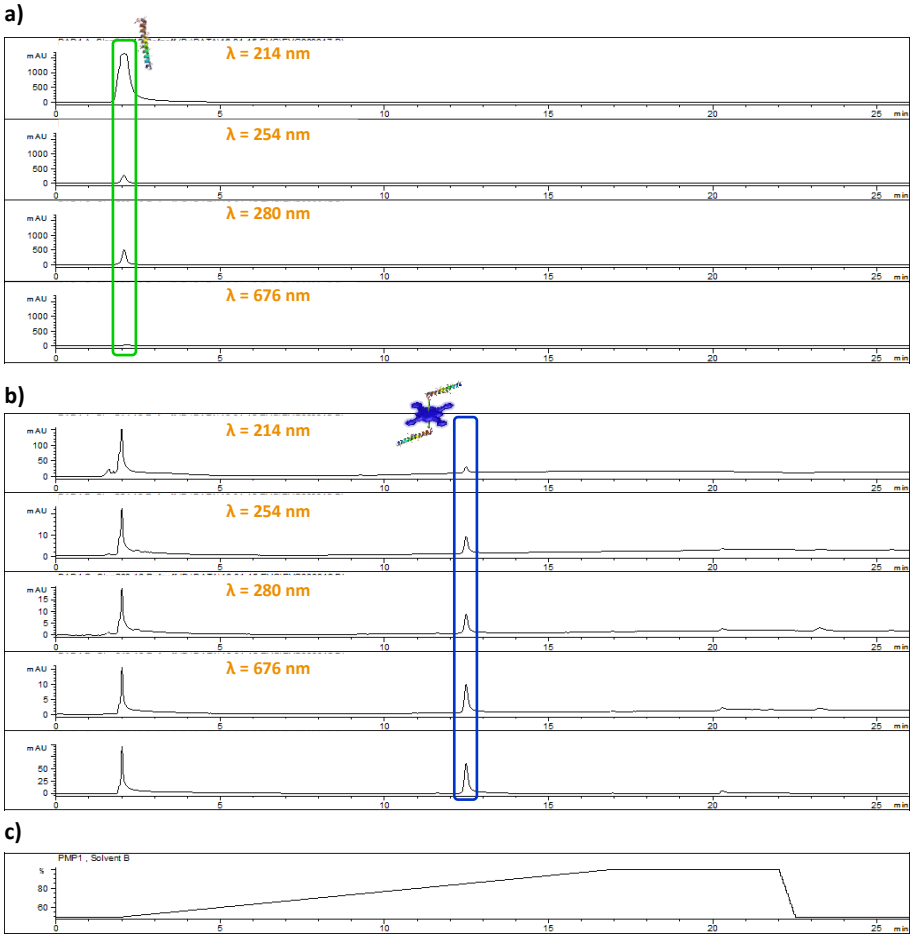

Figure 106. RP-HPLC chromatograms of a) **39**, b) the purified SiPc-CPP conjugate **37**, and c) the solvent mixture used to elute the compounds, consisting of water (Solvent A) and acetonitrile (Solvent B) with a gradient from 50 to 100%B in 25 min. The elution of all compounds is followed at hv= 214, 254, 280 and 676 nm.

1.3 Spectral features and photophysical properties

The normalized absorption spectra of conjugates **37** and **38** and their maleimide-containing precursors **42** and **43** were measured in DMF (Figure 107a – full lines). They all represent the typical spectrum of non-aggregated SiPcs (**37** and **42**) and SubPcs (**38** and **43**) and, with an intense and sharp Q-band around 562 nm and 673 nm respectively, and a broad Soret band with maxima around 300 nm and 360 nm, respectively. For the water-soluble conjugates **37** and **38**, the normalized absorption spectra were also recorded in deionised water (Figure 107a – dashed lines). In this medium, conjugates are also essentially non-aggregated. Their Q-bands show a small bathochromic shift: 10 nm for the SiPc-CPP conjugate **37** (Q-band at 683 nm) and 4 nm for the SubPc-CPP conjugate **38** (Q-band at 566 nm), with respect to their Q-bands in DMF.

The fluorescence emission spectra of all compounds are displayed in Figure 107b. Upon excitation at 520 nm, the SubPcs showed a fluorescence emission around 573 nm in DMF and 580 nm in water. In turn, the SiPcs showed, upon excitation at 610 nm, a fluorescence emission around 683 nm in DMF and 694 nm in water. ϕ_F were determined both in DMF and in water, the results being represented in Table 17 and Table 18, respectively.

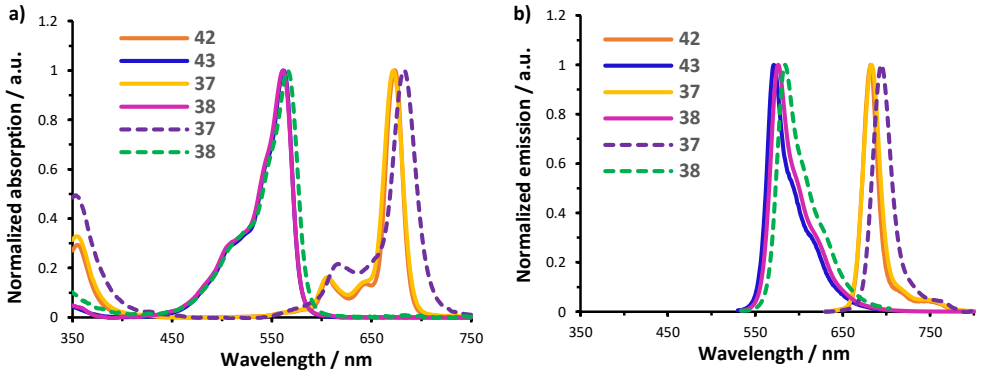

Figure 107. a) Electronic absorption and b) emission spectra of conjugates **37** and **38** and their maleimide-containing precursors **42** and **43** in DMF (full lines) and water (dashed lines).

Table 17. Electronic absorption and photophysical data for conjugates **37** and **38** and their maleimide-containing precursors **42** and **43** in DMF.

Compound	λ_{max} (nm)	λ_{em} (nm)[a]	ϕ_F (%)[a]	ϕ_Δ (%)[b]
42	674	683	34.0	34.4
43	562	571	14.4	27.6
37	671	683	33.4	38.3
38	560	576	29.7	67.6

[a] Excited at 520 nm, using F_{12}SubPcCl in benzonitrile (ϕ_Δ = 0.58) as the reference for SubPcs; Excited at 610 nm, using ZnPc in DMF as the reference (ϕ_F = 0.28) for SiPcs. [b] Using ZnPc in DMF as the reference (ϕ_Δ = 0.56).

Table 18. Electronic absorption and photophysical data for conjugates **37** and **38** in water.

Compound	λ_{max} (nm)	λ_{em} (nm)[a]	ϕ_F (%)[a]
37	682	694	9.2
38	565	580	29.9

[a] Excited at 520 nm, using F_{12}SubPcC in benzonitrile (ϕ_Δ = 0.58) as the reference for SubPcs; Excited at 610 nm, using ZnPc in DMF as the reference (ϕ_F = 0.28) for SiPcs. [b] Using ZnPc in DMF as the reference (ϕ_Δ = 0.56).

The ϕ_Δ of conjugates **37** and **38** and their maleimide-containing precursors **42** and **43** in DMF is also shown in Table 17, and was determined by the relative method based on the photoinduced decomposition of the chemical scavenger DPBF, as described in Chapter 1. On the other hand, similarly as in Chapter 2, ϕ_Δ of cationic compounds **37** and **38** could not be determined in aqueous medium. Thus, in order to examine their relative $^1O_2$ generation efficiency in physiological medium, their relative $^1O_2$ generation capacity was evaluated in PBS (Figure 108).

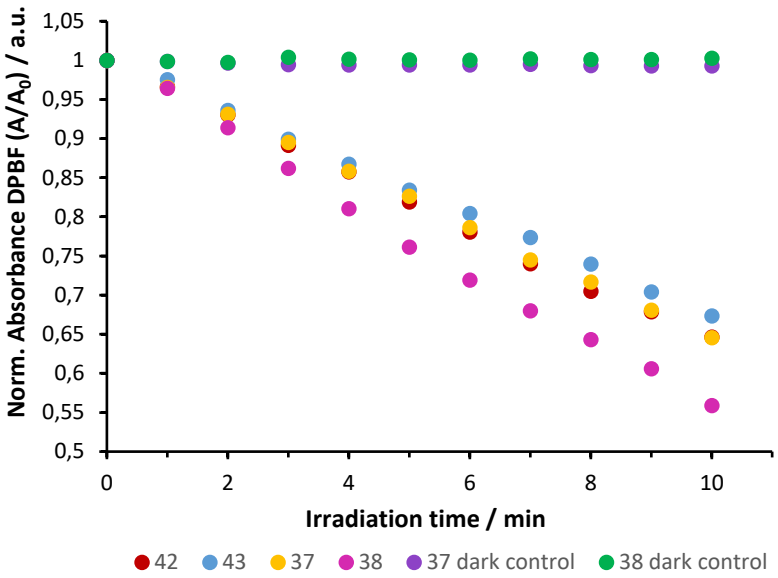

Figure 108. Decay of the absorbance of DPBF at 414 nm, sensitized by conjugates **37** and **38** and their maleimide-containing precursors **42** and **43**, in function of irradiation time (min), in PBS (0.5% Cremophor EL) buffer.

As a first observation, from the obtained data it can be seen that the results for the relative $^1O_2$ generation of all compounds in PBS buffer are in complete concordance with the ϕ_Δ obtained in DMF (Table 17). The SubPc **43** has the lowest capacity for $^1O_2$ generation, followed by SiPc **42** and SiPc-CPP conjugate **37**, which has a slightly higher quantum yield than its precursor. Surprisingly, the ϕ_Δ of SubPc-CPP conjugate **38** is more than double than that of its precursor. This trend is confirmed in the study in PBS buffer, where conjugate **38** is by far the most effective $^1O_2$ generator. Importantly, dark control experiments confirm that, under all conditions, conjugates **37** and **38** are unable to produce $^1O_2$ without $h\nu_{>455nm}$ illumination.

1.4 *In vitro* test of cellular uptake

Cell uptake experiments with the prepared PS-CPP biohybrid conjugates have been performed in collaboration with the research groups of Prof. Annemieke Madder and Prof. Bruno de Geest at the University of Ghent (Belgium), in collaboration with Eva Marina Llamas Garcinuño and Alexandra van Driessche.

The most common method to study the internalization of CPP-bearing compounds consists in quantifying their cell uptake by flow cytometry analysis and visualizing it by fluorescence microscopy. In general, fluorophore-labelled peptides are used for this reason, however in our case the PS serves as fluorophore.

1.4.1 Flow cytometry

The flow cytometry analysis to quantify cell uptake is generally performed with cells incubated in the presence of the CPP-containing compounds at both 4°C and at 37°C.[222] In theory, at 37°C both active transport (receptor-mediated, endocytosis) and passive transport (permeation) through the cell membrane can take place, whereas at low temperature endocytosis is inhibited. If any cell uptake does take place at 4°C, it almost surely has occurred through passive transport induced by the cell penetration capacity of the CPP.

For the experiment chinese hamster ovary (CHO) cells, an epithelial cell line often used in biological and medical research, were grown, counted and plated in 24-well plates with a final concentration of 15×10^4 cells in 900 µL of cell medium per well. The plates were incubated at 37°C for 24h after which half of the cells were cooled on ice for 1 hour. At that time, 100 µL of a 1 µM PBS solution of the PS-CPP biohybrid conjugates was added to the wells, both at 37°C and at 4°C. The plates were left to incubate for another 4h, again either in an incubator at 37°C or on ice, after which the cell medium was removed and a cell dissociation buffer was added to detach the cells from the well bottom. After 15 more min of incubation, the cells were transferred to Eppendorf, centrifuged to remove the cell dissociation buffer, and dissolved in PBS for injection into the flow cytometer.

Inside the flow cytometer, the flow with cells passes through a fluorescence measuring station where the light scattering and fluorescent characteristics of each cell of interest is measured, one cell at a time and up to thousands of cells per second. In this way a fast, objective and quantitative recording of fluorescent signals from individual cells in which uptake of the PS-CPP biohybrid conjugate has taken place (fluorescent) or not (non-fluorescent) are counted separately, quantifying the degree of cell uptake (Figure 109).

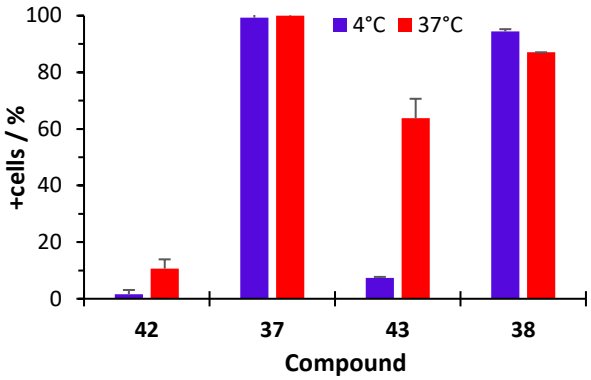

Figure 109. Cell uptake (%) of the precursor compounds **42** and **43** and CPP-PS biohybrid conjugates **37** and **38**, at 4°C and 37°C.

The results indicate that the precursor compounds containing the maleimide moiety but not the CPP (**42** and **43**) show some uptake at 37°C, but their uptake at 4°C is negligible (<10%). The CPP-containing compounds (**37** and **38**), however, show great uptake at both 37°C and 4°C. Uptake at 4°C, where no active transport such as endocytosis is possible, is higher than 90% in both cases, indicating that the CPP moieties are indeed very effective in destabilizing the cell membrane and are successfully introducing the PS inside the cells.

1.4.2 Confocal imaging

In some cases, the fluorescence signal generated in the flow cytometry experiment can be caused by cell binding of the CPP-containing compounds (due to electrostatic interactions between the cationic peptide and the negatively charged cell membrane) instead of actual cell uptake. To confirm cell uptake does take place, it is usually visualized by fluorescence microscopy.

Similarly as for the flow cytometry experiment, for the confocal imaging experiment the CHO cells were grown, counted and plated in 24-well plates, this time with a concentration of 5 x 10^3 cells in 200 µL of cell medium per well. After 24h of incubation at 37°C (with 5% CO_2) half of the cells was cooled on ice for 1h prior to adding 10 µL of a 1 µM PBS solution of the PS-CPP biohybrid conjugates to the wells, both at 37°C and at 4°C. After 4h of incubation, the cells are stained with Hoechst and Phalloidine stain for visualization of the cell nucleus and cell membrane, respectively, by fluorescence microscopy. In a first trial, however, no fluorescence signal could be observed, neither inside the cell or on the surface, due to the compounds being insufficiently fluorescent to allow for proper detection at the excitation wavelength and concentration used in this experiment. Since the excitation wavelength cannot be changed, the confocal imaging experiment will be repeated at higher concentration of PS. Furthermore, *in vitro* PDT experiments are also

planned in the near-feature, in order to assess the efficacy of conjugates **37** and **38** as PS in relation to internalization.

2

Photoantimicrobial biohybrids by supramolecular immobilization of cationic zinc phthalocyanines onto cellulose nanocrystals

2.1 State of the art

Cellulose, made up of some 1500 glucose rings chained together, belongs to the family of carbohydrates which, as mentioned in the introduction of this chapter, are suitable agents for the biological delivery of PS. Since wood consists mostly of cellulose, it is the most abundant biopolymer produced in the biosphere and, as a consequence, it has been industrially processed and consumed for nearly 150 years. In the last two decades, nanoscience has enabled the development of new high-end cellulose derivatives from renewable resources. Rod-shaped cellulose nanocrystals (CNC) have attracted growing attention due to their extraordinary mechanical properties, high aspect ratio and surface area, colloidal stability, biocompatible sugar-based chemical structure, and cheap processing as a well-defined nanomaterial.[248]

[248] a) M. Pääkkö, J. Vapaavuori, R. Silvennoinen, H. Kosonen, M. Ankerfors, T. Lindström, L.A. Berglund and O. Ikkala, *Soft Matter*, **2008**, *4*, 2492-2499. b) S.J. Eichhorn, A. Dufresne, M. Aranguren, N.E. Marcovich, J.R. Capadona, S.J. Rowan, C. Weder, W. Thielemans, M. Roman, S. Renneckar, W. Gindl, S. Veigel, J. Keckes, H. Yano, K. Abe, M. Nogi, A.N. Nakagaito, A. Mangalam, J. Simonsen, A.S. Benight, A. Bismarck, L.A. Berglund and T. Peijs, *J. Mater. Sci.*, **2010**, *45*, 1-33. c) Y. Habibi, L.A. Lucia and O.J. Rojas, *Chem. Rev.*, **2010**, *110*, 3479-3500. d) R.J. Moon, A. Martini, J. Nairn, J. Simonsen and J. Youngblood, *Chem. Soc. Rev.*, **2011,** *40*, 3941-3994. e) H. Rosilo, E. Kontturi, J. Seitsonen, E.

CNCs have been prepared since the mid-20th century, by acid hydrolysis of cellulose employing strong acids, mainly sulfuric and hydrochloric acids. In this way, the amorphous domains are broken and only the crystalline domains remain (Figure 110).[249] The hydrolysis conditions haves thereafter been optimized in order to improve the recovery yield and to tailor the CNCs dimensions.[250]

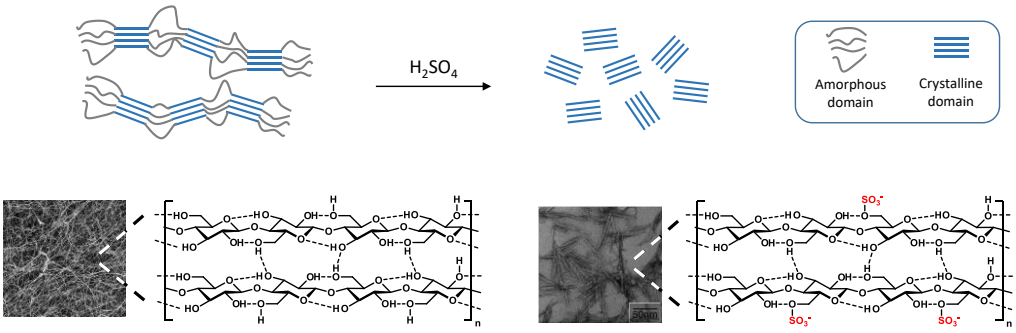

Figure 110. Preparation of CNC from cellulose by acidic hydrolysis with H_2SO_4.

The application potential of these CNCs can be significantly enhanced by surface modification, either by covalent or non-covalent approaches. The latter can be based on hydrophilic affinity, electrostatic attractions, hydrogen bonds or van der Waals forces. The non-covalent approach has mainly been exploited for the adsorption of surfactants to the cellulose surface, to improve the dispersibility of CNCs in organic solvents and hydrophobic matrices.[251] Until now, all examples of non-covalent grafting of molecules to the surface of CNC implicate a previous synthetic modification of the CNC with supramolecular or electrostatic recognition motifs,[251a,252] while the direct non-covalent modification of CNC remains unexplored. The covalent modification of CNC, on the other hand, is mainly based on the introduction of different functional groups such as allyl, thiol, alkyne, and azide functionalities, enabling "click" reactions.[251]

The grafting of CNC with PS molecules leads to photoactive biohybrids that can be used as $^1O_2$ generators for both PDT and/or PDI. Ghiladi and co-workers described the covalent modification of CNC with a cationic Por derivative, employing the Cu(I)-catalyzed Huisgen

Kolehmainen and O. Ikkala, *Biomacromolecules*, **2013**, *14*, 1547-1554. f) J.R. McKee, E.A. Appel, J. Seitsonen, E. Kontturi, O.A. Scherman and O. Ikkala, *Adv. Funct. Mater.*, **2014**, *43*, 2706-2713. g) M. Giese, L.K. Blusch, M.K. Khan and M.J. MacLachlan, *Angew. Chem. Int. Ed.*, **2015**, *54*, 2888-2910. h) A. Boujemaoui, S. Mongkhontreerat, E. Malmström and A. Carlmark, *Carbohydr. Polym.*, **2015**, *115*, 457-464.

249 B. G. Rånby, *Discuss. Faraday Soc.* **1951**, *11*, 158–164.

250 D. Bondeson, A. Mathew, K. Oksman, *Cellulose* **2006**, *13*, 171.

251 a] Y. Habibi, *Chem. Soc. Rev.* **2014**, *43*, 1519–1542; b) A. Boujemaoui, S. Mongkhontreerat, E. Malmström, A. Carlmark, *Carbohydr. Polym.* **2015**, *115*, 457–464.

252 a) S. Eyley and W. Thielemans, *Nanoscale*, **2014**, *6*, 7764-7779. b) J. Zoppe, L. Johansson and J. Seppälä, *Carbohydr. Polym.,* **2015**, *126*, 23-31.

1,3-dipolar cycloaddition (Figure 111).[253] To this end, an azide group had to be introduced onto the CNC, which could be achieved by tosylating the surface hydroxyl groups and reacting them with sodium azide. The resulting Por-CNC biohybrids showed excellent efficacy in the PDI of the Gram-positive bacteria *M. smegmatis* and *S. aureus* and the Gram-negative bacterium *A. baumannii*. Nevertheless, they were ineffective against the Gram negative *E. coli* and *P. aeruginosa* bacteria.

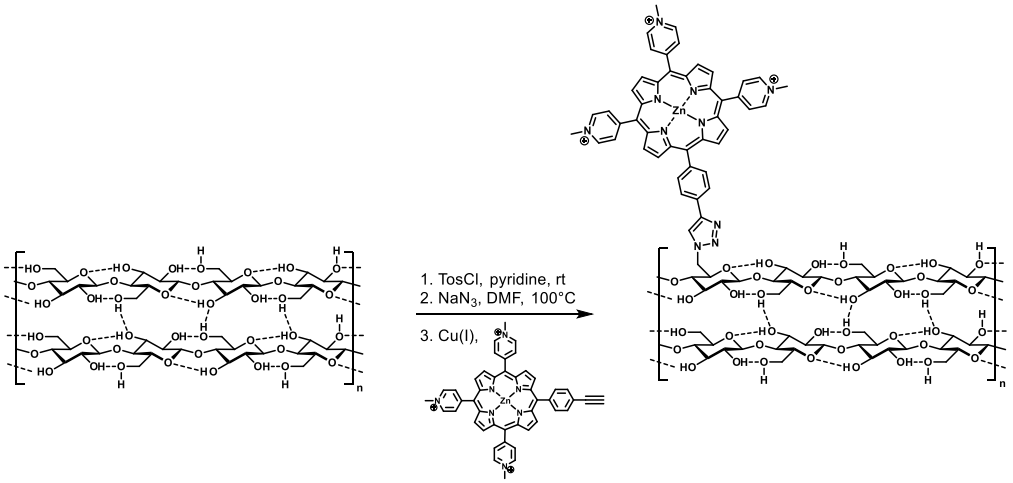

Figure 111. Covalent modification of CNC with Por molecules employing the Cu(I)-catalyzed Huisgen 1,3-dipolar cycloaddition, as published by Ghiladi and co-workers.[253]

Another PS-CNC biohybrid, based on a chlorin, was described by Sol and co-workers (Figure 112).[254] It's *in vitro* PDT efficacy was tested against a HaCat cell line displaying IC_{50} values within the nanomolar range, pointing out the possible applicability of this system. However, as with most of the previously described covalent approaches to modify CNC, the conjugation of the PS on the CNC was tedious and significantly increased production efforts and costs. The conjugation strategy consisted of first oxidizing the glucose units by sodium periodate, and then reacting the resulting carbonyl functions with the amine groups of polyethylenimine by means of reductive amination using sodium cyanoborohydride.

---

[253] a] E. Feese, H. Sadeghifar, H. S. Gracz, D. S. Argyropoulos, R. A. Ghiladi, *Biomacromolecules* **2011**, *12*, 3528–3539; b) B. L. Carpenter, E. Feese, H. Sadeghifar, D. S. Argyropoulos, R. A. Ghiladi, *Photochem. Photobiol.* **2012**, *88*, 527–536.

[254] N. Drogat, R. Granet, C. Le Morvan, G. Bégaud-Grimaud, P. Krausz, V. Sol, *Bioorg. Med. Chem. Lett.* **2012**, *22*, 3648–3652.

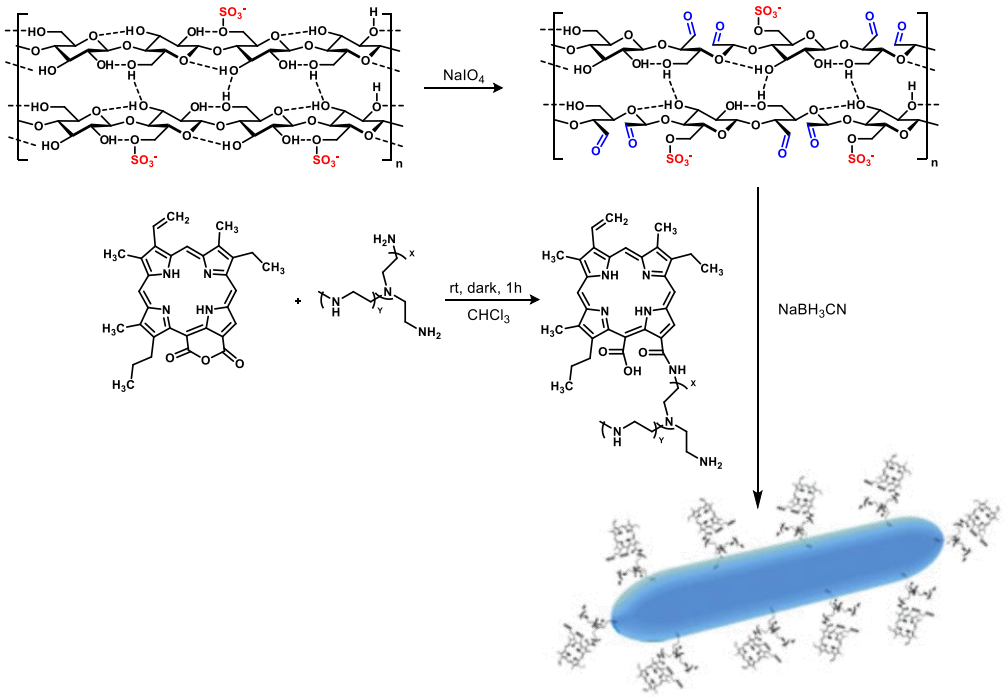

Figure 112. Covalent modification of CNC with chlorin molecules by oxidizing the glucose units and reacting the resulting carbonyl groups with the amine groups incorporated in the chlorine derivative, as published by Sol and co-workers.[254]

2.2 Molecular design, synthesis and characterization of zinc phthalocyanine-CNC biohybrids

To circumvent the above mentioned limitations of covalently attaching PS to CNC, in this chapter we aim to immobilize PS on the surface of sulfated CNC through an easy, non-covalent approach based on electrostatic interactions between positively charged PS and the negatively charged CNC surface (Figure 113). Two cationic ZnPc (**44** and **45**) will be immobilized, whereas a third anionic ZnPc (**46**) was employed as negative control for confirming that binding proceeds through electrostatic interactions.

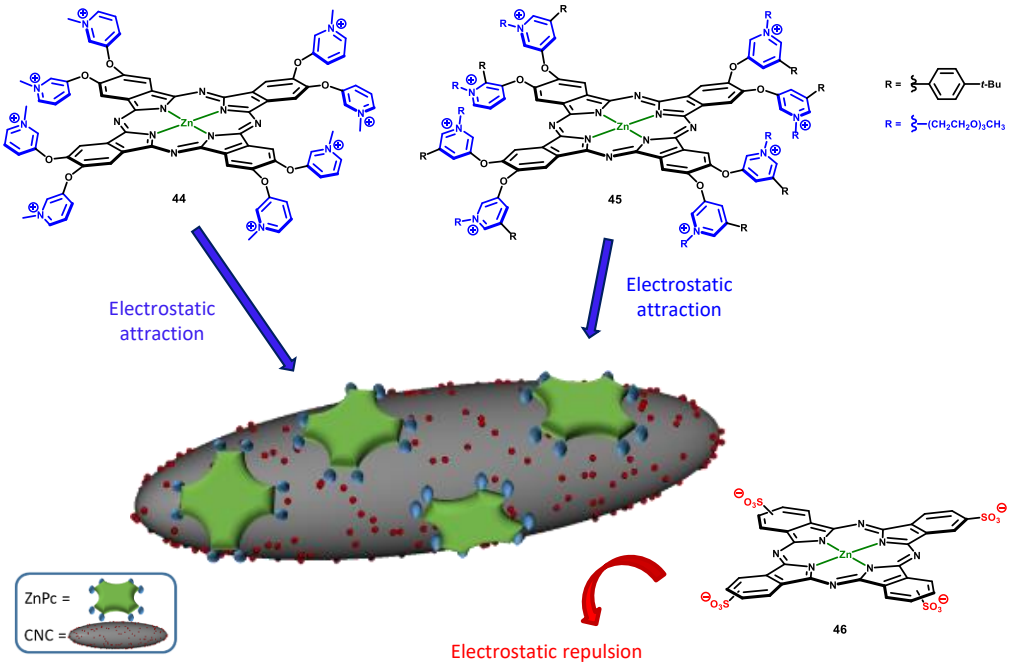

Figure 113. Chemical structure of the cationic ZnPc derivatives **44** and **45,** and the schematic representation of their supramolecular immobilization onto the surface of sulfate-decorated CNC. The anionic ZnPc **46** is a negative control.

*The synthesis of the ZnPc derivatives (**44**-**46**) used in the preparation of the ZnPc-CNC biohybrids has been previously reported by Dr. Eduardo Anaya-Plaza, and will therefore not be detailed in the present thesis. The synthesis of the biohybrids and their characterization has been performed in collaboration with the group of Mauri A. Kostianen from the Aalto University in Espoo (Finland).*

2.2.1 Synthesis and characterization of the ZnPc-CNC biohybrids

CNC with negatively charged surface sulfate groups were isolated from filter paper by sulfuric acid hydrolysis.[255] The ZnPc-CNC hybrids, in turn, were easily prepared by ultrasound bath-assisted dispersion of the CNC (5 mg mL^{-1}, 3 mL) in the corresponding ZnPc aqueous solution (ca. 0.1 mM, 12 mL) for 30 min. The sample was then centrifuged at 10000 rpm (9391 rfc) for 10 min and the pellet was washed five times with water and centrifuged again, until no color was observed in the supernatant (Figure 114).

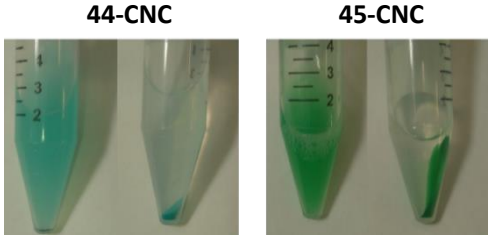

Figure 114. Images of **44-CNC** and **45-CNC** suspensions in PBS before and after centrifugation.

The ZnPc payload in the hybrids was determined through elemental analysis and calculated to be 1.0 x 10^{-5} and 1.7 x 10^{-5} mol of ZnPc per gram of CNC for **44-CNC** and **45-CNC**, respectively. Dynamic light scattering (DLS) was used to estimate the hydrodynamic diameter of pristine CNC (128 ± 8 nm), **44-CNC** (234 ± 17 nm) and **45-CNC** (216 ± 17 nm), at low concentration (0.05 mg mL^{-1}) to minimize the absorption of the ZnPc (Figure 115a, Table 19). A significant increase in size can be observed for the complexes in comparison to pristine CNC. We ascribe this size increase to a slight CNC aggregation and electrostatic cross-linking induced by the immobilized ZnPc. Yet the particle sizes remain in the range of a few hundreds of nanometers and have moderate polydispersity index (PDI) values.

The electric double layer of the system was evaluated by measuring the electrophoretic mobility and ζ-potentials of the hybrid particles at 0.05 mg mL^{-1} (Figure 115b, Table 19). The value found for **44-CNC** (-3.20 x 10^{-8} m^2 V^{-1} s^{-1}) closely resembles that of the pristine CNC (-3.23 x 10^{-8} m^2 V^{-1} s^{-1}), as a consequence of the low percentage of interacting sulfate esters (13.5%) in **45-CNC**, which leaves the electrostatic surface of the particles very similar to that in the absence of ZnPc. On the contrary, the electrophoretic mobility of **45-CNC** (-0.93 x 10^{-8} m^2 V^{-1} s^{-1}) drops drastically, as compared to pristine CNC. We ascribe this effect to the methoxy(triethylenoxy) chains, which render a more neutral solvation sphere and colloidal stabilization of the particle surface.

[255] C. D. Edgar, D. G. Gray, *Cellulose* **2003**, *10*, 299–306.

Table 19. Z-average size and PDI from DLS, mobility and ζ-potential measurements of CNC, **43-CNC** and **44-CNC**.

	Z-avg. (nm)	PDI	Mobility (10^{-8} $m^2 \cdot V^{-1} \cdot s^{-1}$)	ζ-Pot. (mV)
CNC	128 ± 8	0.18	-3.23 ± 0.04	-41.3± 5.5
44-CNC	234 ± 17	0.34	-3.20 ± 0.2	-40.4 ± 2.3
45-CNC	216 ± 17	0.24	-0.93 ± 0.12	-12.0 ± 1.5

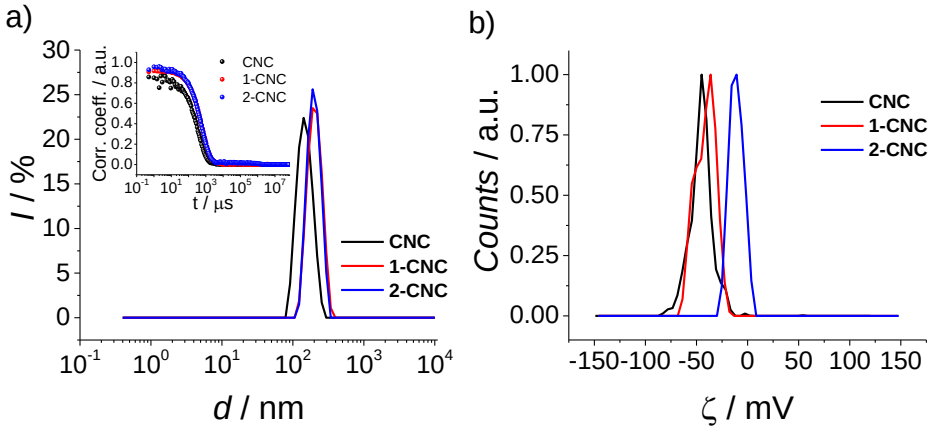

Figure 115. (a) DLS results showing the increase in intensity-averaged size distribution when CNC are coated with **44** (**44-CNC**) and **45** (**45-CNC**) in 5 µg/L solutions. *Inset*: correlograms of selected spectra. (b) ζ-potential of CNC showing no variation in **44-CNC** and a decrease of 29.3 mV in absolute value for **45-CNC**.

In order to characterize aggregation of the ZnPc-decorated CNCs, suggested above by DLS data, electron microscopy studies were also conducted. Cryogenic transmission electron microscopy (cryo-TEM) images of **44-CNC** show clusters of slightly aggregated rod-shaped nanocrystals in different orientations (Figure 116a). This behavior differs from **45-CNC** where all the nanocrystals are shown in flat, highly orientated, well-packed sheets (Figure 116b). We ascribe these differences to the presence of PEG chains in the chemical structure of **45** that hinder the binding to the CNC, yielding thermodynamically favored closed-packed assemblies. In opposition, **44** binds faster due to the exposed cationic surface, yielding kinetically trapped amorphous aggregates.

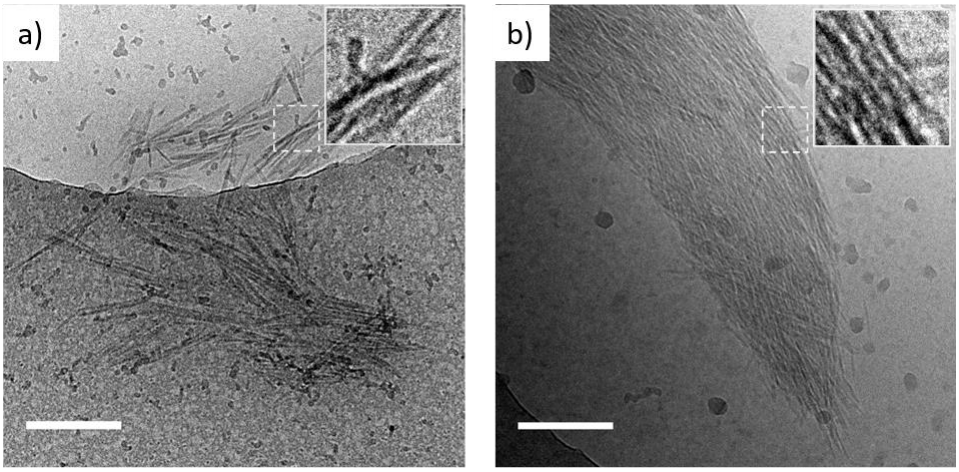

Figure 116. Cryo-TEM image of (a) **44-CNC** and (b) **45-CNC** at 0.5 mg/mL in water. Scale bars: 200 nm. Insets show magnifications of the areas marked by dashed lines.

2.2.2 Electronic absorption and photophysical properties

The electronic absorption and photophysical properties of the CNC-ZnPc biohybrids have been investigated during a predoctoral stay in the research group of Prof. Santi Nonell Marrugat at the Institut Químic de Sarrià of the Universitat Ramon Llull (Barcelona), in collaboration with Roger Bresolí-Obach.

2.2.2.1 Aggregation behaviour

The aggregation behaviour of **44** and **45**, both in solution and bound onto the CNC (**44-CNC** and **45-CNC**, respectively), is assessed by UV-Vis spectroscopy in different solvents (Figure 117).

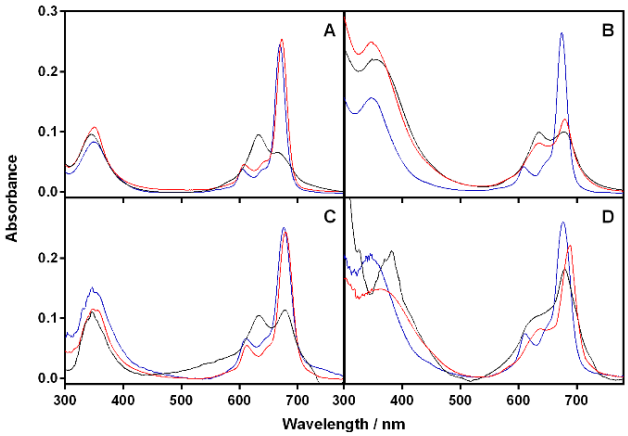

Figure 117. Absorption spectra of compounds a) **44** and b) **45** in methanol (blue), water (red) and PBS (black), as compared to those of hybrids c) **44-CNC** and d) **45-CNC**.

In methanol, both ZnPcs **44** and **45** exist in their monomeric form, displaying a characteristic sharp and intense absorption band at 670 nm and 674 nm, respectively, as is also the case for **44** in water. **45** on the other hand shows the appearance of a strong absorption band at 635 nm in water, an indication of *H*-type ZnPc aggregation.[256] In aqueous phosphate buffer saline (PBS), a physiologically relevant medium, the intensity of this band increases at the expense of the monomer band. Interestingly, **44** appears to be more aggregated than **45**.

The absorption spectra of the ZnPc-CNC hybrids **44-CNC** and **45-CNC** in methanol and water, on the other hand, show the characteristics of non-aggregated ZnPc (i.e., lack of the absorption band at 635 nm), as well as the typical scattering from CNC over the whole

[256] T. Nyokong, *Coord. Chem. Rev.* **2007**, *251*, 1707–1722.

spectral range. In PBS all CNCs showed aggregation, though to a lower extent than **44** and **45**.

2.2.2.2 $^1O_2$ generation efficiency

To demonstrate the photoactive character of the ZnPc-CNC complexes, we proceeded to study their efficacy for photoinduced $^1O_2$ production and to compare it with that of the corresponding free ZnPc derivatives. To this end, time-resolved near-IR spectroscopy was used to monitor the phosphorescence of $^1O_2$ at 1275 nm and compare it to that of suitable references (see Table 20 and Figure 118).[257] The results show that **44** is an intrinsically better PS than **45** in methanol, where both are in monomeric form. In PBS both compounds lose their photosensitising ability due to extensive aggregation. An intermediate behaviour is observed in neat D_2O, used instead of water to increase the $^1O_2$ lifetime, namely **44** behaves as in methanol but **45** is closer to PBS due to its more hydrophobic character.

Table 20. ϕ_Δ of **44**, **45**, **44-CNC** and **45-CNC** in various solvents. All ϕ_Δ values were determined as the average of three different measurements.

	ϕ_Δ [MeOH]	ϕ_Δ [D_2O]	ϕ_Δ [PBS]
44	0.62±0.03	0.74±0.06	0.04±0.01
45	0.02±0.01	~0.01	<0.01
44-CNC	0.20±0.04	0.04±0.01	<0.01
45-CNC	0.02±0.01	~0.01	<0.01

[257] A. Jiménez-Banzo, X. Ragàs, P. Kapusta, S. Nonell, *Photochem. Photobiol. Sci.* **2008**, *7*, 1003–1010.

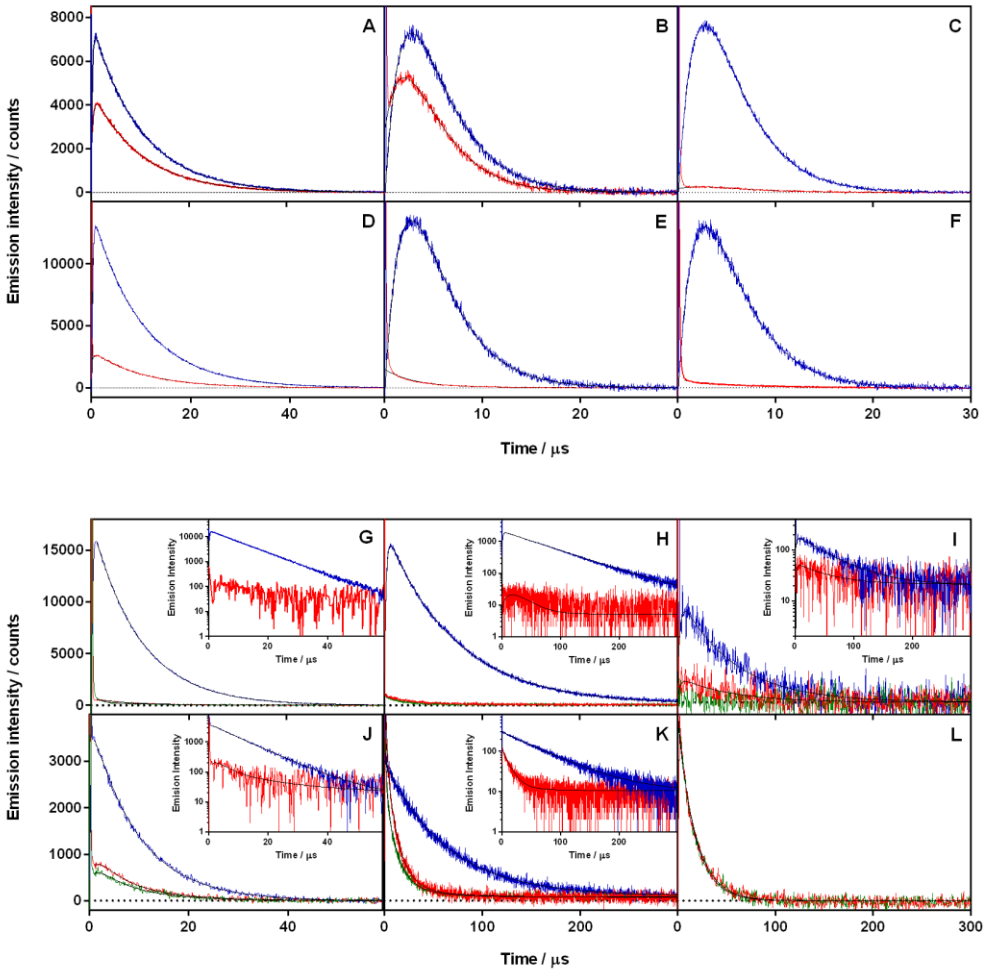

Figure 118. Time-resolved near-IR emission signals at 1275 nm for the free Pcs **44** and **45** and the biohybrids **44-CNC** and **45-CNC** (red lines) as well as for the reference PS used to determine ϕ_Δ values (blue lines). For the biohybrids an additional green line shows the effect of 50 mM NaN_3. a) **44** in methanol, b) **44** in water, c) **44** in PBS, d) **45** in methanol, e) **45** in water, f) **45** in PBS, g) **44-CNC** in methanol, h) **44-CNC** in D_2O, i) **44-CNC** in deuterated-PBS, j) **45-CNC** in methanol, k) **45-CNC** in D_2O and l) **45-CNC** in deuterated-PBS. The insets in G-L show the same data in log scale to facilitate visualization.

Contrary to what could perhaps be expected in view of the almost pure monomeric absorption spectra (Figure 117), the CNC biohybrids show almost no $^1O_2$ production in any solvent. This was thoroughly investigated and the underlying reason seems to be the severe loss of efficiency of oxygen trapping of the Pc's triplet state (^{3}Pc) upon anchoring to the CNC surface, a prerequisite for $^1O_2$ production. This is evidenced by the long ^{3}Pc lifetime in the biohybrids compared to the free molecules in solution (Figure 119; compare

panels A vs E and B vs F) and by the minor effect of sodium azide, a potent $^1O_2$ quencher,[258] on the emission signals at 1275 nm (cf. panels C vs G and D vs H).

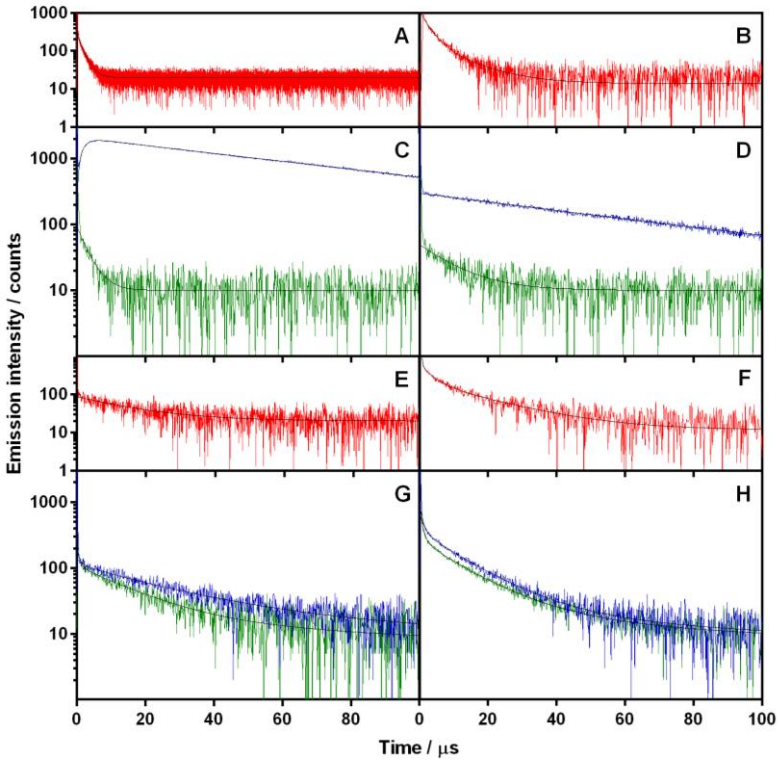

Figure 119. Comparison of the time-resolved near-IR emission signals in D_2O at 1110 nm (^{3}Pc; red line) and 1275 nm (^{3}Pc and $^1O_2$; blue line) for the free phthalocyanines **44** (A, C) and **45** (B, D), and for the biohybrids **44-CNC** (E, G) and **45-CNC** (F, H). The green line shows the effect of 50 mM NaN_3 on the 1275 nm emission. The phthalocyanine concentration was 3 μM in all cases.

It is worth mentioning that the signals at 1275 nm are a combination of ^{3}Pc phosphorescence and $^1O_2$ emission, as demonstrated by the remaining emission observed after adding sodium azide. The actual contribution of $^1O_2$ to the 1275 nm signals can thus be gauged by comparing the signals recorded in the absence and in the presence of azide. It is clear that it is much larger for the free molecules than for the CNC biohybrids, in which the 1275 nm signals are largely dominated by ^{3}Pc phosphorescence. The conclusion from these experiments is that anchoring the Pcs to the CNC surface almost completely inhibits their ability to produce $^1O_2$. Similar results were observed in methanol and PBS (Figure 120 and Figure 121, respectively).

[258] M. Y. Li, C. S. Cline, E. B. Koker, H. H. Carmichael, C. F. Chignell, P. Bilski, *Photochem. Photobiol.* **2001**, *74*, 760–764.

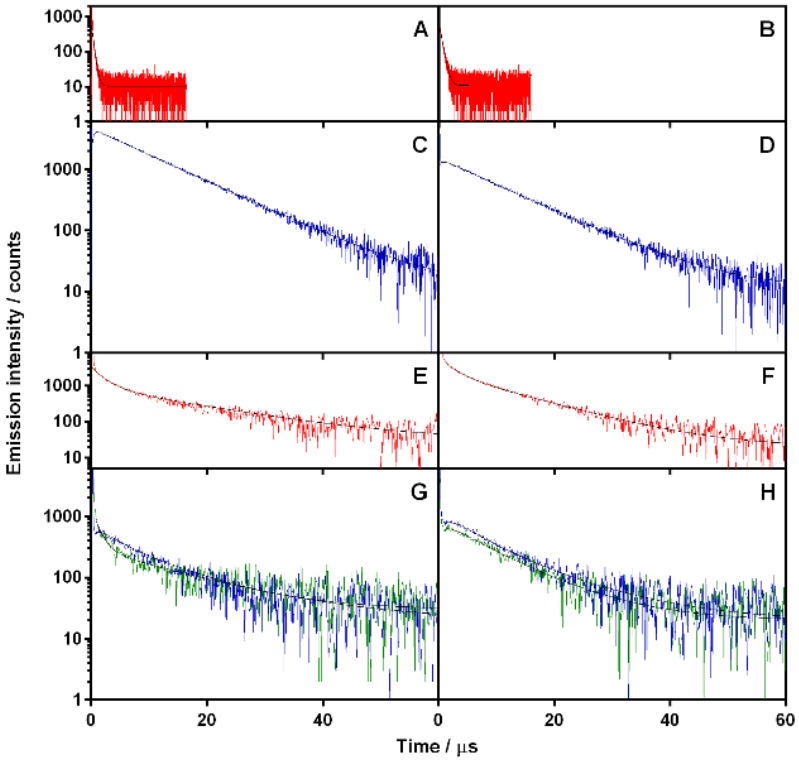

Figure 120. Comparison of the time-resolved near-IR emission signals in methanol at 1110 nm (red line) and 1275 nm (blue line) for the free phthalocyanines **44** (A, C) and **45** (B, D), and for the biohybrids **44-CNC** (E, G) and **45-CNC** (F, H). For the biohybrids, an additional green line shows the effect of 50 mM NaN_3 on the 1275 nm, emission. The phthalocyanine concentration was 3 μM in all cases.

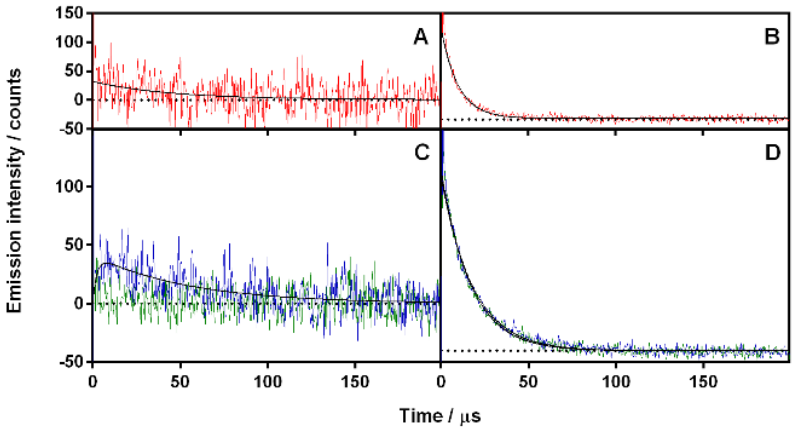

Figure 121. Comparison of the time-resolved near-IR emission signals in deuterated-PBS at 1110 nm (red line) and 1275 nm (in absence (blue line) and in presence (green line) of 50 mM NaN_3) for the biohybrids **44-CNC** (A, C) and **45-CNC** (B, D). The phthalocyanine concentration was 3 μM in all cases.

These results are consistent with the tight packing observed for the two ZnPc-CNC hybrids (see cryo-TEM results, Figure 116), which limits the diffusion of molecular O_2 through the CNC bundles.[259] Thus only the ZnPc molecules in close contact with the solvent (i.e. located at the surface of those bundles) can effectively produce $^1O_2$. The different modes of packing observed for **44-CNC** and **45-CNC** do not alter this general picture.

[259] A. J. Svagan, C. Bender Koch, M. S. Hedenqvist, F. Nilsson, G. Glasser, S. Baluschev, M. L. Andersen, *Carbohydr. Polym.* **2016**, *136*, 292–299.

2.3 *In vitro* photodynamic inactivation of microorganisms

PDI experiments for the CNC-ZnPc biohybrids have been performed during a predoctoral stay in the research groups of Dra. Montserrat Agut Bonsfills at the Institut Químic de Sarrià of the Universitat Ramon Llull (Barcelona), in collaboration with Oscar Gulías.

The microorganisms used in this study were the Gram-positive bacteria *Staphylococcus aureus*, Gram-negative bacterium *Escherichia coli* and the pathogenic yeast *C. albicans*.

In general, fresh bacterial or yeast cultures with a concentration between 1.5 and 3 x 10^8 CFU mL^{-1}, in the presence of the PS, were irradiated by means of a LED-lamp with red light (625 ± 25 nm), coinciding with the absorption maximum of the ZnPcs. Light alone controls without PS, and dark toxicity control with PS in dark were performed in order to rule out any inactivation effect due to the light or the PS alone. Triplicate aliquots of treatments and controls were collected at various time intervals and survival fractions were expressed as ratios of CFUs of cells treated with light and PS to CFUs of untreated cells.

First and foremost, before initiating any photoinactivation study of the newly designed biohybrids, the toxicity of the pristine CNCs on S. aureus is investigated (Figure 122). Favourably, at both low and high concentration (0.5 µM and 5 µM), and both in the dark or upon 30 minutes of irradiation, the CNCs are devoid of any cytotoxity.

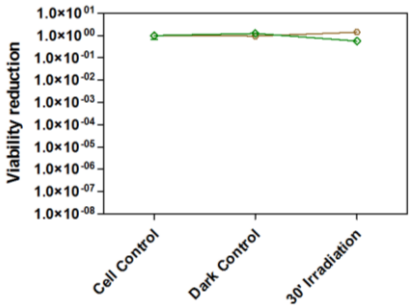

Figure 122. Photoinactivation studies of *S. Aureus*. Working compounds concentrations: 0.5 µM (brown) and 5µM (green).

Consequently, the PDI properties of these new biohybrids were tested against *S. aureus*, a Gram-positive bacterium, and compared with that of the free ZnPc counterparts (Figure 123). Both **44-CNC** and **45-CNC** proved to be highly efficient in inactivating *S. aureus*, resulting in 6 logs and 3 logs CFU reduction, respectively, at concentrations as low as 0,5 µM and light fluencies of only a few J/cm2. Remarkably, both CNC hybrids showed a greater photoinduced antimicrobial effect than the free ZnPcs **44** and **45**, highlighting the importance of their formulation onto CNC. Importantly, **44-CNC** is devoid of any dark toxicity, while that of **45-CNC** is non-zero but almost negligible (1 log CFU reduction).

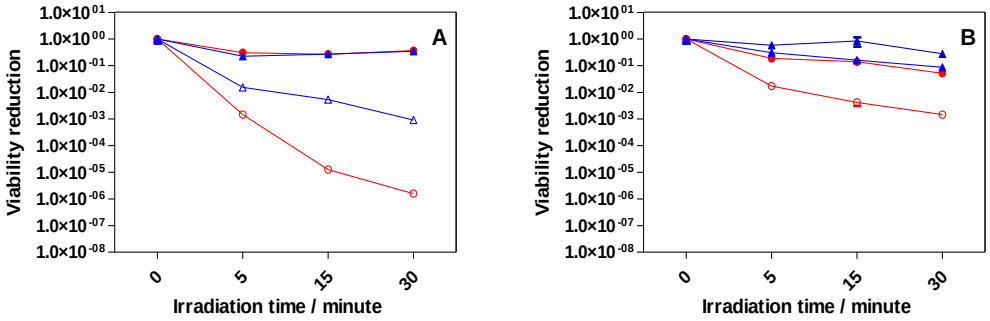

Figure 123. Photoinactivation studies of *S. aureus* with a) **44** and **44-CNC** or b) **45** and **45-CNC** upon red light irradiation (620-645 nm; 18 mW/cm^2). Working compounds concentration: 0.5 μM. **44-CNC** and **45-CNC** are represented with red lines and circle marks, while plain ZnPc **44** and **45** inactivations are depicted in blue with triangle marks. Dark controls are represented with solid marks.

Similar results as those for *S. aureus* were obtained against the Gram-negative *E. coli.* **44-CNC** showed no dark toxicity and reached 8 logs of CFU reduction, i.e., complete eradication, at approximately 3 μM and 64 J/cm^2 (Figure 124a). On the other hand, **45-CNC** induced up to 6 logs CFU reduction under the same conditions, however its dark cytotoxicity was very high (4 logs of CFU reduction; Figure 124b). Significantly, the free compounds **44** and **45** were again 3-4 logs less effective, clearly indicating the added value of their covalent attachment to the CNCs.

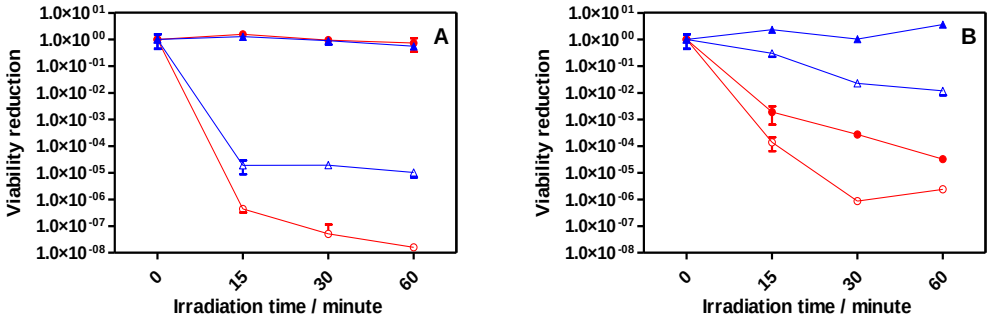

Figure 124. Photoinactivation studies of *E. coli* with a) **44** and **44-CNC** or b) **45** and **45-CNC** upon red light irradiation (620-645 nm; 18 mW/cm^2). Working compounds concentration: 3 μM. **44-CNC** and **45-CNC** are represented with red lines and circle marks, while plain ZnPc **44** and **45** inactivations are depicted in blue with triangle marks. Dark controls are represented with solid marks.

Finally, both **44** and **44-CNC** were also tested against *C. albicans* (Figure 125), whereas **45** and **45-CNC** were discarded in view of the high dark toxicity the biohybrid displayed in both *S. aureus* and *E. coli*. Neither **44** or **44-CNC** showed any dark toxicity. Interestingly, **44** did not show any phototoxicity either, while **44-CNC** was highly phototoxic, reaching more than 6.5 logs CFU reduction at 3 μM and 64 J/cm^2.

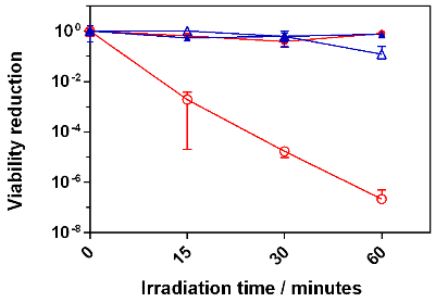

Figure 125. Photoinactivation studies of *C. albicans* with **44** and **44-CNC** upon red light irradiation (620-645 nm; 18 mW/cm^2). Working compounds concentration: 3 µM. **44-CNC** is represented with red lines and circle marks, while plain ZnPc **44** is depicted in blue with triangle marks. Dark controls are represented with solid marks.

In sum, **44-CNC** is a very efficient and broad spectrum photoantimicrobial agent, devoid of any dark toxicity and worth of further consideration. Importantly, the PS concentrations and light doses applied for the PDI of both *S. aureus* and *E. coli* are one- to two order of magnitudes lower than those reported in the literature for similar, but covalently linked systems.[253] The substantial loss of $^1O_2$ photosensitisation ability of **44** and **45** when they are anchored to the CNC surface (see results section 2.3.2) may explain the modest performance of these previously published covalently linked systems. Thus, in our case, the excellent photoantimicrobial ability of **44-CNC** and **45-CNC** suggests that the Pcs, being only non-covalently attached, can be transferred from the negatively charged CNC surface to the negatively charged cell wall of the microorganisms, and in this way result in significantly greater photodamage.

3

Summary and Conclusions

In the present chapter, we have developed two different kinds of PS-based biohybrid systems for PDT and PDI. They are differentiated by both the type of biological delivery agent and the synthetic approach that was employed in each subchapter.

In the first subchapter, the conjugation of a well-known CPP with two different PS, a SiPc and a SubPc, has been discussed. The conjugation strategy was covalent, by incorporation of a cysteine functionality at the C-terminus of the CPP and a maleimide functionality in the PS structure, which allowed the CPP and the PS to react through a maleimide-thiol Michael addition "click" reaction. The resulting PS-CPP biohybrids are water-soluble and their absorption, fluorescence and $^1O_2$ generation capacity have been carefully evaluated in water and/or PBS. These experiments confirmed that both conjugates are efficient $^1O_2$ generators, **37** being a better PS than **38**. Finally, in order to evaluate the cell uptake properties of these PS-CPP conjugates, their cellular internalization properties was quantified *in vitro*, using chinese hamster ovary cells as a model system, by flow cytometry analysis. Both biohybrids were taken up by the cells efficiently at 4°C, where only passive transport is possible, indicating the CPP is responsible for the cell uptake and confirming the utility of our strategy. The visualization of cell uptake by fluorescence microscopy is pending.

In the second subchapter, we have studied supramolecular complexes of Pc molecules and CNC, as a type of optically active biohybrid nanostructures. Preparation of such materials represents a challenging goal from the nanotechnology point of view. Our strategy is based on the immobilization of cationic ZnPc derivatives onto unmodified CNC through an easy and straightforward non-covalent methodology, which is driven by electrostatic interactions. The resulting biohybrids have been characterized by UV-Vis spectroscopy, DLS and cryo-TEM, proving that ZnPc stacking and CNC clustering are key processes that need to be prevented for an optimal photoinduced $^1O_2$ production. To this end, the $^1O_2$ generation of both the ZnPcs and the ZnPc-CPP biohybrids was studied in depth by monitoring the phosphorescence of $^1O_2$ by time-resolved near-IR spectroscopy.

Importantly, $^1O_2$ is a key species in photodynamic therapy, water treatments, diagnostic arrays and photocatalytic technologies. The photodynamic inactivation of bacteria by **44-CNC** and **45-CNC**, for example, show clear advantages of these nanohybrids compared to the free ZnPc and to related nanosystems in which the PS is covalently linked to the CNC surface. The hybrids developed herein are therefore promising photoactive biomaterials, which may find useful applications in biomedicine and nanotechnology.

4

Experimental section

4.1 Materials and methods

The materials and methods used in this experimental section are the same as the ones used in that of Chapter 1, except for:

IR spectra (IR) were recorded on a FTIR Cary 630 (Agilent Technologies) using the ATR technique. Spectral intensity were corrected by the ATR algorism and subsequent baseline correction.

GC-EI spectra were recorded using an GCT Agilent Technologies 6890N spectrometer (Waters), at the Servicio Interdepartmental de Investigación (SIdI) of the Universidad Autónoma de Madrid. The data are expressed with the intensity in percentage between parentheses.

The MALDI-TOF spectra of CPP conjugates (Subchapter 1) were recorded on an Applied Biosystems Voyager-DE STR Biospectrometry Workstation, using freshly prepared α-cyano-4-hydroxycinnamic acid as matrix, in the department of Organic Chemistry at University of Ghent, Belgium. For peptidic compounds, the exact mass, rather than the molecular weight of the compound, is stated, as this allows for an easier evaluation of mass spectrometric data. The data are expressed with the intensity in percentage between parentheses.

RP-HPLC analyses were performed on an Agilent 1100 Series instrument with a Phenomenex Luna C18(2) column (250 x 4.6 mm, 5 µm at 35°C). A flow rate of 1 mL/min and with the following solvent systems:

- For SiPc-CPP **37**: water (A) and acetonitrile (B). The column was flushed for 10 min with 100% B followed by 10 minutes of flushing with 100% A, then a gradient from 50 to 100% B over 25 min was used, followed by 10 min of flushing with 100% B. Samples were dissolved in water (A) and filtered (0.45

μm pore size, Millipore nylon filters) prior to injection. UV-detection was performed at 214, 254, 280 and 676 nm.

- For SubPc-CPP **38**: 0.1% TFA in water (A) and 0.1% TFA in acetonitrile (B). The column was flushed for 10 min with 100% B followed by 10 minutes of flushing with 100% A, then a gradient from 0 to 100% B over 25 min was used, followed by 10 min of flushing with 100% B. Samples were dissolved in 0.1% TFA in water (A) and filtered (0.45 μm pore size, Millipore nylon filters) prior to injection. UV-detection was performed at 214, 254, 280 and 650 nm.

Elemental analysis was carried out in a LECO CHNS-932 analyser. A Zetasizer Nano ZS90 analyzer (Malvern Instruments) with a He–Ne laser of 633 nm was used for measuring the particle size distributions, electrophoretic mobilities and ζ-potentials at a 90° scattering angle. Disposable PMMA cuvettes (Plastibrand) were used for DLS measurements and Universal 'Dip' cell (ZEN1002) for ζ-potential measurements. Cryogenic transmission electron microscopy (cryo-TEM) imaging was carried out with JEOL JEM-3200FSC equipment.

4.1.1 Fluorescence and singlet oxygen quantification

The ϕ_F and ϕ_Δ in Subchapter 1 are determined using the same procedures as those used in Chapter 1. The ϕ_Δ in Subchapter 2 on the other hand are determined by time-resolved near-IR spectroscopy.

The specific near-infrared phosphorescence kinetics were detected by means of a PicoQuant Fluotime 200 lifetime system customized as follows: a diode-pumped pulsed Nd:YAG laser (FTSS355-Q, Crystal Laser, Berlin, Germany) working at 10 or 1 kHz repetition rate at 355 nm (0.5 μJ per pulse) was used for excitation. A 1064 nm rugate notch filter (Edmund Optics, York, UK) and an uncoated SKG-5 filter (CVI Laser Corporation, Albuquerque, USA) were placed at the exit port of the laser to remove any residual component of its fundamental emission in the near-infrared (NIR) region. The luminescence exiting from the sample was filtered by a 1100 nm long-pass filter (Edmund Optics, York, UK) and narrow bandpass filters at either 1110 nm (BP-1110-070-B, Spectrogon, Täby, Sweden) to detect the phthalocyanine phosphorescence emission, or at 1275 nm (BK-1270-70-B, bk Interferenzoptik, Nabburg, Germany) to detect the $^1O_2$ emission. A TE-cooled near-IR sensitive photomultiplier tube assembly (H9170-45, Hamamatsu Photonics, Hamamatsu City, Japan) was used as detector. Photon counting was achieved with a multichannel scaler (NanoHarp 250, PicoQuant, Berlin, Germany).

ϕ_Δ is defined as the number of photosensitized $^1O_2$ molecules per absorbed photon and was determined by fitting the kinetic model below to the time-resolved phosphorescence intensity at 1275 nm, which contains both $^1O_2$ and triplet phthalocyanine emission

components.[260] The pre-exponential factors $S_\Delta(0)$ and $S_T(0)$ are proportional to ϕ_Δ and ϕ_t, respectively

$$S(t) = S_\Delta(0) \times \frac{\tau_\Delta}{\tau_T - \tau_\Delta} \times \left(e^{-t/\tau_T} - e^{-t/\tau_\Delta}\right) \; + \; S_T(0)e^{-t/\tau_T}$$

For the free phthalocyanines ϕ_Δ was determined by comparison of their $S_\Delta(0)$ values to that of an optically-matched reference in the same solvent and at the same excitation wavelength. The references used were 1H-phenalen-1-one in methanol ($\Phi_\Delta = 0.98$)[261] and 1H-phenalen-1-one-2-sulphonate in water or PBS ($\phi_\Delta = 0.97$).[262] For the biohybrids, the references were the corresponding free phthalocyanines at the same concentration.

$$\phi_\Delta(sample) = \frac{S_\Delta(0)_{sample}}{S_\Delta(0)_{reference}} \times \phi_\Delta(reference)$$

4.1.2 Flow cytometry

The cell medium of a cell suspension of CHO cells was removed and the cells were washed with PBS and incubated for 15 minutes in the presence of trypsine. PBS was added for centrifugation of the cells, the supernatant removed and the cells resuspended in cell medium. 180 µL of Trypan blue was added to 20 µL of cell suspension, in order to visualize the cells for cell counting.

Cells were subsequently plated in 24-well plates with a concentration of $15*10^4$ cells in 900 µL per well. Half of the cells was maintained in an incubator at 37°C (5% CO_2), whereas the other half was cooled on ice. After 1h, 100 µL of a PBS solution of the PS-CPP biohybrid conjugates was added to the wells. For each measurement condition two blanks were performed without adding any PS-CPP biohybrids to the cells. The plates were left to incubate for another 4h, again either in an incubator at 37°C (5% CO_2) or on ice, after which the cell medium was removed and 500 µL of cell dissociation buffer was added to detach the cells from the well bottom. After 15 more minutes of incubation the cells were transferred to Eppendorf, centrifuged to remove the cell dissociation buffer, and dissolved in 300 µL of PBS for injection into the flow cytometer. Flow cytometry experiments are performed on a BD Accuri C6 from BD Biosciences with serial number 3863.

---

[260] S. Nonell. and Flors. C., in *Singlet Oxygen: Applications in Biosciences and Nanosciences Vol. 2*, The Royal Society of Chemistry, London, **2016**, pp. 7–26.

[261] a) E. Oliveros, P. Suardi-Murasecco, T. Aminian-Saghafi, A. M. Braun and H.-J. Hansen, *Helv. Chim. Acta*, **1991**, *74*, 79–90; b) R. Schmidt, C. Tanielian, R. Dunsbach and C. Wolff, *J. Photochem. Photobiol. A Chem.*, **1994**, *79*, 11–17; c) C. Martí, O. Jürgens, O. Cuenca, M. Casals and S. Nonell, *J. Photochem. Photobiol. A Chem.*, **1996**, *97*, 11–18.

[262] S. Nonell, M. González and F. R. Trull:, Afinidad, **1993**, *44*, 445–450.

4.1.3 Confocal imaging

Cells were plated in 24-well plates with a concentration of $5*10^3$ cells in 200 µL per well. Half of the cells was maintained in an incubator at 37°C (5% CO_2), whereas the other half was cooled on ice. After 1h, 10 µL of a PBS solution of the PS-CPP biohybrid conjugates was added to the wells. For each measurement condition two blanks were performed without adding any PS-CPP biohybrids to the cells. After 4 more hours of incubation, the cells were stained with Hoechst and Phalloidine stain for visualization of the cell nucleus and cell membrane, respectively, by fluorescence microscopy.

For staining, a dye solution consisting of 2 mL PBS BSA 1% + 5 µL CTB 488 stock + 10 µL Hoechst stock 1 mg/mL was prepared. The cell medium was removed and the cells were washed with 2 x 200 µL PBS, after which 200 µL PFA 4% was added for cell fixation. The cells were incubated for 15 minutes (37°C, 5% CO_2) and washed with 2 x 200 µL PBS before adding the dye solution and incubating another 30 minutes (37°C, 5% CO_2). Upon removal of the dye solution, the cells were again washed and resuspended in PBS, and kept in the dark until the confocal imaging experiment.

Confocal imaging experiments were performed on a Leica DMI6000 B inverted microscope equipped with a Zeiss 63x NA 1.40 oil immersion objective and an Andor DSD2 confocal scanner. Images were treated with Imaris software.

4.1.4 Photoinactivation studies

Three strains obtained from the American Type Culture Collection (*S. aureus* 29213, *E. coli* ATCC 25922 and *C. albicans* ATCC 18804) were tested in this study. All the isolated strains were deposited and maintained at IQS (Institut Químic de Sarrià).

Inactivation of bacterial strains:

Bacteria were grown aerobically overnight at 37°C in Tryptic Soy Broth (TSB, Panreac 413820.1210, Castellar del Vallès, Spain) in an orbital shaking incubator. 10µl of the pre inoculum was added to 10ml of sterile TSB and incubated, until the culture reached an optical density of 0,2 at 600 nm, corresponding to between 1.5 to 3 $\cdot 10^8$ CFU ml^{-1}.

The suspensions were then centrifuged (10 minutes, 3000 g) and suspended with sterile phosphate-buffered saline at pH4 (PBS, Fisher BP399, New Jersey, USA) at the same cellular concentration in the presence of 0.5µM (*S. aureus*) or 3 µM (*E. coli*) of the appropriate compound. Then, bacterial suspensions were incubated in the dark in an orbital shaking incubator at 37°C for 15 minutes.

Next, 300 µl aliquots of the bacterial suspensions were placed in 96-well plates. The plates were illuminated by means of a LED-lamp (Sorisa Photocare) with red light (625 ± 25 nm) from the top of the plates at a fluence of 18 mW/cm^2. At the time point when the requisite fluence had been delivered (0, 5, 15, 30 or 60 minutes), the aliquots were serially diluted in PBS, and 10 µl of each dilution were streaked on Tryptic Soy Agar plates (TSA, TSB added with 1,5% agar-agar, Fisher BP9744, Geel, Belgium) and incubated in the dark for 24 hours at 37°C. After the incubation period, the number of CFU ml^{-1} was determined.

Experiments were carried out in triplicate for each condition. Light alone controls without PS, and dark toxicity control with PS in dark were performed in order to rule out any inactivation effect due to the light or the PS alone. Survival fractions were expressed as ratios of CFU of bacteria treated with light and photo-sensitizer to CFU of untreated bacteria.

Inactivation of *Candida albicans*:

Pre inoculum suspensions were prepared from an overnight culture of the yeast grown in glucose Sabouraud broth (Panreac 413804.1210, Castellar del Vallès, Spain) incubated aerobically at 30ºC in an orbital shaking incubator. 100 µL of the pre inoculum were added to 10 mL of sterile glucose Sabouraud broth and incubated at 30°C until the culture reached an optical density of 0.25 at 600 nm, corresponding to 1 x 10^8 to 2 x 10^8 CFU ml^{-1}. After the incubation period, yeast cultures were centrifuged for 10 minutes and 3,000g and re-suspended in 10 mL of sterile PBS at pH 4 with 3 µM of the desired compound. The suspensions were then incubated in the dark in an orbital shaking incubator at 30°C for 15 minutes. After this, 300 µL aliquots of the suspensions were placed in 96-well plates and illuminated with red light (625 ± 25 nm, 18 mW/cm^2) from the top of the plates. When the desired fluence had been delivered (0, 15, 30 or 60 minutes), the aliquots were serially diluted in PBS and 10 µL of each dilution were streaked on glucose Sabouraud agar (Panreac 4138021210, Castellar del Vallès, Spain) and incubated in the dark for 48 hours at 30°C. After the incubation period, the number of CFU ml^{-1} was determined.

Experiments were carried out in triplicate. Survival fractions were expressed as ratios of CFUs of cells treated with light and PS to CFUs of untreated yeasts. Light-only and PS-only controls were performed.

4.2 Experimental details synthesis

4.2.1 Synthesis of maleimide-containing SiPc and SubPc derivatives

1-(3-((*tert*-butyldimethylsilyl)oxy)propyl)-1H-pyrrole-2,5-dione (**40**):

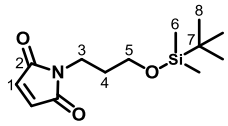

Maleic anhydride (3.500 g, 0.036 mol) was dissolved in ethanol (300 ml) and added dropwise to a solution of **9** (8.101 g, 0.042 mol) and triethylamine (4.9 mL, 0.036 mol) in ethanol (200 mL) at 0°C under vigourous stirring. The reaction mixture was stirred for 4h. The solvent was removed, the residue was redissolved in acetic anhydride (70 mL) and sodium acetate (2.920 g, 0.036 mol) was added. The reaction mixture was heated for 30 min at 60-70°C and cooled to rt. The solvent was evaporated and the crude product purified by column chromatography using EtOAc/heptane (6:1) as the eluent to yield **40** (4.486 g, 47%) as a viscous colorless oil.

^{1}H-NMR (300 MHz, $CDCl_3$): δ(ppm) 6.63 (s, 2H, H_1), 3.68 – 3.46 (m, 4H, H_3, H_5), 1.72 (p, *J* = 7.0 Hz, 2H, H_4), 0.82 (s, 9H, H_8), -0.03 (s, 6H, H_6).

^{13}C-NMR (75 MHz, $CDCl_3$): δ(ppm) 170.32 (C_2), 133.69 (C_1), 60.23 (C_5), 34.93 (C_3), 31.06 (C_4), 25.49 (C_8), 17.85 (C_7), -5.81 (C_6).

MS (GC-EI): 254.1 $[M–CH_3]^+$ (10), 212.1 [M–*t*-Bu]$^+$ (100), 156.0 [M–TBDMS+2H]$^+$ (60), 154.0 [M–TBDMS]$^+$ (40), 110 (10), 75 (10).

HR-MS (GC-EI): [M]$^+$ Calcd. for $C_{12}H_{20}NO_3Si$: 254.1119; Found: 254.1203.

FT-IR (neat) ν (cm^{-1}): 2856, 1701 (C=O), 1444, 1406, 1253, 1152, 1095, 1005, 826, 775.

1-(3-hydroxypropyl)-1H-pyrrole-2,5-dione (**41**):

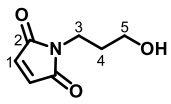

40 (0.121 g, 0.4 mmol) was dissolved in dry methanol (1.7 mL) and the reaction mixture was cooled to 0°C. Acetyl chloride (5 µL, 0.07 mmol) was added dropwise under vigorous stirring. Upon completion of the reaction (30 minutes) the solvent was evaporated at 0°C to yield compound **41** as a colorless oil (0.176 g, 87%). Compound **41** was directly used in the next step without further purification, to reduce the risk of polymerization.

^{1}H-NMR (300 MHz, $CDCl_3$): δ(ppm) 6.98 (s, 2H, H_1), 4.23 (s, 1H, OH), 3.44 (t, *J* = 7.3 Hz, 2H, H_5), 3.38 (t, *J* = 6.2 Hz, 2H, H_3), 1.62 (p, *J* = 6.8 Hz, 2H, H_4).

^{13}C-NMR (75 MHz, $CDCl_3$): δ(ppm) 171.08 5 (C_2), 134.50 (C_1), 58.43 (C_5), 34.83 (C_3), 31.25 (C_4).

MS (GC-EI): *m/z* = 155.0 [M]$^+$ (10), 137.0 (40), 125.0 (40), 110.0 (100), 99.0 (30), 87.0 (30).

HR-MS (GC-EI): [M]$^+$ Calcd for $C_7H_9NO_3$: 155.0582; Found: 155.0590.

Subphthalocyanine **42**:

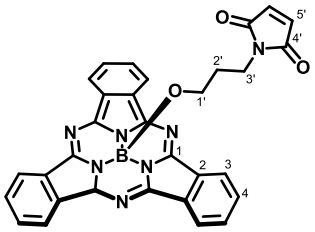

16 (0.080 g, 0.190 mmol) and silver triflate (0.060 g, 0.230 mmol) were dissolved in anhydrous toluene (3 mL) and the mixture was stirred at rt under argon atmosphere **16** is consumed (approx. 40 min). Once the SubPcBOTf was generated, the nucleophile **41** (0.058 g, 0.380 mmol.) and DIPEA (40 µL, 0.230 mmol) were added. The mixture was stirred at 40°C until the reaction is completed. The solvent was removed by evaporation under reduced pressure and the product was directly purified by chromatography on silica gel using a gradient of toluene/THF (30:1 to 10:1) as the eluent. After further SEC purification with Bio-Beads **42** (0.039 g, 38%) was obtained as a dark pink solid.

^{1}H-NMR (300 MHz, $CDCl_3$): δ(ppm) 8.80 – 8.72 (AA'BB' system, 6H, H_3), 7.84 – 7.75 (AA'BB' system, 6H, H_4), 6.30 (s, 2H, $H_{5'}$), 2.73 (t, *J* = 6.8 Hz, 2H, $H_{3'}$), 1.43 (t, *J* = 6.0 Hz, 2H, $H_{1'}$), 0.73 (p, *J* = 6.4 Hz, 2H, $H_{2'}$).

^{13}C-NMR (75 MHz, $CDCl_3$): δ(ppm) 170.39 ($C_{1'', C4''}$), 151.59 (C_5, C_7, C_{12}, C_{14}, C_{19}, C_{21}), 133.71 ($C_{2'', C3''}$), 131.11 ($C_{4a,}$ C_{7a}, C_{11a}, C_{14a}, C_{18a}, C_{21a}), 129.79 ($C_{2,}$ C_3, C_9, C_{10}, C_{16}, C_{17}), 122.23 ($C_{1,}$ C_4, C_8, C_{11}, C_{15}, C_{18}), 56.63 ($C_{1'}$), 34.91 ($C_{3'}$), 28.99 ($C_{2'}$).

MS (MALDI-TOF, DCTB): *m/z* = 806.3 (2), 643.3 (2), 584.3 (2), 549.2 $[M]^+$ (100), 395.2 $[M-L_{axial}]^+$ (2)

HR-MS (FAB, m-NB MALDI-TOF, DCTB A): $[M]^+$ Calcd. for $C_{31}H_{20}BN_7O_3$: 549.1721 ; Found: 549.1714.

FT-IR (neat) ν (cm^{-1}): 2924, 1702 (C=O), 1612, 1455, 1430, 1388, 1286, 1229, 1176, 1128, 825, 737, 695.

Mp: >250°C.

Silicon (IV) phthalocyanine **43**:

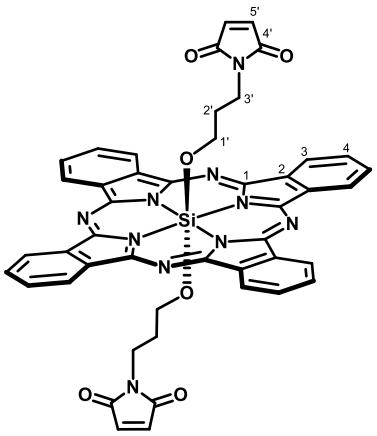

$SiPcCl_2$ (0.025 g, 0.041 mmol), alcohol **41** (0.032 g, 0.204 mmol) and DIPEA (0.15 mL) were heated in dry toluene (5 mL) under reflux and argon atmosphere for 18 h. The solvent was removed under reduced pressure and the crude purified by column chromatography using silica gel, previously neutralized with triethylamine, and DCM as the eluent. After precipitation in methanol, **43** (0.017 g, 51%) was obtained as a dark blue solid.

^{1}H-NMR (300 MHz, $CDCl_3$): δ(ppm) 9.64 (dd, *J* = 5.8, 2.9 Hz, 8H, H_3), 8.34 (dd, J = 5.9, 2.8 Hz, 8H, H_4), 5.85 (s, 4H, $H_{5'}$), 1.08 (t, *J* = 6.9 Hz, 4H, $H_{3'}$), -1.35 (p, *J* = 6.4 Hz, 4H, $H_{2'}$), -2.13 (t, *J* = 5.9 Hz, 4H, $H_{1'}$).

^{13}C-NMR (75 MHz, $CDCl_3$): δ(ppm) 168.86 ($C_{4'}$), 148.88 (C_1), 135.77 (C_2), 132.34 ($C_{5'}$), 130.56 (C_4), 123.42 (C_3), 52.73 (C_1), 33.35 (C_3), 27.50 (C_2).

MS (MALDI-TOF, DCTB): *m/z* = 894.2 $[M+2Na]^+$ (40), 871.3 $[M+Na]^+$ (100), 848.3 $[M]^+$ (10), 734.2 (10), 717.2 (10), 694.2 (100).

HR-MS (MALDI-TOF, DCTB): $[M+Na]^+$ Calcd. for $C_{46}H_{32}N_{10}NaO_6Si$: 871.2168; Found: 871.2151.

FT-IR (neat) ν (cm^{-1}): 1701 (C=O), 1519, 1333, 1287, 1159, 1120, 1080, 920, 839, 758, 733, 694.

Mp: >250°C.

4.2.2 Conjugation with the CPP

Subphthalocyanine **37**:

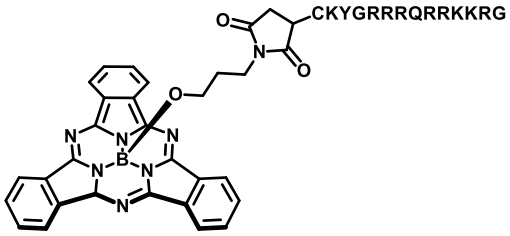

5.0 mg of peptide (2.707 nmol) were dissolved in DMSO (200 mL) and the resulting solution was added to a solution of **42** (4.219 mg, 7.680 nmol) in DMSO (200 mL), containing pyridine (3 µL). The mixture was shielded from light, and was allowed to stand overnight at rt. The mixture was then partitioned between ethyl acetate and deionised 0.1% aq. TFA. The aqueous layer was evaporated to a small volume, and applied to a Discovery DSC-18 solid phase extraction cartridge (Supelco, Gillingham, UK). The desired compound was eluted with a gradient from 5% acetonitrile 01% aq. TFA to 20% acetonitrile 0.1% aq. TFA mobile phase, and then lyophilised to yield **37** (6.201 mg, 95%) as a pink solid.

MS (MALDI-TOF, CHCA): *m/z* = 2395.7 $[M]^+$ (100), 2002.0 $[M_{F2}+H]^+$ (55), 1846.1 $[M_{F1}+H]^+$ (48).

HR-MS (MALDI-TOF, CHCA): $[M^+]$ Calcd. for $C_{106}H_{160}B_1N_{44}O_{19}S_1$: 2396.2730; Found: 2396.2731.

UV-VIS (DMF): λ_{max} (nm) (log ε): 560 (4.74), 508 (sh), 298 (4.66)
(H_2O): λ_{max} (nm) (log ε): 565 (4.78), 513 (sh), 303 (4.55)

FT-IR (neat) ν (cm^{-1}): XXX

Mp: >250°C

RP-HPLC: t_r=12,2 min

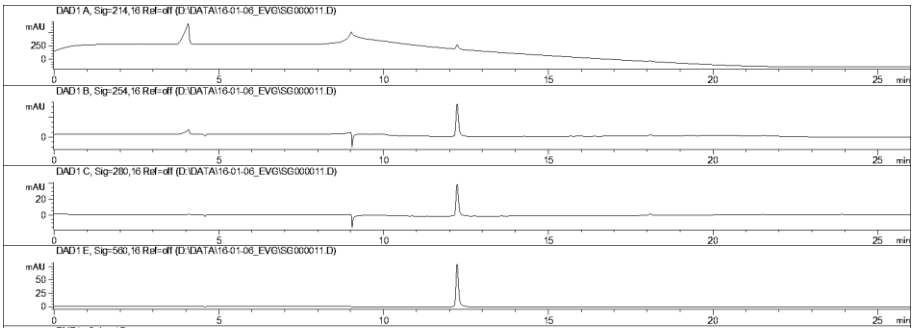

Silicon (IV) phthalocyanine **38**:

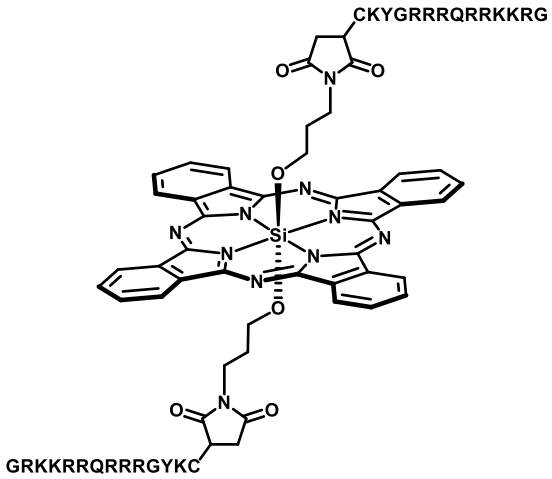

40.0 mg of peptide (0.0216 mmol) were dissolved in DMSO (800 mL), and the resulting solution was added to a solution of **43** (4.219 mg, 0.0072 mmol) in DMSO (200 mL), containing pyridine (3 µL). The mixture was shielded from light, and was allowed to stand overnight at rt. Addition of diethyl ether (10 mL) results in the formation of a blue precipitate. After centrifugation the colorless supernatant was removed and the remaining solid was dissolved in distilled water and washed with DCM. The aqueous phase was lyophilised to yield **38** (15.3 mg, 48%) as a dark blue solid.

MS (MALDI-TOF, CHCA): *m/z* = 2002.0 $[M_{F2}+H]^+$ (100), 1113.1 (64).

UV-VIS (DMF): λ_{max} (nm) (log ε): 671 (5.33), 644 (sh), 606 (4.51), 353 (4.88)
(H_2O): λ_{max} (nm) (log ε): 682 (4.88), 618 (4.40), 353 (4.67)

FT-IR (neat) ν (cm^{-1}): XXX

Mp: >250°C

RP-HPLC: t_R = 12.5 min

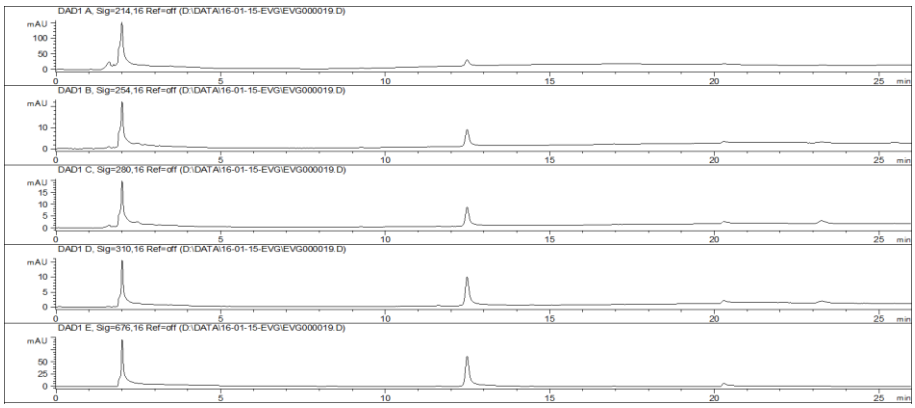

4.2.3 Preparation ZnPc-CNC biohybrids

The ZnPc-CNC hybrids were easily prepared by ultrasound bath-assisted dispersion of the pristine CNC (in PBS, 5 mg mL^{-1}, 3 mL) in the corresponding ZnPc aqueous solution (ca. 0.1 mM, 12 mL) for 30 min. Because of its low water solubility, ZnPc **45** had to be dissolved first in a concentrated solution in DMSO (ca. 10 mM) and subsequently injected into water, with a final DMSO proportion lower than 1%. After sonication of the ZnPc-CNC mixture, the resulting dispersion was centrifuged at 10000 rpm (9391 rfc) for 10 minutes. Colored supernatant was removed and the pellet was washed by adding 10 mL of milli-Q water, re-dispersed by 2 minutes sonication and centrifuged for 10 extra minutes at 10000 rpm (9391 rfc). This procedure was repeated 5 times until no color was observed in the supernatant. In the case of ZnPc **46**, the pellet was colored white, just like the pristine CNC, indicating no dye had been retained. In contrast, in the case of ZnPc **44** and **45** the pellet was blue or green colored, respectively, indicating binding had taken place.

Resumen y Conclusiones en Español

Introducción y Objetivos

El principal objetivo de esta Tesis Doctoral es la síntesis de nuevas ftalocianinas (Pc) y subftalocianinas (SubPc) para su aplicación como fotosensibilizadores (PS) en terapia fotodinámica (PDT: *photodynamic therapy*).

La PDT es una forma de fototerapia aprobada clínicamente que se emplea tanto en el tratamiento de enfermedades oncológicas como en la inactivación de microorganismos. En este último caso, también se puede utilizar el término aPDT (*antimicrobial PDT*) o PDI (*photodynamic inactivation*).

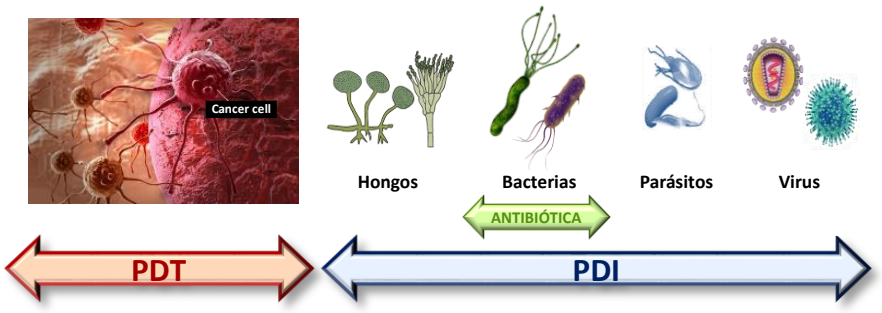

Aparte de un PS, el elemento central en PDT, el tratamiento requiere la presencia de dos componentes más: luz de una longitud de onda adecuada y la presencia de oxígeno molecular ($^3O_2$). Tras la irradiación del PS en su máximo de absorción, éste se excita a su estado singlete excitado ($^1PS^*$), un estado inestable y de corta duración que, a su vez, puede sufrir una inversión del spin del electrón excitado (ISC, *intersystem crossing*) dando lugar al primer estado triplete excitado ($^3PS^*$), un estado más estable y con tiempo de vida más largo. En consecuencia, en este estado el PS tiene la posibilidad de interactuar con el $^3O_2$ presente en el medio biológico, un triplete en su estado fundamental, generando así formas reactivas de oxígeno (ROS, *reactive oxygen species*) y oxígeno singlete ($^1O_2$). Ambos causan daño oxidativo dentro de los tejidos diana, resultando así en la destrucción de células tumorales en el caso de la PDT, y en la inactivación de microorganismos en el caso de la PDI.

Como es bien sabido, el PS ideal debe cumplir con una serie de requisitos básicos para producir resultados óptimos. Debe presentar por ejemplo una elevada estabilidad química y fotoquímica, solubilidad en medios biológicos, y altos rendimientos cuánticos del estado triplete y de generación de $^1O_2$. Además, el PS debe carecer de toxicidad en ausencia de luz y debe mostrar selectividad hacia los tejidos diana. En este sentido, el desarrollo de nuevos PS con mejores propiedades y específicamente diseñados para su aplicación en PDT y/o PDI es un campo de investigación de gran actualidad. En general, los PS se dividen en dos grandes familias: los no porfirinoides y los porfirinoides. Hasta ahora, los porfirinoides han sido la familia más estudiada y con más éxito, dando lugar a varios PS aprobados clínicamente en los últimos años. Por lo tanto, en esta tesis nos

centramos en el desarrollo y el estudio de derivados porfirinoides como PS, más concreto en ftalocianinas de silicio (SiPcs) y SubPcs.

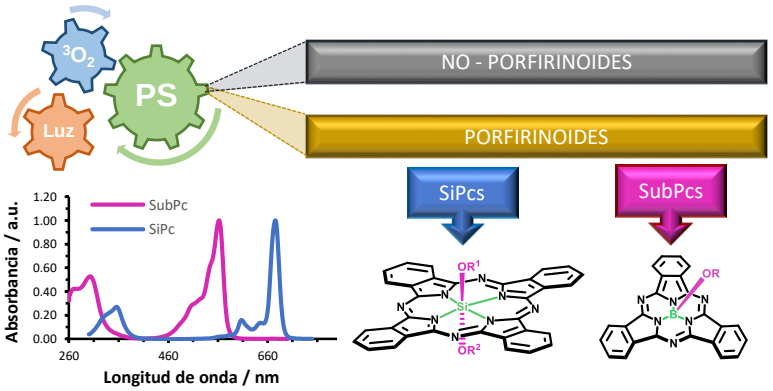

Las Pcs son macrociclos aromáticos constituidos por cuatro unidades de isoindol unidas entre sí por puentes de nitrógeno, cuya nube de 18 electrones π sufre una deslocalización sobre los 16 átomos del anillo interno. En consecuencia, las Pcs poseen una banda Q muy intensa a longitudes de onda relativamente largas (650-750 nm), que se encuentran dentro de la ventana óptica terapéutica, permitiendo así una penetración de luz más profunda en los tejidos. Además, las Pcs presentan una gran versatilidad estructural gracias a que pueden alojar en su cavidad central hasta 70 elementos de la tabla periódica, y a que poseen 16 posiciones periféricas en los anillos bencénicos, en las cuales se pueden introducir diversos sustituyentes. Según la naturaleza del metal alojado, es también posible introducir diferentes sustituyentes en posición axial. Gracias a esta versatilidad química y a sus excelentes propiedades fotofísicas, las Pcs son candidatos prometedores como PS. Sin embargo, debido a su inherente superficie aromática hidrófoba, las Pcs presentan dos principales limitaciones para su uso como PS, como son la ausencia de solubilidad en medio acuoso y la elevada tendencia a formar agregados. Ambos restringen la eficiencia de los procesos relacionados con el estado excitado tales como la fluorescencia o la producción eficiente de $^1O_2$ a través del estado triplete. No obstante, la agregación se evita fácilmente empleando sustituyentes voluminosos en la periferia o en las posiciones axiales del macrociclo. En este sentido, las SiPcs son empleadas con éxito en PDT, ya que permiten la introducción de dos sustituyentes en las posiciones axiales, lo que suprime su tendencia a agregar. Además, una buena selección de los sustituyentes axiales puede proporcionar a la SiPc un aumento de solubilidad en medio acuoso.

Las SubPcs, por otro lado, son homólogos inferiores de las Pcs, constituidas por tres unidades de isoindol unidas entre sí por puentes de nitrógeno. En su cavidad central siempre se aloja un átomo de boro tetracoordinado, que se halla unido a tres átomos de nitrógeno de las unidades de isoindol y a un sustituyente que ocupa la posición axial de la molécula. Parecido a las Pcs, su sistema aromático consta de una nube de 14 electrones π que están deslocalizados sobre el anillo aromático interno, resultando en una banda Q muy intensa a longitudes de onda ligeramente más cortas. Por rayos X se ha determinado

que, a diferencia de las Pcs, las SubPcs no son planas, sino que muestran una estructura cónica. Esto, junto con la presencia del sustituyente axial, implica que las SubPcs son menos susceptibles a agregarse, lo cual es una gran ventaja para su uso como PS. Además, estos macrociclos presentan varias características que justifican su uso como PS, tales como su accesibilidad sintética, altos coeficientes de absorción molar y altos rendimientos cuánticos del estado triplete, de fluorescencia y de generación de $^1O_2$. No obstante, hasta ahora las SubPcs han sido exploradas sobre todo para su aplicación en dispositivos fotovoltaicos y materiales ópticos no lineales, mientras que su uso en aplicaciones biomédicas permanece poco estudiado.

Por otro lado, una nueva tendencia en el desarrollo de PS son los PS de tercera generación, es decir PS conjugados covalentemente, o de modo no covalente, con agentes transportadores para su liberación y acumulación especifica dentro de los tejidos diana, o nanoestructuras biohíbridas que optimizan su solubilidad en medio acuoso, rompen la agregación y proporcionan una elevada biocompatibilidad.

Con el objetivo de extender el conocimiento sobre las propiedades y la eficacia *in vitro* de las SiPcs y SubPcs como PS, en esta tesis hemos preparado varios derivados de ambos, sustituidos con una gran variedad de sustituyentes en las posiciones axiales, y presentando o no cargas positivas en la periferia. Además, algunos de esos PS han sido conjugados con agentes transportadores o nanovehículos en sistemas biohíbridos que mejoran su distribución y liberación en los tejidos diana. Finalmente, se ha investigado la eficacia *in vitro* de los PS obtenidos, tanto para PDT como para PDI. Así, esta tesis se encuentra dividida en tres grandes capítulos.

Capítulo 1: Diseño, síntesis y evaluación *in vitro* de fotosensibilizadores neutros para su uso en terapia fotodinámica

En el Capítulo 1 se describe la síntesis de nuevos derivados de SiPcs y SubPcs para su aplicación en PDT, más específicamente en el tratamiento de enfermedades oncológicas.

➢ En el ***Subcapítulo 1,*** se ha sintetizado una serie de SiPcs que presentan una variedad de sustituyentes con diferentes características, tanto de manera simétrica como asimétrica.

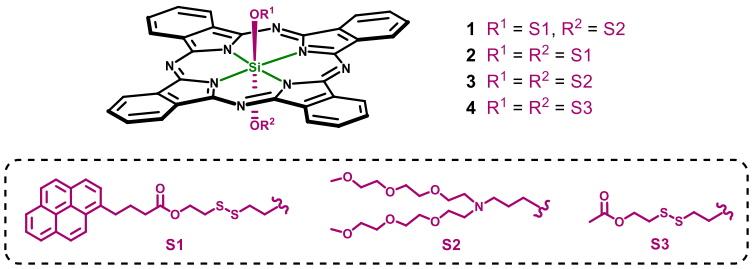

En concreto, los sustituyentes axiales que han sido introducidos tienen la capacidad de inhibir el estado excitado de la SiPc, y como consecuencia su generación de $^1O_2$ y su fluorescencia. Por un lado, se han empleado sustituyentes portadores de grupos pireno, que actuarán como grupos dadores en un proceso de transferencia electrónica de energía (EET: *electronic energy transfer*) en la cual la SiPc actúa como aceptor. Por otro lado, se ha empleado un sustituyente con un grupo amino (**6**), que participará en un fenómeno de transferencia de electrones fotoinducida (PET: *photoinduced electron transfer*). Para todas las SiPcs sintetizadas (SiPc **1**-**3**), tanto su rendimiento cuántico de $^1O_2$ (ϕ_Δ) como de fluorescencia (ϕ_{F680}) han sido evaluados y comparados con los rendimientos cuánticos de una SiPc de referencia desprovista de dichas unidades inhibidoras (SiPc **4**), confirmando la estrategia empleada. Además, en el caso de las SiPcs portadoras de grupos pireno también la fluorescencia de los propios grupos pireno (ϕ_{F377}) está inhibida de manera muy eficaz, permitiendo su uso en teranóstica.

En el caso de los grupos amino, la inhibición es claramente reversible; una vez protonado el grupo amino ya no puede producirse el proceso de PET, y la SiPc recupera su capacidad para generar $^1O_2$ y su fluorescencia. En el caso de los grupos pireno, la eficacia de la EET depende de la distancia entre el dador y el aceptor. De este modo, se puede revertir la inhibición rompiendo el puente disulfuro que enlaza el pireno y la SiPc, empleando un reductor. Así, la SiPc asimétrica que presenta ambas unidades inhibidoras (SiPc **1**) es la molécula con mayor interés, y su comportamiento en función de los dos parámetros que suprimen la inhibición (medio ácido y presencia de un reductor) ha sido estudiado en detalle en la *Seccion 1.3*. Hay que destacar que ambas vías para invertir la inhibición son particularmente relevantes para la aplicación final de este PS, ya que un medio ligeramente ácido y un ambiente reductor son dos características de las células

tumorales. De esta manera, tanto la generación de $^1O_2$ como la fluorescencia de la SiPc y de los grupos pirenos (F_{377}) se activarían solo una vez dentro del tejido diana, las células tumorales, incrementando la selectividad del PS estudiado.

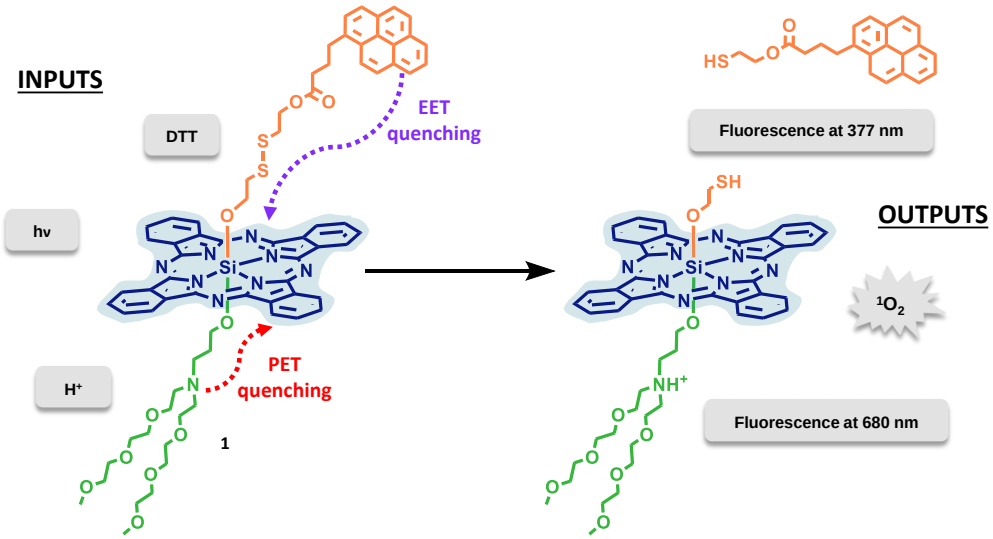

Para algunas SiPcs seleccionadas (SiPc **1**, **3** y **4**), su eficacia *in vitro* ha sido estudiada en varias líneas de células tumorales, durante una colaboración con el laboratorio de microbiología de Ángeles Juarranz de la Fuente, en el Departamento de Biología de nuestra propia universidad. Tal y como se describe en la *Sección 1.4*, la SiPc **3**, la más anfifílica de la serie, es la que ha dado lugar a los mejores resultados, tanto en cantidad de absorción celular como en eliminación de las células tumorales.

➢ En el ***Subcapítulo 2***, se ha llevado a cabo el diseño, la preparación y la caracterización de una serie de SubPcs para su uso como PS en PDT.

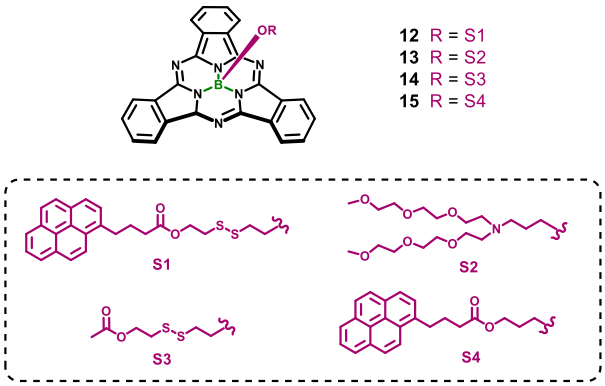

Tanto los rendimientos cuánticos de fluorescencia (ϕ_{F571} y ϕ_{F377}) como de generación de $^1O_2$ (ϕ_Δ) de todas las SubPcs de esa serie han sido determinados, indicando que en este caso la inhibición de F_{377} causada por EET entre los pirenos y la SubPc es muy efectiva,

más que en el caso de las SiPcs, lo cual permite el uso de estas SubPcs (**15** y **16**) en diagnóstica. Por otro lado, aunque la inhibición de la fluorescencia de la SubPc (F_{571}) y de la generación de $^1O_2$ (ϕ_Δ) no es tan efectiva, toda la serie de SubPcs resulta interesante para su uso como PS en PDT, ya que los valores de ϕ_Δ son muy altos y prometedores. En consecuencia, la eficacia de esos compuesto *in vitro* se está estudiando en el laboratorio de Ángeles Juarranz, y se espera obtener los primeros resultados próximamente.

➢ En el ***Subcapítulo 3***, se han combinado los dos PS usados en las secciones anteriores en una sola molécula. En concreto, se ha sintetizado una tríada compuesta por una SiPc portadora de dos SubPcs en sus posiciones axiales. Su generación de $^1O_2$ y su fluorescencia han sido diseñadas para ser sensibles al ambiente de las células tumorales, de manera similar al caso de las SiPc del *Subcapítulo 1*. Con la intención de mejorar la eficacia del proceso de inhibición por EET, se han elegido las SubPcs como unidades dadoras en vez de los grupos pirenos, ya que su espectro de emisión solapa con la banda Q de la SiPc, en vez de con la banda Soret, lo cual ha resultado en una inhibición de su estado singlete excitado más eficaz, tal como se ha estudiado en la *Sección 3.3*. Además, hay que destacar que las SubPcs absorben en regiones de baja absorción de las SiPcs, por lo cual la conjugación de ambos macrociclos permite obtener una fotosensibilización pancromática que en principio debe maximizar la generación de $^1O_2$. No obstante, la estabilidad de la triada ha resultado ser baja, por lo cual no se han podido llevar a cabo estudios de su eficacia *in vitro*.

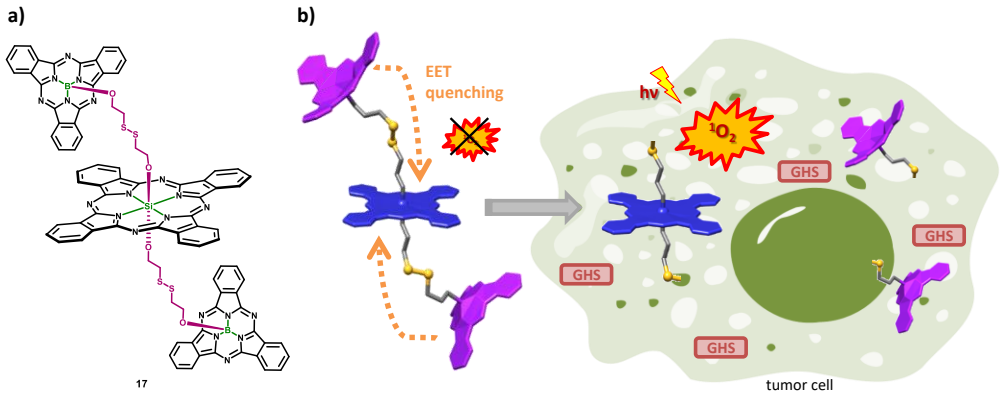

Capítulo 2: Diseño, síntesis y evaluación *in vitro* de fotosensibilizadores catiónicos para su uso en la inactivación fotodinámica de microorganismos

En el Capítulo 2, se describe la síntesis de nuevos derivados de SiPcs y SubPcs catiónicas, para su aplicación en PDI.

Para su uso en PDI, es favorable que los PS estén cargados positivamente, ya que la inactivación de microorganismos está basada en causar daño a la membrana citoplasmática de los microorganismos, la cual suele estar cargada negativamente. De esta manera, los PS catiónicos son en principio capaces de inactivar una gran variedad de microorganismos, tales como hongos, levaduras, protozoos parásitos, bacterias Gram-positivas e incluso bacterias Gram-negativas. Estas últimas son, debido a la presencia de una segunda membrana celular, las especias más difíciles de inactivar, e imposibles de inactivar con PS neutros o cargados negativamente. Aparte de ser catiónicos, los PS deben demostrar las características generales requeridas para PDT, tales como coeficientes de absorción altos en la zona del infrarrojo cercano (NIR: *near infrared*) y altos rendimientos cuánticos de formación del estado triplete y generación de $^1O_2$.

➢ Con esto en mente, en el ***Subcapítulo 1*** de este capítulo se ha sintetizado una serie de SiPcs catiónicas. En paralelo a la serie de SiPcs neutras descrita en el Capítulo 1, se ha introducido una variedad de sustituyentes axiales, mientras que la periferia de las SiPcs presenta invariablemente ocho grupos de tipo piridinio, resultando en una serie de SiPcs octacatiónicas.

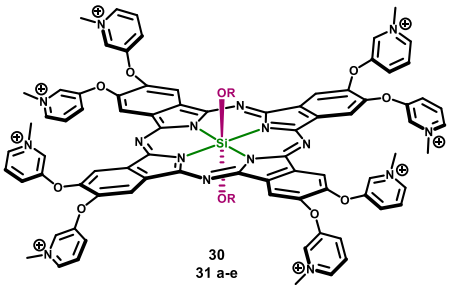

30
31 a-e

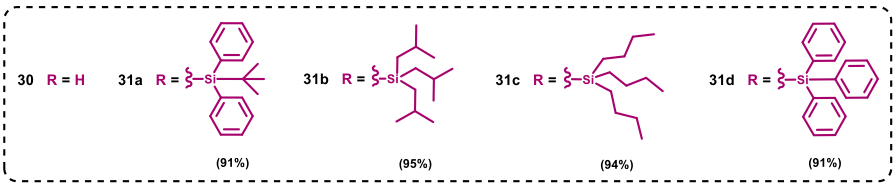

La influencia del ligando axial ha sido evaluada en detalle, determinando el estado de agregación y los rendimientos cuánticos de fluorescencia y $^1O_2$ para toda la serie. Además, se ha valorado la eficiencia de la inactivación de los PS frente a *S. aureus*, una bacteria Gram-positiva, y Methicillin-resistant *S. aureus*, una variante más resistente a varios tipos de antibióticos. En ambos casos, la SiPc **30**, desprovista de toxicidad en

oscuridad y con niveles de inactivación de los microorganismos de hasta el 99,99%, ha dado los mejores resultados.

➢ En el ***Subcapítulo 2***, por otro lado, se ha expuesto la idea de sintetizar una serie de SubPcs hexacatiónicas, para el mismo fin. Sin embargo, tras sintetizar el derivado clorado de la SubPc hexacatiónica, con seis grupos piridinio en la periferia, ha quedado claro que este tipo de SubPc es inestable y su uso como PS en PDT ha sido descartado.

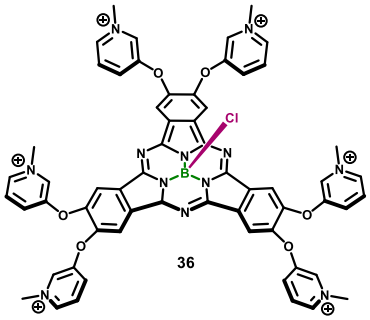

Capítulo 3: Diseño, síntesis y evaluación *in vitro* de sistemas fotosensibilizadores biohíbridos para su uso en terapia fotodinámica y/o la inactivación fotodinámica de microorganismos

El Capítulo 3 se ha dedicado a la preparación de diferentes materiales biohíbridos, para su aplicación en PDT y/o PDI, mediante la combinación de un PS con dos biomoléculas diferentes. Estas biomoléculas han sido seleccionadas cuidadosamente, con el objetivo de mantener o incluso mejorar las características de los PS, mediante desagregación de los mismos en medios acuosos, además de resultar en materiales biocompatibles y monodispersos que dan lugar a sistemas fotoactivos nanoestructurados.

➢ En el ***Subcapítulo 1*** se describe la conjugación de una SiPc y una SubPc con un péptido de penetración celular (CPP: cell penetrating peptide). La conjugación y subsiguiente caracterización han sido llevadas a cabo durante una estancia predoctoral en el laboratorio de Annemieke Madder en la Universidad de Gante (Bélgica). Para este fin, se han sintetizado previamente una una SiPc (**42**) y SubPc (**43**) portadoras de un sustituyente con un grupo maleimida en la posición axial. La elección de este grupo funcional se basa en que puede reaccionar de manera sencilla y eficaz con una unidad de cisteína, presente en el péptido, mediante una reacción tiol-eno de tipo “click”. Los biohíbridos resultantes (**37** y **38**) son totalmente solubles en agua, y sus propiedades

fotofísicas, tales como su fluorescencia y generación de $^1O_2$, han sido examinadas tanto en agua como en tampón fosfato salino (PBS: phosphate buffered saline), un medio representativo desde el punto de vista biológico. Su elevada tendencia a la internalización ha sido confirmada por análisis de citometría de flujo (FACS, *fluorescence activated cell sorting*) en el laboratorio de Bruno de Geest, también en la Universidad de Gante, confirmando la utilidad de esta estrategia. Queda pendiente la visualización de la absorción celular por microscopía de fluorescencia confocal. Estos PS biohíbridos podrían ser utilizados tanto en el tratamiento de enfermedades oncológicas (PDT) como en la inactivación fotodinámica de microorganismos (PDI).

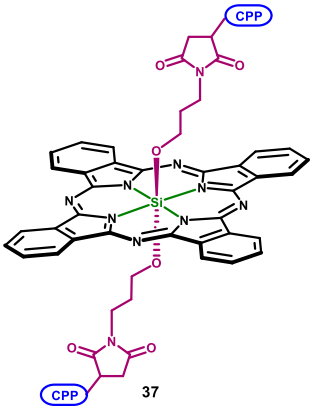

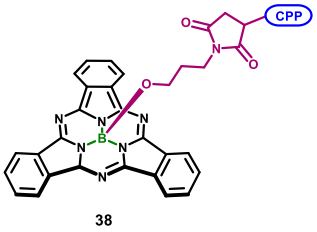

➢ En el ***Subcapítulo 2*** se describe la preparación y caracterización de complejos supramoleculares de ftalocianinas de zinc (ZnPcs) catiónicas y nanocristales de celulosa (CNCs, *cellulose nanocrystals*), como una nueva clase de PS nanoestructurados para la fotogeneración de $^1O_2$. Este trabajo sigue una estrategia basada en la inmovilización mediante interacciones electrostáticas entre derivados catiónicos de ZnPc (**44** y **45**) y la superficie no modificada de los CNCs, que presentan grupos sulfónicos como consecuencia de su síntesis. Los híbridos resultantes han sido caracterizados mediante diversas técnicas, demostrando que no solo la agregación de la ZnPc, sino también la tendencia a la agregación de los CNCs juegan un papel clave en la producción de $^1O_2$. Las propiedades fotofísicas de estos compuestos, junto con su eficacia *in vitro* frente a una serie de microorganismos, han sido estudiadas en detalle durante una estancia predoctoral en los laboratorios de Santi Nonell Marrugat y Montserrat Agut Bonsfills en el Institut Químic de Sarrià de la Universitat Ramon Llull (Barcelona), tal y como se describe en las *Secciones 2.3 y 2.4*. En consecuencia, la inactivación fotodinámica de microorganismos por **44-CNC** y **45-CNC** muestra mejoras evidentes en comparación con la inactivación causada por las ZnPcs libres. Además, es importante destacar que los sistemas **44-CNC** y **45-CNC** demuestran una eficacia significativamente mayor que otros sistemas biohíbridos previamente mencionados en la literatura, en los cuales el PS se ha unido covalentemente a la superficie de los CNC. En este sentido, los biohíbridos desarollados en esta Sección han demostrado ser biomateriales fotoactivos muy

prometedores, que pueden encontrar aplicaciones útiles en biomedicina y nanotecnología.